



**HAL**  
open science

# Application of Time Reversal (TR) Technique to Ultra wideband (UWB) and multi antenna (MIMO) communication systems

Ijaz Haider Naqvi

► **To cite this version:**

Ijaz Haider Naqvi. Application of Time Reversal (TR) Technique to Ultra wideband (UWB) and multi antenna (MIMO) communication systems. Signal and Image processing. INSA de Rennes, 2009. English. NNT: . tel-00499469

**HAL Id: tel-00499469**

**<https://theses.hal.science/tel-00499469>**

Submitted on 9 Jul 2010

**HAL** is a multi-disciplinary open access archive for the deposit and dissemination of scientific research documents, whether they are published or not. The documents may come from teaching and research institutions in France or abroad, or from public or private research centers.

L'archive ouverte pluridisciplinaire **HAL**, est destinée au dépôt et à la diffusion de documents scientifiques de niveau recherche, publiés ou non, émanant des établissements d'enseignement et de recherche français ou étrangers, des laboratoires publics ou privés.

N° d'ordre : D09-26

# Thèse

présentée devant

**l'Institut National des Sciences Appliquées de Rennes**

pour obtenir le titre de

**Docteur**

spécialité : *Electronique et Télécommunications*

---

## **Application of Time Reversal (TR) Technique to Ultra wideband (UWB) and multi antenna (MIMO) communication systems**

**"Application du retournement temporel (RT) aux systèmes de communications ultra large  
bande (ULB) et multi-antennes (MIMO)"**

---

par

Ijaz Haider NAQVI

Soutenue le 15 décembre 2009 devant la commission d'Examen

*Composition du jury*

***Rapporteurs***

Claude OESTGES    Professeur à l'UCL Belgique  
Alain SIBILLE    Professeur à l'ENSTA ParisTech

***Examineurs***

Gilles BUREL    Professeur à l'UBO Brest  
Arnaud TOURIN    Maître de Conférences à l'ESPCI ParisTech  
Bernard UGUEN    Professeur à l'Université de Rennes 1  
Philippe BESNIER    Chercheur CNRS à l'INSA de Rennes  
Ghaïs EL ZEIN    Professeur à l'INSA de Rennes

---

Institut d'électronique et de télécommunications de Rennes  
Institut National des Sciences Appliquées de Rennes



# Contents

<b>Contents</b>	<b>i</b>
<b>List of Figures</b>	<b>v</b>
<b>List of Tables</b>	<b>xi</b>
<b>List of Acronyms and Abbreviations</b>	<b>xiii</b>
<b>Résumé étendu</b>	<b>xv</b>
<b>General Introduction</b>	<b>xxxiii</b>
<b>1 State-of-the-Art of Pulsed UWB and Time Reversal UWB</b>	<b>1</b>
1.1 Introduction . . . . .	3
1.2 Pulsed UWB Technology . . . . .	4
1.2.1 Introduction: What is UWB ? . . . . .	4
1.2.1.1 Definition . . . . .	4
1.2.2 Historical Developments . . . . .	4
1.2.2.1 Strengths and Weaknesses of UWB . . . . .	6
1.3 PSD Constraints for UWB Systems . . . . .	7
1.4 Principle of Pulsed UWB . . . . .	10
1.4.1 Pulse Position Modulation . . . . .	10
1.4.2 Pulse Amplitude Modulation . . . . .	12
1.4.3 Orthogonal Pulse Modulation . . . . .	12
1.4.4 Transmit Reference Scheme . . . . .	13
1.4.5 Direct Sequence UWB . . . . .	13
1.4.6 Multi-band Orthogonal Frequency Division Multiplexing . . . . .	15
1.5 UWB Propagation Channels . . . . .	16
1.5.1 UWB Channel Characterization Parameters . . . . .	17
1.5.2 Channel Modeling and Practical Constraints . . . . .	18
1.6 UWB Channel Models . . . . .	19
1.6.1 Empirical Models . . . . .	19
1.6.1.1 Path Loss Models . . . . .	19
1.6.1.2 Power delay profile . . . . .	20
1.6.1.3 Delay spread . . . . .	20

1.6.2	Statistical Models . . . . .	20
1.6.2.1	Channel impulse response model . . . . .	21
1.6.2.2	Statistics of channel delays . . . . .	21
1.6.2.3	Power delay profile statistics . . . . .	21
1.6.2.4	Auto-regressive models for UWB channels . . . . .	22
1.7	Receiver Used for UWB Systems . . . . .	22
1.7.1	Coherent Receivers . . . . .	22
1.7.1.1	Rake Receiver . . . . .	22
1.7.2	Non Coherent Receivers . . . . .	23
1.7.2.1	Energy Detector . . . . .	23
1.7.2.2	Transmit Reference Receiver . . . . .	24
1.8	Introduction of Time Reversal . . . . .	24
1.8.1	Time Reversal Acoustics . . . . .	25
1.8.2	Stoke's Time Reversal Experiment . . . . .	25
1.8.3	Principle of Reciprocity . . . . .	26
1.8.4	Time Reversal Cavity . . . . .	27
1.8.5	Time Reversal for Electromagnetic Waves . . . . .	27
1.8.5.1	Time Reversal of a Carrier Based Signal . . . . .	28
1.8.6	TR in UWB . . . . .	29
1.8.6.1	Time Reversal Properties . . . . .	32
1.8.6.2	Spectral Analysis of TR Scheme . . . . .	34
1.9	Conclusion . . . . .	35
<b>2</b>	<b>Validation of TR Scheme</b> . . . . .	<b>37</b>
2.1	Introduction . . . . .	39
2.2	Simulation Approach for TR Validation . . . . .	40
2.2.1	Description of Used Channel Model . . . . .	40
2.2.1.1	Channel Model . . . . .	40
2.2.1.2	Channel Model Parameters . . . . .	41
2.2.1.3	Properties of Channel Impulse Response . . . . .	42
2.2.2	TR Validation with Existing Channel Models . . . . .	46
2.2.3	TR Validation with TD-TLM Simulations . . . . .	47
2.2.3.1	Simulation Setup . . . . .	48
2.2.3.2	Simulation Results . . . . .	49
2.3	Semi Measurement Approach for TR Validation . . . . .	51
2.3.1	Experimental Setup . . . . .	52
2.3.2	Spatial Focusing in an Indoor Environment . . . . .	52
2.3.3	Effects of Bandwidth on Spatial Focusing of the TR Scheme . . . . .	54
2.3.3.1	Experimental Setup . . . . .	54
2.3.3.2	Bandwidth Effects . . . . .	54
2.4	Full Measurement Approach for TR Validation . . . . .	56
2.4.1	Experimental Setup . . . . .	56
2.4.2	Validation Procedure . . . . .	57

2.4.3	Comparison of Measured Channel Response in Different Measurement Configurations . . . . .	58
2.4.4	Comparison of different TR Properties . . . . .	59
2.4.5	TR in a Reverberation Chamber . . . . .	63
2.4.5.1	Experimental Setup . . . . .	63
2.5	Effect of Different Antennas on TR . . . . .	65
2.5.1	Experimental Results in RC . . . . .	66
2.5.2	Experimental Results in the Indoor Environment . . . . .	67
2.6	Effect of Different Bandwidths on TR . . . . .	69
2.6.1	Experiments in RC . . . . .	69
2.6.2	Experiments in Indoor Environment . . . . .	71
2.7	TR with Multi-Antenna Configurations . . . . .	72
2.7.1	MIMO-TR in RC . . . . .	74
2.7.1.1	Experimental Setup . . . . .	74
2.7.1.2	Experimental Results . . . . .	75
2.7.2	SISO and SIMO-TR in the Indoor Environment . . . . .	76
2.7.2.1	Experimental Results . . . . .	76
2.8	Multiplexing Gain of SIMO-TR . . . . .	77
2.8.1	Capacity Comparison of the TR Multi Antenna Configurations . . . . .	79
2.8.2	Experimental Validation of SIMO-TR . . . . .	81
2.8.2.1	Experimental Setup . . . . .	81
2.9	Conclusion . . . . .	82
<b>3</b>	<b>Robustness of TR Scheme</b>	<b>85</b>
3.1	Introduction . . . . .	86
3.2	Experiments in RC . . . . .	87
3.2.1	Experimental Setup . . . . .	88
3.2.2	Measurement Results and Analysis . . . . .	88
3.2.2.1	Experiments with a Rotating Stirrer . . . . .	88
3.2.2.2	Experiments with Moving Receiver . . . . .	94
3.3	TR Robustness in Realistic Channels . . . . .	98
3.3.1	Measurement Procedure . . . . .	98
3.3.2	Experiments With a Changing Environment . . . . .	98
3.3.2.1	Measurement Campaign 1 . . . . .	98
3.3.2.2	Measurement Campaign 2 . . . . .	103
3.3.3	Experiments With a Moving Receiver . . . . .	105
3.4	Conclusion . . . . .	107
<b>4</b>	<b>UWB Time Reversal Communication</b>	<b>109</b>
4.1	Introduction . . . . .	110
4.2	Novel Modulation Scheme for TR Communication . . . . .	111
4.2.1	Description of the Novel Modulation Scheme . . . . .	111
4.2.2	Effects of Shift on the Received Signal . . . . .	115
4.2.3	Theoretical Performance . . . . .	116

4.2.4	Information Rate of the Modulation Scheme . . . . .	117
4.2.5	Validation of the New Modulation Scheme by Experiments and Simulations . . . . .	120
4.2.5.1	Measurement Campaign 1 . . . . .	121
4.2.5.2	Measurement Campaign 2 . . . . .	124
4.3	High Data Rate TR Communication . . . . .	127
4.3.1	Experimental Setup . . . . .	127
4.3.2	Experimental Results . . . . .	128
4.3.2.1	Channel Estimation . . . . .	128
4.3.2.2	Data Transmission . . . . .	128
4.3.2.3	<i>Signal, Interference</i> and <i>Noise</i> Extraction . . . . .	129
4.3.2.4	SIR and BER Performance of the Classical TR Scheme	131
4.3.3	Sub-Band TR Transmission Scheme . . . . .	135
4.3.3.1	Experimental Results with SB-TRTS . . . . .	137
4.4	Conclusion . . . . .	138
<b>5</b>	<b>Multi User TR Communication</b>	<b>141</b>
5.1	Introduction . . . . .	142
5.2	Circular Shift Time Reversal . . . . .	142
5.2.1	Effects of CSTR on Received Signal Peak . . . . .	145
5.3	Effects of CSTR on Signal to Interference Ratio (SIR) . . . . .	146
5.3.1	Experimental Setup . . . . .	147
5.3.2	Simulation Results . . . . .	147
5.4	Modified Transmission Scheme . . . . .	149
5.4.1	Interference Analysis of the Proposed Scheme . . . . .	150
5.4.2	Effects of Shift on Received Signal Peak . . . . .	151
5.4.3	Experimental Setup and Simulation Results . . . . .	153
5.4.3.1	BER Performance . . . . .	154
5.5	Conclusion . . . . .	155
	<b>General Conclusion and Prospects</b>	<b>157</b>
	<b>Research Publications</b>	<b>161</b>
	<b>Bibliography</b>	<b>163</b>

# List of Figures

1	Systèmes radio présents dans les bandes UHF et SHF . . . . .	xvii
2	Masque spectral ULB dans différents pays . . . . .	xvii
3	Transmission en multi-bandes OFDM . . . . .	xix
4	Focalisation spatiale du RT . . . . .	xxii
5	Focalisation spatiale du RT . . . . .	xxiii
6	PPR de RCM et de réponse RT pour une configuration NLOS et des polarisations identiques . . . . .	xxiii
7	Pour une largeur de bande de 2.0 GHz, PPR de la réponse RT pour différentes $\theta$ . . . . .	xxv
8	Pour différentes $\theta$ et largeurs de bande a) Puissance crête normalisée b) Rapport signal à lobe secondaire c) Gain de focalisation d) Augmentation de puissance moyenne . . . . .	xxvi
9	Pour une largeur de bande de 2.0 GHz et différents variation dans le canal a) PPR b) caractéristiques du RT . . . . .	xxvi
10	Performances en TEB avec la nouvelle technique de modulation pour différents ordres de modulation a) TEB théorique b) TEB par simulation	xxix
11	TEB avec RT à haut débit en indoor . . . . .	xxx
12	Performances en TEB avec 5, 10, et 20 utilisateurs simultanés avec a) RT-simple b) RTPC c) RT modifié d) toutes les techniques avec 15 utilisateurs simultanés . . . . .	xxxi
1.1	Comparison of the spectrum allocation for different wireless radio systems . . . . .	5
1.2	Channel capacity as a function of SNR for different bandwidths . . . . .	7
1.3	Different radio systems present in UHF and SHF bands . . . . .	8
1.4	UWB Spectral Mask in USA and Europe . . . . .	9
1.5	Illustration of bit '0' and bit '1' using TH-PPM . . . . .	11
1.6	The DS-UWB spectrum. . . . .	14
1.7	Spectrum of multi-band OFDM . . . . .	15
1.8	Block diagram of Rake receiver . . . . .	23
1.9	Block diagram of an energy detector based on OOK . . . . .	24
1.10	Block diagram of the transmit reference receiver . . . . .	24

1.11	Reflection and transmission of a plane wave along the interface separating two media of different sound velocities. (b) Time reversal of FIG. 1.11a . . . . .	26
1.12	a) CIR in an indoor environment b) Received signal with TR scheme in an indoor environment . . . . .	30
1.13	PSD of a a pulse train and single pulse for a) Pulsed UWB b) TR UWB	34
2.1	Power Delay Profiles and Power Decay Profiles for CIRs in LOS and NLOS configuration for an indoor residential environment . . . . .	44
2.2	Power Delay Profiles and Power Decay Profiles for CIRs in LOS and NLOS configuration for an indoor office environment . . . . .	44
2.3	Power Delay Profiles and Power Decay Profiles for CIRs in LOS and NLOS configurations for the industrial environment . . . . .	45
2.4	Power Delay Profiles and Power Decay Profiles for TRRs in LOS and NLOS configuration for an indoor residential environment . . . . .	45
2.5	Power Delay Profiles and Power Decay Profiles for TRRs in LOS and NLOS configuration for an indoor office environment . . . . .	46
2.6	Power Delay Profiles and Power Decay Profiles for TRRs in LOS and NLOS configurations for the industrial environment . . . . .	46
2.7	Simulation setup . . . . .	48
2.8	Normalized PDP of the CIR with TD-TLM simulation at a) corner of the rectangular surface b) center of the rectangular surface . . . . .	49
2.9	Normalized PDP of the TRR with TD-TLM simulation . . . . .	50
2.10	Normalized peak power with the TR scheme in a square surface with TD-TLM simulation . . . . .	50
2.11	Normalized PDP with the TR scheme with TD-TLM simulation for x, y and z polarizations . . . . .	51
2.12	Measurement layout for the measurement in an indoor environment . .	52
2.13	Normalized TR received peak power over a rectangular surface in an indoor environment . . . . .	53
2.14	Measurement layout for measuring the frequency responses in a RC . .	54
2.15	Normalized peak power with the TR scheme in a square surface with different bandwidths (BW) but constant lower frequency ( $f_L$ ) . . . . .	55
2.16	Normalized peak power with the TR scheme in a square surface with a constant bandwidth (BW) of 3 GHz but different lower frequencies ( $f_L$ ) . . . . .	55
2.17	Measurement environment layout . . . . .	56
2.18	Experimental Setup . . . . .	56
2.19	Channel sounding pulse . . . . .	57
2.20	Power Delay Profiles of the CIRs in LOS and NLOS configurations in a typical indoor office environment . . . . .	59
2.21	Power Delay Profiles of TRRs in LOS and NLOS configurations in a typical indoor office environment . . . . .	61
2.22	Measurement setup for the TR experiment in the reverberation chamber	63

2.23	PDP of the MCR in the RC . . . . .	64
2.24	PDP of the measured TR received signal in the RC . . . . .	65
2.25	A snapshot of horn, log-periodic and CMA . . . . .	66
2.26	PDP of the TR received signal with CMA, horn and log-periodic antennas in the RC . . . . .	67
2.27	PDP of the TR received signal with CMA, horn and log-periodic antennas in an indoor environment . . . . .	68
2.28	A snapshot of one CMA in the RC . . . . .	70
2.29	PDP of the TR received signal with different bandwidths in the RC . . . . .	70
2.30	PDP of the TR received signal with different bandwidths in an indoor environment with NLOS cross-polar configuration . . . . .	71
2.31	Multiplexing and diversity gains for different multi antenna configurations . . . . .	74
2.32	Experimental setup for different multi-antenna configurations in the RC . . . . .	75
2.33	The interior of the reverberation chamber with two conical monopole antennas . . . . .	76
2.34	PDP of the received TR signal with SISO, SIMO and MIMO configurations . . . . .	76
2.35	PDP of the received TR signal with SISO and SIMO configurations in an indoor environment . . . . .	77
2.36	Block diagram of the novel transmission approach for SIMO-TR . . . . .	79
2.37	Capacity of the SISO-TR, MISO-TR with different number of antennas at the transmitting and SIMO-TR with different number of antennas at the receiving end. . . . .	81
2.38	Power delay profile of the received signal with SISO-TR and two individual signals with SIMO-TR . . . . .	82
3.1	A snapshot of the interior of the reverberating chamber with horn antenna and the stirrer . . . . .	87
3.2	Measurement setup for the TR experiment in the reverberation chamber . . . . .	88
3.3	Cross-correlation coefficients ( $\rho_h(\theta^\circ)$ ) between the MCRs $h'_j(\theta^\circ)$ and $h'_j(0^\circ)$ . . . . .	89
3.4	Cross-correlation coefficients ( $\rho_y(\theta^\circ)$ ) between the TR received signals $y_j(\theta^\circ)$ and $y_j(0^\circ)$ . . . . .	90
3.5	PDP of the TR received signals a) $y_j(\theta^\circ)$ b) $y_j(1^\circ)$ c) $y_j(2^\circ)$ d) $y_j(3^\circ)$ for a bandwidth of 2.0 GHz . . . . .	90
3.6	Partial correlation between the $a_i$ and $b_i$ extracted from MCRs $h'_j(0^\circ)$ and $h'_j(3^\circ)$ respectively for bandwidth of 2.0 GHz . . . . .	92
3.7	Correlated part of the MCRs $h'_j(0^\circ)$ and $h'_j(3^\circ)$ for a bandwidth of 2.0 GHz . . . . .	92
3.8	Received TR signal with a 2% threshold for a) $\theta = 1^\circ$ b) $\theta = 5^\circ$ . . . . .	93
3.9	For varying $\theta$ and different bandwidths, a) Received peak power b) Signal to side-lobe ratio c) Focusing gain d) Increased average power . . . . .	94

3.10	Pattern of the movement of the receiver for the TR experiments in the RC . . . . .	95
3.11	Cross-correlation coefficients ( $\rho_h$ ) of the MCR at a reference position and MCR at a) all measurement points b) first 6 measurement points .	95
3.12	Cross-correlation coefficients ( $\rho_y(d)$ ) of the TR received signal at different distance ( $d$ cm) from the reference position ( $d = 0$ cm) . . . . .	96
3.13	Partial correlation between $a_i$ and $b_i$ extracted from the MCRs $h'_j(d = 0$ cm) and $h'_j(d = 10$ cm) respectively for a bandwidth of $1.5$ GHz . . . . .	96
3.14	For varying positions of the receiver and different bandwidths, a) Received peak power b) Signal to side-lobe ratio c) Focusing gain d) Increased average power . . . . .	97
3.15	Measurement environment layout . . . . .	99
3.16	Experimental Setup . . . . .	99
3.17	Two metallic strips used to induce variations in the channel . . . . .	100
3.18	Correlation coefficient of the MCR and the TRR with different induced variations in the channel . . . . .	101
3.19	Relative strength of different TR properties with different induced variations in the channel . . . . .	101
3.20	PDP of the received TR signal with different variations induced in the channel or a bandwidth of $2.0$ GHz . . . . .	102
3.21	PDP of the received TR signal with different variations induced in the channel different bandwidths . . . . .	102
3.22	Measurement environment layout for the second measurement campaign	103
3.23	Correlation coefficient of the MCR and the TRR with different induced variations in the channel . . . . .	104
3.24	Relative strength of different TR properties with different induced variations in the channel for second measurement campaign . . . . .	104
3.25	PDP of the received TR signal with different variations induced in the channel for a bandwidth of $2.0$ GHz . . . . .	105
3.26	Respective correlation coefficients of the MCR ( $\rho_h(d)$ ) and the measured TRR ( $\rho_y(d)$ ) with the MCR and measured TRR at $d = 0$ cm with different displacements of the receiver for a bandwidth of $2.0$ GHz	106
3.27	PDP of TR received signal with different displacements of the receiver	107
4.1	Conceptual block diagram of the new modulation scheme . . . . .	112
4.2	Pattern for the left and right shifts . . . . .	113
4.3	Received signal peak power with left and right shifts normalized to the peak with no shift . . . . .	115
4.4	Average and bit by bit signal to interference ratio for the received signal with 4 simultaneous bits ( $m = 4$ ) with different shift steps (in percentage of the transmitted signal length ( $T_{sig}$ )) . . . . .	116
4.5	Signal space representation of the new modulation scheme with $M = 4$ and $M = 8$ . . . . .	118

4.6	Data rate for $m$ number of simultaneous bits normalized to the data rate of BPEM ( $m = 1$ ) . . . . .	120
4.7	Data rate of the proposed modulation scheme against both SNR and SIR normalized to the data rate of $m = 1$ for two different values of $m$ . . . . .	121
4.8	Environment layout of the first measurement campaign . . . . .	121
4.9	BER performance of the new modulation scheme for different modulation orders a) Theoretical curves b) simulated curves with a shift step of $0.02 T_{sig}$ . . . . .	122
4.10	BER performance for different modulation orders in the AWGN channel for a) QAM b) PAM . . . . .	123
4.11	Simulation curves for BER performance of the new modulation scheme for different modulation orders with a shift step of $0.05 T_{sig}$ . . . . .	124
4.12	Measurement environment layout of the measurement campaign 2 . . . . .	125
4.13	Experimental Setup of the measurement campaign 2 . . . . .	125
4.14	Received signal for $M = 16$ with the new modulation scheme . . . . .	126
4.15	BER performance of the new modulation scheme for different modulation orders with using the experimental results of measurement campaign 2 . . . . .	126
4.16	Amplitude distribution of the received signal without separating the <i>Interference</i> and <i>Noise</i> components for different values of $T_s$ . . . . .	130
4.17	Amplitude distribution of <i>Signal</i> , <i>Interference</i> and <i>Noise</i> and the sum of three components for $SNR = 15 dB$ in a reverberation chamber for two different values of $T_s$ . . . . .	131
4.18	<i>Signal</i> , <i>Interference</i> and <i>Noise</i> component $SNR = 15 dB$ in an indoor environment for different values of $T_s$ . . . . .	132
4.19	BER performance of TR system for $1 ns \leq T_s \leq 64 ns$ in an indoor environment . . . . .	134
4.20	BER performance of TR system for $1 ns \leq T_s \leq 64 ns$ in a reverberating chamber . . . . .	134
4.21	PSD of a classic TR transmitted signal . . . . .	135
4.22	Block diagram of the modified TR scheme . . . . .	135
4.23	PSD of a modified TR transmitted signal . . . . .	136
4.24	BER performance of TR system for $1 ns \leq T_s \leq 64 ns$ in an indoor environment with sub-band filtering . . . . .	138
5.1	Time Reversed CIR a) without CS b) with right CS of 3 taps c) with left CS of 3 taps . . . . .	144
5.2	Received <i>Signal</i> and <i>Image</i> with right circular shift of $0.25N$ taps . . . . .	145
5.3	Variation of the received signal peak values normalized to the received signal peak without circular shift with different values of circular shift . . . . .	146
5.4	Measurement layout for the measurement in an indoor environment . . . . .	147
5.5	CDF of SIR with right circular shift for User5 with different shift % . . . . .	148
5.6	CDF of SIR with left circular shift for User5 with different shift % . . . . .	148

- 5.7 Received signal peak power with left and right shifts normalized to the peak with no shift . . . . . 152
- 5.8 PSD of transmitted signal with simple TR and modified TR schemes . 153
- 5.9 BER performance with 5, 10, and 20 simultaneous users with a) simple TR b) TR with circular shift c) modified TR scheme d) 15 simultaneous users with all three schemes for  $\delta = 0.05 L$  taps . . . . . 155

# List of Tables

2.1	Channel model parameters for residential, office and industrial indoor environments . . . . .	43
2.2	Time Reversal characteristics with different measurement configurations	48
2.3	Time Reversal characteristics with different measurement configurations	60
2.4	Time Reversal characteristics in a reverberation chamber . . . . .	65
2.5	Time Reversal characteristics with different types of antennas in a RC	67
2.6	Time Reversal characteristics with different type of antennas in an indoor environment . . . . .	68
2.7	Time Reversal characteristics with different bandwidths in a RC . . . .	69
2.8	Time Reversal characteristics with different bandwidths in an indoor environment with NOS cross-polarconfiguration . . . . .	72
2.9	Time Reversal characteristics in the reverberation chamber with different polarizations and multi antenna configurations . . . . .	77
2.10	Time Reversal characteristics in the indoor environment with different SISO and SIMO configurations . . . . .	78
3.1	Comparison of delay spread of the TR received signal ( $y_j(\theta^\circ)$ ) and the MCR ( $h'_j(\theta^\circ)$ ) for different $\theta$ and bandwidths . . . . .	93
3.2	For different bandwidths, comparison of delay spread of the TR received signal ( $y_j(d\text{ cm})$ ) and the MCRs ( $h'_j(d\text{ cm})$ ) at different distances ( $d\text{ cm}$ ) from the reference position ( $d = 0\text{ cm}$ ) . . . . .	97
3.3	Comparison of different TR properties with different displacements of the receiver ( $d\text{ cm}$ ) with respect to the reference position ( $d = 0\text{ cm}$ ) . .	106
4.1	Comparison of SIR for different $T_s$ in the reverberation chamber and in the indoor channel for $SNR = 15\text{ dB}$ with classic TR scheme . . . .	133
4.2	Comparison of SIR for different $T_s$ in the indoor channel for $SNR = 15\text{ dB}$ with SB-TRTS . . . . .	137



# List of Acronyms and Abbreviations

<b>APDcP</b>	<b>A</b> verage <b>P</b> ower <b>D</b> elay <b>P</b> rofile
<b>AWG</b>	<b>A</b> rbitrary <b>W</b> aveform <b>G</b> enerator
<b>AWGN</b>	<b>A</b> dditive <b>W</b> hite <b>G</b> aussian <b>N</b> oise
<b>BER</b>	<b>B</b> it <b>E</b> rror <b>R</b> ate
<b>BPAM</b>	<b>B</b> inary <b>P</b> ulse <b>A</b> mplitude <b>M</b> odulation
<b>BPSK</b>	<b>B</b> inary <b>P</b> hase <b>S</b> hift <b>K</b> eying
<b>BPF</b>	<b>B</b> and <b>P</b> ass <b>F</b> ilter
<b>CDF</b>	<b>C</b> umulative <b>D</b> istribution <b>F</b> unction
<b>CDMA</b>	<b>C</b> ode <b>D</b> ivision <b>M</b> ultiple <b>A</b> ccess
<b>CIR</b>	<b>C</b> hannel <b>I</b> mpulse <b>R</b> esponse
<b>CS</b>	<b>C</b> ircular <b>S</b> hift
<b>CSTR</b>	<b>C</b> ircular <b>S</b> hift <b>T</b> ime <b>R</b> eversal
<b>DCS</b>	<b>D</b> igital <b>C</b> ellular <b>S</b> ystem
<b>DECT</b>	<b>D</b> igital <b>E</b> nhanced <b>C</b> ordless <b>T</b> elecommunication
<b>DSO</b>	<b>D</b> igital <b>S</b> torage <b>O</b> scilloscope
<b>DSUWB</b>	<b>D</b> irect <b>S</b> equence <b>U</b> ltra <b>W</b> ide <b>B</b> and
<b>EIRP</b>	<b>E</b> ffective <b>I</b> sotropic <b>R</b> adiated <b>P</b> ower
<b>ECC</b>	<b>E</b> uropean <b>C</b> ommunications <b>C</b> ommission
<b>ED</b>	<b>E</b> nergy <b>D</b> etector
<b>ETSI</b>	<b>E</b> uropean <b>T</b> elecommunications <b>S</b> tandards <b>I</b> nstitute
<b>FCC</b>	<b>F</b> ederal <b>C</b> ommunications <b>C</b> ommission
<b>FFT</b>	<b>F</b> ast <b>F</b> ourier <b>T</b> ransform
<b>FG</b>	<b>F</b> ocusing <b>G</b> ain
<b>GPR</b>	<b>G</b> round <b>P</b> enetrating <b>R</b> adar
<b>GPS</b>	<b>G</b> lobal <b>P</b> ositioning <b>S</b> ystem
<b>GSM</b>	<b>G</b> lobal <b>S</b> ystem for <b>M</b> obile communications
<b>HIPERLAN</b>	<b>H</b> igh <b>P</b> erformance <b>R</b> adio <b>L</b> ocal <b>A</b> rea <b>N</b> etwork
<b>IAP</b>	<b>I</b> ncreased <b>A</b> verage <b>P</b> ower
<b>IDA</b>	<b>I</b> nfocomm <b>D</b> evelopment <b>A</b> uthority
<b>IEEE</b>	<b>I</b> nstitute of <b>E</b> lectrical and <b>E</b> lectronics <b>E</b> ngineers
<b>IETR</b>	<b>I</b> nstitute of <b>E</b> lectronics and <b>T</b> elecommunications of <b>R</b> ennes
<b>IFFT</b>	<b>I</b> nverse <b>F</b> ast <b>F</b> ourier <b>T</b> ransform

<b>ISI</b>	<b>Inter Symbol Interference</b>
<b>ISM</b>	<b>Industrial Scientific and Medical</b>
<b>LOS</b>	<b>Line Of Sight</b>
<b>LNA</b>	<b>Low Noise Amplifier</b>
<b>M-BOK</b>	<b>M-ary Bi-Orthogonal Keying</b>
<b>MB-OFDM</b>	<b>Multi-Band Orthogonal Frequency Division Multiplexing</b>
<b>MCR</b>	<b>Mow Pass Filter</b>
<b>MHP</b>	<b>Measured Channel Response</b>
<b>MIMO</b>	<b>Multiple Input Multiple Output</b>
<b>MISO</b>	<b>Multiple Input Single Output</b>
<b>NLOS</b>	<b>Non Line Of Sight</b>
<b>OFDM</b>	<b>Orthogonal Frequency Division Multiplexing</b>
<b>OOK</b>	<b>On Off Keying</b>
<b>OPM</b>	<b>Orthogonal Pulse Modulation</b>
<b>PAP</b>	<b>Pulse to Amplitude Modulation</b>
<b>PDF</b>	<b>Probability Density Function</b>
<b>PL</b>	<b>Path Loss</b>
<b>PPM</b>	<b>Pulse Position Modulation</b>
<b>PSD</b>	<b>Power Spectral Density</b>
<b>PSM</b>	<b>Pulse Shape Modulation</b>
<b>QAM</b>	<b>Quadrature Amplitude Modulation</b>
<b>QPSK</b>	<b>Quadrature Phase Shift Keying</b>
<b>RC</b>	<b>Reverberation Chamber</b>
<b>RF</b>	<b>Radio Frequency</b>
<b>RMS</b>	<b>Root Mean Square</b>
<b>SB-TRTS</b>	<b>Sub-Band Time Reversal Transmission Scheme</b>
<b>SIMO</b>	<b>Single Input Multiple Output</b>
<b>SIR</b>	<b>Signal to Noise Ratio</b>
<b>SIR</b>	<b>Signal to Information Ratio</b>
<b>SISO</b>	<b>Single Input Single Output</b>
<b>SSR</b>	<b>Signal to Side-lobe Ratio</b>
<b>TD-TLM</b>	<b>Time Domain Transmission Line Matrix</b>
<b>TR</b>	<b>Time Reversal</b>
<b>TRR</b>	<b>Time Reversal Response</b>
<b>UMTS</b>	<b>Universal Mobile Telecommunications System</b>
<b>UNII</b>	<b>Unlicensed National Information Infrastructure</b>
<b>UWB</b>	<b>Ultra Wide Band</b>
<b>WLAN</b>	<b>Wireless Local Area Network</b>
<b>WLAN</b>	<b>Wireless Personal Area Network</b>
<b>ZF</b>	<b>Zero Filling</b>

# Résumé étendu

## Introduction

Avec la croissance rapide et continue du marché et l'évolution des technologies radio, les communications sans fil sont de plus en plus compétitives chaque jour. Les avancées dans les technologies sans fil vont de plus en plus affecter notre vie quotidienne. Le WiFi, le Bluetooth et les systèmes radio de nouvelle génération ont déjà commencé à remplacer les anciennes connexions filaires. Ces technologies, non seulement permettent de se débarrasser de ces fils gênants, mais offrent aussi la mobilité à l'utilisateur qui peut ainsi accéder à un large éventail d'informations de n'importe où et à n'importe quel moment. Les nouveaux systèmes de communication sans fil doivent donc répondre à un besoin croissant en termes de débit et de capacité. Les services des connexions sans fil doivent être plus rapides et plus sécurisés avec une qualité supérieure. Ainsi, de nouvelles technologies à l'étude cherchent à trouver leur place dans le spectre des radio-fréquences (RF) déjà bien encombré.

Cet encombrement du spectre rend difficile, voire impossible, l'émergence de ces nouvelles technologies. Toutefois, avec la technologie UWB (Ultra-Wide Band), qui est en cours d'études, il est possible de coexister avec d'autres technologies, à condition de respecter le spectre attribué en termes de bande et de puissance émise. Les exigences strictes contribuent à maintenir les interférences au minimum et ainsi le spectre peut être utilisé avec une efficacité accrue.

L'UWB est donc une technologie potentielle pour un grand nombre de nouvelles applications comme les réseaux locaux et personnels sans fil (WLAN-WPAN). Compte tenu de la bande passante ultra large, les signaux UWB sont immunisés contre les évanouissements dus aux multi-trajets et permettent des communications avec des débits de données élevés. Leur principale limitation porte sur la distance maximale à laquelle la communication peut avoir lieu avec de faibles taux d'erreur binaire (TEB). En outre, la transmission UWB peut potentiellement être mise en oeuvre avec un coût réduit et une faible consommation de puissance, ce qui représente une solution intéressante pour les applications de contrôle à distance et de réseaux de capteurs. Dans un système de communication UWB impulsionnel, l'information est codée par des impulsions très brèves. La capacité de l'UWB par impulsions à résoudre les trajets multiples est exploitée dans les recherches récentes pour les applications de communications à courte portée. Toutefois, l'exploitation de cette diversité de multi-trajets et les limitations de puissance d'émission rendent le système de réception

complexe. Pour recueillir l'énergie du signal reçu, des techniques telles que la réception par un Rake, ou par corrélation à retour de décision ou encore la transmission de référence, peuvent être mises en oeuvre. Les deux premières techniques sont assez complexes, tandis que la troisième réduit sensiblement le débit du système.

Une façon de surmonter ces inconvénients est de faire usage d'une technique qui permet de déplacer la complexité du récepteur vers l'émetteur. Le retournement temporel (RT) a été proposé comme une technique répondant à ce besoin. Classiquement, le RT a été appliqué en acoustique et dans des communications sous-marines, mais récemment, il est largement étudié pour les communications UWB. Le signal reçu dans un système RT est considérablement concentré dans les domaines spatial et temporel. En conséquence, la puissance reçue est concentrée dans quelques fentes temporelles (taps) et les effets des interférences entre symboles (IES) sont fortement réduits. Le système de réception devient plus simple que sans RT et le signal peut être recueilli au moyen de simples détecteurs d'énergie à seuil. La focalisation spatiale permet de réduire les interférences multi-utilisateurs et co-canal dans les réseaux cellulaires à grande capacité.

## Chapitre 1 : Etat de l'art de la technologie UWB et du retournement temporel

Dans ce chapitre, un aperçu de l'état de l'art de la technologie UWB, ses principaux avantages et ses applications en transmission sans fil sont décrits. Après avoir défini les signaux UWB, la réglementation du spectre à travers le monde est discutée. La figure 1 montre certains systèmes radio opérant dans les bandes UHF et SHF. Nous notons que plusieurs systèmes occupent les bandes réservées tels que la norme de téléphonie cellulaire GSM (900 MHz), DCS (1,8 GHz) et UMTS (2 GHz).

Le système de positionnement par satellite GPS a également une bande réservée (1,5 GHz). Autres bandes de fréquences peuvent être occupées par les systèmes de communication sans licence. Par exemple, la bande ISM (consacrée aux applications industrielles, scientifiques et médicales) est utilisée par Bluetooth, WiFi ou les fours à micro-ondes. La bande UNII est celle de fonctionnement du WiFi 802.11a et HIPER-LAN 1.1.

Afin de limiter l'interférence des signaux ULB aux autres systèmes radio, les différentes autorités de régulation se sont mises d'accord sur l'utilisation de la bande des 3,1 GHz-10,6 GHz pour des signaux ULB. Ainsi, une bande passante de 7,5 GHz peut être utilisée pour des signaux ULB sans interférence notable aux systèmes de téléphonie et GPS. La très faible limite de la densité spectrale de puissance, en dessous du niveau des émissions non intentionnelles, est imposée par la FCC (-41 dBm/MHz). Cette faible valeur est compensée par la large bande passante pour transmettre une puissance totale de 0,6 mW. Les règles imposées à l'émission des signaux ULB sont différentes aux Etats-Unis, en Europe et en Asie. La réglementation en Europe est

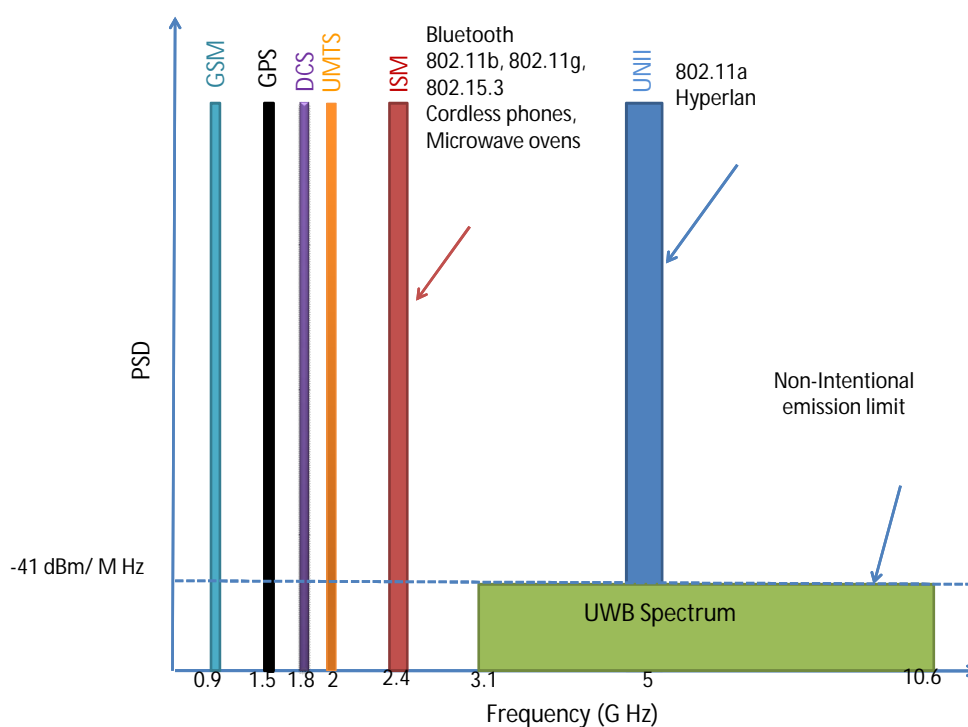


Figure 1: Systèmes radio présents dans les bandes UHF et SHF

plus stricte que celle aux Etats-Unis. Excepté le Japon, la réglementation dans certains pays d'Asie est moins stricte que celle aux Etats-Unis et en Europe.

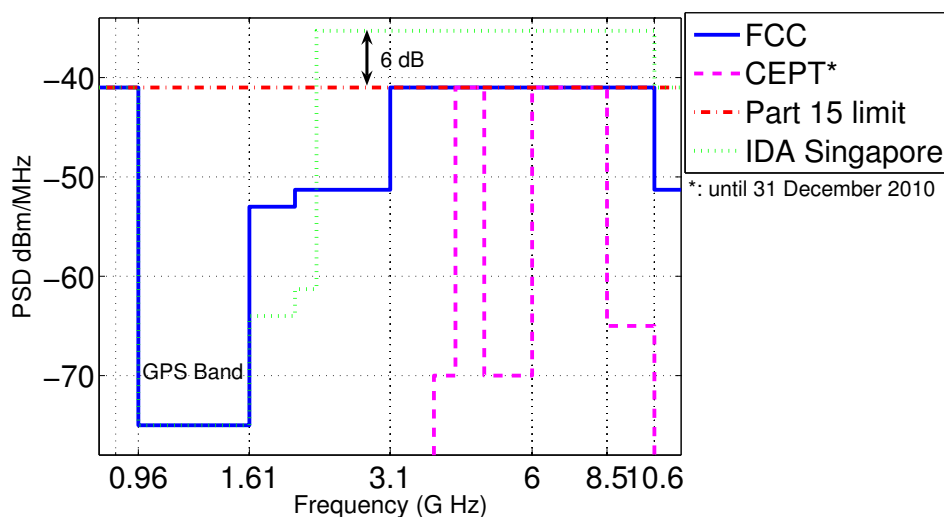


Figure 2: Masque spectral ULB dans différents pays

Le masque du spectre d'une communication autorisée dans un environnement intérieur est montré par la figure 2. Le masque spectral est établi pour assurer la protection des systèmes sensibles, en particulier le GPS (1,2 à 1,5 GHz) et les bandes dédiées à l'aviation civile. Une restriction sur la crête PIRE est également imposée et peut être exprimée par :

$$\text{EIRP}_{peak} = 20 \log_{10} \left( \frac{\text{RBW}}{50} \right) \quad (1)$$

En raison de leur bande passante extrêmement large, les signaux ULB se traduisent par un grand nombre de trajets multiples résolubles en réception, ce qui permet de réduire les interférences provoquées par la superposition de ces trajets. En outre, les systèmes ULB par impulsion peuvent utiliser différents types de modulation, comme par exemple, la modulation de position d'impulsions (PPM), la modulation d'amplitude d'impulsions en (PAM) et la modulation d'impulsions orthogonales (OPM). Avec la PPM, plusieurs utilisateurs peuvent accéder au canal par saut temporel (time hopping ou TH) en utilisant des codes pseudo-aléatoires. Avec l'approche TH-PPM, la collision entre les différents utilisateurs peut être évitée.

La séquence directe (DS) est une autre solution pour la transmission ULB. Ce système utilise l'allocation de fréquences sous forme de deux bandes, couvrant respectivement de 3,1 à 4,85 GHz et de 6,2 à 9,7 GHz. Cette configuration protège les systèmes de la bande UNII à 5 GHz utilisée par le WiFi. Sur ces bi-bandes, les impulsions émises ont une durée d'environ 0,3 à 0,5 ns, et se composent de plusieurs cycles. Au début, seule la bande inférieure a été utilisée afin de simplifier l'architecture des systèmes de transmission. Comme dans la modulation PPM, les trames DS-ULB sont divisées en plusieurs fentes temporelles. Cependant, une impulsion peut être transmise dans chaque fente. Par conséquent, le signal est transmis d'une façon continue et n'est pas comme les signaux radio impulsionnels à faible rapport cyclique. Les symboles transmis sont représentés par des codes d'étalement ternaires (composés de 1, 0 et -1) sur la longueur de la trame. En vertu de la norme proposée par l'IEEE Task Group, tous les systèmes DS-ULB doivent être capables de générer ces codes en utilisant la modulation BPSK en bande de base.

La technique de multiplexage par répartition de fréquences orthogonales en multi-bandes (Multi-Band Orthogonal Frequency Division Multiplexing ou MBOFDM) est également l'une des solutions pour les communications ULB, proposée par le Task Group 3 bis - IEEE 802.15. Dans cette technique, le spectre défini par la FCC est divisé en 14 sous-bandes de 528 MHz sans recouvrement. Ces sous-bandes sont ensuite réparties en cinq groupes. La figure 3 présente ces sous-bandes classées en différents groupes. Dans chaque sous-bande, la modulation OFDM est appliquée et le signal est distribué à travers 128 sous-porteuses, ce qui conduit à une séparation entre sous-porteuses de  $\Delta f = 4,125 \text{ MHz}$ . La modulation à déplacement de phase à 4 états (QPSK) est utilisée pour chaque sous-porteuse. Cette configuration permet une gestion souple du spectre radio. Aussi, il est bien plus facile de respecter les réglementations des différents pays sur le masque spectral.

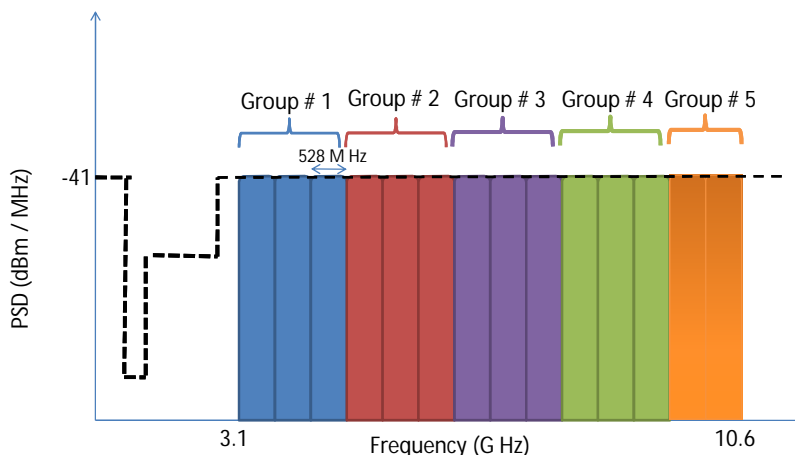


Figure 3: Transmission en multi-bandes OFDM

Un grand nombre de recherches a aussi été effectué sur la modélisation des canaux pour les signaux ULB. Les modèles empiriques et statistiques ont été étudiés. Pour les modèles empiriques, les pertes de puissance, le profil puissance-retard (PPR) et les modèles pour l'étalement des retards sont présentés. La description de modèles statistiques ULB est également présentée dans la thèse : modèle de la réponse impulsionnelle du canal, des statistiques sur le retard, les statistiques sur le profil puissance-retard et les modèles à auto-régression. Pour la réponse impulsionnelle du canal, les modèles à base de clusters sont généralement utilisés comme dans le célèbre modèle de Saleh-Valenzuela ou dans les modèles standardisés IEEE.

Différents types de récepteurs ont été proposés dans la littérature. Afin de rassembler efficacement l'énergie des signaux ULB, les récepteurs sont généralement complexes. Ils sont généralement classés en récepteurs cohérents et non cohérents. Le principe du récepteur Rake est rappelé. Les récepteurs à détection d'énergie ou les systèmes à transmission de référence sont décrits comme des récepteurs non cohérents.

Aussi, nous présentons l'état de l'art de la technique de communication ULB par retournement temporel (RT). A l'origine, le RT a été proposé comme une technique permettant de déplacer la complexité du récepteur vers l'émetteur. Classiquement, le RT a été appliqué en acoustique et dans les applications de communications sous-marines. Pour commencer, l'expérience de Stoke du RT est présentée et le principe de réciprocité est illustré. Le comportement des ondes électromagnétiques avec le RT est examiné. En particulier, les effets de la fréquence porteuse et de la bande passante sur la focalisation spatiale et temporelle du signal reçu par RT sont discutés. Enfin, le RT est discuté pour des signaux ULB. Le RT a été étudié comme une approche de communication possible pour les systèmes ULB. Dans un système de communication RT-ULB, la réponse impulsionnelle du canal (RIC) renversée dans le temps est employée comme un pré-filtre à l'émetteur. La technique RT est composée de deux étapes. Dans la première étape, la RIC est estimée et enregistrée côté émetteur. Dans

la deuxième étape, la RIC conjuguée et inversée dans le temps est transmise dans le même canal. L'onde RT se propage alors dans un canal invariant suivant les mêmes voies dans l'ordre inverse. Ainsi, au niveau du récepteur, toutes les composantes de l'onde, empruntant des chemins différents, se combinent de manière cohérente au point source. Pour des canaux de propagation denses en multi-trajets, la compression temporelle et spatiale peut être réalisée avec un gain de focalisation d'environ 8 dB [1]. Pour les communications, ce gain améliore la portée radioélectrique des transmissions. De même, les effets des interférences entre symboles (IES) et des interférences multi-utilisateurs (IMU) sont atténués respectivement par la focalisation temporelle et spatiale des signaux en réception.

Dans notre étude, différents paramètres caractéristiques du RT ont été définis :

- La puissance crête normalisée (PCN) de réception RT est définie comme la puissance d'un pic reçu pour une puissance d'émission donnée par rapport à un schéma SISO.
- Le gain de focalisation (GF) d'un système RT est défini comme le rapport du plus fort pic reçu en RT sur le plus fort pic reçu par un système impulsif (ULB) classique :

$$GF = 20 \log_{10} \left( \frac{\max |y_j(t)|}{\max |h'_j(t)|} \right) \quad (2)$$

Ce paramètre GF est également important et traduit le gain apporté par le RT en terme de couverture radioélectrique par rapport à un système de communication impulsif ULB classique, pour une puissance de transmission donnée.

- Le rapport signal à lobe secondaire (RSS) est défini comme le rapport de puissance entre les deux premiers pics les plus forts dans un signal reçu RT :

$$RSS = 20 \log_{10} \left( \frac{y_j(t_{pic})}{y_j(t'_{pic})} \right) \quad (3)$$

où  $t_{pic}$  est le temps relatif au pic le plus fort et  $t'_{pic}$  est le temps relatif au second pic. Le RSS est un paramètre important et constitue un indicateur de la qualité du signal reçu.

- L'augmentation de la puissance moyenne (APM) est définie par le rapport des puissances moyennes reçues avec et sans RT :

$$APM(dB) = 10 \log_{10} \left( \frac{E(y_j^2)}{E(h_j^2)} \right) \quad (4)$$

où  $E(\cdot)$  représente l'espérance mathématique

- Une autre caractéristique importante du RT est l'écart type des retards ( $\sigma_\tau$ ). Il peut être calculé par les premier et second moments de la réponse RT mesurée :

$$\sigma_\tau = \sqrt{\frac{\sum_{l=1}^N PDP(l)\tau_l^2}{\sum_{l=1}^N PDP(l)} - \left(\frac{\sum_{l=1}^N PDP(l)\tau_l}{\sum_{l=1}^N PDP(l)}\right)^2} \quad (5)$$

où  $PDP(l) = |y_j(l)|^2$  ou  $|h'_j(l)|^2$ ,  $y_j$  est la réponse RT mesurée,  $h'_j$  est la RI mesurée,  $l$  est le retard et  $N$  est le nombre total de pas dans le profil puissance-retard (PPR). L'écart type des retards constitue une métrique pour la compression temporelle dans les systèmes RT.

Par la suite, une étude comparative de l'ensemble de ces caractéristiques RT est effectuée pour différentes configurations multi-antennes à l'intérieur d'une chambre réverbérante (CR) et en indoor.

## Chapitre 2 : Validation du retournement temporel

Dans ce chapitre, nous étudions le RT de point de vue de la propagation. La validation du RT au laboratoire est effectuée pour étudier les différents paramètres RT en utilisant des simulations, des mesures ou des méthodes mixtes. La validation du RT pour les canaux ULB se compose de deux étapes. Dans la première étape, la réponse du canal est estimée. La deuxième étape consiste à transmettre le signal inversé dans le temps et mesurer la réponse RT. Dans l'approche par simulation, les deux étapes de validation RT sont réalisées à travers des simulations. Le RT est validé en considérant les modèles de canaux existants actuellement dans la littérature et la simulation du RT par programmation. Dans la méthode dite mixte, les réponses impulsionnelles des canaux sont mesurées en laboratoire en utilisant des équipements dans le domaine fréquentiel et le RT est simulé en utilisant des outils de programmation. Dans l'approche basée sur la mesure, des étapes intervenant dans la validation RT sont effectuées à l'aide d'équipements opérant dans le domaine temporel. Dans ce cas, la réponse du canal est mesurée par la transmission d'une impulsion très étroite dans le temps. Par la suite, la réponse du canal mesurée (RCM) est inversée dans le temps et transmise de nouveau dans le canal (qui est supposé être statique pendant cette période) pour mesurer la réponse RT. Différentes propriétés du RT sont étudiées en utilisant les résultats de ces validations.

Les résultats de la validation RT par simulation sont utilisés pour analyser les profils de puissance-retard (PPR) des réponses impulsionnelles du canal (RIC) et les réponses RT dans différents types de canaux indoor. Trois environnements de canaux sont considérés : résidentiels, bureaux et industriels. Le PPR est analysé à la fois en visibilité directe (LOS) et sans visibilité directe (NLOS). Par ailleurs, le RT est démontré par simulation électromagnétique (EM) du canal de propagation. La réponse du canal, entre l'antenne d'émission et des capteurs de champ en réception supposés

idéaux, est calculée par la méthode des lignes de transmission en trois dimensions (3D) dans le domaine temporel (TD-TLM). La version renversée dans le temps de la réponse calculée est utilisée comme signal d'émission. La solution EM est répétée avec la nouvelle forme d'onde d'excitation et la réponse du canal équivalent est obtenue. L'environnement simulé est entouré par des surfaces métalliques, sauf d'un côté qui est choisi comme surface absorbante. La focalisation spatiale du RT est étudiée dans cet environnement.

Les résultats de l'approche mixte pour les validations RT sont utilisés pour étudier la focalisation spatiale du RT dans un environnement intérieur et une chambre réverbérante (CR). Les effets de différentes largeurs de bande et différentes valeurs de fréquence minimale ( $f_L$ ) sont étudiés sur la focalisation spatiale du RT. La largeur de bande des signaux est modifiée de deux façons : dans le premier cas, la fréquence basse ( $f_L$ ) est maintenue constante et la bande passante est accrue en augmentant la fréquence supérieure ( $f_U$ ), alors que dans le second cas, la fréquence centrale ( $f_C$ ) de la bande est maintenue constante et la bande passante du signal est augmentée de façon symétrique autour de  $f_C$ . La figure 4 compare la focalisation spatiale du RT pour des largeurs de bande de 1 GHz et de 3 GHz, mais pour une  $f_L = 0,7$  GHz. La dimension de la tache de focalisation ne diminue pas beaucoup.

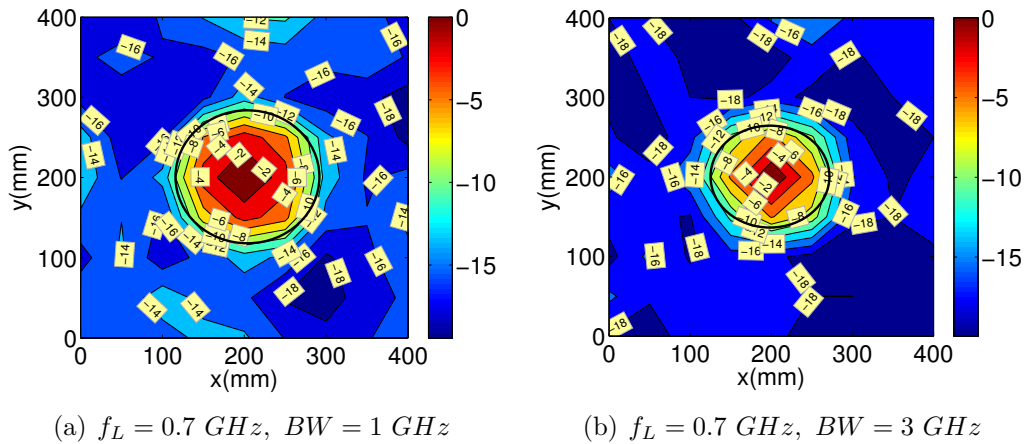


Figure 4: Focalisation spatiale du RT

La figure 5 compare la focalisation spatiale du RT pour une bande passante constante de 3 GHz mais avec des fréquences  $f_L = 0,7$  et 2 GHz. Dans ce cas, la dimension de la tache de focalisation diminue significativement avec l'augmentation de la fréquence inférieure. Ces résultats expérimentaux suggèrent que la dimension de la tache de focalisation est contrôlée par  $f_L$ . Pour des valeurs supérieures de  $f_L$ , une petite zone de focalisation peut être observée, même si la bande passante n'est pas trop large. D'autre part, pour des valeurs inférieures de  $f_L$ , une très faible augmentation du gain de focalisation est observée, même avec une forte augmentation de la largeur de bande du signal.

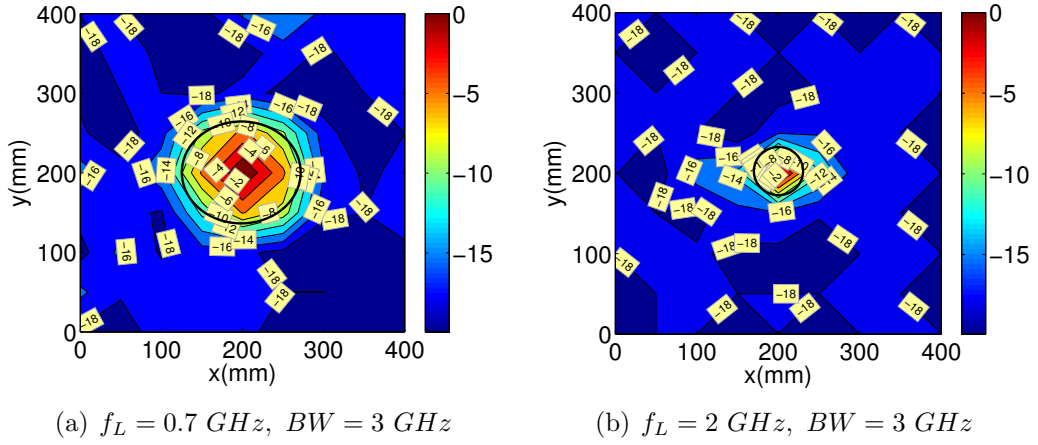


Figure 5: Focalisation spatiale du RT

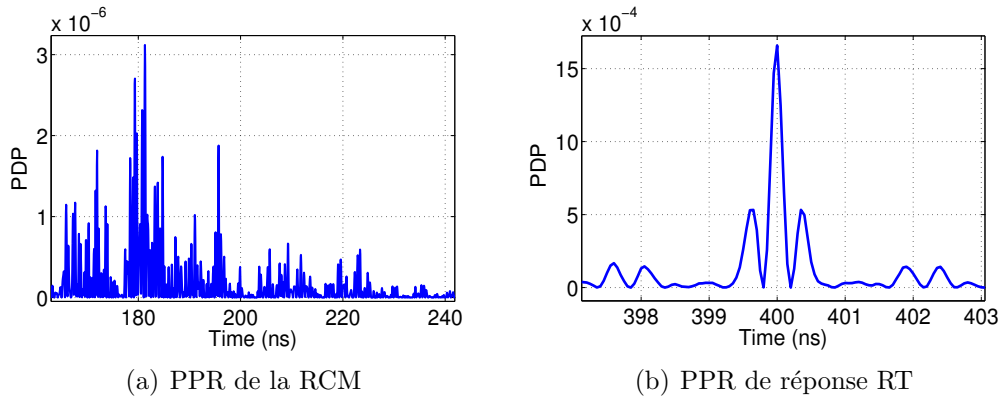


Figure 6: PPR de RCM et de réponse RT pour une configuration NLOS et des polarisations identiques

En utilisant les résultats de l'approche par mesure, la faisabilité de la technique RT est évaluée en communication ULB. Un canal de propagation indoor typique est sélectionné pour l'étude. Différentes caractéristiques du RT, telles que le gain de focalisation (GF), l'augmentation de la puissance moyenne (APM), le rapport signal à lobe secondaire (RSS), la puissance crête normalisée (PCN) et l'écart type des retards ( $\sigma_\tau$ ), sont étudiées en configurations LOS et NLOS, avec des polarisations émission-réception identiques ou croisées.

La figure 6 montre le PPR mesuré de la RCM et de la réponse RT en configuration NLOS avec des polarisations identiques. La RCM a un PPR qui s'étale dans le temps, où plusieurs trajets multiples peuvent être observés, alors qu'avec le RT, le signal reçu est comprimé dans le temps et a une durée effective très courte. La largeur du lobe principal du signal reçu est d'environ  $0,4 \text{ ns}$ . Nous pouvons observer que le signal RT

a un RSS élevé. Toutes les autres mesures de performances sont comparées en détail dans la thèse pour toutes les configurations.

Les mesures dans le domaine temporel sont aussi menées en ULB, dans une CR et toutes les propriétés du RT sont étudiées. La validation RT est effectuée avec différents types d'antennes et pour différentes largeurs de bande du signal transmis RT. Enfin, différentes configurations multi antennes (SISO, SIMO, MISO et MIMO) sont sélectionnées pour la validation RT dans l'environnement indoor et dans la CR. Différentes propriétés du RT sont analysées et comparées à celles d'un système RT en configuration mono-antennaire (SISO).

### Chapitre 3 : Etude de la robustesse du retournement temporel

Comme on l'a vu dans les chapitres précédents, le signal reçu dans un système à retournement temporel (RT) est considérablement concentré dans les domaines spatial et temporel. En conséquence, la puissance reçue est concentrée dans des fentes temporelles étroites et les effets de l'interférence entre symbole (IES) sont fortement réduits. La technique RT déplace la complexité de la conception du récepteur vers l'émetteur. Le système récepteur devient plus simple que sans RT et le signal peut être recueilli à l'aide d'un simple détecteur à seuil d'énergie. La focalisation spatiale permet de réduire les interférences co-canal dans un système cellulaire, ce qui entraîne une utilisation efficace de la bande passante dans le réseau global.

Un des points faibles de la technique RT est que ses performances sont largement tributaires de la disponibilité des informations sur l'état du canal (CSI) à l'émetteur. Dans le cas d'un canal non stationnaire, les performances du RT se détériorent rapidement. Par conséquent, il est impératif d'estimer le canal de manière régulière, ce qui rend le système de transmission très complexe. De même, si l'estimation du canal est imparfaite, les performances du RT seront affectées. Toutefois, si le système RT est robuste et peut résister aux changements de l'environnement, la fréquence des cycles d'estimation sera inférieure entraînant une augmentation du débit utile du système. De même, la robustesse du RT aidera à résister à une estimation imparfaite du canal. Pour étudier la robustesse du système de RT par rapport à un canal variant dans le temps, une campagne de mesure est effectuée dans une chambre réverbérante à brassage de modes (CRBM). La CR est une grande cavité électromagnétique à haut facteur de qualité, qui permet d'obtenir des champs statistiquement uniformes soit par brassage mécanique ou par balayage de fréquence. Ainsi, la CR est un environnement de test hautement contrôlable et peut être considéré comme un environnement de référence. Il nous aide à tirer quelques conclusions importantes qui, autrement, seront difficiles à atteindre. Une présentation plus détaillée de la CR est donnée au Chapitre 2.

Il y a plusieurs facteurs qui peuvent changer le canal d'un système de communication. Si l'émetteur et le récepteur ne changent pas leur position, les variations

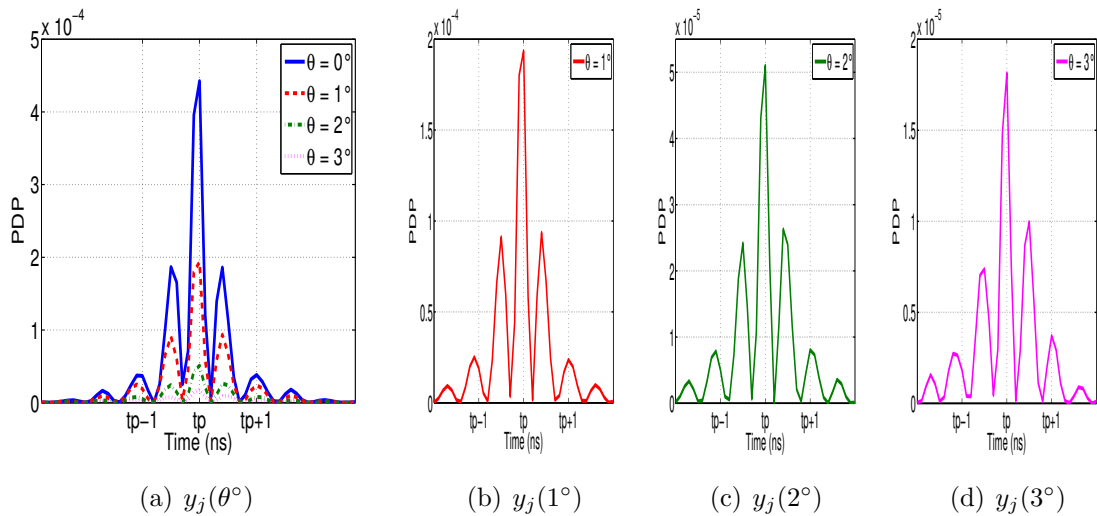


Figure 7: Pour une largeur de bande de  $2.0 \text{ GHz}$ , PPR de la réponse RT pour différentes  $\theta$

temporelles de l'environnement peuvent conduire à des variations du canal. Le canal sera également modifié si l'émetteur ou le récepteur change de position. Pour les mesures, le canal est modifié avec la rotation du brasseur présent à l'intérieur de la CR ou à l'aide d'un positionneur robotique précis pour changer la position du récepteur. Les réponses impulsionnelles du canal (RIC) et les réponses RT sont mesurées pour différentes positions du brasseur ou du récepteur. Les coefficients de corrélation entre les RIC et les réponses RT sont étudiés pour les signaux des différentes largeurs de bande dans un canal variant dans le temps. En outre, les différentes caractéristiques telles que le gain de focalisation (GF), l'augmentation de la puissance moyenne (APM), le rapport signal à lobe secondaire (RSS) et la puissance crête normalisée (PCN), sont étudiées pour différentes bandes passantes.

La figure 7a montre le PPR de la réponse RT dans la CR pour  $\theta \in \{0^\circ, 1^\circ, 2^\circ, 3^\circ\}$ , pour le même signal transmis ( $\theta = 0^\circ$ ) ayant une bande passante de  $2 \text{ GHz}$ . Les PPRs des signaux reçus pour  $\theta \geq 1^\circ$  sont indiqués séparément dans la figure 7 b,c,d. Le résultat montre que même si la puissance pic du signal reçu est réduite, les signaux sont focalisés dans le temps avec un RSS assez élevé.

La figure 8 montre les effets de la rotation du brasseur sur différentes caractéristiques du RT. Même si la RCM change rapidement avec  $\theta$ , la PCN ne diminue pas aussi sévèrement avec  $\theta$  (figure 8a). En plus, le RSS ne se dégrade pas beaucoup avec  $\theta$  (figure 8b). Ainsi, la qualité du signal reste presque constante. Le GF (figure 8c) et l'APM (figure 8d) diminuent aussi avec  $\theta$ , mais cette diminution peut être considérée comme faible par rapport à la dé-corrélation du canal.

Des expériences sont également réalisées en indoor pour les différentes variations introduites dans le canal. La figure 9 montre le PPR et la comparaison de différents paramètres pour les variations suivantes induites dans le canal: présence d'une per-

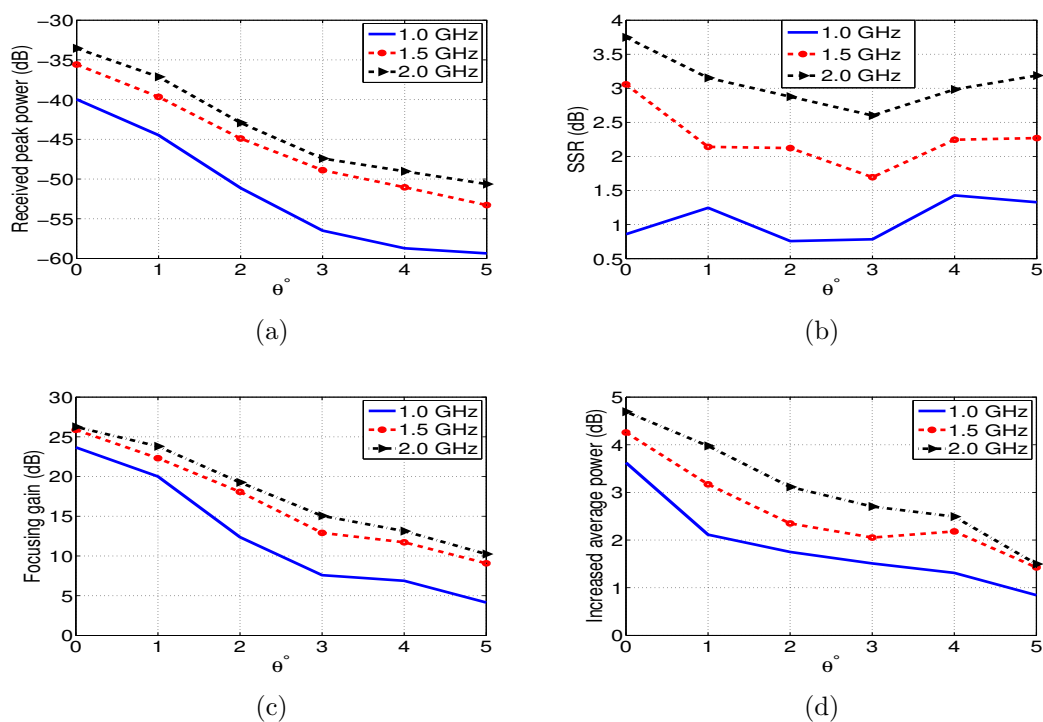


Figure 8: Pour différents  $\theta$  et largeurs de bande a) Puissance crête normalisée b) Rapport signal à lobe secondaire c) Gain de focalisation d) Augmentation de puissance moyenne

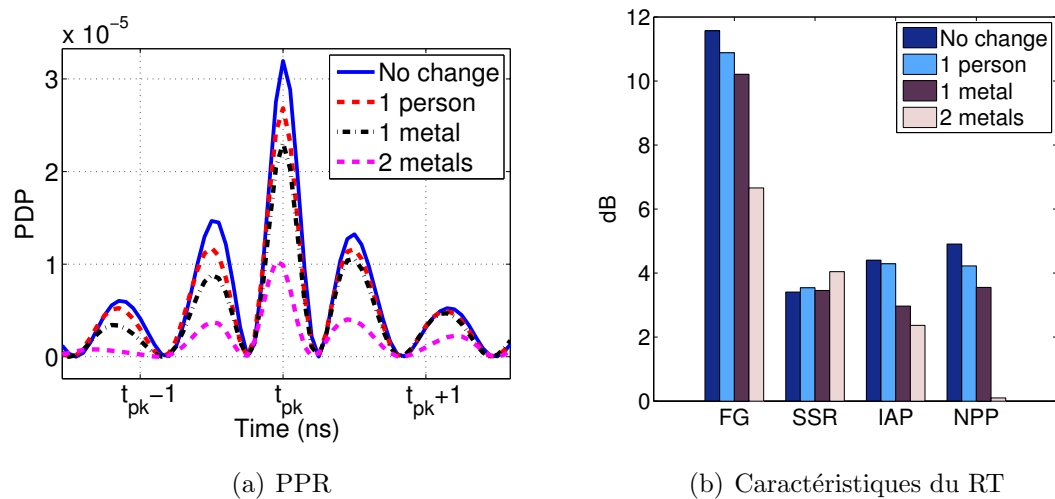


Figure 9: Pour une largeur de bande de 2.0 GHz et différents variation dans le canal a) PPR b) caractéristiques du RT

sonne, une surface métallique et 2 surfaces métalliques près du récepteur. Le GF, l'APM et la PCN ne diminuent pas beaucoup. Le RSS reste presque constant, même avec les variations induites dans le canal. Par exemple, lorsque le canal est modifié par la présence d'une personne dans le canal, toutes les propriétés du RT subissent un changement minimal bien que le canal modifié a une corrélation de 0,7 avec le canal précédent.

Ces résultats montrent que le système RT peut résister à un changement partiel de la RCM. Tant qu'une partie de la RCM maintient sa forme, le système RT donne de bonnes performances. Dans un environnement réel, par exemple un environnement intérieur typique, ce résultat est d'une importance significative. Dans ce cas, si le canal est changé en raison de la variation de l'environnement, par exemple à cause du mouvement des personnes, il est très probable qu'une partie de la RCM restera intacte en fonction de la position et le nombre de personnes. Dans ce cas, la robustesse du RT peut jouer un rôle vital. Il n'est pas nécessaire de réestimer la RCM s'il y a des changements mineurs dans l'environnement, dus par exemple au mouvement des personnes. Cette propriété peut être très intéressante pour les applications sans fil (WLAN et streaming). Toutefois, lorsque le récepteur se déplace, ou s'il y a un changement notable dans la disposition du mobilier, les canaux peuvent subir une décorrélation rapide et une réestimation de la RCM devient nécessaire. Ainsi, le RT reste opérationnel dans un canal non stationnaire où la non stationnarité est causée par des changements dans l'environnement. Les expériences dans la CR ont fourni une bonne base pour l'étude de la robustesse d'un système RT. Des environnements réalistes (tels que l'environnement indoor) créent moins de multi-trajets. Dans ce cas, le RT est moins sensible aux changements que dans la CR. Ainsi, il peut être intuitivement possible de dire que les changements naturels dans le canal ne décorrélaient pas complètement la RCM, qui garde une meilleure corrélation partielle avec l'état antérieur qu'en CR. Par conséquent, le RT sera encore plus robuste dans de tels cas. Toutefois, si la modification de la RCM est survenue en raison du mouvement de l'émetteur ou du récepteur, le canal subit une décorrélation rapide avec son état d'origine (moins rapidement qu'en CR). Dans ce cas, le RT ne sera pas robuste et une réestimation du canal est nécessaire.

## Chapitre 4 : Communication ULB par retournement temporel

Les chapitres précédents de cette thèse ont expliqué la validation et la robustesse du RT. Différentes propriétés du RT ont été étudiées, telles que le gain de focalisation (GF), l'augmentation de la puissance moyenne (APM), le rapport signal à lobe secondaire (RSS), la puissance crête normalisée (PCN) et l'écart type des retards ( $\sigma_\tau$ ). Bien que ces paramètres donnent une indication de la façon dont le RT se produira dans un système de communication, ils ne peuvent pas être considérés comme une métrique directe des performances pour la communication RT. De vraies métriques

de performances pour un système de communication sont le taux d'erreur binaire (TEB), le rapport signal sur interférences (RSI) et le débit. L'ULB radio impulsionnelle est une technique de communication à haut débit qui peut être réalisée en faisant usage de bande passante ultra large. La capacité de l'ULB par impulsions à résoudre les trajets multiples est exploitée dans les recherches récentes pour les applications de communications à courte portée.

Dans ce chapitre, la technique RT est étudiée comme base pour des communications de données à haut débit. Dans la première partie du chapitre, nous proposons un nouveau schéma de modulation qui améliore le débit des données transmises. Ce schéma a été présenté dans l'un des brevets soumis par l'IETR. Plusieurs bits de données sont combinés après décalage dans une même durée symbole pour ajouter un niveau supplémentaire de modulation par rapport à la modulation classique BPAM. Les bits de données compressés sont associés à des formes d'ondes quasi-orthogonales, minimisant l'interférence entre symboles. Ainsi, les bits reçus peuvent être distingués et démodulés assez facilement. Les performances en TEB de la nouvelle modulation et le débit numérique maximal atteignable sont théoriquement analysés. Deux campagnes de mesures distinctes sont effectuées pour analyser les performances de cette nouvelle modulation.

En utilisant les résultats de mesure de la première campagne, la communication RT est simulée. Les résultats de simulation sont comparés aux résultats théoriques. La figure 10 montre les performances théoriques et par simulation pour la nouvelle technique de modulation. Les performances en TEB par simulation de la nouvelle technique de modulation sont en accord avec les performances théoriques. En outre, les performances de cette nouvelle modulation sont comparées aux performances de la modulation d'amplitude en quadrature (QAM) et de la modulation d'impulsions en amplitude (PAM) dans un canal à bruit blanc additif gaussien (AWGN).

Avec la seconde campagne de mesure, la nouvelle modulation a été expérimentalement validée en utilisant des instruments opérant dans le domaine temporel. Les performances de la modulation proposée sont comparées pour les deux campagnes de mesures.

La nouvelle technique de modulation donne de très bonnes performances lorsque le débit n'est pas très élevé. Le débit peut être considérablement augmenté par rapport au RT-simple. Pour une communication à haut débit, un grand nombre de bits doit être ajouté dans la même durée symbole. Comme le nombre de bits transmis simultanément augmente, les performances vont se dégrader. Par conséquent, une communication peut être envisagée sans l'introduction du décalage de sorte que les limitations introduites par ce décalage peuvent être évitées. Ainsi, des résultats à très haut débit avec la modulation d'amplitude d'impulsion binaire (BPAM) sont présentés. La communication RT est étudiée expérimentalement pour des temps symbole ( $T_s$ ) allant de 64 ns à 1 ns, soit pour un débit allant de 15,62 Mbit/s à 1 Gbit/s, dans des canaux de propagation denses en trajets multiples. Des expériences ont été réalisées dans un environnement intérieur typique et dans une chambre réverbérante.

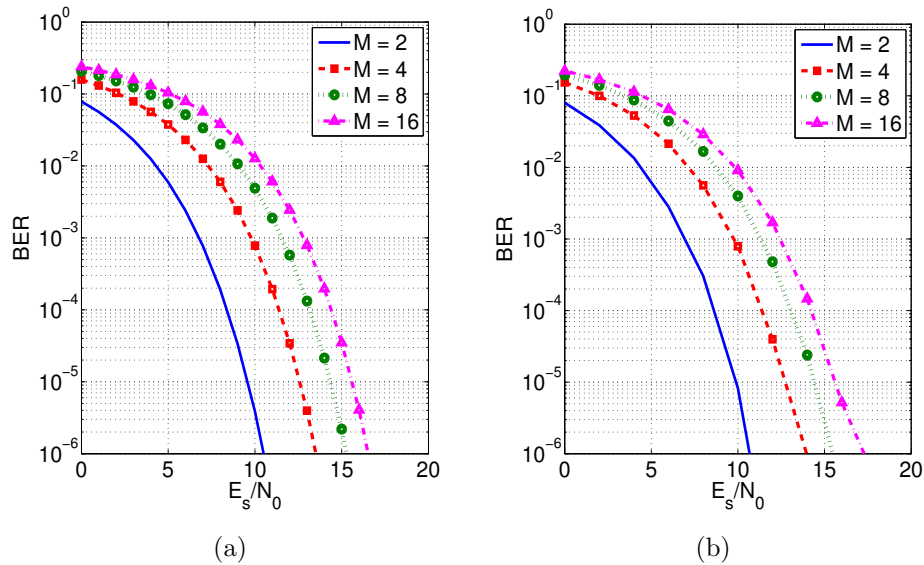


Figure 10: Performances en TEB avec la nouvelle technique de modulation pour différents ordres de modulation a) TEB théorique b) TEB par simulation

Il est démontré que les performances en TEB pour un environnement indoor sont meilleures qu'en CR. En outre, des expériences sont réalisées en utilisant le RT modifié qui divise la bande passante totale du signal transmis en plusieurs sous-bandes, chacune contribuant également à la densité spectrale de puissance (DSP). Ce processus permet d'atteindre une DSP plate. Le RT modifié constitue une sorte d'égalisation, ce qui permet d'améliorer sensiblement le TEB. La figure 11 montre les performances en indoor, avec ou sans filtrage en sous-bandes. On peut constater que les performances du système sont considérablement améliorées avec le filtrage en sous-bandes. Par exemple, l'amélioration obtenue avec le RT modifié est de  $2.4 \text{ dB}$  par rapport au RT classique, pour un débit de  $62,5 \text{ Mbit/s}$  et un TEB fixé à  $10^{-6}$ .

## Chapitre 5 : Communications multi-utilisateurs par retournement temporel

Les communications multi-utilisateurs peuvent être envisagées dans l'un des deux cas suivants :

- Liaison descendante : une station de base communique avec les utilisateurs multiples.
- Liaison montante : différents utilisateurs communiquent avec la station de base.

En cas de communication multi-utilisateurs, la station de base émet normalement un signal différent pour les différents utilisateurs. Par conséquent, cette émission est

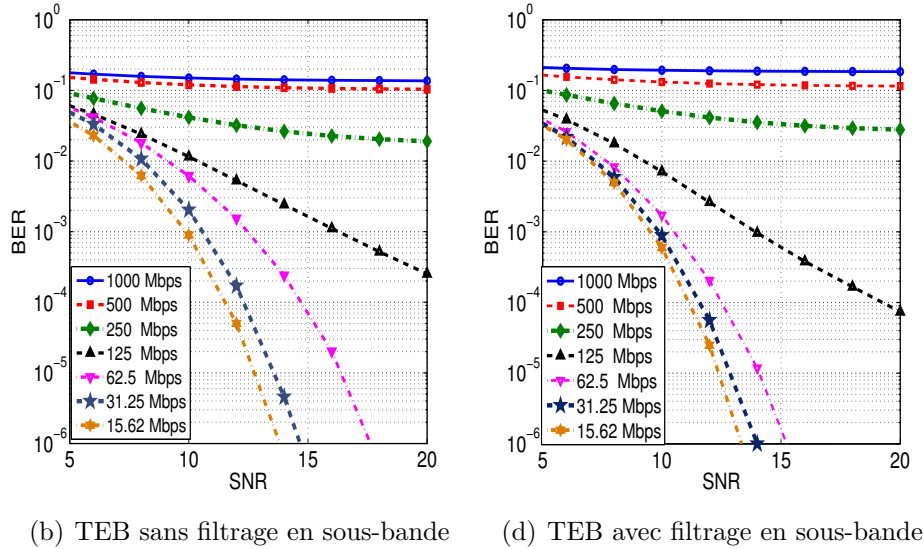


Figure 11: TEB avec RT à haut débit en indoor

fondamentalement différente de la diffusion de la télévision ou de la radio où la station de base émet généralement le même signal pour tous les utilisateurs. Dans ce travail, nous considérons un émetteur RT-ULB communiquant avec plusieurs utilisateurs.

Dans le chapitre 4, un nouveau schéma de modulation est proposé pour un système de communication basé sur le RT-ULB. Plusieurs bits sont combinés après décalage et transmis simultanément dans la même durée symbole. Dans ce chapitre, la communication RT multi-utilisateurs est étudiée en détail en suivant la même approche. Dans un premier temps, nous examinerons la communication RT multi-utilisateurs avec une modification du pré-filtre en utilisant la permutation circulaire. Par la suite, les signaux pour les différents utilisateurs sont emballés dans la même durée symbole et sont transmis simultanément. Par conséquent, un meilleur débit est atteint. Nous avons effectué l'étude analytique du RT avec permutation circulaire (RTPC). Certains inconvénients de cette technique sont mis en évidence. Dans un premier temps, on fait varier le décalage appliqué à la permutation circulaire (PC) pour un utilisateur donné, et on étudie les performances en terme de rapport signal à interférence (RSI).

Par la suite, la communication RT multi-utilisateurs a été étudiée en utilisant l'opération de décalage proposé (décrit dans le chapitre 4). Le schéma proposé traite des limites du RTPC et donne des performances nettement meilleures que celles obtenues avec le RT et le RTPC. L'amélioration des performances augmente avec l'augmentation du nombre d'utilisateurs. Les expressions mathématiques pour le signal reçu et l'interférence du nouveau schéma de transmission proposé sont dérivées. Des expériences sont effectuées dans un environnement indoor. Le nombre maximum d'utilisateurs simultanés est calculé avec le schéma proposé. Notre analyse considère comme constante l'énergie transmise après que les données des utilisateurs soient

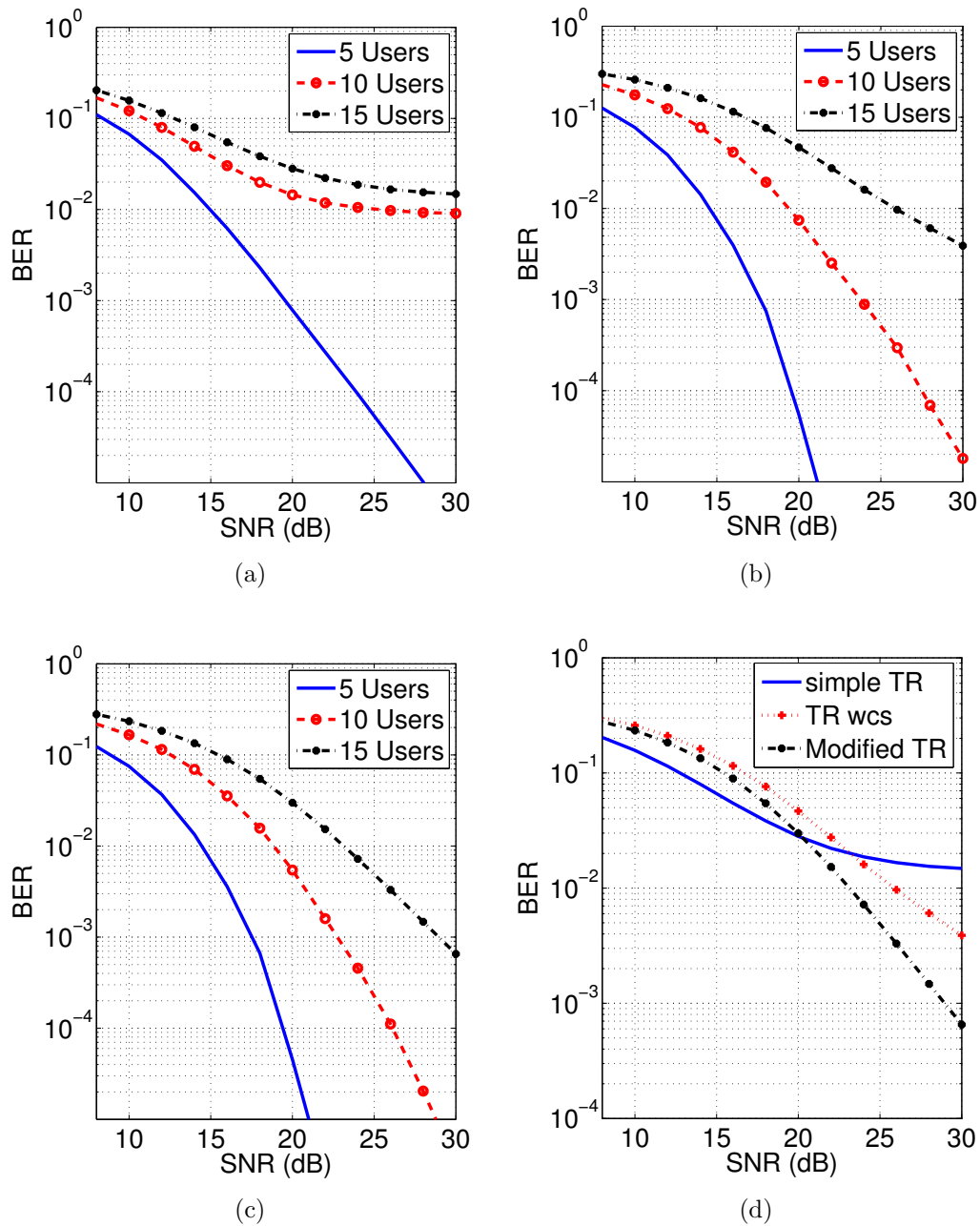


Figure 12: Performances en TEB avec 5, 10, et 20 utilisateurs simultanés avec a) RT-simple b) RTPC c) RT modifié d) toutes les techniques avec 15 utilisateurs simultanés

compactées dans un intervalle de temps symbole, de sorte que la comparaison entre les systèmes avec un nombre différent d'utilisateurs devienne valide.

La figure 12a-c montre les performances en TEB avec le RT-simple, le RTPC, le RT modifié pour 5, 10 et 15 utilisateurs simultanés. Le RT modifié présente de meilleures performances que le RT-simple ou le RTPC, en particulier pour un nombre

d'utilisateurs simultanés plus élevé (10, 15). Par exemple, pour 10 utilisateurs simultanés, le RT modifié améliore les performances de 1,4  $dB$  par rapport au RTPC pour un TEB de  $10^{-4}$ , alors que les performances du RT-simple présentent une saturation. Pour effectuer une analyse en présence de fortes interférences multi-utilisateurs, les performances en TEB sont étudiées pour 15 utilisateurs simultanés. La figure 12d compare ces performances. Le RT modifié donne des résultats nettement meilleurs que les deux autres techniques. L'amélioration est de l'ordre de 4,5  $dB$  ou plus.

## Conclusion

Le retournement temporel (RT) est une approche qui permet d'utiliser des récepteurs simples en déplaçant la complexité vers l'émetteur. Dans cette thèse, nous étudions la technique du RT-ULB et son application aux communications haut débit. Les principales contributions de ce travail de recherche sont:

- La validation de la technique du RT en laboratoire
- Etude paramétrique du RT avec différentes configurations multi-antennes (SISO, SIMO, MISO et MIMO)
- Démonstration de la robustesse du RT dans des environnements non stationnaires
- Validation expérimentale d'une nouvelle technique de modulation pour un système de communication RT-ULB
- Validation expérimentale d'une communication RT à haut débit
- Proposition d'une technique de transmission RT modifiée pour améliorer les performances dans un contexte multi-utilisateurs

L'ensemble des résultats présentés dans cette thèse suggère que le RT-ULB, qui peut être facilement combiné avec les systèmes MIMO, est une approche prometteuse pour les futurs réseaux locaux et personnels (WLAN et WPAN) sans fils.

Enfin, plusieurs perspectives de ce travail sont proposées dans la thèse.

# General Introduction

Ultra wide band (UWB) technology gained a renewed interest after February 2002, when the FCC approved the First Report and Order (R&O) for commercial use of UWB technology under strict power emission limits for various devices. The permission to transmit signals in a wide unlicensed band, opened the doors for the coexistence of UWB technology along with other narrow band and spread spectrum technologies. In UWB communication, extremely narrow RF pulses are employed to communicate between transmitters and receivers. Because of its extremely wide bandwidth, UWB signals result in large number of resolvable multi-paths and thus reduce the interference caused by the super position of unresolved multi-paths. However, it also results in a complex receiver system.

Time reversal (TR) is a transmission approach which shifts the complexity from the receiver to the transmitter. The received signal in the TR scheme is very focused in time and spatial domains and thus can be detected by using very simple receivers. Temporal and spatial focusing also help to reduce inter symbol interference and multiuser interference respectively.

In this Ph.D. thesis, we investigate the TR UWB scheme and its application to high data rate communication. The thesis comprises of two main parts. In the first part, we explain the validation of the TR scheme in the laboratory with different mono and multi-antenna configurations and study different TR parameters. In the second part, TR scheme is investigated from the communication point of view.

In **Chapter 1**, the state of the art of the pulsed UWB and TR UWB has been presented. The spectrum regulations throughout the world are discussed. Thereafter, an overview of pulsed UWB technology, popular transmission and modulation schemes, its key benefits and applications for wireless transmission are described. UWB channel models are discussed and some of the receiver systems for UWB signals are illustrated. Furthermore, the state of the art for TR technique is presented. Historic background of TR scheme is provided. The use of TR for the acoustic and Stoke's TR experiment are presented. Thereafter, an overview of TR technique for communication with electromagnetic waves and UWB signals is elaborated. Finally, some definitions of different TR parameters are provided.

In **Chapter 2**, we investigate the TR scheme from propagation point of view. Validation of TR technique is presented. In the laboratory, validation of the TR scheme is performed using simulation, semi-measurement and measurement approaches. Thereafter, a parametric analysis of the TR technique is carried out using the results of these

validation approaches. The results of the simulation based TR validation are used to analyze the power delay profiles (PDP) and average power decay profiles (APDcP) of the channel impulse responses (CIR) and the TR responses in residential, office and industrial indoor environments. The results of the semi-measurement approach for the TR validations are used to study the spatial focusing property of the TR scheme in an indoor environment and in a reverberation chamber (RC). Using the results of measurement approach, the feasibility of time-reversal technique for ultra wide-band (UWB) communication system is assessed. Different TR properties such as normalized peak power (NPP), focusing gain (FG), increased average power (IAP), signal to side lobe ratio (SSR) and root mean square (RMS) delay spread are studied in LOS and NLOS configurations with both co-polar and cross-polar antenna orientations. TR validation is performed with different types of antennas and for different bandwidths of the TR transmitted signal. Finally, different multi-antenna configurations (SISO, SIMO, MISO and MIMO) are selected for TR validation in the indoor and RC environments.

In **Chapter 3**, robustness of the TR technique is investigated in non stationary channel environments for bandwidths of  $2.0\text{ GHz}$ ,  $1.5\text{ GHz}$  and  $1.0\text{ GHz}$ . Measurement campaigns are conducted in a mode stirred reverberation chamber (RC) and in the indoor environments. In the RC, the channel is changed with the rotation of the stirrer present inside the RC or with the help of a precise robotic positionner to change the position of the receiver. In the indoor environment, changes in the channel are induced with the presence of a person or metallic strips near a receiver terminal. The channel responses and the TR responses are measured with the time varying channel environments. Cross-correlation coefficients between the measured channel responses (MCR) and TR responses and different TR properties such as NPP, FG, SSR, IAP and RMS delay spread are studied for the signals of different bandwidths in time varying channel environments.

In **Chapter 4**, high data rate TR communication is studied. In the first part of the chapter, we present a novel modulation scheme for a TR system. The bit error rate (BER) performance of the new modulation scheme and the maximum achievable data rate are theoretically analyzed. Two separate measurement campaigns are carried out to analyze the performance of the modulation scheme. TR communication is simulated using the measurement results of the first measurement campaign. The simulated and the theoretical results are compared to each other. Furthermore, the performance of the new modulation scheme is compared with the performance of the quadrature amplitude modulation (QAM) and the pulse amplitude modulation (PAM) in an AWGN channel. With the second measurement campaign, the new modulation scheme is experimentally validated using time domain instruments. The performance of the proposed modulation scheme is compared for the two measurement campaigns. In the latter part of the chapter, high data rate communication for a Time Reversal UWB communication system is experimentally studied for data rates ( $R_b$ ) ranging from  $15.62\text{ Mbps}$  to  $1\text{ Gbps}$  using binary pulse amplitude modulation (BPAM) in dense multi-path propagation channels. Furthermore, a modified

transmission approach is introduced which divides the total bandwidth of the signal into multiple sub-bands. High data rate communication is also validated with the modified transmission approach.

In **Chapter 5**, Multiuser TR communication has been studied by using a TR filter which uses a circular shift operation (CSTR). We have carried out the analytical study of CSTR scheme. Some inherent drawbacks in the scheme are highlighted. At first, amount of CS is varied for a given user and SIR performance of the CSTR scheme is independently analyzed for each user. Thereafter, time reversal (TR) communication is investigated by further modifying the transmission pre-filter. Mathematical expressions for received signal and the interference of the proposed transmission scheme are derived. Experiments are performed in a typical indoor environment and the BER performance of the proposed transmission approach is analyzed for different number of simultaneous users. Maximum number of simultaneous users is calculated with the proposed scheme.

In the end, the significance of the results and future perspectives are discussed in the thesis conclusion.

This work was carried out in the framework of ANR project MIRTEC and financially supported by the French research ministry.



# Chapter 1

## State-of-the-Art of Pulsed UWB and Time Reversal UWB

### Contents

---

<b>1.1</b>	<b>Introduction</b> . . . . .	<b>3</b>
<b>1.2</b>	<b>Pulsed UWB Technology</b> . . . . .	<b>4</b>
1.2.1	Introduction: What is UWB ? . . . . .	4
1.2.2	Historical Developments . . . . .	4
<b>1.3</b>	<b>PSD Constraints for UWB Systems</b> . . . . .	<b>7</b>
<b>1.4</b>	<b>Principle of Pulsed UWB</b> . . . . .	<b>10</b>
1.4.1	Pulse Position Modulation . . . . .	10
1.4.2	Pulse Amplitude Modulation . . . . .	12
1.4.3	Orthogonal Pulse Modulation . . . . .	12
1.4.4	Transmit Reference Scheme . . . . .	13
1.4.5	Direct Sequence UWB . . . . .	13
1.4.6	Multi-band Orthogonal Frequency Division Multiplexing . . . . .	15
<b>1.5</b>	<b>UWB Propagation Channels</b> . . . . .	<b>16</b>
1.5.1	UWB Channel Characterization Parameters . . . . .	17
1.5.2	Channel Modeling and Practical Constraints . . . . .	18
<b>1.6</b>	<b>UWB Channel Models</b> . . . . .	<b>19</b>
1.6.1	Empirical Models . . . . .	19
1.6.2	Statistical Models . . . . .	20
<b>1.7</b>	<b>Receiver Used for UWB Systems</b> . . . . .	<b>22</b>
1.7.1	Coherent Receivers . . . . .	22
1.7.2	Non Coherent Receivers . . . . .	23
<b>1.8</b>	<b>Introduction of Time Reversal</b> . . . . .	<b>24</b>

1.8.1	Time Reversal Acoustics . . . . .	25
1.8.2	Stoke's Time Reversal Experiment . . . . .	25
1.8.3	Principle of Reciprocity . . . . .	26
1.8.4	Time Reversal Cavity . . . . .	27
1.8.5	Time Reversal for Electromagnetic Waves . . . . .	27
1.8.6	TR in UWB . . . . .	29
<b>1.9</b>	<b>Conclusion . . . . .</b>	<b>35</b>

---

## 1.1 Introduction

With the rapid and continuous increase in the commercial demands and the growth in technology, wireless communication is becoming more and more challenging every day. The advancements in the wireless technology are certainly affecting our daily lives. WiFi, Bluetooth and the new generation radio systems have already started replacing the old wired connections. These technologies not only get rid of the troublesome wires but also permit mobility to the end user enabling consumers to access wide range information from anywhere and anytime. As our insatiable desire for higher data rates and power efficient systems continues, new wireless communication systems offering higher capacity, faster service and more secure wireless connections with higher quality will continue to evolve. Thus, new enhanced technologies have to find their place in the already overcrowded radio frequency (RF) spectrum.

The RF spectrum is so crowded that emergence of any technology is quite difficult if not impossible. However, UWB technology is evolving fast as with this technology, there is a possibility to coexist with other technologies by using the spectrum allocated to other technologies with strict power spectral density (PSD) limitations. The stringent requirements help to keep the interference to minimum and thus the spectrum is used with an increased efficiency. UWB is therefore a potential technology for large number of new applications including wireless LAN and wireless PAN applications. Given the ultra large bandwidth, UWB signals are immune to multi-path fading and have the ability to communicate with high data rates. The limitation is the distance over which communication can be held with sustainable low bit error rates. Furthermore, UWB signaling can potentially be implemented with very low cost and low power consumption components, representing an interesting solution for remote control and sensor network applications. In a pulsed UWB communication system, the information is encoded in very narrow pulses. The ability of pulsed UWB to resolve individual multi-path components is exploited in the recent research for short range communication applications. However, large number of resolvable paths and low PSD limitations necessitate a complex receiver system. To collect the received signal energy, transmit-reference, Rake receiver, or decision feedback auto-correlation receiver can be implied. The latter two techniques are quite complex while the former decreases the data rate of the system significantly. One way to overcome these drawbacks is to make use of the technique that shifts the design complexity from the receiver to the transmitter.

Time reversal (TR) has been proposed as a technique to shift the design complexity from the receiver to the transmitter. Classically, TR has been applied in acoustics and under water communication applications, but recently, it has been widely studied for UWB communication. The received signal in a TR system is considerably focused in spatial and temporal domains. As a result, the received signal energy is concentrated within few taps and the effects of inter symbol interference (ISI) are greatly reduced. The receiver system becomes simpler than without TR and signal can be collected using a simple energy threshold detectors. Spatial focusing enables low multi-user and co-channel interference in a multi-user and multi cell systems respectively.

In this chapter, an overview of state of the art UWB technology, its key benefits and applications for wireless transmission are described. The spectrum regulations throughout the world are also discussed. Thereafter, an overview of pulsed UWB technology, popular transmission and modulation schemes, its key benefits and applications for wireless transmission are described. UWB channel models are discussed and some of the receiver systems for UWB signals are illustrated. Furthermore, the state of the art for TR technique is presented. Historic background of TR scheme is provided. The use of TR for the acoustic and Stoke's TR experiment are presented. Thereafter, an overview of TR technique for communication with electromagnetic waves and UWB signals is elaborated. Finally some definitions of different TR parameters are provided.

## 1.2 Pulsed UWB Technology

### 1.2.1 Introduction: What is UWB ?

#### 1.2.1.1 Definition

Ultra wide-band (UWB) is a generic term used to represent a radio access technique which has been studied under different names. These include the terms impulse radio (IR), carrier-free radio, baseband radio, time domain radio, non-sinusoid radio, orthogonal function radio and relative bandwidth radio etc. [2]. The fractional bandwidth of a communication system is defined as:

$$B_f = 2 \frac{f_H - f_L}{f_H + f_L} \quad (1.1)$$

where  $f_H$  and  $f_L$  are respectively the higher and the lower frequency boundaries at a threshold (e.g. 3 dB) below the strongest radiated emission. A UWB signal was first defined as a signal having a 3 dB fractional bandwidth ( $B_{f_{3dB}}$ ) greater than 25 %. In 2002, the FCC defined a UWB signal as any signal having a -10 dB fractional bandwidth larger than 20 % and/or an absolute bandwidth of more than 500 MHz [3]. Typically, the bandwidth of UWB signals ranges from 500 MHz to several GHz. FIG. 1.1 compares the power spectral density (PSD) of conventional narrow band systems which generally modulate the narrow band signals on a frequency carrier, spread spectrum (UMTS) system which has lower PSD and a bandwidth of 5 MHz, and UWB system having very low PSD.

### 1.2.2 Historical Developments

In 1901, Guglielmo Marconi employed the very first transmission system based on the UWB technology to transmit Morse code across the Atlantic Ocean. Approximately half a century after, modern pulsed base systems started intrusion in the military applications. The study of electromagnetism in the time domain started in early sixties. Early research was focused on radar applications due to the nature of broadband

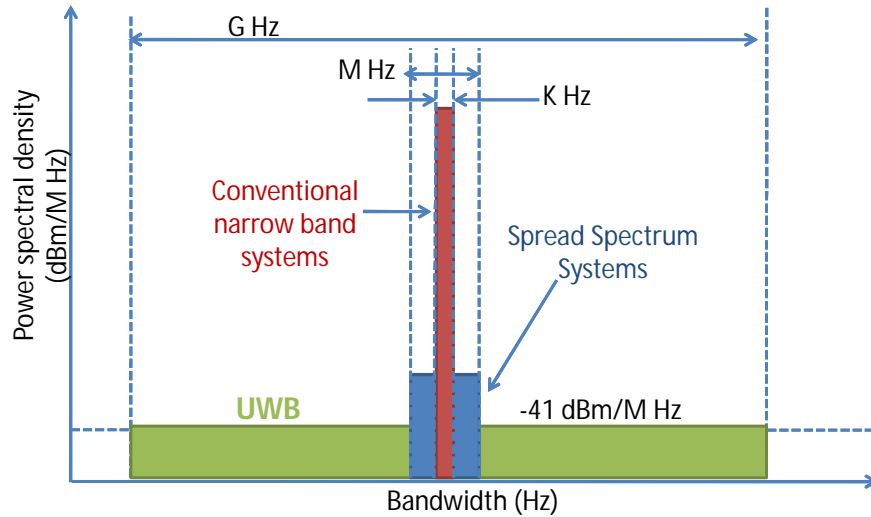


Figure 1.1: Comparison of the spectrum allocation for different wireless radio systems

signals, which provide a strong temporal resolution. A comprehensive survey of early research in this field was presented by Bennett and Ross [4], while Taylor [5] presents the foundations of the technology applied to UWB radar. Regular research advances have been made since the mid-60s, as revealed by the historical study of Barrett [2]. However, the use of UWB signals in the field of radio communication was not envisaged before the end of the 20<sup>th</sup> century. In 1990, the department of defense of United States of America (USA) government published the results of its evaluation of the UWB technology, which focused exclusively on the radar, since no other application of UWB communication systems were then proposed [6]. More recently, research has been focused on UWB signals for radio communication, [7, 8], developing the main characteristics of this technique: A temporal resolution in the order of nanoseconds due to the frequency bandwidth, low duty cycle allowing multiple access without a transmission carrier, which simplifies the architecture of radio systems [9]. Since 1998, the FCC launched a first study on UWB. In February 2002, a first regulatory report is published, allowing wireless communications in particular in the band of 3.1 GHz - 10.6 GHz with strong constraints on the power spectral density [3].

UWB technology is opening the doors for a range of new applications as well as complementing existing wireless systems. One of the important applications, which is not always a low power application is the radar. UWB radars are used for maritime and air navigation and as remote speedometers. There are many commercial applications of UWB radar and imaging, such as intrusion-detection radars, ground-penetrating radar (GPR) and precision geo-location systems. Some new applications include automotive security and rescue operations. In these applications one active device transmits narrow pulses and analyzes the echoes from the target, which is usu-

ally passive and unaware of the signal. Among the low power applications for the UWB are the ranging and short range communication applications. The communication system can either utilize entire bandwidth and achieve very high data rate over one link or can have multiple low data rate links (e.g. sensor networks) with very high aggregate data rate.

### 1.2.2.1 Strengths and Weaknesses of UWB

One of the biggest strengths of the UWB technology is derived by its ultra large bandwidth. Owing to such a large bandwidth, UWB systems can attain very high data rates. The information theory tells us that it is possible to transmit data at a bit error rate (BER) below an arbitrarily low threshold, if the data rate is below the capacity of the transmission channel. The channel capacity  $C$  is thus an indication of maximum data rate which is theoretically possible for a given channel. In the presence of additive white Gaussian noise (AWGN), it can be calculated by the famous theorem of Shannon [10]:

$$C = B \log_2 \left( 1 + \frac{S}{N} \right) \quad (1.2)$$

where  $C$  is the capacity in bits per second (bps),  $B$  is the bandwidth in  $Hz$  and  $\frac{S}{N}$  is the signal to noise ratio (SNR). Note that the channel capacity increases quasi linearly with the bandwidth and logarithmically with SNR. FIG. 1.2 shows the channel capacity as a function of SNR with different bandwidths. In a context of growing demand for high data rate wireless communication, systems working with large frequency bands are more likely to achieve adequate data rate. Thus, UWB with frequency bandwidth of up to several  $GHz$ , is more adapted to the increasing consumer's demands [9].

Because of their wide bandwidth, UWB signals have very high temporal resolution, typically in the order of nanosecond. A first implication of this involves localization: with an ability to detect the delay of a signal with precision in the order of 0.1 to 1  $ns$ , it is possible to obtain information about the location of the transmitter with an accuracy of 3 to 30  $cm$ . Temporal resolution of UWB radio signal also provides robustness against fast fading of the propagation channels caused by the multi-paths. As narrow UWB waveforms detect multiple reflections of the radio channel separately, therefore destructive recombination of the multi-paths is no longer experienced at the receiver.

From the implementation point of view, the conventional radio systems are generally heterodyne in design: the baseband data signals are modulated by using a carrier of higher frequency. UWB communication system allows the transmission of baseband pulse directly over the radio channel without any carrier modulation. The carrier free transmission simplifies the architecture of the radio systems. One of the weaknesses of UWB signals is their low PSD. This property is not intrinsic to the UWB signal as we defined above (1.1), but is imposed by the regulatory authorities of the radio spectrum radio. In fact, the vast spectral range of UWB signals occupies frequencies already allocated to other radio systems. To allow the peaceful co-existence of UWB with other radio narrow band technologies, the federal communication commission

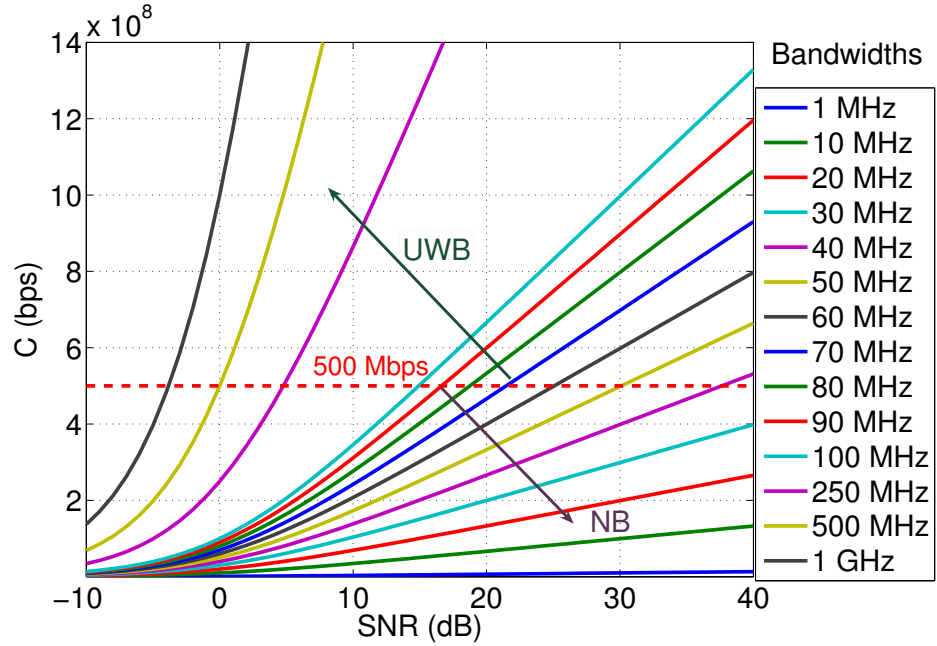


Figure 1.2: Channel capacity as a function of SNR for different bandwidths

(FCC) has limited the PSD of signals UWB to  $-41 \text{ dBm/MHz}$ , which corresponds to the limit of PSD allowed for unintentional radio emission. This low PSD results in a secure communication as transmitted signals becomes harder to detect. Another consequence of this peculiarity concerns the distance of propagation, which is limited to few meters. Therefore, UWB applications are limited to short-range and high data rate telecommunication systems, and are therefore particularly suited to the development of ad-hoc networks.

### 1.3 PSD Constraints for UWB Systems

UWB signals require strict regulation on their transmission spectrum as their spectrum spans over a whole range of frequencies already occupied by other technologies. To enable the transmission of signals over several  $\text{GHz}$ , regulators must impose a severe limitation on the transmission PSD. FIG. 1.3 shows some radio systems in the UHF and SHF bands. We note that several systems occupy the reserved bands such as standard cell phone GSM ( $900 \text{ MHz}$ ), DCS ( $1.8 \text{ GHz}$ ) and UMTS ( $2 \text{ GHz}$ ). The satellite positioning system GPS has also a reserved band ( $1.5 \text{ GHz}$ ). Other frequency bands can be occupied by the non licensed communication systems. For example, the ISM band is used by Bluetooth, WiFi and DECT and authorizes the emission due to industrial equipment such as microwave ovens. The UNII band is the band where WiFi 802.11a and HIPERLAN 1.1 operate.

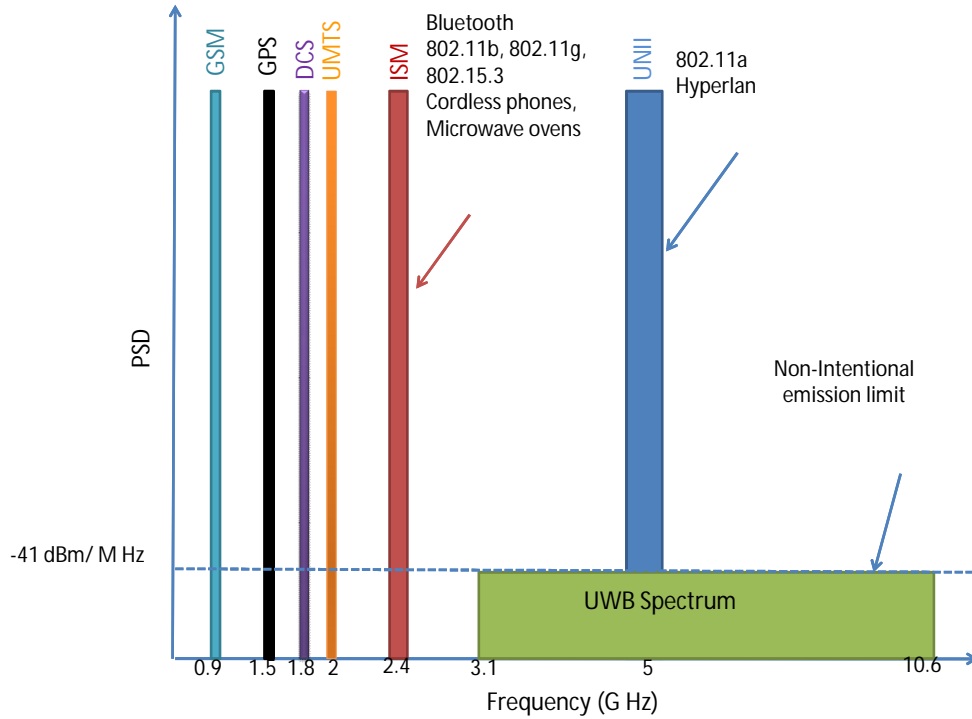


Figure 1.3: Different radio systems present in UHF and SHF bands

To limit the interference from UWB signals to other radio systems, different regulatory authorities agreed on the use of the band  $3.1\text{ GHz} - 10.6\text{ GHz}$  for UWB signals [11]. Thus, a bandwidth of  $7.5\text{ GHz}$  can be used for UWB signals without any interference to sensitive telephony systems and GPS. A very strict PSD limit, under the level of non-intentional emission, is imposed by the FCC ( $-41\text{ dBm/MHz}$ ). The low PSD is compensated by the large bandwidth to transmit a total power of  $0.6\text{ mW}$ .

The regulations imposed on the emission of UWB signals are different in USA, Europe and Asia. The regulations in Europe are stricter than the regulations in USA, while barring Japan, regulations in some Asian countries are less strict than the regulations in USA and Europe.

The emission regulations in USA are imposed by Federal Communications Commission (FCC). FCC launched its work on UWB in 1998 and published its first proposal for regulation (Notice of Proposed Rule Making) in May 2000. In 2002, FCC permitted the deployment of UWB on unlicensed basis in the frequency band of  $3.1\text{ GHz}$  to  $10.6\text{ GHz}$ . The limit on average effective isotropic radiated power (EIRP) at the transmitter is  $-41.25\text{ dBm}$  or  $75\text{ nW}$  per  $\text{MHz}$ . The whole spectrum mask for communication and measurements in an indoor environment is shown in the FIG. 1.4. The spectral mask is established to ensure protection of sensitive systems, particularly the GPS ( $1.2\text{ GHz}$  to  $1.5\text{ GHz}$ ), and bands dedicated to civil aviation. A restriction on the peak EIRP is also imposed and can be expressed as:

$$\text{EIRP}_{peak} = 20 \log_{10}\left(\frac{\text{RBW}}{50}\right) \quad (1.3)$$

where  $\text{RBW}$  is the resolution bandwidth in  $\text{MHz}$ . For  $\text{RBW} = 50 \text{ MHz}$ , the peak EIRP is limited to  $0 \text{ dBm}$  or  $1 \text{ mW}$ .

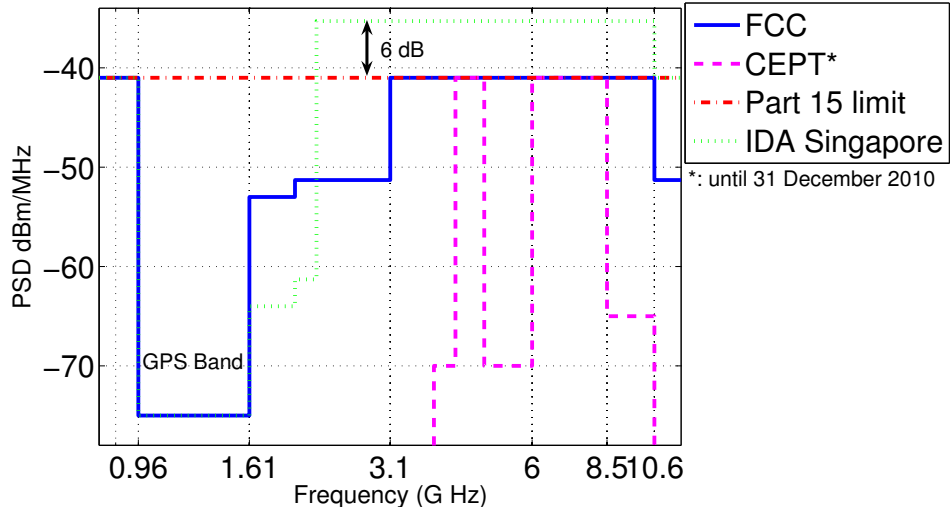


Figure 1.4: UWB Spectral Mask in USA and Europe

In Europe, the standards body European Telecommunications Standards Institute (ETSI) started working in 2001 to develop a European standard for UWB systems. The studies are carried out in close cooperation with the SE24 group of the European Conference Posts and Telecommunications (CEPT), which analyzed more particularly the impact of UWB on existing systems. In February 2007, the European Communication Commission (ECC) permitted the emission in the UWB. The commission decision contains two separate masks for before and after 31<sup>st</sup> December 2010 [12]. The mask shown in FIG. 1.4 is valid till 31<sup>st</sup> December 2010. The regulations beyond 2010 are stricter. These regulations are applicable to only indoor communication. The band in which  $-41 \text{ dBm/MHz}$  PSD is acceptable is reduced from  $7.5 \text{ GHz}$  by FCC to  $3.1 \text{ GHz}$  by ECC and that also in two separate bands.

In Asia, different countries have different spectral masks. In 2003, Infocomm Development Authority (IDA) of Singapore created an area of UWB Research known as UWB friendly zone. In this UWB friendly zone, an emission PSD up to 6 dB above the limit of the FCC is permitted in the band  $2.2 \text{ GHz} - 10.6 \text{ GHz}$  [13], [14]. The spectral mask for Singapore is also shown in FIG. 1.4. In this way, the IDA is trying to lead the advancements of the new communication technologies, in order to remain scientifically and economically competitive. In August 2006, the official gazette of the Japanese government announced regulations for the radio transmission using UWB. The allocated frequency bands are from  $3.4 \text{ GHz} - 4.8 \text{ GHz}$  and from  $7.5 \text{ GHz} - 10.25 \text{ GHz}$ . For the lower band, the interference caused by the transmitted

signal is required to be reduced by an interference reducing mechanism. Furthermore, the average transmission PSD is limited to  $-41.3 \text{ dBm/MHz}$  or lower (the peak value is limited to  $0 \text{ dBm}/50\text{MHz}$  or lower) on both bands. In  $3.4 \text{ GHz} - 4.8 \text{ GHz}$  band without any interference technology, the average transmission PSD is limited to  $-70 \text{ dBm/MHz}$  or lower (the peak value is limited to  $-30 \text{ dBm}/50\text{MHz}$  or lower).

## 1.4 Principle of Pulsed UWB

Developed from studies on the radar, the concept of impulse radio is based on very short duration transmission pulse (about 100 ps to 1 ns). Typically, this type of pulse has a very broad spectrum (in the order of 1 to a few GHz). Therefore, it follows a mono-band approach. Different pulse shapes have been adopted for UWB applications which include Gaussian pulse, its first derivative (Gaussian monocycle) and its second derivative. Gaussian pulse is not usually preferred to the other two pulse shapes because of its non-zero average value, which corresponds to an important DC component in the frequency domain. Different types of modulation schemes are used for the communication with the pulsed UWB principle. Pulse position modulation (PPM), pulse amplitude modulation (PAM), bi-phase modulation, on off keying (OOK) and pulse shape modulation (PSM) are few of the modulation schemes used for the communication in UWB.

### 1.4.1 Pulse Position Modulation

By far the most common modulation scheme used for UWB communication in the literature is PPM. The transmitted signal is delayed or sent in advance to the establish communication of different bits. By specifying time delays for multiple pulses, an M-ary communication system can also be created. The transmitted signal for a PPM modulated signal can be written as:

$$s(t) = \sum_{k=1}^{\infty} w(t - kT_f - a_k\delta) \quad (1.4)$$

where  $w(t)$  is pulse waveform,  $T_f$  is the frame time and  $a_k \in \{0, \dots, M-1\}$  is encoded by the transmitted signal,  $M$  is the modulation order or the number of states of modulation and  $\delta$  is the shift distance between two modulation states.  $T_f$  must be greater than  $M\delta$  to avoid inter symbol interference (ISI) and some guard interval might be added as well. Optimum value for  $\delta$  can be found depending upon the correlation properties of the pulse waveform. An optimum value of  $\delta$  is the one which satisfies the following equation:

$$\int_{-\infty}^{+\infty} w(t) w(t + \delta_{opt}) dt = 0 \quad (1.5)$$

As PPM does not involve an antipodal approach, the demodulator for the modulation scheme can work on the energy detection principle. The received signal can

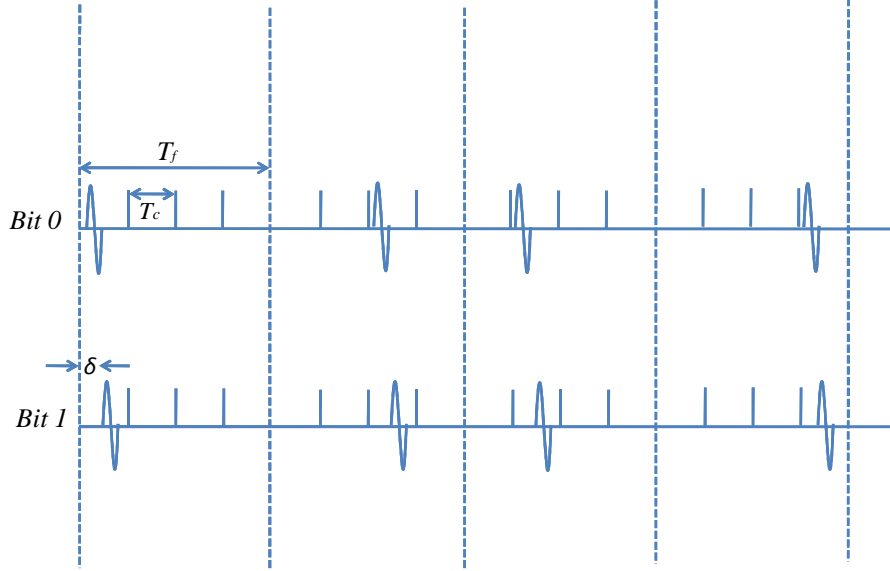


Figure 1.5: Illustration of bit '0' and bit '1' using TH-PPM

be squared before taking the decision. The term  $kT_f$  permits the uniformly placed impulses. The signal,  $\sum_k w(t - kT_f)$ , corresponds to an equally spaced impulse train with a period of  $T_f$  seconds.  $T_f$  is generally called symbol time or frame time and is about 100 to 1000 times greater than the width of pulse. These low duty cycle impulses help to have a very low PSD. The periodicity of the impulse train of this signal generates parasite lines in the radio spectrum of the transmitted signal. This problem is solved by a code of pseudo random time hopping. The frame duration  $T_f$  is divided into a number of time intervals (chips) of duration  $T_c$ . Each user has a pseudo-random code ( $c_j$ ) of length  $N_s$  which indicates the chip of the frame in which the pulse must be transmitted. The use of a pseudo-random code reduces the appearance of lines due to the periodicity of the frame, and the spectrum becomes much more smoothed. Furthermore, time hopping can be used as a multiple access technique and can avoid the collision of the signals of different users. FIG. 1.5 shows an illustration of TH-PPM. From [15], the transmitted signal for the time hopping pulse position modulation (TH-PPM) signal is written as:

$$s^{(j)}(t) = \sum_{k=-\infty}^{\infty} w(t - kT_f - c_k^{(j)}T_c - \delta d_{\lfloor \frac{k}{N_s} \rfloor}^{(j)}), \quad (1.6)$$

where  $c_k^{(j)}$  is the time hopping sequence specific to the  $j_{th}$  user,  $d_k$  is the transmitted symbol 0 or 1 and  $N_s$  is the number of pulses required to transmit one symbol. The

indice  $\lfloor \frac{k}{N_s} \rfloor$  indicates that the same symbol is used for the whole length of the code. With the TH-PPM approach, the catastrophic collision between different users is avoided as each user (indexed by  $j$ ) is assigned a distinctive time-shift pattern called a time hopping sequence.

At the receiver end, a correlation receiver is usually used to detect symbols. The received signal is correlated with a template which allows the demodulation of the signal. The template is a given pseudo random code. The pseudo random code helps in the multiple access. If multiple users transmit at the same time, then by using the orthogonal pseudo random codes, only the signal corresponding to the selected code will be demodulated. The other signals will appear as a noise.

### 1.4.2 Pulse Amplitude Modulation

Pulse Amplitude Modulation (PAM) is an alternative to PPM. In PAM, the amplitude of the transmitted pulse is varied to encode data symbols for different modulation states. Theoretically, an unlimited number of levels of amplitude can be used but in practice, PAM is often limited to two states ( $\pm 1$ ). In these conditions, 2-PAM modulation is a form of bi-phased modulation or binary phase shift keying (BPSK). BPSK provides good robustness to the channel variations and simplifies the synchronization. The transmitted signal for 2-PAM can be written as:

$$s(t) = \sum_{k=-\infty}^{+\infty} d_k w(t - kT_f) \quad (1.7)$$

where  $d_k \in \{-1, +1\}$  represents the transmitted symbol and  $T_f$  is the frame time or pulse repetition interval. Another variant of the PAM is on off keying (OOK) where  $d_k \in \{0, 1\}$ . A pulse is transmitted when data symbol is '1' and no pulse is transmitted when data symbol is '0'. OOK has a reduced complexity and low implementation cost. The transmitter for OOK consists of a simple RF switch which turns on and off to represent data. This saves power of the transmitter as well. At the receiver end, the signal can be detected by using either coherent or non coherent receivers. Finally, there are also hybrid modulations. For example, we can create a modulation of 512 states by combining a 256-PPM modulation with a 2-PAM modulation.

### 1.4.3 Orthogonal Pulse Modulation

Pulse shapes other than Gaussian mono cycles can also be used for the communication in UWB. In [16], authors have used orthogonal pulses to modulate the data symbols. These pulses are generated from Hermite polynomials and are used to represent the symbols for M-ary modulation; therefore, it is called orthogonal pulse modulation (OPM). The Hermite polynomial is defined as:

$$\begin{aligned}
 p_0(t) &= 1 \\
 p_n(t) &= (-1)^n e^{\frac{t^2}{2}} \frac{d^n}{dt^n} \left( e^{-\frac{t^2}{2}} \right)
 \end{aligned} \tag{1.8}$$

As these pulses are not orthogonal, Gram-Schmidt procedure [17] was adopted to make the pulses orthogonal to each other called modified Hermite pulses (MHP). Using these MHPs, a multiple-access scheme can easily be designed. Different users are assigned different pairs of polynomials for binary data transmission. Each pair contains two orthogonal polynomials. In short, each user uses an orthogonal pair of pulse polynomials, which is in turn orthogonal to signals of other users. The BER performance in a two user environment using the MHP-based OPM has been studied in [16], where the signal from one of the users acts as an interference. It is shown that MHP-based OPM has a significant performance improvement over traditional PPM.

#### 1.4.4 Transmit Reference Scheme

Due to its simplicity, a renewed interest has been developed in transmitted-reference signaling scheme for the communication in UWB systems. In this scheme, a pair of pulses or doublets separated in time [18, 19] or frequency [20] are transmitted simultaneously. One pulse acts as a reference pulse while the other contains the information of the transmitted data symbol. The data symbols are modulated with reference to the polarity of the reference pulse. If both the pulses are of same polarity, data symbol ‘0’ is transmitted whereas for data symbol ‘1’, the data pulse is of different polarity to the reference pulse. This kind of signaling was first proposed in 1950 where it was proposed for military spread spectrum communications. It is supposed that both of the pulses experience the same channel. For this to happen either the time separation must be lesser than the coherence time or the frequency separation must be lesser than coherence bandwidth. The receiver can be a simple auto-correlation receiver (AcR) with the reference pulse acting as a template to its subsequent data pulse. There are certain drawbacks of this scheme also. As the received reference pulse is affected by noise and the overlap of the data and the reference pulse, the correlation with the noisy reference degrades the performance of the system. Also, with the insertion of the reference pulse with every data pulse, the data rate of the system is heavily affected.

#### 1.4.5 Direct Sequence UWB

Modulation for spread spectrum UWB, or direct sequence ultra wide-band (DSUWB) is the solution advocated by the IEEE standardization task group [21]. It uses frequency band allocation for UWB in the form of two dual-bands, spanning respectively from 3.1 GHz to 4.85 GHz and 6.2 GHz to 9.7 GHz. This configuration protects the UNII band systems at 5 GHz used by WiFi. FIG. 1.6 shows the spectrum of

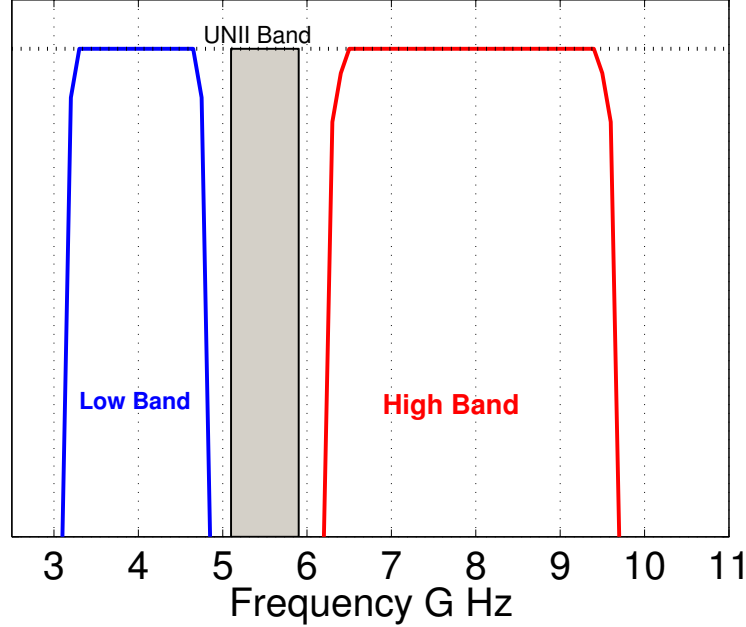


Figure 1.6: The DS-UWB spectrum.

DS-UWB system. On these dual-bands, the transmitted pulses have a duration of about 0.3 to 0.5 *ns*, and consist of several cycles. At first, only the lower band was used in order to simplify the architecture of the radio transmission systems.

As in the PPM modulation, DS-UWB frames are divided into several chips. However, a pulse can be transmitted in each chip of the frame. Therefore, the signal is transmitted in a continuous fashion and is not like the low duty cycle impulse radio signals. The transmitted symbols are represented by ternary spreading codes (consist of 1, 0 and -1) spanning the length of the frame. Under the proposed standard by IEEE task group, all DS-UWB systems must be able to generate these codes by using baseband BPSK modulation. M-ary bi-orthogonal keying (M-BOK) can also be used as an optional scheme in order to increase the efficiency of the system. To ensure a more robust transmission, the length of spreading codes varies from 1 to 24 chips depending on the desired speed. The proposed data rates for DS-UWB systems extend from 28 *Mbps* to 1320 *Mbps*. The multiple access, grouped into sub-networks called piconets, is achieved by the use of orthogonal codes. In this case, the DS-UWB modulation follows the CDMA approach used in UMTS. Finally, it has been seen that the isolation of the users of different piconets is improved by the use of slightly different chip frequencies in each piconet. More information about this technology are available in [22].

Compared to the impulse radio systems, DS-UWB seems easier to implement, because the bands involved are less wide, which requires less constraints on the RF side. The modulation used is always based on pulses, the radio access technology

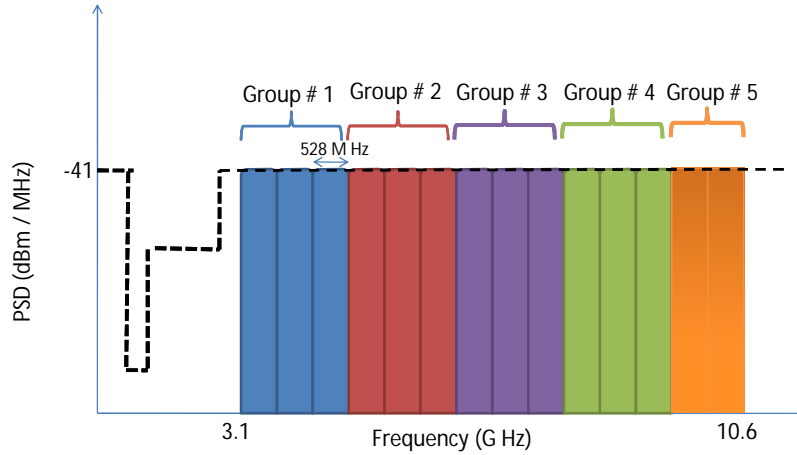


Figure 1.7: Spectrum of multi-band OFDM

remains robust to the effects of multi-path channel. The separation into two bands allows protection to the sensitive frequency bands but the transmission spectrum becomes less flexible.

#### 1.4.6 Multi-band Orthogonal Frequency Division Multiplexing

Multi-band orthogonal frequency division multiplexing (MB-OFDM) technique is also one of the solution for UWB communication, proposed by IEEE 802.15 Task Group 3a [23]. In this technique, the spectrum defined by the FCC is divided into 14 non overlapping sub-bands of 528 MHz each. These sub-bands are then divided into five groups. FIG. 1.7 presents these sub-bands classified into different groups. In each sub-band, OFDM modulation is applied and the signal is distributed among 128 sub-carriers [23] which leads to a sub-carrier separation of  $\Delta f = 4.125 \text{ MHz}$ . Quadrature phase shift keying (QPSK) modulation is used as a modulation scheme for each sub carrier. This configuration allows a flexible management of radio spectrum. Also, it is quite easier to abide by the regulations on the spectral mask of different countries. Multiple access within the users of a same group of a particular sub-band is made by the use of time-frequency codes. In a group of sub-bands, the communication of a particular user passes regularly from one band to another. This pattern of the change of bands depends on the time-frequency code, which is unique for every user. The advantages of MB-OFDM radio access technology lies mainly in its low complexity. If the frequency bands are limited to the first group of bands, existing RF systems and components can also be used for the implementation of the system. However, the transmitted signals are not pulsed based, therefore, this technology does not benefit from advantages linked to the ultra wide bandwidth such as the robustness to the channel variations.

Initially used for the radar applications, UWB technology has now been studied for almost fifteen years for wireless communications. The characteristics such as very wide spectrum or high temporal resolution have allowed the scientific and the industrial community to propose some very attractive applications: WLAN/ WPAN high-speed applications and home automation, etc. As we have seen, different types of modulation schemes have been proposed for UWB standardization, including the spread spectrum technology and multi-band OFDM. As in all radio access technologies, knowledge of the propagation channel is a pre-requisite for the development of communication system. In the next section, we will study the propagation channel for UWB systems.

## 1.5 UWB Propagation Channels

Channel is the medium in which a signal propagates from the transmitter to the receiver. A good understanding of the propagation phenomena allows to model the propagation channels adapted to the constraints of UWB. A signal propagating in the free space is only affected by the attenuation and a delay which is a function of the distance between the transmitter and the receiver. However, antenna gains and antenna efficiencies make it frequency dependent as well. The path gain in the free space is given by the formula as under:

$$G_{pr} = \frac{P_R}{P_T} = G_{TX}(f)\eta_{TX}(f)G_{RX}(f)\eta_{RX}(f) \left( \frac{c}{4\pi df} \right)^2 \quad (1.9)$$

where  $P_R$  and  $P_T$  are the received and the transmitted powers respectively,  $G_{TX}(f)$  and  $G_{RX}(f)$  are the frequency dependent antenna gains for the transmitter and the receiver respectively,  $\eta_{TX}(f)$  and  $\eta_{RX}(f)$  are the antenna efficiencies of the transmitter and the receiver respectively,  $f$  is the frequency of the transmitted signal, and  $d$  is the distance between the transmitter and the receiver. This equation is normally interpreted such that the path gain decreases with the square of frequency. However, the above formulation also shows us that this is valid only if the antenna gains are constant over frequency [24]. The antenna area,  $A_{RX}$ , is also related to the antenna gain and can be written as:

$$A_{RX} = \frac{G_{RX}}{4\pi} \left( \frac{c}{f} \right)^2 \quad (1.10)$$

In real environments, there are multiple obstacles which disturb the signal propagation. The received signal is a recombination of multiple waves, which have either been attenuated or experienced different phase shifts and reach the receiver with a delay corresponding to the path they have traversed. The presence of multi-paths in the propagation channel can lead to significant distortions in the received signal. Furthermore, especially in the indoor environment (which is often the propagation environment for UWB signals), a line of sight (LOS) path is not always available. Therefore, the signals propagating in the real environment undergo different phenomena such as reflection, transmission, diffraction, diffusion and wave guide effect etc.

If the propagating signal reflects from or transmits through dielectric or conductive objects, then resulting propagation process is also dependent on the frequency as the dielectric properties of most materials show strong variations over the frequency range of the interest for UWB systems. The diffraction and the scattering on the rough surfaces are other properties which show strong dependence on the frequency [24].

Along with the frequency, the propagation is also affected largely by the distance between the transmitter and the receiver. One of the most important propagation parameter which is a function of the distance is the path loss or the attenuation caused by the propagation to a certain distance  $d$ . Different obstacles present in the channel further attenuate the transmitted wave. Generally, the attenuation of the wave is a function of distance  $d$  between the transmitter and the receiver which is characterized by the coefficient of the propagation loss,  $\alpha$ . The received power decreases in proportion to  $d^{-\alpha}$ . The value of  $\alpha$  in the free space is 2, whereas it varies between 2 and 5 in a non line of sight (NLOS) configuration. In LOS configuration, in the presence of wave guide effects,  $\alpha$  is usually less than 2.

### 1.5.1 UWB Channel Characterization Parameters

Different parameters affect the channel in different ways. The transmitted signal propagating in a given propagation channel can experience constructive or destructive interference, frequency selectivity and Doppler effect etc. depending upon the channel and its variations. Considering a narrow band carrier based signal, the constructive and destructive interference are caused by overlapping of two waves received with certain delay in time. If the received signals are in phase then the amplitude will add up and an enforced signal will be formed, whereas if the received signals are out of phase, then the amplitude will be nearly canceled out resulting in a weaker signal. The phase shift between the two signals depends upon the wavelength of the signal and the difference in the path followed by the signals. In case of mobile displacement, the phase rotation of each path leads to a succession of maxima and minima which represents a signal with fast fading. When this phenomenon applies to a large number of multi-paths, the received signal appears as a random process. As the signal covers a narrow band, we can suppose that all the frequency components of the signal experience similar phase shifts and the power attenuation of all the frequency components is constant throughout the considered band. This phenomenon is also termed as flat fading.

If however, the transmitted signal has a large bandwidth, diverse frequency components are attenuated in different ways. The signal thus undergoes a frequency selective fading and therefore, the received power varies with the frequency. The bandwidth over which the spectral components of the signal are affected in the same way is called coherence bandwidth or correlation bandwidth. In the time domain, frequency selectivity results in a reception of different signals with delays in the order of nanoseconds. Depending on the bandwidth of the signal, these echoes overlap and thus cause significant attenuation of the signal. For signals with very wide spectrum, for example

UWB signals, the resolution of multi-path becomes very low and thus limits the interference between the different versions of the delayed signal. In this case, the fading power is less important. Some advanced techniques for the reception of the signals such as channel equalization can be applied to maximize the received energy present in the multi-paths [25, 26, 27]. Therefore, we can say that the large bandwidth is responsible for the temporal spread of the transmitted signal. The knowledge of this dispersion is necessary for calibrating the communication systems and avoiding the problems of inter-symbol interference (ISI).

The phenomenon of constructive or destructive interference shows that the properties of the radio propagation channel may differ significantly when the receiving antenna is positioned at different locations. Therefore, the behavior of the propagation channel becomes of special interest when the transmit antenna, the receiving antenna (or both), are moving. The Doppler effect corresponds to the frequency shift introduced in the electromagnetic signal caused by the variation of the path.

### 1.5.2 Channel Modeling and Practical Constraints

In the rest of the chapter, we will use the term ‘narrow band’ for all the signals which are not UWB. The channel impulse response (CIR) of narrow band signals can be modeled as the sum of different multi path components (MPCs) [28]. The channel model will only be deterministic if all of the echoes of the received signal are resolvable. However, because of the narrow bandwidth, not all of the MPCs are resolvable. Therefore, the CIR can be written as:

$$h(t, \tau) = \sum_{i=1}^N a_i \delta(t - \tau_i) = \sum_{i=1}^{N'} \sum_k \tilde{a}_{ik} \delta(t - \tau_i) = \sum_{i=1}^{N'} c_i \delta(t - \tau_i) \quad (1.11)$$

where  $N$  is the number of MPCs, while  $N'$  is the number of resolvable MPCs where one resolvable MPC consists of  $k$  physical MPCs,  $c_i$  is the resultant amplitude of the resolvable multi-path components. In the case of UWB systems, CIR differs from the narrow band propagation channel in many respects:

- Due to the fine temporal resolution, the number of physical MPCs which form one resolvable MPC is lower
- Each of the MPCs is subjected to some distortions due to the frequency dependent effects

From [24], the CIR for a UWB channel can be written as:

$$h(t, \tau) = \sum_{i=1}^N a_i(t) \chi_i(t, \tau) \otimes \delta(t - \tau_i) \quad (1.12)$$

where  $\chi_i(t, \tau)$  denotes the (time-averaging) distortion of the  $i_{th}$  echo due to the frequency selectivity of the interactions with the environment. No matter how wide

the bandwidth of the UWB signal is, every practical signal is still band limited. As long as the system is band limited, any deterministic CIR can be represented by a tapped delay line model implying that the distortion due to the frequency has not fundamentally changed the description method. It is assumed that the tap spacing is at least as dense as required by the Nyquist sampling theorem (time sampling must be carried out at a rate of at least twice the highest spectral frequency). On the other hand, the number of taps that is required to represent the impulse response can increase due to the pulse distortion.

Depending upon the bandwidth of the UWB signal, the UWB channels can be categorized as *sparse* and *dense*. The *sparse* channel is the one in which the arrival time of certain MPCs is larger than the inverse of the bandwidth of the channel. Therefore, every resolvable MPC might not carry significant amount of energy. On the other hand, in the *dense* channel, the inter arrival time of the MPCs is smaller than the resolvable bandwidth. This significantly impacts the design of Rake receivers [24]. *Dense* or *sparse* power delay profiles (PDP) depend on the considered bandwidth and the considered environment. Channels with larger bandwidths are more likely to be *sparse* than the channels with lesser bandwidths. However, large number of reflecting and diffracting objects in the propagation environment will lead to *dense* channels even for extremely large bandwidths. For instance, *dense* channels are observed for a large bandwidth of 7.5 GHz in an industrial environment [29], while residential environments [30] show *sparse* behavior at that bandwidth. More information on UWB channels can be found in [24].

## 1.6 UWB Channel Models

In this section, we will discuss some empirical as well as statistical channel models for the UWB systems.

### 1.6.1 Empirical Models

#### 1.6.1.1 Path Loss Models

The average power loss experienced in the radio propagation at a given distance  $d$  is described by the path loss models. A log distance model is generally adopted for UWB communications [31, 32] which gives the average path loss in  $dB$ :

$$\overline{PL}_{dB}(d) = \overline{PL}_{dB}(d_0) + 10n \log_{10}\left(\frac{d}{d_0}\right) \quad (1.13)$$

where  $\overline{PL}_{dB}(d_0)$  is the mean path loss at a reference distance  $d_0$  and  $n$  represent the environment-specific path loss decay exponent. In practice, the path loss can be approximately calculated from the measured frequency response of the channel:

$$\overline{PL}_{dB}(d) = 10 \log_{10} \left( \frac{1}{N} \sum_{i=1}^N |H(d, f_i)|^2 \right) \quad (1.14)$$

where  $H(d, f_i)$  is the measured frequency response at a frequency  $f_i$  and  $N$  is the total number of points in the response. As mentioned previously, the path loss decay exponent is usually less than 2 in the LOS scenarios while it varies from 2 to 5 in NLOS scenarios.

### 1.6.1.2 Power delay profile

The average power delay profile for UWB channels has been experimentally studied by a number of researchers. [33, 34, 35] are few examples. Some common observations about the UWB channels are:

1. Distinct clusters of scatterers are present in the PDP.
2. The PDP decays exponentially with cluster dependent decay exponents.
3. A large number of resolvable multi paths are present in the PDP.

### 1.6.1.3 Delay spread

The mean excess delay spread of channel can be extracted from the PDP of a certain channel. It is defined as the first moment of the PDP and can be written as:

$$\tau_m = \frac{\sum_{i=1}^N a_i^2 \tau_i}{\sum_{i=1}^N a_i^2} \quad (1.15)$$

where  $a_i$  is the  $i_{th}$  tap of the CIR with a time delay of  $\tau_i$  and  $N$  is the total number of taps in the CIR. The instantaneous root mean square (RMS) delay spread is an important parameter which indicates the time dispersion of the channel due to the presence of multi-paths [36]. It can be calculated by the first and the second moment of the measured channel power delay profile (PDP):

$$\tau_{rms} = \sqrt{\frac{\sum_{i=1}^N a_i^2 (\tau_i - \tau_m)^2}{\sum_{i=1}^N a_i^2}} \quad (1.16)$$

Typical values of the RMS delay spread vary from 5 – 25 ns depending on configurations (LOS and NLOS) and the environments (office, home and industrial etc.) [37].

## 1.6.2 Statistical Models

Statistical models for the path loss, large scale fading, general shape of the CIR, path interval times are presented in [24]. In this section, we present the statistical models for the CIR and channel delays.

### 1.6.2.1 Channel impulse response model

Generally, a tapped-delay line model with clusters is adopted for the CIR of a UWB channel. The most famous way to mathematically represent the CIR of the UWB channel is known as ‘Saleh Valenzuela (SV)’ model [38]. According to SV model, the CIR of the UWB channel can be written as:

$$h(t) = \sum_{l=1}^L \sum_{k=1}^K a_{k,l} \exp(j\phi_{k,l}) \delta(t - T_l - \tau_{k,l}) \quad (1.17)$$

where  $L$  is total number of clusters,  $K$  is the number of MPCs within a cluster,  $a_{k,l}$  is the coefficient of the  $k_{th}$  tap in the  $l_{th}$  cluster,  $T_l$  is the cluster arrival time for the  $l_{th}$  cluster,  $\tau_{k,l}$  is the delay of the  $k_{th}$  MPC relative to the  $T_l$ . The number of clusters can either be assumed fixed [38], or considered to be a stochastic variable [39]. The number of clusters is usually a function of bandwidth and the considered environment. In UWB channels, on the basis of the results of the measurement campaigns, it can be stated that the tap amplitudes of CIR differ significantly from the famous Rayleigh and Rice distributions. Therefore, some other distributions such as Nakagami [40]-[42] and the log-normal [41] are adopted for UWB channels. The phases  $\phi_{k,l}$  are uniformly distributed, i.e., for a bandpass system, the phase is taken as a uniformly distributed random variable from the range  $[0, 2\pi]$  [24].

### 1.6.2.2 Statistics of channel delays

For the modeling of multiple echoes of the MPCs, two models are generally used in the literature. One is the  $\Delta - K$  model and the other is Neyman-Scott model [42]. The inter arrival time of two of MPCs is modeled as a two state Markov model in  $\Delta - K$  model. At a time  $t_0$ , the process changes from the state  $S_1$  to  $S_2$  on the arrival of a MPC. If at the end of time interval  $[t_0 + \Delta]$ , no MPC arrives, the state changes again from  $S_2$  to  $S_1$ .

The Neyman-Scott model is the most popular model for the arrival of MPCs. It assumes that the arrival times within a cluster is a Poisson process. It is used in the SV model [38] as well as in the IEEE 802.15.4a channel model [39]. Although the  $\Delta - K$  and Neyman-Scott models are in good agreement with the experimental data but their parameters cannot be easily evaluated. For this reason, simpler stochastic models have been proposed which uses the split-Poisson model for the arrival of different MPCs [43]. This assumes the existence of only two clusters each with a different arrival frequency.

### 1.6.2.3 Power delay profile statistics

According to the cluster based UWB models, the power delay profile of a UWB channel is usually approximated as a double exponential. The average power of the

$k_{th}$  echo in the  $l_{th}$  cluster of 1.17 is given by:

$$E\{a_{k,l}^2\} = \Omega_0 \exp\left(-\frac{T}{\Gamma_l}\right) \exp\left(-\frac{\tau_{kl}}{\gamma}\right) \quad (1.18)$$

where  $\Omega_0$  is the average power of the first multi-path component, and  $\Gamma$  and  $\gamma$  are the intra cluster and inter cluster decay time constants of the clusters respectively. The inter-cluster decay time constant  $\Gamma$  is typically around 10 – 30 ns, while widely differing values (between 1 – 60 ns) have been reported for the intra-cluster constant  $\gamma$ . The information about the fast fluctuations of the received power due to fading is however not provided in 1.18.

#### 1.6.2.4 Auto-regressive models for UWB channels

The models based on the description of CIR such as given by 1.17 need a large number of parameters for a satisfactory description of the CIR. An accurate modeling of the channel frequency response can be done by making use of a second order auto-regressive model in the frequency domain [44]. Furthermore, these models closely match the experimental data even with a small number of required parameters.

## 1.7 Receiver Used for UWB Systems

Different types of receivers have been used for pulsed UWB communication system. UWB receivers can be broadly classified into coherent and non coherent receivers.

### 1.7.1 Coherent Receivers

#### 1.7.1.1 Rake Receiver

As it has already been described that because of its very large bandwidth, the UWB received signal is composed of large number resolvable MPCs. Rake receiver exploits the inherent time diversity of the MPCs and tries to collect maximum amount of energy coherently. However, because of the large number of MPCs, collection of significant energy requires large number of fingers in the RAKE receiver. For instance according to [45], to capture 80% of the received signal energy, Rake receiver requires more than 200 fingers. Depending upon the configuration (LOS or NLOS) and the environment (residential, office or industrial) different UWB channels require different number of RAKE fingers. For the SV model, number of fingers to capture 85% of energy varies from 22 – 123 for different LOS and NLOS configurations. Therefore, only a subset of MPCs is used for the collection of energy. Selective (S-RAKE) and partial (P-RAKE) are the examples of rake receiver with limited number of fingers. But using these kind of receivers degrade the performance of the receiver and are more prone to the errors. Therefore, there is a compromise between the quality and the complexity.

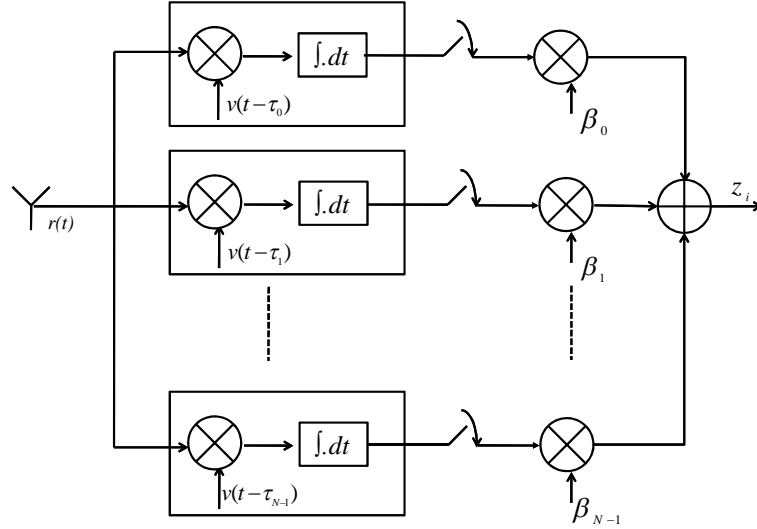


Figure 1.8: Block diagram of Rake receiver

FIG. 1.8 shows the block diagram of the Rake receiver with  $N$  fingers. The received signal is correlated with a given template ( $v(t - \tau_i)$ ) for the  $i$ th finger and then combined based on the combining scheme used. Two of the well known combining schemes are maximum ratio combining (MRC) and equal gain combining (EGC). In MRC, the amplitudes of the MPCs are estimated and used as the weighting vector ( $\beta_i$ ). Therefore, performance of the MRC Rake receiver depends upon the receiver's knowledge of the channel. Whereas, in the case of EGC, all the MPCs are combined with equal gain and thus only the phase of the corresponding MPC is required. Therefore, EGC Rake receiver is simpler to implement than MRC Rake receiver but performance is also affected.

## 1.7.2 Non Coherent Receivers

Non coherent receivers do not require channel state information (CSI) at the receiver. From the implementation point of view, non coherent receivers give a simple option at the cost of performance loss. Energy detectors and transmit reference receiver are two common non coherent receivers.

### 1.7.2.1 Energy Detector

Energy detector (ED) is one of the famous non coherent receivers. After being filtered, the received signal is passed through a square law device followed by an integrator and a decision mechanism. FIG. 1.9 shows the block diagram of an energy detector

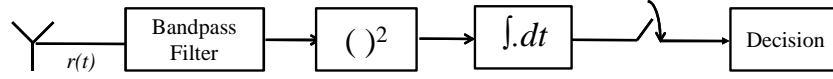


Figure 1.9: Block diagram of an energy detector based on OOK

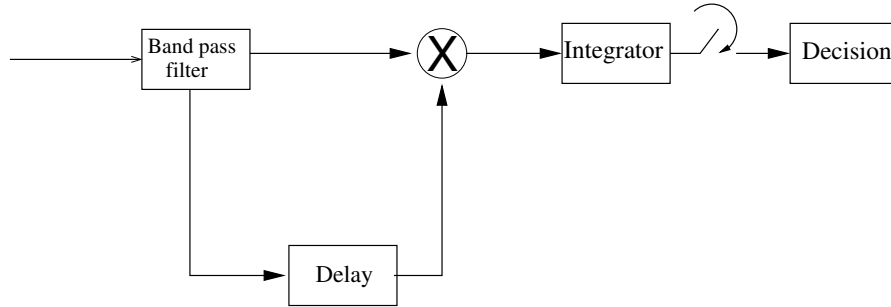


Figure 1.10: Block diagram of the transmit reference receiver

based on OOK. PPM modulated signal can also be detected using energy detection. The low complexity of the ED receiver is at the cost of performance [16, 46].

### 1.7.2.2 Transmit Reference Receiver

Transmit reference receiver is another non coherent receiver which, due to its simplicity, has gained much interest among the researchers. In every frame of the transmit reference signal, a reference pulse is transmitted along with the data pulse. The receiver delays the reference signal and correlates it with the data signal in every time frame. FIG.1.10 shows the block diagram of the transmit reference receiver. Transmit reference scheme has no stringent requirements of channel estimation but it exploits the inherent multi path diversity of the UWB signals. However, as the reference pulse is transmitted in every time frame, it experiences a 3 dB penalty compared to the coherent receivers. Furthermore, the performance of the transmit reference receiver is also limited due to the noisy reference. This drawback can be partially removed by averaging the reference signal before correlating [47].

## 1.8 Introduction of Time Reversal

As explained in the previous Section, UWB receivers are either complex or result in a significant performance degradation as a cost of receiver simplicity. One way to overcome these drawbacks is to make use of a technique that shifts the design complexity from the receiver to the transmitter. Time Reversal (TR) has been proposed as a technique to shift the design complexity from the receiver to the transmitter. Classi-

cally, TR has been applied in acoustics and under water communication applications. In this section, we will first discuss the evolution of TR. We will start from TR acoustics and then discuss TR in electromagnetic waves and finally we will describe TR in UWB.

### 1.8.1 Time Reversal Acoustics

Time reversal (TR) invariance is a fundamental symmetry that holds nearly everywhere in microscopic physics, which can be exploited in macroscopic physics to create a variety of useful instruments as well as elegant experiments in pure physics [48]. In acoustics, TR has been widely applied for focusing and source localization as well [49]- [51]. The wave propagation in acoustics is governed by the following equation:

$$\rho_0(r)\Delta\cdot\left(\frac{1}{\rho_0(r)}\cdot\Delta\Phi(r,t)\right)=\frac{1}{c_0^2(r)}\frac{\partial^2\Phi(r,t)}{\partial t^2} \quad (1.19)$$

where  $\Phi(r,t)$  is the acoustic potential of the wave at point  $r$ ,  $c_0(r)$  is the spatial distribution of sound velocity in the medium and  $\rho_0(r)$  is the density distribution of the medium. One can note that it contains only a second-order time-derivative operator. This property is the starting point of the time-reversal principle, valid only for a lossless propagation medium. As an immediate consequence, if  $\Phi(r,t)$  is a pressure field solution of the propagation equation, then  $\Phi(r,-t)$  is another solution of the problem because of the presence of time derivative. This property is specific to the invariance under a time-reversal operation. However, if the propagation medium has a frequency-dependent attenuation, the propagation equation may contain odd order time-derivative operator and therefore, the invariance under time-reversal is lost. The special property of time reversal has been observed by Stokes in the framework of the classical experiment of reflection and transmission of a plane wave along the interface separating two media of different sound velocities [52].

### 1.8.2 Stoke's Time Reversal Experiment

If a plane incident wave of amplitude 1 is propagating from medium 1 to medium 2, it will be reflected into a plane wave of amplitude  $R$  and a transmitted wave of amplitude  $T$  (Fig. 1.11a). If we assume a configuration in which the pressure field  $\Phi(r,t)$  is resulted from these three plane waves, Stoke investigated whether this experiment could be time-reversed or not. He used the plane wave property that time reversal can be accomplished by reversing the wave vector direction. The time reversed  $\Phi(r,-t)$  can be described by a new set of three waves: two incident waves of amplitudes  $R$  and  $T$ , one incident from medium 1 to medium 2 while other incident from medium 2 to medium 1, followed by a transmitted wave of amplitude 1 propagating in medium 1 as shown in FIG. 1.11b. If we define  $R'$  and  $T'$  as the reflection and transmission coefficients for an incident wave coming from medium 2, and applying the superposition principle, the two incident waves lead to the generation of four plane waves, two of them propagating in medium 1 with a resulting amplitude  $R^2 + TT'$ , and the other

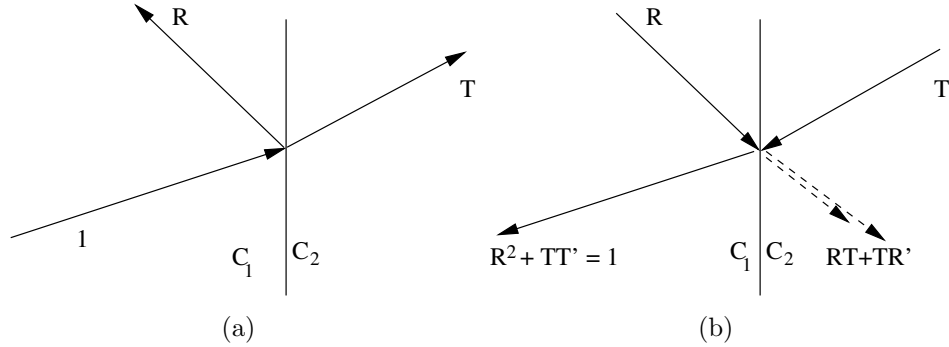


Figure 1.11: Reflection and transmission of a plane wave along the interface separating two media of different sound velocities. (b) Time reversal of FIG. 1.11a

two propagating in medium 2 with a resulting amplitude  $RT + TR'$ . An elementary computation of the reflection and transmission coefficients  $R$ ,  $T$ ,  $R'$ , and  $T'$  allows us to verify the following relations [52]:

$$\begin{aligned} R^2 + TT' &= 1 \\ RT + TR' &= 0 \end{aligned} \quad (1.20)$$

The above example suggests that the wave equation can be directly interpreted as the time-reversal of the previous situation. In fact, these arguments can be generalized for different kinds of incident acoustic fields and other geometries of inhomogeneities. It is important to note that the two relations written above are only valid, if the reflected and transmitted plane waves have a real propagative wavenumber. Due to the finite bandwidth of the incident field, some information is lost in the time-reversal process.

### 1.8.3 Principle of Reciprocity

Helmholtz-Kirchhoff's principle of reciprocity is demonstrated by the system of linear equations which resulted from the evolution of acoustic waves. In the case of linear acoustics, the system can be written under the assumption of adiabatic process, i.e. without any source term and without any outflow:

$$\begin{aligned} \frac{\partial}{\partial t} \rho(r, t) &= -\Delta \cdot (\rho_0(r) v(r, t)) \\ \rho_0(r) \cdot \frac{\partial}{\partial t} v(r, t) &= -\Delta p(r, t) \\ p(r, t) &= c_0^2(r) \cdot \rho(r, t) \end{aligned} \quad (1.21)$$

where  $\rho(r, t)$  is the variation of the density distribution,  $v(r, t)$  is a particular velocity, and  $p(r, t)$  is the variation of the pressure of the medium at point  $r$  and time  $t$ . Here if

we change the variable  $t$  with  $-t$ , the velocity  $v(r, t)$  which corresponds to the velocity of the divergent wave becomes  $-v(r, -t)$  which is the velocity of the convergent wave. This can be explained as the velocity vector is a time derivative of the position vector. It is possible to achieve an instantaneous time reversal by recording at once all the pressure and the velocity fields and then retransmitting the pressure unchanged and the velocity in the opposite direction. Indeed, in a three dimensional system, such an approach is technically impossible. In fact, the knowledge of the pressure and the velocity fields of a 2-D surface is sufficient to predict the fields in all the volume covered by that surface [52].

#### 1.8.4 Time Reversal Cavity

In any propagation experiment, a unique solution to the wave equation  $\Phi(r, t)$  is determined based on the initial conditions. In the TR experiments, the objective is to modify the initial conditions in such a manner that  $\Phi(r, -t)$  also becomes a solution. However, due to the causal nature of the physical phenomena,  $\Phi(r, -t)$  is not an experimentally valid solution. Therefore, the goal is limited to the generation of  $\Phi(r, T - t)$ . As mentioned earlier, measuring the pressure field  $p(r, t)$  during a time interval  $T$  in the whole three-dimensional (3-D) volume is technically impossible. Huygens principle can be used to resolve this problem: the wave field in any point of a volume can be predicted by the knowledge of the field and its normal derivative on a closed surface surrounding the volume. The problem is therefore simplified from a 3-D to a 2-D time reversal. The time reversal focusing consists of two phases. First is the phase of recording in which the source surrounded by a closed surface transmits a spherical wave front and the transducer elements in the cavity measures the pressure fields and its normal derivative which are distorted by the inhomogeneous propagation medium. In a second phase, each transducer element of the cavity becomes a source and transmits the time reversed signals measured in the first phase. The time-reversed pressure field back-propagates inside the surface and is distorted by the interaction with the inhomogeneities. It has been shown that the fields transmitted by the transducers on the cavity focus on the initial source position [52]. We can obtain fine focusing which only depends upon the size of the point source. If we define the focal point as the size as half of the length of the zone in which the energy is concentrated then the dimension of the focal point is limited by diffraction. Its dimension is of the order of half of the wavelength ( $\frac{\lambda}{2}$ ). More details about the TR in acoustics can be found in the articles [52]- [55].

#### 1.8.5 Time Reversal for Electromagnetic Waves

The electromagnetic fields obey the theorem of reciprocity. It states that an electric field in the direction of polarization of the source remains unchanged if the position of the transmitter and the receiver is interchanged. Mathematically, it can be written as:

$$p_1 \cdot E_2(r_1, \omega) = p_2 \cdot E_1(r_2, \omega) \quad (1.22)$$

where  $p_{1,2}$  is the vector of polarization of the elementary source dipole,  $E_{1,2}(r_{1,2}, \omega)$  is the electric field at the position  $r_1$  or  $r_2$ .

### 1.8.5.1 Time Reversal of a Carrier Based Signal

In most of the communication systems, the transmitted signal is modulated on a high frequency carrier. Communication with the signals of low frequency (i.e. large wavelengths) is quite difficult as it requires antenna of very large dimensions. Often a high-frequency sinusoidal signal is used as carrier signal to transmit the information. The three key parameters of a sine wave are its amplitude, its phase and its frequency, all of which can be modified exclusively or in combination in accordance with an information signal to obtain the modulated signal. If  $f_0$  is the carrier frequency, the modulated signal can be represented as:

$$x(t) = x_p(t) \cos(2\pi f_0 t) - x_q(t) \sin(2\pi f_0 t) \quad (1.23)$$

where  $x_p(t)$  and  $x_q(t)$  are the baseband signals having a PSD centered at 0 and are called in-phase and quadrature components of  $x(t)$  respectively. The representation of the modulation scheme becomes simpler if the complex envelope of the initial signal is used. The modulated signal can alternatively represented as:

$$x(t) = \Re(x_e(t) \exp(j2\pi f_0 t)) \quad (1.24)$$

where  $x_e(t) = x_p(t) + jx_q(t)$  is the complex envelope of the signal  $x(t)$ . In the frequency domain, this signal can be expressed as:

$$x(f) = \frac{1}{2} x_e(f) \star \delta(f \pm f_0) \quad (1.25)$$

where  $x(f)$  and  $x_e(f)$  are the Fourier transforms of  $x(t)$  and  $x_e(t)$  respectively and  $\star$  denotes the convolution product. It is clear that the signal is translated to the carrier frequency  $f_0$ . As the signal  $x(t)$  is a real signal, its frequency spectrum has a Hermitian symmetry.

At high frequencies, if the technique of time reversal is to be used, the signal must be sampled at a very high sampling rate. Furthermore, the digital signal must be converted into analog form in order to be transmitted. These two processes are quite expensive at high frequencies. The received signal in any channel without noise can be written as:

$$r(t) = r_p(t) \cos(2\pi f_0 t) - r_q(t) \sin(2\pi f_0 t) \quad (1.26)$$

where  $r_p(t)$  and  $r_q(t)$  are the respective in-phase and quadrature components of the baseband received signal. It is important to note that the baseband signals contain all the information about the propagation in the medium. The time reversed received signal can be written as:

$$r(-t) = r_p(-t) \cos(2\pi f_0 t) + r_q(-t) \sin(2\pi f_0 t) \quad (1.27)$$

The above equation (1.27) is the definition of the TR in modulated signal which is carried out by time reversing the inphase and quadrature components in time followed by a phase conjugation. In the context of TR with a carrier modulated signals, it is observed that temporal compression and spatial focusing properties depend directly on the bandwidth of the signal. The TR is quite advantageous with a carrier based modulation. Even the low frequency baseband signals can achieve high spatial focusing due to the presence of a high frequency carrier. It is observed that the size of the spatial focusing zone depends on the carrier frequency even if the frequency of the baseband signal is significantly lower than the carrier frequency. Thus, a fine spatial focusing can be achieved only by varying the carrier frequency and not disturbing the whole spectrum. Time compression, which is the ratio of the TR peak amplitude to the mean amplitude of the secondary lobes, depends on the ratio of the bandwidth of the signal to the coherence bandwidth of the propagation channel. In other words, it depends on the ratio of the RMS delay spread to the duration of the initial pulse. Thus, time compression depends primarily on the bandwidth and the characteristics of the medium rather than the carrier frequency. To conclude, the increase in carrier frequency can increase the time compression of the signal but it is also limited by the product  $\Delta v \tau$  where  $\tau$  is the reverberation time and  $\Delta v$  is the bandwidth of the signal [56].

### 1.8.6 TR in UWB

As discussed in Section 1.8.5, the temporal and spatial focusing of the TR scheme improves with the bandwidth of the signal. Therefore, systems with ultra wide bandwidth are inherently suitable for the TR scheme. Classically, TR has been applied to acoustics [48, 52] and underwater systems [53], but recently, it has been widely studied for broadband and UWB communication systems [1]- [58]. One of the very first experimental study for TR with wideband electromagnetic waves is carried out in [59]. In a TR UWB communication systems, a time reversed channel impulse response (CIR) is employed as a transmitter pre-filter. The TR technique comprises of two steps. In the first step, the CIR is estimated at the transmitter end. In the second step, the complex conjugated and time reversed CIR is transmitted in the same channel. The TR wave then propagates in an invariant channel following the same paths in the reverse order. Finally at the receiver, all the paths add up coherently in the delay and spatial domains. Experimental demonstration of TR has been performed in [1, 60]. The performance of MISO TR systems has been analyzed in [61, 62]. TR performance in a multi-user scenario is studied in a number of articles [63, 64]. The performance of TR UWB for different bandwidths is analyzed in [65]. For dense multi-path propagation channels, strong temporal compression and high spatial focusing can be achieved with a focusing gain of about 8 dB [1]. For communication purposes, this gain improves the transmission range. ISI effects are mitigated by temporal compression and multi-user

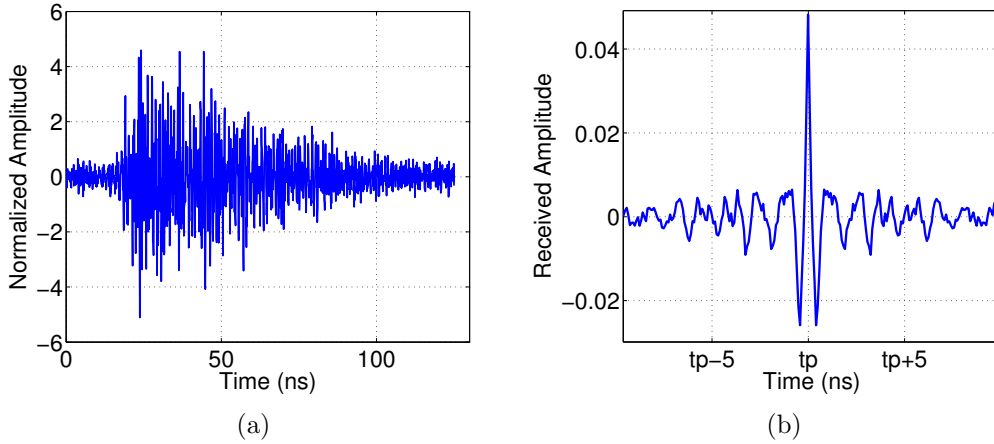


Figure 1.12: a) CIR in an indoor environment b) Received signal with TR scheme in an indoor environment

interference is reduced due to spatial focusing. The noiseless received signal ( $y_j(t)$ ) at the intended receiver ( $j$ ) can be mathematically represented as:

$$y_j(t) = s(t) \star h_{ij}(-t)^* \star h_{ij}(t) = s(t) \star R_{ij}^{auto}(t) \quad (1.28)$$

where  $h_{ij}(t)$  is the CIR from the transmitting point to an intended receiver,  $s(t)$  is the transmitted signal,  $\star$  denotes convolution product and  $(.)^*$  means the complex conjugate of the function and  $R_{ij}^{auto}(t)$  is the auto-correlation of the CIR between the transmitting antenna ( $i$ ) and receiving antenna ( $j$ ). The received signal with the TR scheme has a very strong peak at time  $t = 0$  (from the properties of auto-correlation function) and is considerably focused in spatial and temporal domains. FIG. 1.12 shows a measured CIR in an indoor environment (IETR<sup>(1)</sup> laboratory) and the received signal with the TR scheme. Temporal focusing property of TR can easily be observed. As a result, the received power is concentrated within few taps and the effects of ISI are greatly reduced. The receiver system becomes simpler than without TR and signal can be collected using a simple energy threshold detector. Spatial focusing enables very low co-channel interference in a multi cell system, resulting in an efficient use of bandwidth in the overall network. It can be noted that in order to apply TR, the knowledge of the CIR is mandatory at the transmitter. In a reciprocal channel, the CIR for the forward link (from the transmitter to the receiver) is similar to the CIR of the backward link (from the receiver to the transmitter). Channel reciprocity for the UWB channels is studied experimentally with TR scheme in [66]. If the channel is assumed to be reciprocal, the channel estimation of the backward link can be performed. The noiseless received signal at any non intended receiver ( $k$ ) is:

$$s(t) \star h_{ij}(-t)^* \star h_{ik}(t) = s(t) \star R_{ikj}^{cross}(t) \quad (1.29)$$

<sup>(1)</sup>Institute of Electronics and Telecommunications of Rennes

where  $h_{ik}(t)$  is the CIR from the transmitting point to an un-intended receiver and  $R_{ikj}^{cross}(t)$  is the cross-correlation of the CIR  $h_{ik}(t)$  and the time reversed complex conjugated version of the transmitted signal  $h_{ij}(-t)^*$ . If the channels are uncorrelated, then the signal transmitted for one receiver will act as a noise for a receiver at any other location. This means that the channel itself codes the transmitted signal (quasi) orthogonally and results in a secure communication with low probability of detection and low probability of interception. In a MIMO scenario, if there are  $N_t$  transmitting antennas and  $N_r$  receiving antennas, the received signal by the  $j$ th receiving antenna is:

$$y_j(t) = \underbrace{s_j(t) \star \sum_{i=1}^{N_t} R_{ij}^{auto}(t)}_{Signal(j)} + \underbrace{\sum_{i=1}^{N_t} \sum_{k=1; k \neq j}^{N_r} s_k(t) \star R_{ikj}^{cross}(t)}_{Interference(j)} + \underbrace{n_j(t)}_{Noise(j)} \quad (1.30)$$

where  $s_j(t)$  and  $s_k(t)$  are the transmitted signals intended for the  $j$ th and the  $k$ th receiving antenna respectively. The equivalent CIR,  $h^{eq}$ , denoted by the sum of the auto-correlation functions  $R_{ij}^{auto}$  in (1.30) can be written as:

$$h_j^{eq}(t) = \sum_{i=1}^{N_t} R_{ij}^{auto}(t) \quad (1.31)$$

As long as the channels are uncorrelated, the interference part in (1.30) is not significant. Thereby, it might be possible to communicate simultaneously with all receiving antennas with a simple detection scheme at each antenna. Consequently, the throughput of the system can be significantly increased. The above equation thus can be used to describe either a  $N_t \times N_r$  MIMO system or  $N_r$  simultaneously operating MISO systems each one representing a different user. Signal to interference ratio (SIR) is a metric representing the spatial focusing characteristics of TR [67]. The instantaneous SIR for the  $j$ th user can be calculated as:

$$SIR_j = 10 \log_{10} \frac{|Signal_j(t = t_{peak})|^2}{|Interference_j(t = t_{peak})|^2} \quad (1.32)$$

where  $t_{peak}$  is the decision time or the time at which the *Signal* peak is received.

In the practical implementation of the TR system, the pre-coding filter is truncated in time to reduce the filter length and thus the system complexity. The truncated response is represented as  $h'(-t)$ . For data communication purpose, the transmitted symbols are modulated by binary pulse amplitude modulation (BPAM) scheme. The  $k$ th symbol,  $d_k$ , of the symbol sequence is equal to 1 or -1 for the data bits 1 or 0

respectively. Therefore, the received signal at the intended receiver is written as:

$$\begin{aligned}
 y'(t) &= A \underbrace{\sum_k d_k h'(-t - k T_s)}_{\text{Transmitted RF signal}} \star \underbrace{h(t)}_{\text{CIR}} + n(t) \\
 &\approx A \sum_k d_k R_{hh}(t - k T_s) + n(t)
 \end{aligned} \tag{1.33}$$

where  $A$  is a normalization factor and  $T_s$  is the symbol duration.  $n(t)$  is the noise and  $R_{hh}(t)$  is the auto-correlation function of the CIR ( $h(t)$ ). For the sake of simplicity, we have supposed that the  $T_s$  is equal to the length of the measured time reversed CIR ( $h'(-t)$ ). As the amplitude of the peak of the received signal is proportional to the energy of the transmitted signal ( $\int h^2 dt$ ), the truncation process decreases the peak of the received signal. Due to BPAM, the polarity of the received signal peaks depends on the transmitted data bit and is used for the detection of the data bits.

As the received TR signal is quite focused in time, the detection of the TR signal can be done with a rather simple energy detection method [63]. Because of a strong TR peak, the synchronization of the main peak of the received signal is expected to be easy. Therefore, very simple or no equalizer is needed. The complexity thus shifts from the receiver side to the transmitter side. The application of TR with MMSE equalizer is studied in [68]. Performance evaluations of the pre-Rake scheme for UWB systems can be found in [69, 70].

### 1.8.6.1 Time Reversal Properties

Some of the TR characteristics are defined in the following:

- TR received peak power is an important performance metric for the TR scheme. In case of TR communication, TR peak power acts as a core performance metric. It is defined as the power of the received peak for a TR system with a fixed transmitted power. TR peak performance can vary depending upon the environment (LOS or NLOS), antenna polarization (co-polar or cross polar) and antenna configurations (SISO, SIMO, MISO and MIMO). In the next chapters, we have compared the TR received peak power with respect to a given reference, therefore it is often referred as normalized peak power (NPP), i.e. TR received peak power normalized to some given reference.
- Focusing gain (FG) of a TR system is defined as the ratio of the strongest tap power of the received signal in time reversal scheme to the strongest tap power of the pulse system; where the transmitted signal power and bandwidth is kept constant for both the schemes. Mathematically, it can be written as:

$$FG = 20 \log_{10} \left( \frac{\max |y_j(t)|}{\max |h'_j(t)|} \right) \tag{1.34}$$

It is also an important TR property as higher FG can translate into higher communication range for a communication system as compared to a pulsed UWB communication system.

- As the data rate of the transmission scheme becomes large, the signal to side lobe ratio (SSR) becomes more and more important. It is defined as the ratio of the power of the first to second strongest peak in a TR received signal:

$$SSR = 20 \log_{10} \left( \frac{y_j(t_{peak})}{y_j(t'_{peak})} \right) \quad (1.35)$$

where  $t_{peak}$  is the time for strongest peak and  $t'_{peak}$  is the time for the second strongest peak. SSR is an important parameter and is a measure of the quality of the received signal. In case of high data rate TR communication system, SSR affects directly the BER performance.

- The average received power with the TR scheme increases as compared to the pulsed system for a fixed transmitted power. The increased average power (IAP) is defined as the ratio of the mean power with the TR scheme and the pulsed UWB scheme. Mathematically, the increased average power (IAP) is defined as:

$$IAP(dB) = 10 \log_{10} \left( \frac{E(y_j^2)}{E(h_j^2)} \right) \quad (1.36)$$

where  $E(\cdot)$  denotes the expected value.

- Another important TR characteristic is the instantaneous RMS delay spread ( $\sigma_\tau$ ). It can be calculated by the first and the second moment of the measured TR response or the CIR:

$$\sigma_\tau = \sqrt{\frac{\sum_{l=1}^N PDP(l) \tau_l^2}{\sum_{l=1}^N PDP(l)} - \left( \frac{\sum_{l=1}^N PDP(l) \tau_l}{\sum_{l=1}^N PDP(l)} \right)^2} \quad (1.37)$$

where  $PDP(l) = |y_j(l)|^2$  or  $|h'_j(l)|^2$ ,  $y_j$  is the measured TR response,  $h'_j$  is the measured CIR,  $\tau_l$  is the excess time delay and N is the total number of taps in the PDP. The knowledge of the RMS delay spread allows to estimate the frequency selectivity of the propagation channel. RMS delay spread is considered as a metric for temporal compression in TR systems.

In simple TR scheme, the transmitted power of each symbol for each transmission link is equal to the power of the estimated CIR. It can be problematic when there is a simultaneous transmission for different communication links. As the intended transmitted power for different receiving antennas can be different, the interference power can be a large fraction of the intended signal. The solution is equal power

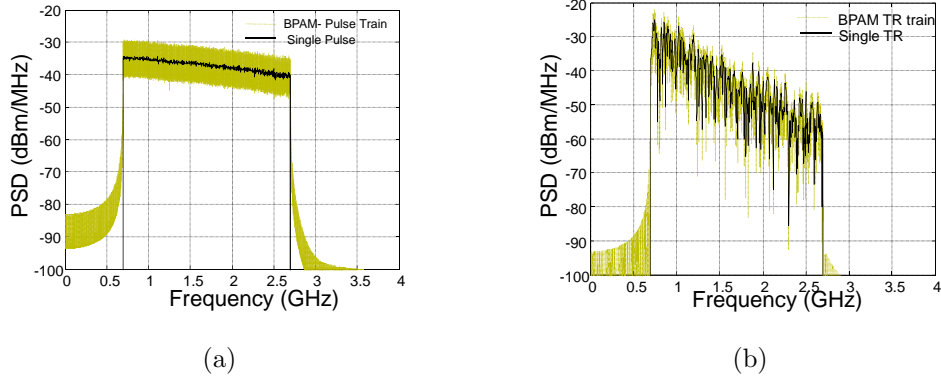


Figure 1.13: PSD of a a pulse train and single pulse for a) Pulsed UWB b) TR UWB

control as described in [63]. The time reversed CIR is normalized with the measured wide-band power so that the intended power for each receiving antenna is equal:

$$h_{ij}^{TR}(t) = \frac{h_{measured_{ij}}(-t)^*}{\|h_{measured_{ij}}(t)\|} \quad (1.38)$$

where  $\|\cdot\|$  denotes the Frobenius norm operation.

### 1.8.6.2 Spectral Analysis of TR Scheme

In a pulsed UWB system, strong spectral lines are observed at the multiples of pulse repetition frequency. On the contrary, the spectrum of the single pulse does not have such spectral lines. FIG. 1.13a shows the PSD of the transmitted short pulse and the short pulse train with BPAM modulated data. Welch's method is used for computing the PSD [71]. To reduce the spectral lines in the pulse train, some randomizing techniques such as direct sequence (DS) and time-hopping (TH) are applied for UWB communication systems. These techniques spread the spectrum of the transmitted pulse train to get rid of the spectral lines. In TR wireless communications, the transmitted signal is constructed from multiple short pulses with different amplitudes and polarities. Thus, the spectrum of the TR-signal train is inherently spread and is very similar to a single TR signal. FIG. 1.13b shows the PSD of a single TR-signal and the TR-signal train with BPAM modulated data. As shown, in contrast to the PSD of the pulse train, the spectrum of the TR-signal train is covered by the spectrum of a single TR-signal. Thus, the randomizing process to break up the large spikes of the spectrum to reduce the interference with other communication systems is not efficient for the TR signaling. Furthermore, due to the spatial focusing property of the TR scheme, the collision among the users in the multi-user systems is inherently reduced (without randomizing). Consequently, the receiver system is simplified by eliminating the randomizing circuits.

The second issue concerning the spectrum of the TR-UWB signal is the effective bandwidth of the scheme. The effective bandwidth in pulse radio is specified by the spectrum of the transmitted short pulse. However, for TR scheme, the transmitted signal and the related spectrum are enforced by the wave propagation medium. The PSD of the TR transmitted signal depends on the effects of the propagation channel including path loss and the antennas. Therefore, the PSD has a descending shape. The components of the signal at higher frequencies are attenuated as compared to the components at lower frequencies. Thus, the spectrum of the TR signal is emphasized at the lower frequencies of a given bandwidth (see FIG. 1.13b). This inherent property of the TR signal makes it difficult to employ efficiently to an ultra wide bandwidth signal. Therefore, large percentage of energy is contained at the components of the signals at lower frequencies.

## 1.9 Conclusion

In this chapter, the state of the art of the pulsed UWB and the TR UWB is presented. Pulsed UWB has gained attention of the researchers from all over the world from February 2002 onwards, after which an unlicensed communication can be carried out over very large bandwidth. Because of its extremely wide bandwidth, UWB signals result in large number of resolvable multi-paths and thus reducing the interference caused by the super position of unresolved multi-paths. Different modulation schemes such as PPM, PAM, OPM, OOK, transmit reference transmission and direct sequence UWB are used for the pulsed UWB systems. Another approach of utilizing the UWB is to divide the bandwidth into a number of sub-bands and use multi-band OFDM approach. A lot of research has also been done on different channel models for the UWB signals. Both empirical and statistical models have been studied. For the channel impulse response, cluster based models are generally used as in the famous Saleh-Valenzuela or in the IEEE standardized models. Different types of receivers (coherent and non coherent) have been suggested in the literature. In order to collect significant energy of the UWB signals, the receivers are generally complex. Time reversal (TR) has been proposed as a transmission scheme which shifts the design complexity from the receiver to the transmitter end. Initially used for acoustics and underwater application, TR has now been studied as a potential communication approach for UWB systems. The received signal in a TR scheme is time compressed and spatially focused. Therefore, it can be detected by using simple threshold detectors. Different performance metrics for TR scheme have been defined and will be repeatedly used in the chapters to come.



# Chapter 2

## Validation of TR Scheme

### Contents

---

<b>2.1</b>	<b>Introduction</b>	<b>39</b>
<b>2.2</b>	<b>Simulation Approach for TR Validation</b>	<b>40</b>
2.2.1	Description of Used Channel Model	40
2.2.2	TR Validation with Existing Channel Models	46
2.2.3	TR Validation with TD-TLM Simulations	47
<b>2.3</b>	<b>Semi Measurement Approach for TR Validation</b>	<b>51</b>
2.3.1	Experimental Setup	52
2.3.2	Spatial Focusing in an Indoor Environment	52
2.3.3	Effects of Bandwidth on Spatial Focusing of the TR Scheme	54
<b>2.4</b>	<b>Full Measurement Approach for TR Validation</b>	<b>56</b>
2.4.1	Experimental Setup	56
2.4.2	Validation Procedure	57
2.4.3	Comparison of Measured Channel Response in Different Measurement Configurations	58
2.4.4	Comparison of different TR Properties	59
2.4.5	TR in a Reverberation Chamber	63
<b>2.5</b>	<b>Effect of Different Antennas on TR</b>	<b>65</b>
2.5.1	Experimental Results in RC	66
2.5.2	Experimental Results in the Indoor Environment	67
<b>2.6</b>	<b>Effect of Different Bandwidths on TR</b>	<b>69</b>
2.6.1	Experiments in RC	69
2.6.2	Experiments in Indoor Environment	71
<b>2.7</b>	<b>TR with Multi-Antenna Configurations</b>	<b>72</b>
2.7.1	MIMO-TR in RC	74

2.7.2	SISO and SIMO-TR in the Indoor Environment . . . . .	76
<b>2.8</b>	<b>Multiplexing Gain of SIMO-TR . . . . .</b>	<b>77</b>
2.8.1	Capacity Comparison of the TR Multi Antenna Configurations . . . . .	79
2.8.2	Experimental Validation of SIMO-TR . . . . .	81
<b>2.9</b>	<b>Conclusion . . . . .</b>	<b>82</b>

---

## 2.1 Introduction

In this chapter, we investigate the TR scheme from propagation point of view. The validation of the TR scheme in the laboratory is performed and a parametric analysis of TR technique is carried out using simulation, semi-measurement and measurement approaches. The validation of the TR scheme for UWB channels consists of two steps. In the first step, the channel response is estimated. The second step consists of transmitting the time reversed signal and measuring the time reversal response (TRR). In the simulation approach, both the steps involved for validating TR scheme are performed through simulations. TR is validated by taking the existing channel models present in the literature and simulating the TR scheme through programming. In the semi-measurement approach, channel impulse responses are measured in the laboratory using frequency domain equipment and the TR is simulated using programming tools. In the measurement approach, both of the steps involved in the TR validation are performed experimentally using time domain equipment. In this case, the channel response is measured by transmitting a very narrow pulse in time. Thereafter, the measured channel response (MCR) is time reversed and transmitted again in the channel (which is assumed to be static during this period) to measure the TRR. Different TR properties are studied by making use of the results of these validations.

The results of the TR validation by simulation are used to analyze the power delay profiles (PDP) and average power decay profiles (APDcP) of the channel impulse responses (CIR) and the TR responses (TRRs) in different types of indoor channels. Three channel environments are used; residential, office and industrial. PDP and APDcP are analyzed for both line of sight (LOS) and NLOS (non-LOS) configurations. Furthermore, TR is demonstrated by electromagnetic (EM) simulation of a sample wave propagation channel. Channel response between transmitting antenna and receiving ideal field sensors is computed using three dimensional (3D) time-domain transmission line matrix (TD-TLM) method. Time reversed version of the computed response is used as the source signal of the transmitting antenna. A simulated environment with metallic faces except one is (which is an absorbing boundary) is chose and spatial focusing of the TR scheme is studied in this environment.

The results of the semi-measurement approach for the TR validations are used to study the spatial focusing property of the TR scheme in an indoor environment and in a reverberation chamber (RC). The effects of different bandwidths and lower frequency ( $f_L$ ) are studied on the spatial focusing property of TR.

Using the results of measurement approach, the feasibility of TR technique in ultra wide-band (UWB) communication is assessed. A typical indoor propagation channel is selected for the exploration. Different TR properties such as focusing gain (FG), increased average power (IAP), signal to side lobe ratio (SSR), normalized peak power (NPP) and root mean square (RMS) delay spread are studied in LOS and NLOS configurations with both co-polar and cross-polar antenna orientations. Time domain measurements are also conducted for ultra wide-band (UWB) signals in the RC and all the TR properties are studied for RC as well. TR validation is performed with different

types of antennas and for different bandwidths of the TR transmitted signal. Finally, different multi antenna configurations (SISO, SIMO, MISO and MIMO) are selected for TR validation in the indoor environment and the RC. Different TR properties are analyzed and compared to that of a single-input single-output (SISO) TR system.

## 2.2 Simulation Approach for TR Validation

### 2.2.1 Description of Used Channel Model

Before entering the details for the validation of the TR scheme with simulation approach, the channel model used for the validation is described in the following. Since Saleh and Valenzuela [38] proposed their model for UWB channel in 1987, a lot of work has been done after that which is almost always based on the SV model. The research on UWB channel geared up especially after 2002 when FCC allowed a license free communication with UWB signals. IEEE 802.15.3a model was proposed followed by IEEE 802.15.4a standard model for UWB signals which provided the modeling of attenuation and delay dispersion [39]. Both of these models are based on the initial SV model. The difference from the original SV channel model is that the number of clusters in the IEEE 802.15.4a standard model is considered to be a stochastic variable rather than a constant. We have used IEEE 802.15.4a standard model for the validation of the TR scheme.

#### 2.2.1.1 Channel Model

The impulse response (in complex baseband) for both SV and IEEE models is given as:

$$h(t) = \sum_{l=1}^L \sum_{k=1}^K a_{k,l} \exp(j\phi_{k,l}) \delta(t - T_l - \tau_{k,l}) \quad (2.1)$$

where  $L$  is the total number of clusters,  $K$  is the number of multi-path components (MPCs) within a cluster,  $a_{k,l}$  is the coefficient of the  $k_{th}$  tap in the  $l_{th}$  cluster,  $T_l$  is the cluster arrival time for the  $l_{th}$  cluster,  $\tau_{k,l}$  is the delay of the  $k_{th}$  MPC relative to the  $T_l$ . The number of clusters is an important parameter and is assumed to be Poisson-distributed:

$$pdf_L(L) = \frac{|\bar{L}^L \exp(-\bar{L})|}{L!} \quad (2.2)$$

here  $\bar{L}$  completely characterizes the distribution. The cluster arrival times are by definition given by a Poisson process:

$$p(T_l|T_{l-1}) = \Lambda_l \exp[-\Lambda_l(T_l - T_{l-1})], \quad l > 0 \quad (2.3)$$

where  $\Lambda_l$  is the cluster arrival rate (assumed to be independent of  $l$ ). The IEEE 802.15.4a standard for the UWB channels has proposed to model the ray arrival times with a mixture of two Poisson processes to overcome the discrepancy of the classical SV model to fit for the indoor residential, indoor office and outdoor environments. The IEEE model can be written as:

$$p(\tau_{k,l}|\tau_{(k-1),l}) = \beta\lambda_1 \exp[-\lambda_1 (\tau_{k,l} - \tau_{(k-1),l})] + (\beta - 1)\lambda_2 \exp[-\lambda_2 (\tau_{k,l} - \tau_{(k-1),l})] \quad (2.4)$$

To determine power and shape of the clusters, the power delay profile (PDP) is constructed with an exponential curve within each cluster:

$$E\{|a_{k,l}|^2\} = \Omega_l \frac{1}{\gamma_l [(1 - \beta)\lambda_1 + \beta\lambda_2 + 1]} \exp(-\tau_{k,l}/\gamma_l) \quad (2.5)$$

where  $\Omega_l$  is the integrated energy of the  $l_{th}$  cluster and  $\gamma_l$  is the intra cluster decay time constant which depends linearly on the arrival time of the cluster:

$$\gamma_l \propto k_\gamma T_l + \gamma_0 \quad (2.6)$$

where  $k_\gamma$  is the increase of the decay constant with delay. The mean energy of the cluster experiences an exponential decay:

$$10 \log(\Omega_l) = 10 \log[\exp(-T_l/\Gamma)] + M_{cluster} \quad (2.7)$$

where  $M_{cluster}$  is a normally distributed variable with a standard deviation of  $\sigma_{cluster}$ . In the case of some NLOS environments (e.g. office and industrial), the shape of the power delay profile can be of a log-linear shape:

$$E\{|a_{k,l}|^2\} = (1 - \chi \cdot \exp(-\tau_{k,l}/\gamma_{rise})) \cdot \exp(-\tau_{k,l}/\gamma_1) \cdot \frac{\gamma_1 + \gamma_{rise}}{\gamma_1} \frac{\Omega_l}{\gamma_1 + \gamma_{rise}(1 - \chi)} \quad (2.8)$$

where  $\chi$  describes the attenuation of the first component,  $\gamma_{rise}$  describes the rate of PDP increase to its local maximum and  $\gamma_1$  tells the decay at the late times.

### 2.2.1.2 Channel Model Parameters

Different channel model parameters are described in the following. These parameters are obtained from [39]. A complete list of all parameters is as under:

- $PL_0$  pathloss at 1m distance
- $n$  pathloss exponent
- $\sigma_S$  shadowing standard deviation

- $A_{ant}$  antenna loss
- $\kappa$  frequency dependence of the pathloss
- $\bar{L}$  mean number of clusters
- $\Lambda$  inter-cluster arrival rate
- $\lambda_1, \lambda_2, \beta$  ray arrival rates (mixed Poisson model parameters)
- $\Gamma$  inter-cluster decay constant
- $k_\gamma, \gamma_0$  intra-cluster decay time constant parameters
- $\sigma_{cluster}$  cluster shadowing variance
- $m_0, k_m$  Nakagami m factor mean
- $\hat{m}_0, \hat{k}_m$  Nakagami m factor variance
- $\tilde{m}_0$  Nakagami m factor for strong components
- $\gamma_{rise}, \gamma_1, \chi$  parameters for alternative PDP shape

The parameters for different indoor environments for both LOS and NLOS configurations are tabulated in TABLE 2.1

### 2.2.1.3 Properties of Channel Impulse Response

The PDP gives the intensity of a signal received through a multi-path channel as a function of time delay. It is easily measured empirically and can be used to extract certain channel's parameters such as the delay spread. The APDcP of a signal is a measure of how quickly the average power of the signal decays to an arbitrarily low level. It also gives an indication of the delay spread of the signal. APDcP of a CIR is more than just an indication of the delay spread of the CIR. It helps to understand the propagation channel and the measurement configuration. The pattern in which the power decays is an interesting observation. For LOS configurations, generally the power decays sharply at the start and then the decay rate slows down whereas in NLOS configurations, the decay rate is generally constant. Based on the channel models described in the Section 2.2.1, a sample PDP of an arbitrary channel and the average power decay profile (APDcP) of 100 channels in different configurations are compared in FIG. 2.1, FIG. 2.2 and FIG. 2.3. The PDP and APDcP are plotted in three different indoor environments (residential, office and industrial) with both LOS and NLOS configurations.

In NLOS configuration, a lot more multipath components (MPCc) are received. In LOS configurations, a significant difference can be observed in the APDcP. The APDcP decays rapidly at the start showing the difference in the received power for the direct path and the other paths. After few nano-seconds, the APDcP decays

Parameters	Residential		Office		Industrial	
	LOS	NLOS	LOS	NLOS	LOS	NLOS
Path loss						
$PL_0$	43.9	48.7	35.4	57.9	56.7	56.7
$n$	1.79	4.58	1.63	3.07	1.2	2.15
$\sigma_S$	2.22	4.51	1.9	3.9	6	6
$A_{ant}$ (dB)	3	3	3	3	3	3
$\kappa$	$1.12 \pm 0.12$	$1.53 \pm 0.32$	0.03	0.71	-1.103	-1.427
Power delay profile						
$\bar{L}$	3	3.5	5.4	1	4.75	1
$\Lambda$ (1/ns)	0.047	0.12	0.016	NA	0.0709	NA
$\lambda_1$ (1/ns)	1.54	1.77	0.19	NA	NA	NA
$\lambda_2$ (1/ns)	0.15	0.15	2.97	NA	NA	NA
$\beta$	0.095	0.045	0.0184	NA	NA	NA
$\Gamma$ (ns)	22.61	26.27	14.6	NA	13.47	NA
$k_\gamma$	0	0	0	NA	0.926	NA
$\gamma_0$	12.53	17.50	6.4	94	0.651	NA
$\sigma_{cluster}$ (dB)	2.75	2.93	NA	NA	4.32	NA
Small scale fading						
$m_0$ (dB)	0.67	0.39	0.42	0.50	0.36	0.30
$k_m$	0	0	0	0	0	0
$\hat{m}_0$ (dB)	0.28	0.32	0.31	0.25	1.13	1.15
$\hat{k}_m$	0	0	0	0	0	0
$\tilde{m}_0$	NA	NA	NA	NA	12.99	NA
$\chi$	NA	NA	NA	0.86	NA	1
$\gamma_{rise}$	NA	NA	NA	15.21	NA	17.35
$\gamma_1$	NA	NA	NA	11.84	NA	85.36

Table 2.1: Channel model parameters for residential, office and industrial indoor environments

slowly and gradually to reach a level of  $-40$  dB. In the residential environment, the APDcP takes significantly longer time to decay to  $-40$  dB level in NLOS than the LOS configuration (see FIG. 2.1). In the office environment, even in the LOS configuration, a large number of MPCs is observed. The APDcP takes a little longer time in NLOS to decay to  $-40$  dB level than LOS configuration (see FIG. 2.2). The industrial environment gives some very interesting results. In the LOS configuration, the MPCs other than the direct paths are significantly attenuated than the direct path. The APDcP is attenuated to  $-20$  dB within 10 ns. However, after that the profile decays slowly and takes almost 80 ns to reach  $-40$  dB level. In the NLOS

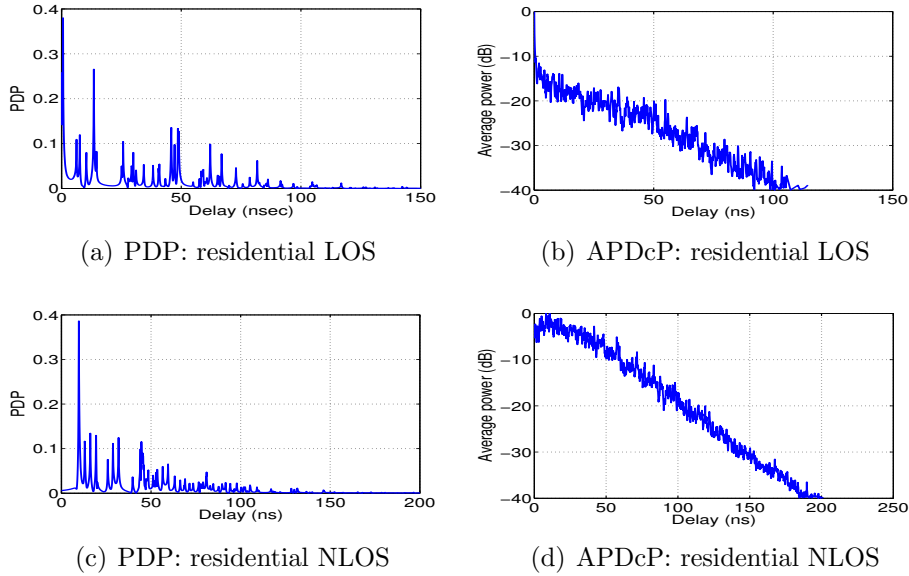


Figure 2.1: Power Delay Profiles and Power Decay Profiles for CIRs in LOS and NLOS configuration for an indoor residential environment

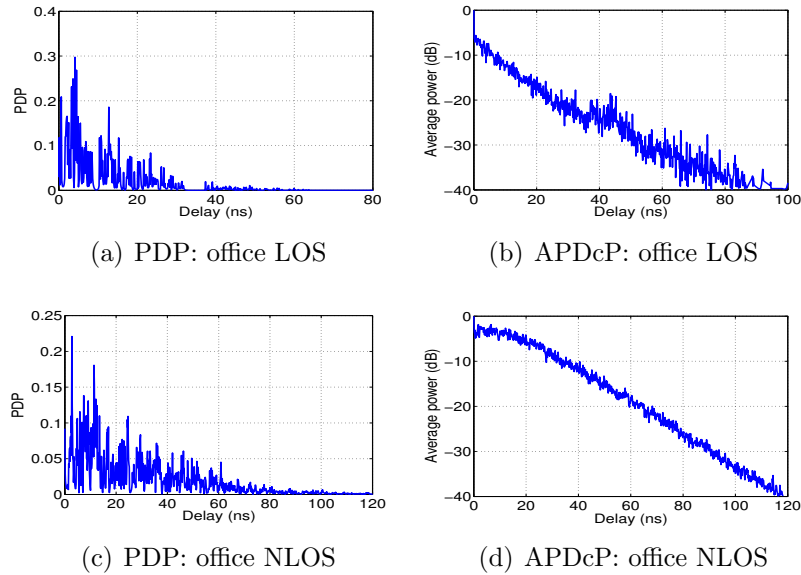


Figure 2.2: Power Delay Profiles and Power Decay Profiles for CIRs in LOS and NLOS configuration for an indoor office environment

industrial environment, large number of MPCs is observed and the PDP has a very large delay spread. More than 800 ns are required to decay to  $-40$  dB level. One more interesting observation in the APDcP of the industrial environment is that the maximum average power is not observed at the origin but after a few nano-seconds

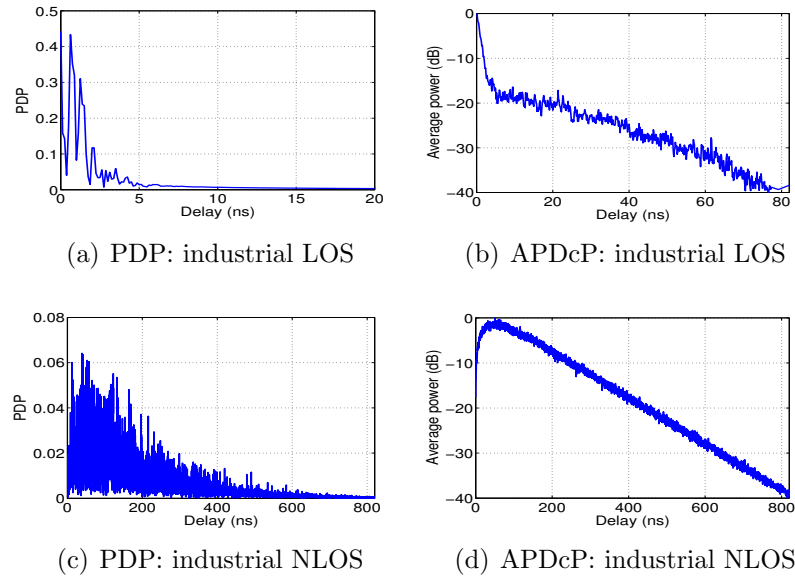


Figure 2.3: Power Delay Profiles and Power Decay Profiles for CIRs in LOS and NLOS configurations for the industrial environment

(see FIG. 2.3), suggesting that the first received MPC is not usually the strongest MPC.

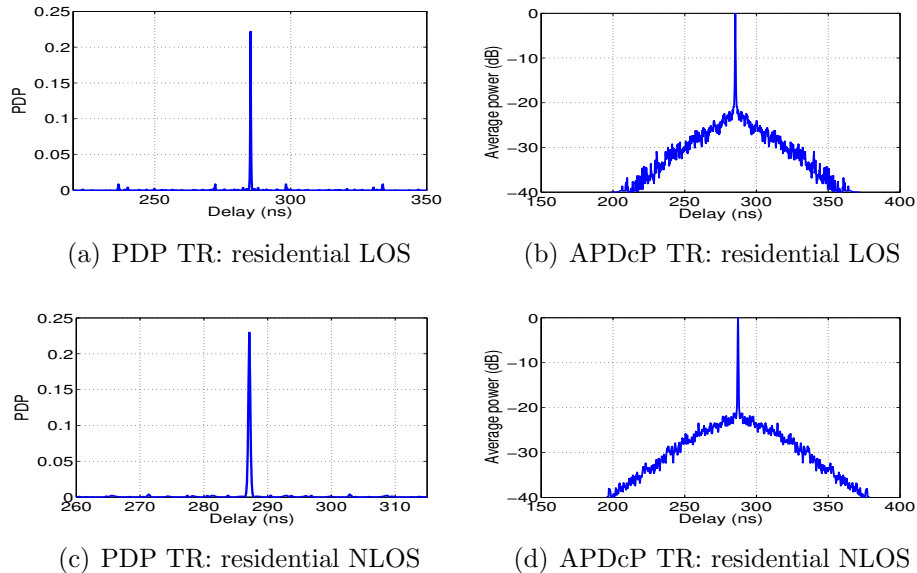


Figure 2.4: Power Delay Profiles and Power Decay Profiles for TRRs in LOS and NLOS configuration for an indoor residential environment

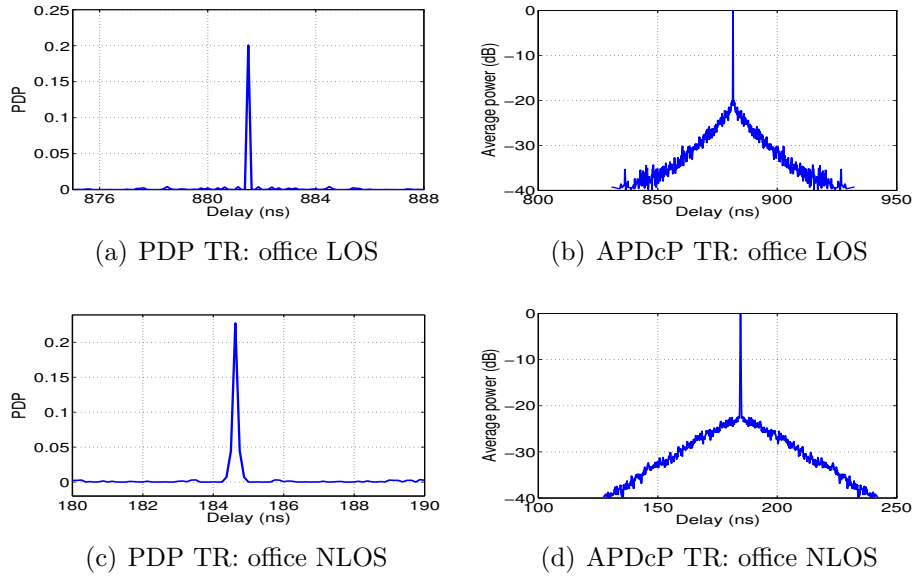


Figure 2.5: Power Delay Profiles and Power Decay Profiles for TRRs in LOS and NLOS configuration for an indoor office environment

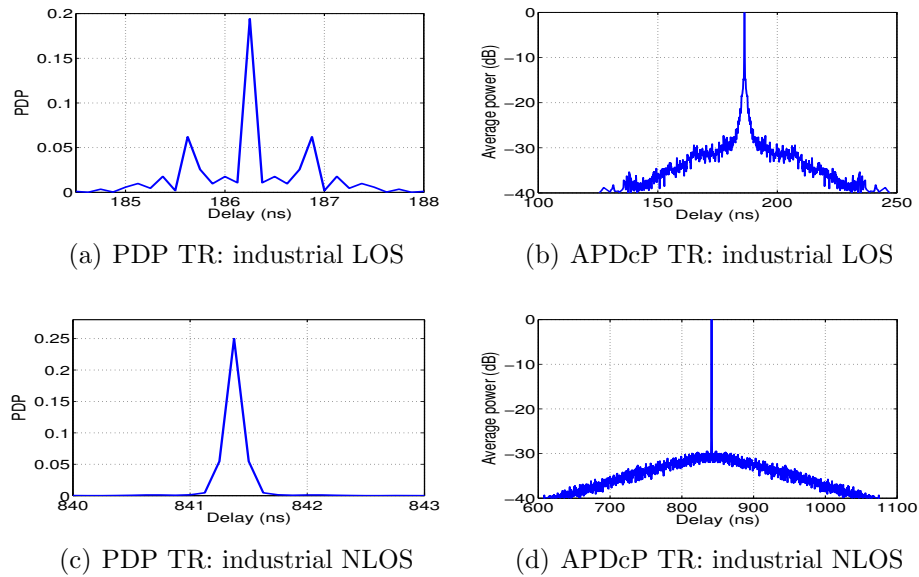


Figure 2.6: Power Delay Profiles and Power Decay Profiles for TRRs in LOS and NLOS configurations for the industrial environment

## 2.2.2 TR Validation with Existing Channel Models

The TR validation with the existing model is simulated by the impulse responses acquired by the IEEE 802.15.4a channel models [39]. The time reversed version of the

CIR is transmitted in the same channel to acquire the noiseless TR received signal. FIG. 2.4, FIG. 2.5 and FIG. 2.6 show the PDP and the APDcP of the TRRs for the three indoor environments. It can be seen that the received signal is very focused in time. These signals are not normalized to the equal transmitted power, therefore, the received power cannot be compared. One important observation is that the average power decays very quickly at the start and then decays slowly to  $-40$  dB threshold level. Another important observation is that, higher the number of MPCs in the PDP of the channel, the better is TRR. In residential environment, both LOS and NLOS configurations give similar performances but, side lobes are fewer and weaker in case of NLOS configuration. Both LOS and NLOS configurations have a similar APDcP. They take almost same amount of time to decay to  $-40$  dB threshold level (see FIG. 2.4). In the office environment, the NLOS configuration again has lesser and weaker side lobes. The presence of the side lobes in the PDP of the LOS configuration can be observed for LOS configuration while the NLOS APDcP has no significant side lobe (see FIG. 2.5). In industrial environment, large number of MPC is present in the PDP of the CIR in NLOS configuration while very few MPCs are there for LOS configuration. Significant side lobes can be observed in the PDP for LOS configuration. In case of NLOS configuration, MPCs help to build a strong main peak in the TRR. The TRR for the industrial NLOS environment results in a TRR of very good quality. There are hardly any side lobes in the PDP of the TRR in NLOS. The APDcP decays to  $-30$  dB within  $50$  ns and then decays slowly to  $-40$  dB threshold level(see FIG. 2.6).

The time taken by the average power to decay to  $-40$  dB threshold level and  $-30$  dB level is summarized in TABLE 2.2 for both CIRs and the TRRs. Decay times for the CIR and TRR are denoted by  $\tau_{dec,CIR}^{-40\text{ dB}}$  and  $\tau_{dec,TR}^{-40\text{ dB}}$  respectively for a  $-40$  dB threshold level. In residential LOS environment, the TRR takes larger time than the CIR to decay to  $-40$  dB and  $-30$  dB threshold levels. In residential NLOS environment,  $\tau_{dec,TR}^{-40\text{ dB}}$  and  $\tau_{dec,TR}^{-30\text{ dB}}$  are lesser than  $\tau_{dec,CIR}^{-40\text{ dB}}$  and  $\tau_{dec,CIR}^{-30\text{ dB}}$  respectively. The results suggest that  $\tau_{dec,TR}^{-30\text{ dB}}$  is significantly lower than  $\tau_{dec,CIR}^{-30\text{ dB}}$ , whereas  $\tau_{dec,TR}^{-40\text{ dB}}$  is mostly comparable and in some cases larger than  $\tau_{dec,CIR}^{-40\text{ dB}}$  except industrial NLOS environment for which  $\tau_{dec,TR}^{-40\text{ dB}}$  is significantly lower than  $\tau_{dec,CIR}^{-40\text{ dB}}$ . Largest time compression is observed for industrial NLOS environment, where  $\tau_{dec,TR}^{-30\text{ dB}}$  is lesser than  $\tau_{dec,CIR}^{-30\text{ dB}}$  by a factor of 12.

### 2.2.3 TR Validation with TD-TLM Simulations

We introduce a three dimensional electromagnetic approach to the modeling of TR technique. Time-domain transmission line matrix (TD-TLM) method is used for the computation of the channel response in a rich scattering environment. The time reversed version of the computed channel response is used as the source signal of the transmitting antenna. The electromagnetic solution is repeated to study the characteristic of the TR scheme.

Channel Environment	$\tau_{dec,CIR}^{-40\text{ dB}} (ns)$	$\tau_{dec,TR}^{-40\text{ dB}} (ns)$	$\tau_{dec,CIR}^{-30\text{ dB}} (ns)$	$\tau_{dec,TR}^{-30\text{ dB}} (ns)$
residential LOS	114.5	174	79.6	94
residential NLOS	201.25	183.5	152.8	99.5
office LOS	126.6	101.75	74.37	31.75
office NLOS	118.12	114.75	93.75	52.25
industrial LOS	82.7	121.5	62.75	42.25
industrial NLOS	840.75	469	655.37	54.5

Table 2.2: Time Reversal characteristics with different measurement configurations

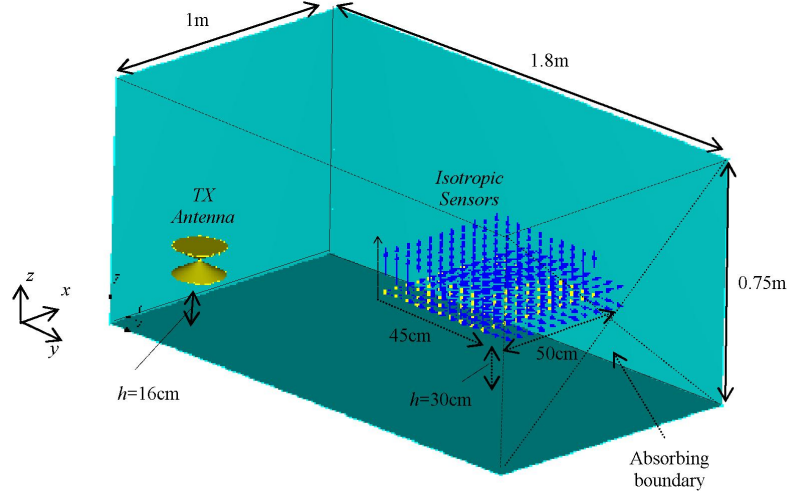


Figure 2.7: Simulation setup

### 2.2.3.1 Simulation Setup

FIG. 2.7 shows the modeled environment which has the dimensions of  $1.8\text{ m} \times 1\text{ m} \times 0.75\text{ m}$ . The dimensions are kept small to minimize the simulation time and memory. In the selected environment, all faces are metallic except the indicated face that is selected as an absorbing boundary. Such an environment is selected to study the performance of TR scheme in the presence of both reflective and absorbing boundaries. Furthermore, such a selection also reduces the delay spread of the signals and consequently the simulation time. The chamber is fed by a vertically polarized bi-conical antenna located at the lower left side,  $16\text{ cm}$  over the floor and  $20\text{ cm}$  distance from the walls. The antenna dimensions are optimized to cover the frequency range of  $0.5 - 3\text{ GHz}$  with a good free space impedance matching. To simulate the receiver, an array of  $11 \times 10$  ideal isotropic sensors is selected at the height of  $30\text{ cm}$  from the floor.

Three-dimensional TD-TLM code is used for the solution of Maxwell equations in the propagation environment. The transmitting antenna is excited by a short pulse

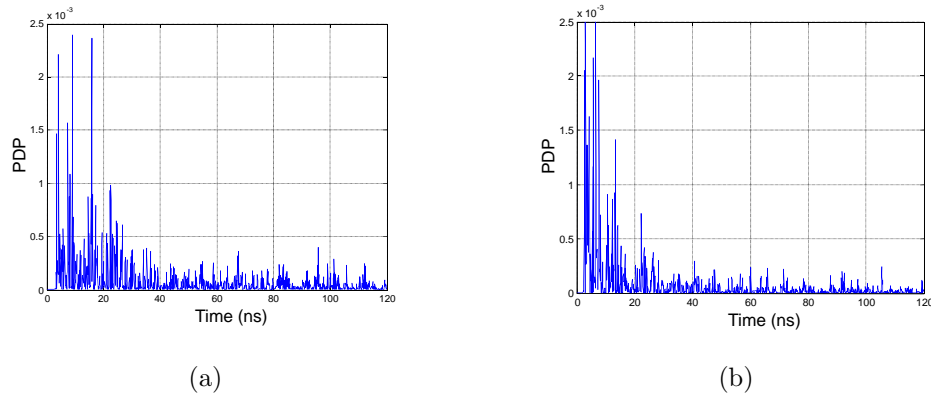


Figure 2.8: Normalized PDP of the CIR with TD-TLM simulation at a) corner of the rectangular surface b) center of the rectangular surface

with a spectrum that has a 10 *dB* bandwidth of 0.5 – 2.5 *GHz*. The channel response between the transmitting antenna and the receiving virtual sensors are simulated. The received waveforms for all polarization components on the virtual locations are extracted. The simulation uses 433878 number of cells and has an allocated memory of 57 *MB*. The simulation time is in the order of 15 minutes. Time-domain solution based on TLM code has the features of fast computation time and small allocated memory.

### 2.2.3.2 Simulation Results

The noise-free instantaneous power delay profile (PDP) at two different locations, i.e. at the center and the corner of the rectangular surface is shown in FIG. 2.8. It can be seen that the modeled environment is very dispersive and the channel responses are significantly different. The transmitted signal is *z*-polarized but due to the reflection of the wave from the metallic walls and the chamber corners, the received field at the rectangular surface has all polarization components. We have observed that the average power of *z*-polarization component is 2.5 and 1.5 times more than the average power of *x*- and *y*-polarizations respectively.

In the second simulation step, the computed *z*-polarized waveform at the center of the rectangular surface is selected for TR simulation. The model achieved in the last step is used and the electromagnetic simulations are repeated by introducing the novel waveform at the antenna excitation port. FIG. 2.9 shows the received instantaneous PDP with the TR scheme at the selected location. As expected, the simulated TRR is quite compressed in time.

To compare the characteristics of the simulated TRR, total excited signal power for the simulation of the CIR and TRR is normalized to a constant. A FG of 14 *dB* is observed for the simulated environment. The SSR of the time compressed signal is 6 *dB*. FIG. 2.10 shows the instantaneous PDP of the TR channel at the in-

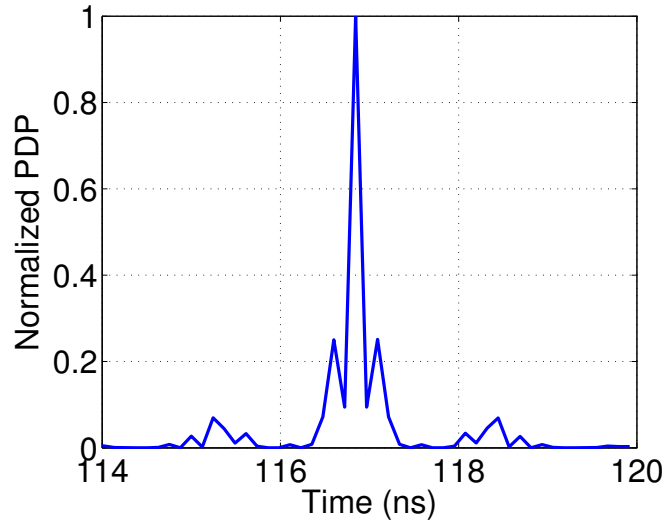


Figure 2.9: Normalized PDP of the TRR with TD-TLM simulation

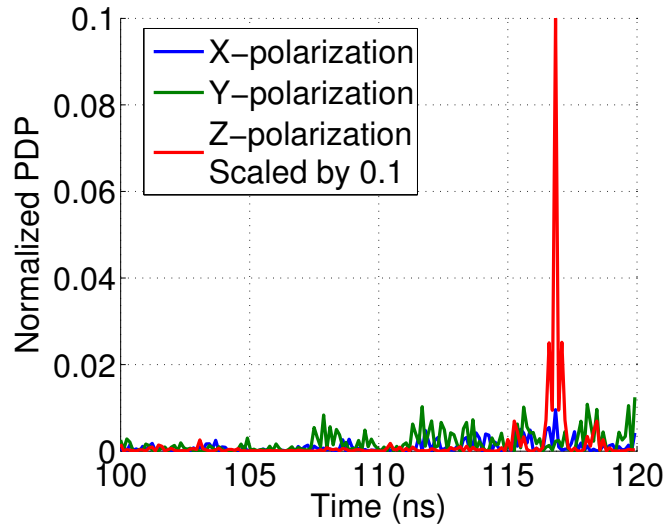


Figure 2.10: Normalized peak power with the TR scheme in a square surface with TD-TLM simulation

tended location for different polarizations, x, y and z. For the sake of comparison, the PDP of z-polarization is scaled by 0.1. As shown, the peak power with the intended polarization (z-polarization) is extremely large than the other polarization components. This result shows the possibility to imply polarization diversity in multiple antenna configuration for example, TR multiple-input single-output (TR-MISO) or TR multiple-input multiple-output (TR-MIMO) systems.

Spatial focusing is another inherent property of the TR scheme. This means that the spatial profile of the power peaks at the intended location and decays rapidly away

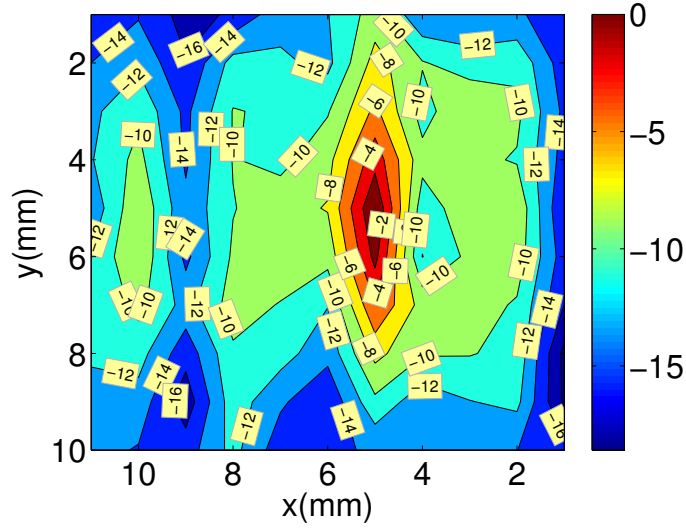


Figure 2.11: Normalized PDP with the TR scheme with TD-TLM simulation for x, y and z polarizations

from it. To illustrate this property, the received peak power is computed as a function of space. The intended signal is at the center of the rectangular surface. The signal for the intended signal is transmitted and the received signal is measured over whole of the rectangular surface. FIG. 2.11 shows the 2-D plot of the normalized received peak power (normalized to the peak power at the intended receiver) over the given surface. As shown, the maximum spatial focusing gain is generated at the intended location and the gain decreases non-symmetrically in x and y-axis directions away from it. The focusing zone is more concise in x-axis direction compared to y-axis direction due to the presence of two metallic walls of the chamber in x-axis direction which make large number of reflections. On the other hand, in y-axis direction, the reflections are limited by the absorbing boundary. This find may be applicable to determine the field angle of arrivals in multi-path propagation environments.

## 2.3 Semi Measurement Approach for TR Validation

In the Section 2.2.2, the validation of the TR scheme with the existing models was explained. The second type of validation involves some experimentation. The procedure of the validation has two steps. In the first step, the frequency responses of a typical indoor channel are measured using frequency domain equipment. To observe the spatial focusing property of the TR, the measurements are performed for varying positions of the receiver over a rectangular surface. A vector network analyzer

is used to measure the frequency responses. Thereafter in the second step, a TR communication is simulated through MATLAB.

### 2.3.1 Experimental Setup

Experiments are performed in a typical indoor environment. The environment is an office space of  $14\text{ m} \times 8\text{ m}$  in the IETR<sup>(1)</sup> laboratory. FIG. 2.12 shows the measurement layout in a typical indoor environment of IETR lab. The frequency response of the channel in the frequency range of  $0.7 - 6\text{ GHz}$  is measured using vector network analyzer (VNA) with a frequency resolution of 3.3 MHz. Two wide-band conical mono-pole antennas (CMA) are used in a non line of sight (NLOS) configuration. The height of the transmit antenna and the receive antenna is 1.5 m from the floor. The receiver antenna is moved over a rectangular surface ( $65\text{ cm} \times 40\text{ cm}$ ) with a precise positioner system. Respective spatial resolution of  $2.5\text{ cm}$  and  $5\text{ cm}$  is used for the x-axis and y-axis of the horizontal plane. Thus 243 ( $27 \times 9$ ) measurements are taken over the rectangular surface. The frequency responses between the transmitting antenna and receiving virtual array (of 243 antennas) are measured. The time domain CIRs are computed using the inverse fast Fourier transformation (IFFT) of the measured frequency responses.

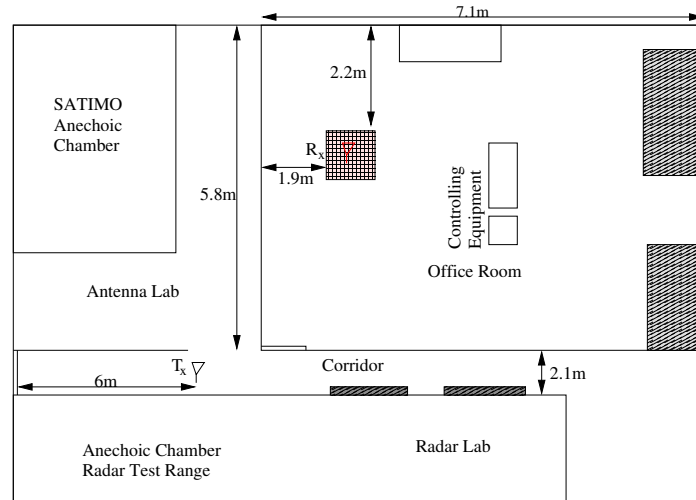


Figure 2.12: Measurement layout for the measurement in an indoor environment

### 2.3.2 Spatial Focusing in an Indoor Environment

Once the CIR of 243 channels has been recovered, TR scheme is validated through MATLAB and different TR characteristics are compared. One of the interesting properties of TR scheme is the spatial focusing of the TR. As the channels de-correlate

<sup>(1)</sup>Institute of Electronics and Telecommunications of Rennes

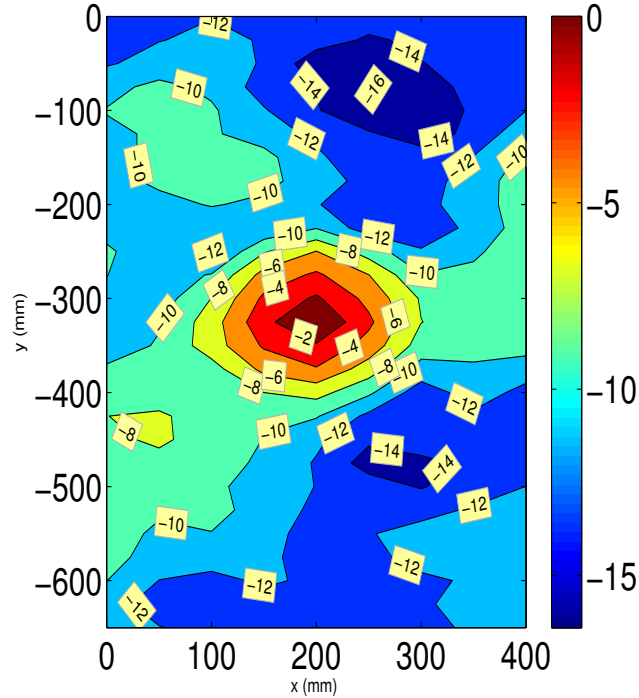


Figure 2.13: Normalized TR received peak power over a rectangular surface in an indoor environment

very quickly in space and the transmitted signal of the TR scheme is pre-coded by the time reversed version of the CIR, the spatial focusing of the TR received signal is linked with the channel de-correlation in space.

FIG. 2.13 shows the received peak power of the TR received signal in an indoor environment over a rectangular surface when the intended signal is for the receiver at the center of the rectangle. The received power is normalized to the received power of the intended receiver. The received power has decreased by 10 dB for only 10 cm movement of the receiver. The inherent spatial focusing property of the TR scheme has its advantages and disadvantages. For the application where secure communication is required between stationary transmitter receiver pair, the spatial focusing of the TR scheme makes it an ideal scheme for such applications. The channel between the transmitter and the receiver acts as a unique code for the transmitter receiver pair. Any non intended receiver at a location other than the intended receiver will receive a noise like signal. Thus, the transmitter and the receiver can communicate with very low probability of detection and probability of interception. However, the dependence of the transmitted signal on the channel makes it a relatively complex transmission scheme for mobile communication. As soon as the receiver changes its position, the TR scheme cannot communicate with the receiver and fresh estimation of the channel is required.

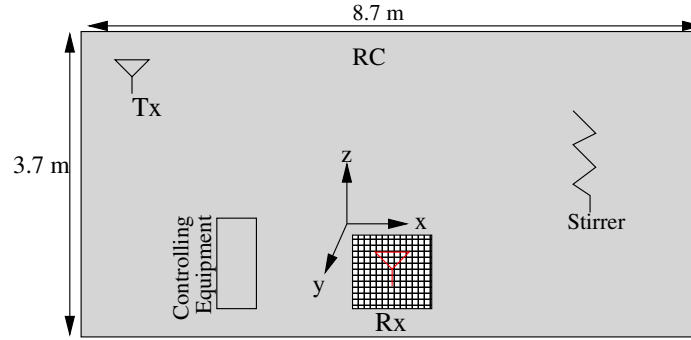


Figure 2.14: Measurement layout for measuring the frequency responses in a RC

### 2.3.3 Effects of Bandwidth on Spatial Focusing of the TR Scheme

Spatial focusing is one of the inherent properties of the TR scheme. It is interesting to note whether use of different bandwidths affects the spatial focusing of the TR scheme. To verify the effects of different bandwidths on the spatial focusing, a measurement campaign is carried out in the RC. The CIR is measured by using the frequency domain equipment (VNA) in a reverberation chamber for a frequency range of 0.7 to 5 GHz.

#### 2.3.3.1 Experimental Setup

Experiments are performed in the RC having dimensions of  $8.7m \times 3.7m \times 2.9m$ . FIG. 2.14 shows the measurement layout in the RC present inside the IETR laboratory. The frequency response of the channel in the frequency range of 0.7 – 5 GHz is measured using vector network analyzer (VNA) with a frequency resolution of 2.7 MHz. Two wide-band conical mono-pole antennas (CMA) are used for the measurements. The height of the transmit antenna and the receive antenna is 1.5 m from the floor. The receiver antenna is moved over a rectangular surface ( $40\text{ cm} \times 40\text{ cm}$ ) with a precise positioner system with a spatial resolution of 5 cm. Thus 81 ( $9 \times 9$ ) measurements are taken over the square surface. The frequency responses between the transmitting antenna and receiving virtual array (of 81 antennas) are measured. The time domain CIRs are computed using the inverse fast Fourier transformation (IFFT) of the measured frequency responses.

#### 2.3.3.2 Bandwidth Effects

Once the CIRs are extracted from the measured frequency responses, the TRRs are simulated by making use of MATLAB. The bandwidth of the signals are varied in two ways; in the first case the lower frequency ( $f_L$ ) is kept constant and the bandwidth is increased by increasing the upper frequency ( $f_U$ ), whereas in the second case, the center frequency ( $f_C$ ) of the band is kept constant and bandwidth of the signal is

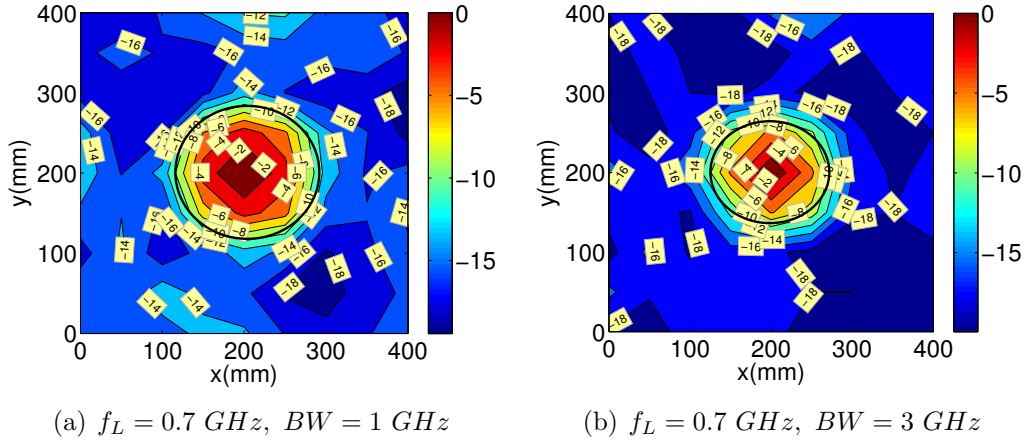


Figure 2.15: Normalized peak power with the TR scheme in a square surface with different bandwidths (BW) but constant lower frequency ( $f_L$ )

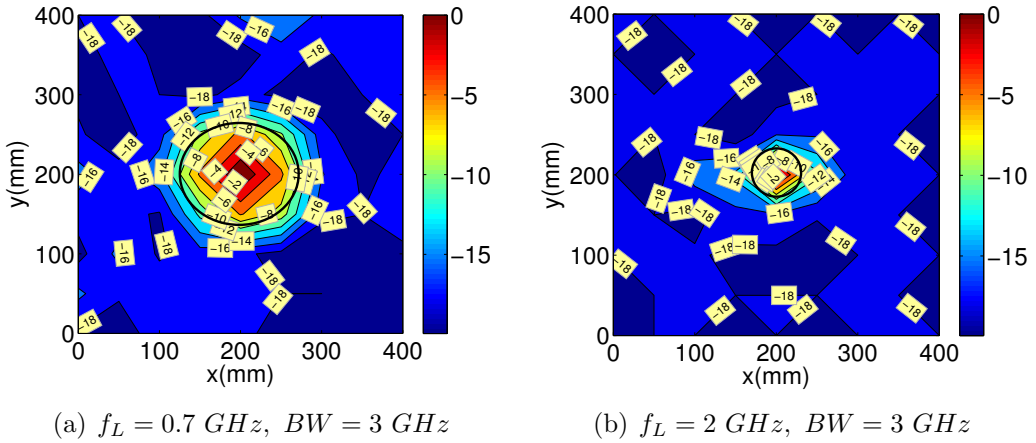


Figure 2.16: Normalized peak power with the TR scheme in a square surface with a constant bandwidth (BW) of  $3 \text{ GHz}$  but different lower frequencies ( $f_L$ )

increased symmetrically on both sides  $f_C$ . To compare the spatial focusing property of the TR scheme, we suppose that the intended receiver is the receiver at the center of the square. The signal intended for the center receiver is transmitted and the received signal is measured over whole square. Thereafter, the received peak power over a square surface is compared with the received peak power of the intended receiver. The received peak powers are normalized to the received peak power at the center of the square. FIG. 2.15 compares the spatial focusing property of the TR scheme for bandwidths of  $1 \text{ GHz}$  and  $3 \text{ GHz}$  but for a constant  $f_L$  of  $0.7 \text{ GHz}$ . The dimension of focusing zone does not decrease a great deal.

FIG. 2.16 compares the spatial focusing property of the TR scheme for a constant bandwidth of  $3 \text{ GHz}$  but with lower frequencies of  $0.7 \text{ GHz}$  and  $2 \text{ GHz}$ . In this case,

the dimension of the focusing zone decreases significantly with the increase in the lower frequency. The experimental results suggest that the dimension of the focusing zone is controlled by  $f_L$ . For higher values of  $f_L$ , a small focusing zone can be observed even if the bandwidth is not too large. On the other hand, for lower values of  $f_L$ , little increase in the focusing gain is observed even with a large increase in the signal bandwidth.

## 2.4 Full Measurement Approach for TR Validation

A time domain validation of the TR scheme is performed by making use of an arbitrary waveform generator (Tektronix AWG 7052) and a high speed digital storage oscilloscope (Tektronix DSO 6124C). For this purpose, measurements are carried out in a typical indoor office environment.

### 2.4.1 Experimental Setup

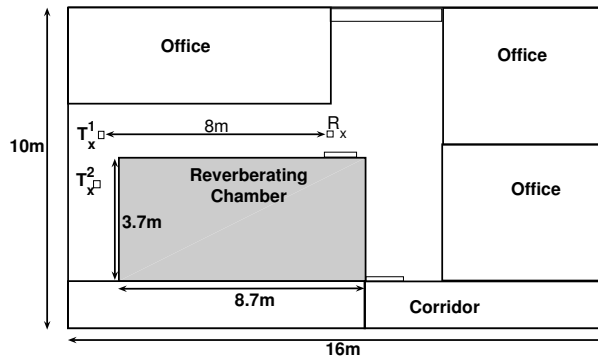


Figure 2.17: Measurement environment layout

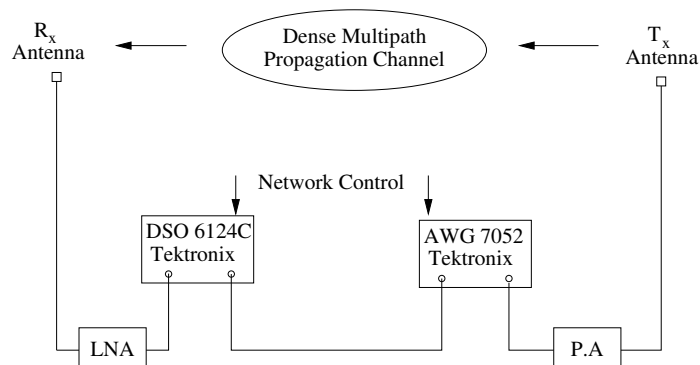


Figure 2.18: Experimental Setup

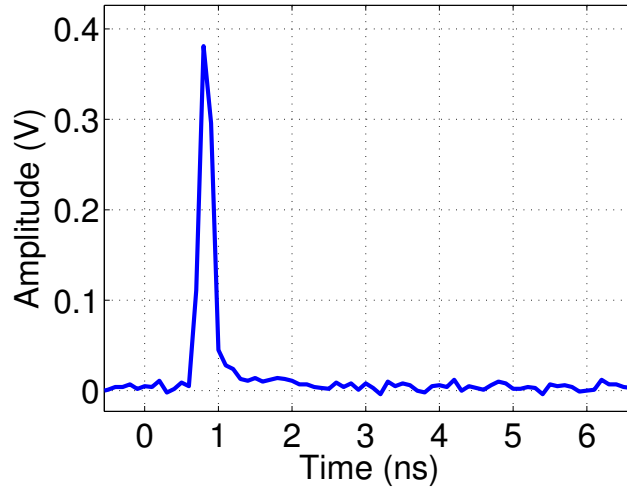


Figure 2.19: Channel sounding pulse

To evaluate the performance of time reversal in indoor propagation channel, an experimental setup is established in a typical indoor environment (IETR laboratory) having the plan shown in FIG. 2.17. All rooms are furnished with office equipments: tables, PCs and seats. Moreover, there is a large reverberating chamber in the laboratory, which increases the wave reflections in the environment. The experimental setup is shown in the Fig. 2.18. Two conical mono-pole antennas (CMA-118/A), are used as the transmitter and the receiver. The distance between the transmitter and the receiver is 8 m in LOS environment and 8.35 m in NLOS while the height is 1 m from the ground.

### 2.4.2 Validation Procedure

The pulse is generated with an AWG which has a maximum sampling rate of 5 GS/s. Because of such a high sampling rate, an extremely narrow channel sounding pulse with a power spectrum of DC-2.7 GHz and a rise time of 200 ps is generated with the AWG. FIG. 2.19 shows the transmitted pulse having a very sharp rise time and extremely spread spectrum. The output signal of the AWG is amplified to a level to drive the power amplifier (PA), Mini-Circuits ZHL-42. The given PA provides a constant gain of 30 dB and covers the frequency range of 700 – 4200 MHz. The amplified signal is transmitted with an ultra wide-band CMA antenna having a frequency range of 0.7 – 18 GHz. Therefore, the effective bandwidth of the transmitted pulse is 0.7 – 2.7 GHz. At the receiver end, the received signal is amplified by an ultra wide-band low noise amplifier (LNA) that covers the frequency range 0.1 – 12 GHz having a gain of 34 dB. The amplified RF signal is attenuated by 17 dB and is sampled and stored by using a DSO with a maximum sampling rate of 40 GS/s. To further suppress the effects of the additive noise from the received signals, the DSO

is operated in average acquisition mode and a common trigger signal is used to synchronize the AWG and the DSO. In the average acquisition mode, multiple measures of the received signals are conducted and then averaged together. The number of measurements for the averaging process improves the quality of the signal at the receiver. In our case, the received signals are averaged 1028 times to reduce the noise considerably. The selected sampling rate of the DSO is 20 GS/s which results in a delay resolution of 0.05 ns. The acquisition time for operating in the average mode for the delay of 400 ns is in the order of few seconds. It is assumed that the channel remains quasi-static during this time interval.

### 2.4.3 Comparison of Measured Channel Response in Different Measurement Configurations

Different propagation scenarios are accomplished by either changing the environment scenario i.e. LOS or NLOS or by changing the antenna polarization i.e. co-polar or cross-polar. The results on the time domain validation of TR scheme have been published or presented in [1]. The influence of these measurement configurations on measured channel responses (MCR) and on the TRR is studied. In all measurements, two CMAs are used as a transmitter receiver pair. The conical monopole antenna provides good impedance matching (return loss  $< -10$  dB) for the frequency range 0.7 – 8 GHz. The radiation pattern of the antenna is approximately omni-directional with a constant phase center. The constant phase center makes the antenna pattern independent of the frequency. For the LOS measurements, the transmitting antenna is installed at the  $T_x^1$  position and for the NLOS configuration, the transmitting antenna is placed behind the metallic chamber ( $T_x^2$ ) to avoid the direct visibility between the antennas (see FIG. 2.17). In the measurements with the co-polar orientation, the transmitting and the receiving antennas are both vertically polarized. In the cross-polar orientation, the transmitting antenna is vertically polarized whereas the receiving antenna is horizontally polarized.

To measure the channel response, a narrow ultra wide-band pulse with a spectrum in the frequency range 0.7 – 2.7 GHz is transmitted in the propagation channel with the AWG. The detected signal with the DSO gives us the MCR. This MCR is then filtered with a rectangular band-pass filter (BPF) for the specified frequency range to eliminate the out-of-band spurious signals. The static power delay profile (PDP) of the MCR ( $|h(t)|^2$ ) with different measurement configurations are illustrated in FIG. 2.20. Because of the wave diffraction and reflections from the propagation channel, the received waveforms are spread in the delay time. The LOS co-polar configuration has the least number of multi-paths and the highest received power. The NLOS cross-polar configuration has the largest number of multi-paths and the least received power. For the other two configurations, both the number of multi-paths and the received power are somewhere in between. The RMS delay spread for the PDP of the MCR ( $\sigma_\tau^{MCR}$ ) in different measurement configurations is tabulated in TABLE 2.3. The delay spread is increased for LOS channel with the antennas in cross-polar orientation.

The reason is the suppression of the direct coupling between the antennas, thus the received signal is most constructed by the multi-path portion of the incident field instead of the LOS path. In the case of NLOS channel, the change in the polarization of the antennas only slightly modifies the RMS delay spread.

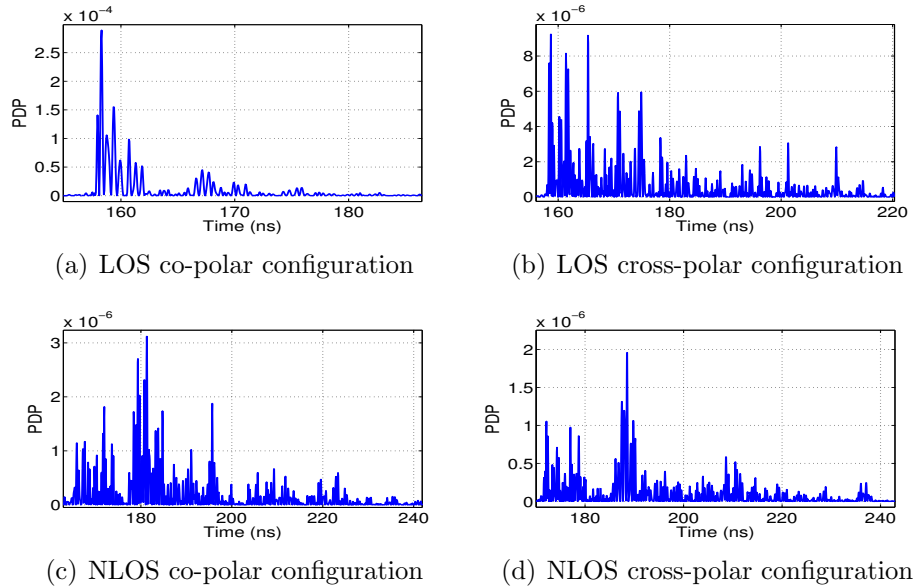


Figure 2.20: Power Delay Profiles of the CIRs in LOS and NLOS configurations in a typical indoor office environment

In any communication system, the average signal energy at the receiver is reduced due to the propagation loss, impedance mismatching of the antennas, and the multi-path fading. The measured power loss (PL) for different measurement configurations is tabulated in TABLE 2.3. In NLOS configurations, the PL is the largest and effect of the antenna polarization in the order of 3 dB is observed. The strongest path component at the NLOS co-polar channel is more important than the cross-polar channel (see FIG. 2.20). In LOS channel, the cross-polar orientation has 9 dB more PL than the co-polar orientation as the direct coupling between the antennas decreases considerably with cross-polar orientation.

#### 2.4.4 Comparison of different TR Properties

The time reversed signal is constructed with processing the measured channel response. First, the channel response is truncated to a length that captures 98% of the total signal energy. As the sampling rate of the DSO (20 GS/s) is larger than the maximum sampling rate of the AWG (5 GS/s), the truncated signal is resampled to construct a time reversal waveform compatible with the AWG. The resampling based on this criterion is conducted and the resulted signal is time reversed and amplified before programming on the AWG by a network data connection line. Therefore, the

TR Property	LOS		NLOS	
	co-polar	cross-polar	co-polar	cross-polar
$\sigma_{\tau}^{MCR}(ns)$	8.34	22.02	20.76	22.49
PL (dB)	16.26	25.38	29.76	32.50
NPP (dB)	0	-9.99	-14.19	-16.49
FG (dB)	7.83	12.79	13.3	13.03
SSR (dB)	3.58	4.60	3.95	4.60
IAP (dB)	7.93	5.59	6.90	7.84
$\sigma_{\tau}^{TR}(ns)$	5.39	13.53	17.07	18.10

Table 2.3: Time Reversal characteristics with different measurement configurations

channel state information (CSI) is available at the transmitter. The generated time reversed signal is amplified with the same PA and re-transmitted in the channel. The received signal at receiver gives the TRR which is measured by the DSO and then filtered with the rectangular BPF in the frequency range of  $0.7 - 2.7 GHz$ . Note that the LNA is not used in the measurement of TRRs.

FIG. 2.21 shows the measured PDP of the TRR for the specified measurement configurations. The received signal is time compressed and has a very short effective length. The width of the main lobe of the received signal is around  $0.4 ns$ . We can observe that the LOS co-polar configuration has the strongest peak but the side lobes for this configuration are also stronger than other configurations. The NLOS cross-polar configuration has the weakest main peak but the side lobes of this configuration are weaker than the other configurations. In the following, we will discuss different TR properties one by one.

The normalized peak power (NPP) acts as a core performance metric for the TR scheme. It is calculated as the TR received peak power normalized to some reference. Here the received peak powers are normalized to the LOS co-polar configuration who has the maximum received peak power. Using the measurement results, the NPP is analyzed for all configurations. The received signal peak power varies considerably depending upon the measurement configuration. The NPP for different configurations is compared in TABLE 2.3. As shown, all other configurations have considerable less NPP especially for NLOS configurations. The LOS cross-polar configuration has  $10 dB$  lesser power than LOS co-polar configurations while the NLOS co-polar and cross-polar configurations have  $14.2 dB$  and  $16.5 dB$  lesser power than the LOS co-polar configuration respectively.

Focusing gain (FG) of the TR scheme is the ratio of the strongest peak of the TR received signal to the strongest peak of the MCR. For different measurement configurations, it is evaluated while keeping the same total transmitted power for the detection of MCR and the TRR. In both cases, total transmitted power (power of the pulse and the TR waveform) is normalized to a constant. Thus, the TR waveform has smaller peak-to-peak signals but has a larger length than the short pulse. Under this criterion, the FG (defined in CHAPTER 1) for different measured configurations is

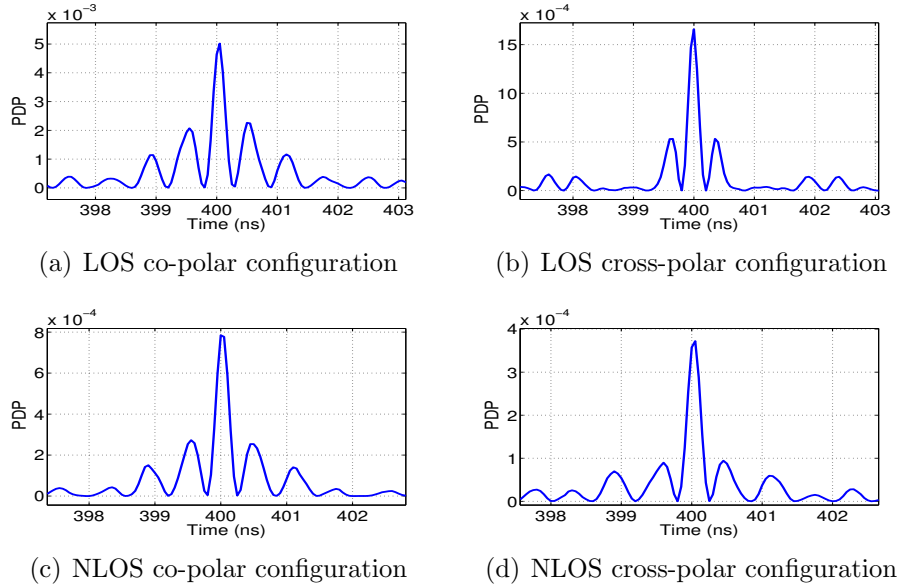


Figure 2.21: Power Delay Profiles of TRRs in LOS and NLOS configurations in a typical indoor office environment

tabulated in TABLE 2.3. In LOS co-polar configuration, a gain of  $7.8 \text{ dB}$  is observed which is the lowest as compared to the other configurations. All other configurations have a FG in the order of  $13 \text{ dB}$ . In LOS co-polar configuration, a strong main peak is received in the MCR whereas in all other configurations, the main peak is suppressed. Although the strongest peak of the TRR is  $7.83 \text{ dB}$  higher than the strongest peak of MCR in LOS co-polar configuration, but still the FG is quite lower than the other configurations. The results suggest that the FG is a result of the inherent multi-path diversity combining offered by the TR technique. Due to this gain, communication range and the signal quality of TR scheme is significantly improved. Moreover, the transmitted signal power can be reduced for a specified range and a moderate data throughput can be obtained with a longer battery life.

Using the TR scheme, the channel delay response is significantly compressed. Thus, the effects of ISI in the data communication system can be alleviated. However, for high data rate applications, the temporal side lobes can cause considerable ISI and degrade the system performance. The temporal side lobes may capture large part of the received signal energy depending on the antenna configuration and the signal bandwidth. Therefore, signal to side lobe ratio (SSR) becomes an important performance metric which is directly related to the signal to interference ratio (SIR) performance and bit error rate (BER) performance of the system. For different measurement configurations, the SSR is tabulated in TABLE 2.3. The cross-polar antenna orientations give the highest SSR whereas the LOS co-polar configuration gives the lowest value of SSR.

Another important property is increased average power (IAP). Considering the same transmitted power for the initial pulse and the TR signal, an important amelioration of the average signal power with the TR scheme is observed. The IAP for different measurement configurations is tabulated in TABLE 2.3. As shown, for different measurement configurations, an IAP in the order of 6 – 8 dB is measured with the TR scheme. Two reasons explain this observation. Firstly, the spectrum of the TR signal undergoes fading effects at some frequencies. The fading effects of the propagation scenario are already known to the transmitter, thus in the TR signal, the allocated power to the faded frequencies is reduced. Thus, with the power normalization, more power is allocated to the non-faded frequencies in the transmitted signal. Therefore, a priori knowledge of the CSI causes an increase in the received signal power. Secondly, due to the ultra wide-band transmission, the propagation loss at the higher frequencies is more significant than at the lower frequencies. Therefore, the spectrum of the TR signal has a descending shape. When the power normalization of the transmitted signal is carried out, all frequency components of the spectrum are amplified with the same manner. Therefore, the lower frequencies in the transmitted signal spectrum are emphasized as compared to the higher frequency components thus most part of the transmitted signal energy lies in the lower frequencies. When this signal passes through the channel, lower frequency band components experience less attenuation and consequently the average signal energy at the receiver is increased.

Another performance metric is the RMS delay spread of the received signal, which is not only a performance metric for the TR scheme but also a performance metric for any communication system. For any communication system, the RMS delay spread is an indicator of the frequency selectivity of the channel. If the RMS delay spread is greater than the symbol duration, the channel is likely to be selective in frequency and may introduce ISI. It is thought to be very strongly but inversely proportional to the coherence bandwidth of the channel. From the TR perspective, as the transmitter has a priori CSI, the pre-coding of time reversed MCR reduces the RMS delay spread considerably. However, it is considered as a metric for temporal compression in TR systems. TABLE 2.3 compares the RMS delay spread for the PDP of the TRRs ( $\sigma_{\tau}^{TR}$ ) for different measurement configurations. The RMS delay spread for the TRRs is considerably lower than the respective delay spread of the CIRs. The delay spread for NLOS configurations is in the order of 17 – 18 ns. The lowest value of the delay spread is observed for LOS co-polar configuration. LOS cross-polar configuration has an intermediate value of the delay spread approximately 13.5 ns.

The comparison of all these measurement configurations suggests that different configurations have different advantages and disadvantages. The LOS co-polar configuration has the maximum received peak power but the least FG and the SSR. The NLOS configurations have better FG and SSR but the received peak power is very low and they have relatively large RMS delay spreads. The LOS cross-polar configuration is a good compromise between the two. The LOS cross-polar configuration has a quite better NPP and lower delay spread than NLOS configuration and has equally good

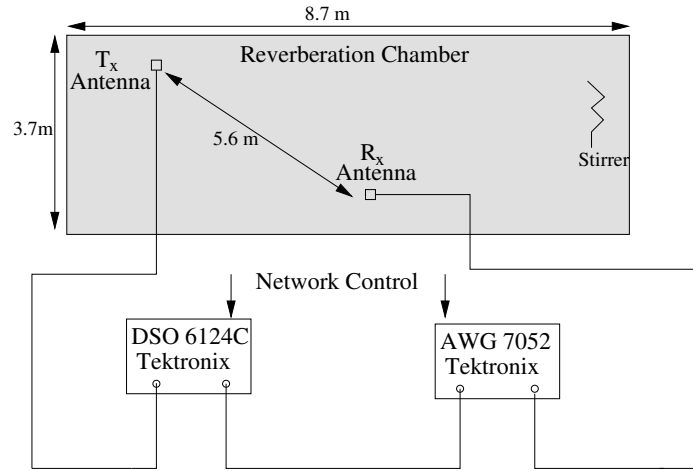


Figure 2.22: Measurement setup for the TR experiment in the reverberation chamber

FG and SSR. Therefore, for our given channel, LOS cross-polar configuration can be considered as one of the better choices of TR communication.

## 2.4.5 TR in a Reverberation Chamber

The validation of the TR scheme is also carried out in a reverberating chamber (RC). A RC is an over-sized Faraday cage with respect to the wavelength. In such an environment, an electromagnetic source generates a large number of propagation modes, resulting in a complex stationary wave pattern. This pattern may also be interpreted as a combination of plane waves or rays that are reflected with the highly conductive walls, giving a very dense multi-path environment. Stochastically, this combination may be altered with the rotation of a large metallic stirrer, which permanently modifies the field distribution in the reverberating enclosure. Over a complete rotation, it can be shown that a component of the electric field follows a Rayleigh distribution. An alternative way to stir the modes is to change the source parameters (frequency, position etc.). From a TR perspective, this rich multi-path environment favors the TR scheme but at the same time the TRR is also spread in the delay time, although the side lobes other than the main lobe are significantly weaker than the strength of the main lobe. The RC is an isolated and highly controllable test environment and can be considered as a reference environment.

### 2.4.5.1 Experimental Setup

A large RC is present inside the IETR laboratory with the dimensions of  $8.7\text{ m} \times 3.7\text{ m} \times 2.9\text{ m}$ . Measurement setup is illustrated in Fig. 2.22. A set of two conical mono-pole antennas (CMA) are used as the transmitter and receiver and are used in co-polar orientation. Note that the PA and LNA are not used at the transmission and receiving end respectively. The height of the transmitter and the receiver is  $1\text{ m}$  from

the ground. The distance between the transmitter and receiver is  $5.6\text{ m}$ . The channel sounding pulse with a rise time of  $200\text{ ps}$  (see FIG. 2.19) is generated by the AWG to measure the channel response inside the RC. The effective bandwidth of the pulse is  $0.7 - 2.7\text{ GHz}$  as explained in SECTION 2.3.1. The received signal is measured by the DSO. The DSO is operated in average mode so that 256 samples are taken and averaged together to reduce the noise in the received signal.

The PDP of the MCR in the RC is shown in FIG. 2.23. There is one strong multi-path component which can be considered as the direct path. The MCR is quite spread in delay time. The RMS delay spread of the PDP of the MCR in the RC is  $2.14\text{ }\mu\text{s}$  (see TABLE 2.4). If antennas are placed in such a manner to avoid direct path coupling, the delay spread increases further and becomes in the order of few micro seconds. The average power loss due to the wave propagation, impedance mismatching of the antennas, and the multi-path fading is observed to be  $20.2\text{ dB}$ . There are two reasons for the lesser loss than the indoor environment. First, the distance between the transmitter and the receiver is only  $5.6\text{ m}$  in the RC whereas it was around  $8\text{ m}$  in the indoor environment. Secondly, the walls of the RC have very high reflective index and absorbs very little energy, thus a lot of energy reaches the receiver from the multi-path components.

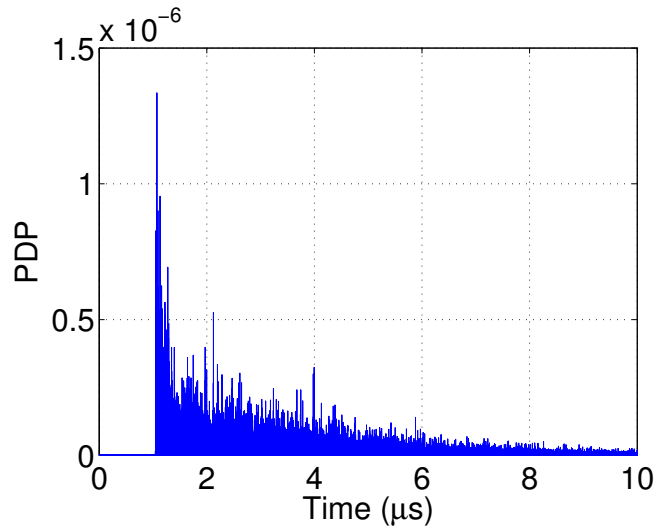


Figure 2.23: PDP of the MCR in the RC

Once the MCR in the RC is recorded, it is truncated to a length that captures 88% of the total signal energy. Furthermore, the truncated version of the MCR is down sampled to make it suitable for the generation with the AWG. The resulting signal is time reversed and amplified before programming on the AWG by a network data connection line. The generated time reversed signal is re-transmitted in the channel. The TRR which is measured by the DSO and then filtered with the rectangular BPF has a frequency range of  $0.7 - 2.7\text{ GHz}$ .

TR Property	Value
FG (dB)	23.4
SSR (dB)	4.42
IAP (dB)	3.67
PL (dB)	20.2
$\sigma_{\tau}^{MCR}(\mu s)$	2.14
$\sigma_{\tau}^{TR}(ns)$	0.65

Table 2.4: Time Reversal characteristics in a reverberation chamber

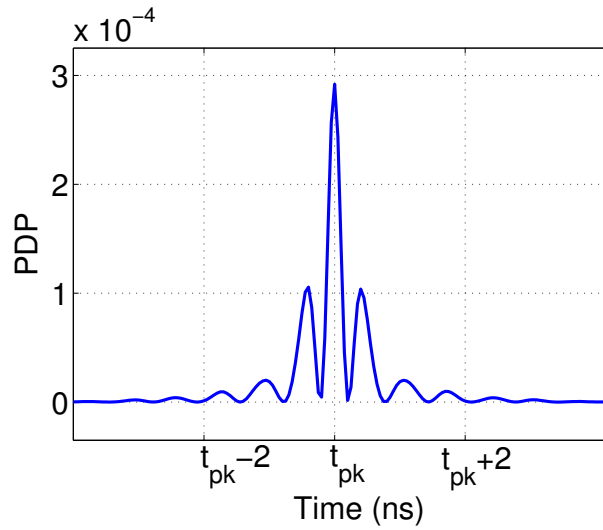


Figure 2.24: PDP of the measured TR received signal in the RC

FIG. 2.24 shows the measured PDP of the TRR in a RC. The received signal is time compressed and has a very short effective length. A delay spread of only 0.65 ns is observed. Large number of multi-paths combines to give a very strong main lobe. The secondary lobes are significantly weaker than the main lobe. TABLE 2.4 gives the values of different TR properties in the RC. As expected, by using the multi-path diversity, a very good TR performance is achieved in the RC. A FG of approximately 23.4 dB is observed whereas it was at most 13.3 dB in the indoor environment. It shows the extent to which the RC environment is conducive for the TR technique. The TR received signal has a very high SSR of 4.42 dB. Furthermore, the IAP of 3.66 dB is calculated with the TR scheme. All these TR properties show that the received signal with the TR scheme in the RC is of very good quality.

## 2.5 Effect of Different Antennas on TR

The performance of the TR scheme is studied for different types of antennas. To analyze how different types of antennas affect the performance of the TR scheme,



Figure 2.25: A snapshot of horn, log-periodic and CMA

experiments are conducted under similar conditions with different types of antennas. Conical monopole antenna (CMA), double ridged waveguide horn antenna and log periodic antenna are used for the experiments. The choice of the antennas is carried out so that these include both quasi omni-directional antenna (CMA) and directive antennas (horn and log periodic). The CMA provides good impedance matching (return loss  $< -10$  dB) for the frequency range  $0.7 - 8$  GHz. The radiation pattern of the antenna is approximately omni-directional with a constant phase center. The horn antenna is a double ridged waveguide antenna covering a frequency range of  $1$  GHz to  $18$  GHz. It has a directive pattern and acts as a spatial filter which captures most of the signal energy from the main lobe. Log-periodic antenna is also a directive antenna. The phase center and the radiation pattern are variable with the operated frequency and the impulse response has significant ringing effect that causes the spread of the transmitted input short pulse in the time delay. A snapshot of all these antennas is presented in the FIG. 2.25. The data sheets of these three antennas can be found in their data sheets.

To compare the performance of the TR scheme with different antennas, similar conditions are chosen. The RC allows examining different characteristics of the TR scheme with different antennas by providing the same channel model. Experiments are also conducted in the indoor environment with NLOS co-polar configuration.

### 2.5.1 Experimental Results in RC

Experimental setup in the RC is the same as presented in FIG. 2.22 for all type of antennas. Fig. 2.26 shows the PDP of the TR received signal in the RC. RC is an environment which has a uniform multi-path floor. As all the walls of the RC are metallic and have a very high reflective index, multi-path components can be received from every direction. Therefore, in this case the CMA whose radiation pattern is close to the radiation pattern of an omni directional antenna performs a little better than the directive antennas. Nevertheless, the directive antennas perform at a good level. A comparison of different TR properties are tabulated in TABLE 2.5. It can be seen that for the horn and log periodic antennas, the performance is comparable to CMA. The received peak power is normalized to the received peak power of the CMA. The NPP of the other two antennas is slightly lesser than NPP of CMA. A very high FG is observed with all types of antennas. It was expected that the SSR will be worse

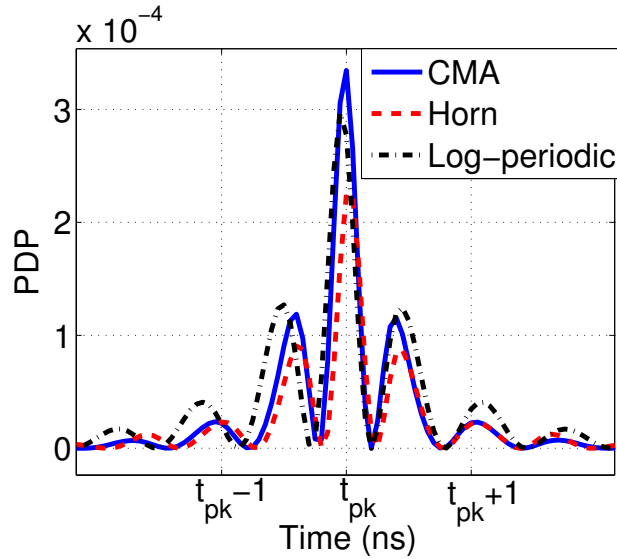


Figure 2.26: PDP of the TR received signal with CMA, horn and log-periodic antennas in the RC

TR Property	CMA	Horn	Log-periodic
$\sigma_{\tau}^{MCR}(\mu s)$	2.20	2.02	2.04
PL (dB)	19.93	21.51	21.02
NPP (dB)	0	-1.67	-0.47
FG (dB)	25.41	24.67	25.69
SSR (dB)	4.49	3.93	3.67
IAP (dB)	3.51	4.05	4.67
$\sigma_{\tau}^{TR}(ns)$	0.53	0.68	0.91

Table 2.5: Time Reversal characteristics with different types of antennas in a RC

for log-periodic antenna because of the ringing effects inherent to the antenna. SSR with the log-periodic antenna is 0.82 dB lesser than that of the CMA. The IAP is however greater for the directive antennas than CMA. The RMS delay spread of the TR received signal with the log periodic antenna is greater than the delay spread with the other two antennas.

## 2.5.2 Experimental Results in the Indoor Environment

Experiments are also performed in the indoor environment in NLOS co-polar configuration for all antennas. The experimental setup is the same as presented in FIG. 2.18. Now, as most of the multi-paths are expected to come from one particular direction, the directive antennas are expected to perform far better than the omni directional antenna if they are placed such that the main lobe of the radiation pattern coincides with the angle of arrival of the multi-path components.

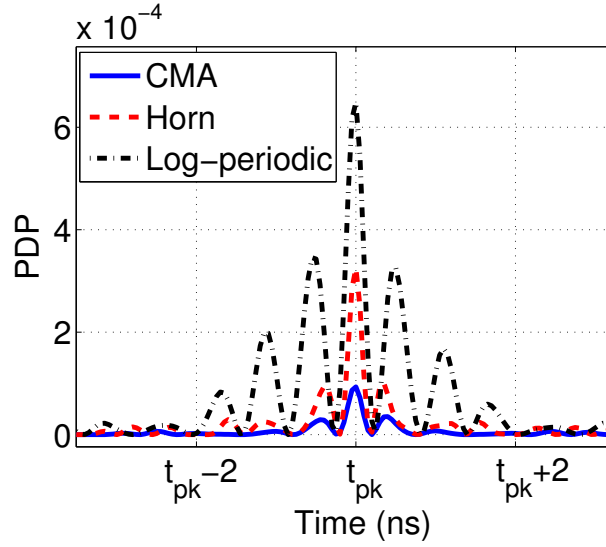


Figure 2.27: PDP of the TR received signal with CMA, horn and log-periodic antennas in an indoor environment

TR Property	CMA	Horn	Log-periodic
$\sigma_{\tau}^{MCR}(ns)$	24.96	18.54	17.19
PL (dB)	19.93	22.37	19.23
NPP (dB)	0	5.39	8.41
FG (dB)	13.41	10.39	12.32
SSR (dB)	4.19	5.09	2.75
IAP (dB)	7.18	5.13	7.90
$\sigma_{\tau}^{TR}(ns)$	19.63	9.43	14.64

Table 2.6: Time Reversal characteristics with different type of antennas in an indoor environment

FIG. 2.27 shows the PDP of the TR received signal with the three antennas in the given indoor environment. As expected, the received signal power is far greater with the directive antennas than the omni directional antenna as directive antenna has significantly greater gain in the direction from where the multi-path components are arriving. The log periodic antenna gives significantly better TR peak performance than the other two antennas. The horn antenna also has quite large received peak power as compared to the CMA. TABLE 2.6 compares different TR properties with different antennas in the indoor environment. The received peak power is normalized to the received peak power of the CMA. Horn antenna has almost 5.39 dB better NPP than the CMA. All other TR properties with the horn antenna are comparable with the CMA. The log-periodic antenna has a NPP of 8.4 dB better than the CMA, but it has a significantly lower SSR compared to the other two antenna types. All other properties are comparable to with the CMA. Therefore, the TR performance

TR Property	1.0 GHz	1.5 GHz	2.0 GHz
$\sigma_{\tau}^{MCR}(\mu s)$	2.09	2.12	2.14
PL (dB)	21.52	20.98	20.28
NPP (dB)	0	3.77	6.67
FG (dB)	23.36	24.32	23.40
SSR (dB)	1.07	2.61	4.42
IAP (dB)	2.89	3.26	3.66
$\sigma_{\tau}^{TR}(ns)$	0.77	0.64	0.65

Table 2.7: Time Reversal characteristics with different bandwidths in a RC

with different antennas depends upon the environment. An omni-directional antenna is expected to perform better in the environments with a constant multi path floor or where the direction of arrival for majority of the multi-paths is uniformly spread, whereas a directive antenna is expected to perform significantly better than the omni-directional antenna if the direction of arrival for most of the multi-paths is within the main lobe of the radiation pattern of the antenna.

## 2.6 Effect of Different Bandwidths on TR

### 2.6.1 Experiments in RC

Effects of different bandwidths are studied on different TR properties. The experiments are performed inside the RC with two CMAs. The interior of the RC with a CMA and the stirrer is shown in Fig. 2.28. The RC produces large number of wave reflections and allows accomplishing very high temporal and spatial focusing. Measurement setup has already been illustrated in FIG. 2.22. The height of the transmitter and the receiver is 1 m from the ground. The distance between the transmitter and receiver is 5.6 m. The DSO is operated in average mode so that 256 samples are taken and averaged together to reduce the captured noise. TR experiments are performed for three different bandwidths i.e. 1 GHz, 1.5 GHz and 2.0 GHz with a center frequency of 1.7 GHz. These bandwidths are selected because our system is lower bounded by the antenna as it filters the frequencies lower than 0.7 GHz and upper bounded by the AWG because it can generate the frequencies up to 2.7 GHz.

FIG. 2.29 shows the PDP of the TRR with different bandwidths in the RC. The TRR with 2 GHz bandwidth has a 6.67 dB and 3.77 dB better TR peak performance than the TRRs with 1.5 GHz and 1.0 GHz bandwidth respectively. Different TR properties are compared for different bandwidths and the results are tabulated in TABLE 2.7. The RMS delay spread of the PDP of the MCR ( $\sigma_{\tau}^{MCR}$ ) is not affected by different bandwidths. It remains in the order of 5 – 5.2  $\mu s$  for all bandwidths. TR performance improves significantly with the increase in the bandwidth. The NPP and SSR increase with the increase in the bandwidth while the IAP increases slightly. The NPP increases by 6.67 dB while SSR is increased by 2.94 dB for an increase in



Figure 2.28: A snapshot of one CMA in the RC

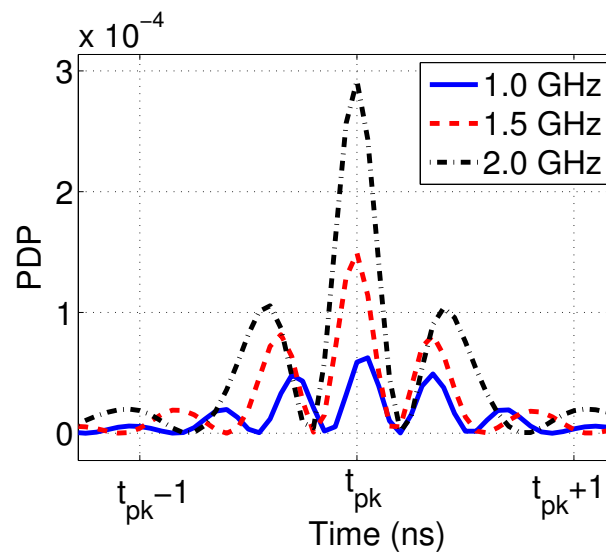


Figure 2.29: PDP of the TR received signal with different bandwidths in the RC

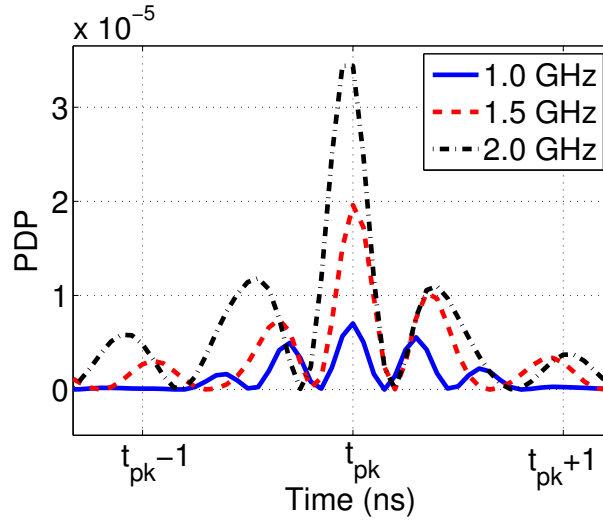


Figure 2.30: PDP of the TR received signal with different bandwidths in an indoor environment with NLOS cross-polar configuration

bandwidth from 1  $GHz$  to 2  $GHz$ . There is no significant impact of an increased bandwidth on the FG. In fact, the received peak power increases for a higher bandwidth but the received peak power for the channel impulse response also increases in the same manner. Therefore, FG, which is the ratio of peak power with or without TR, remains almost constant for all bandwidths. The RMS delay spread of the PDP of the TRRs ( $\sigma_{\tau}^{TR}$ ) decreases slightly with increase in the bandwidth.

## 2.6.2 Experiments in Indoor Environment

Experiments are also performed in the indoor environment with different bandwidths. A NLOS environment is chosen with the antennas in a cross-polar polarization. Experimental setup and measurement layout has already been shown in FIG. 2.18 and FIG. 2.17 respectively. As in the case of experiments in the RC, TR experiments in the indoor environment are also performed for three different bandwidths i.e. 1  $GHz$ , 1.5  $GHz$  and 2.0  $GHz$  with a center frequency of 1.7  $GHz$ .

FIG. 2.30 shows the PDP of the TRR with different bandwidths in the indoor environment. The TRR with 2  $GHz$  bandwidth has a 6.97  $dB$  and 4.60  $dB$  better TR peak performance than the TRRs with 1.5  $GHz$  and 1.0  $GHz$  bandwidth respectively. This increase in the TR performance is slightly better than the performance in the RC. Different TR properties are compared for different bandwidths and the results are tabulated in TABLE 2.8. The RMS delay spread and the path loss for the MCR are not affected a great deal with the bandwidth. The FG also remains comparable for all bandwidths. SSR increases with the increase in bandwidth as was observed for the experiments in the RC. There is a significant increase in the IAP with 1.5  $GHz$  and 2.0  $GHz$  bandwidths.

TR Property	1.0 GHz	1.5 GHz	2.0 GHz
$\sigma_{\tau}^{MCR}(ns)$	21.53	18.81	21.10
PL (dB)	33.58	33.58	33.21
NPP (dB)	0	4.60	6.97
FG (dB)	12.26	10.93	12.69
SSR (dB)	1.04	2.82	4.64
IAP (dB)	4.90	8.84	7.98
$\sigma_{\tau}^{TR}(ns)$	10.79	17.42	16.96

Table 2.8: Time Reversal characteristics with different bandwidths in an indoor environment with NOS cross-polarconfiguration

## 2.7 TR with Multi-Antenna Configurations

The temporal compression and spatial focusing properties of the TR scheme makes it an attractive transmission scheme for MIMO systems. One of the main differences between a classical MIMO system and a TR-MIMO system is that in the classic system, the receiving antennas receive multiple superposed signals while in the TR system, each antenna receives only one dominant signal. The spatial focusing property of the TR means that the antennas which are separated in space will have uncorrelated channel impulse responses. Thus, the interference caused by the transmitted signals for unintended receiving antennas is suppressed. At the same time, the time dispersive characteristics of the channel are mitigated by the temporal compression inherent to the TR scheme. Therefore, simultaneous communication with all receiving antennas can be performed using simple detectors at the receiver [63]. As described in CHAPTER 1, the received signal with MIMO-TR for  $N_t$  transmitting antennas and  $N_r$  receiving antennas is given by the expression:

$$\begin{aligned}
 y_j(t) = & \underbrace{s_j(t) \star \sum_{i=1}^{N_t} R_{ij}^{auto}(t)}_{Signal(j)} + \underbrace{\sum_{i=1}^{N_t} \sum_{k=1; k \neq j}^{N_r} s_k(t) \star R_{ikj}^{cross}(t)}_{Interference(j)} \\
 & + \underbrace{n_j(t)}_{Noise(j)}
 \end{aligned} \tag{2.9}$$

where  $s_j(t)$  and  $s_k(t)$  are the transmitted signals intended for the  $j_{th}$  and the  $k_{th}$  receiving antenna respectively. There are two types of MIMO communications; one is the multiuser scenario and second is the single user MIMO scenario. In the first case, multiple transmitting antennas communicate with multiple receiving antennas well separated in space. In multi user TR communication, the interference part in (2.9) may be suppressed because of the large distances between the receiving antennas.

In a single user MIMO scenario, it might be possible to simultaneously transmit signals over several independent channels. (2.9) is valid in this case as well. Note that the number of users then becomes the number of the receiving antennas. Since

the interference power increases with the number of receiving antennas, one cannot send more information by simply adding more receiving antennas. However, with reasonably smaller number of receiving antennas than the number of transmitting antennas and a rich multi-path environment, the desired signal's magnitude might become larger than that of the interference [67]. In this case, application of TR in wireless MIMO could be possible.

MISO-TR has been investigated in a number of papers to benefit from the antenna diversity of the configuration. In [61, 72], using the data from a fixed wireless  $8 \times 1$  MISO measurement, a delay compression by a factor of 3 was shown to be possible. In [62], using the experimental results, temporal focusing and an increase in collected energy with the number of antennas in MISO-TR systems is verified. Also, the reciprocity of realistic channels is demonstrated with the help of MISO-TR. MISO-TR system is investigated for UWB communication over ISI channels in [73]. TR is studied for a multi user scenario in [63, 64, 67].

The use of multiple element antenna (MEA) systems in wireless communications has recently become a well-known technique to increase the transmission reliability and channel capacity [67]. Antenna and diversity gain can be achieved using available combining methods (selection, equal gain, maximum ratio combining). However, for wide-band MEA systems where signals are mixed both in time and space, a combination of advanced signal processing algorithms is required to overcome the effects of multi-path fading and ISI. Therefore, the receiver is expected to have a rather high complexity. Since the setup of MEA systems has some similarity to TR, it becomes an interesting question whether TR can be applied in MEA wireless systems. If this is the case, the advantages will be three fold: i) reducing ISI without the use of an equalizer ii) focusing the signal on the point of interest thereby reducing the interference and iii) applying a rather simple receiver structure.

In this chapter, validation of TR scheme is carried out with different multi-antenna configurations in the RC and the indoor environment. A single user approach is applied for all configurations. Different multi-antenna configurations include SISO, SIMO ( $1 \times 2$ ), MISO ( $2 \times 1$ ) and MIMO ( $2 \times 2$ ). Time reversal (TR) measurements are conducted for ultra wide-band (UWB) signals in a reverberation chamber (RC) for these multi-antenna configurations. A comparison is made among the four configurations. Channel measurement is done by using an AWG at the transmitter and a high speed DSO at the receiver. For all these configurations, the received signals are time reversed and re-transmitted from the transmitting antenna. TR performance is analyzed and compared for all the configurations by considering different TR characteristics i.e. NPP, FG, SSR, IAP and RMS delay spread.

There are two types of gains associated with the configurations having more than one antenna either at the transmitting end or at the receiving end or both. One gain is the diversity gain achieved through the antenna diversity. The upper bound for the diversity gain is the product,  $N_t N_r$ , where  $N_t$  is the number of transmitting antennas and  $N_r$  is the number of receiving antennas. The upper bound for the multiplexing

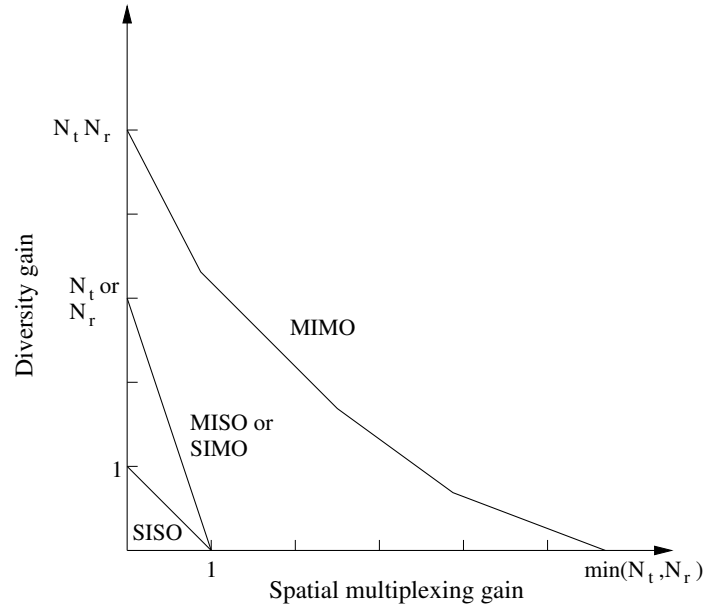


Figure 2.31: Multiplexing and diversity gains for different multi antenna configurations

gain is  $\min(N_t, N_r)$  [74]. FIG. 2.31 further elaborates the limits of spatial multiplexing gain and the diversity gain for different multi antenna configurations.

In a TR system, same bounds for the multiplexing gain and diversity gain apply. We have compared different TR properties for different cases of MIMO configurations. The diversity gain is taken into account and the received signal in the case of SIMO and MIMO configurations is combined (or added) whereas transmitted signal is combined for MISO configuration. The results for the MIMO TR validation have been accepted for publication in [75, 76].

## 2.7.1 MIMO-TR in RC

A comparison of TR with different multi antenna configurations is first made in the RC. These experiments show performance of the TR scheme in an ideal static environment. Multi-antenna TR in the RC makes full use of the multi-path diversity inherent to the environment. The performance evaluation in an ideal environment gives a general trend of the TR performance, thereafter, experiments are carried out in more realistic environments to verify the results.

### 2.7.1.1 Experimental Setup

An experimental setup is established in the RC for the validation of the TR in multi-antenna configurations. Measurement setup is illustrated in FIG. 2.32. A set of four conical mono-pole antennas (CMA) are used at the transmitter and receiver with both co-polar and cross-polar antenna orientations and different multi-antenna

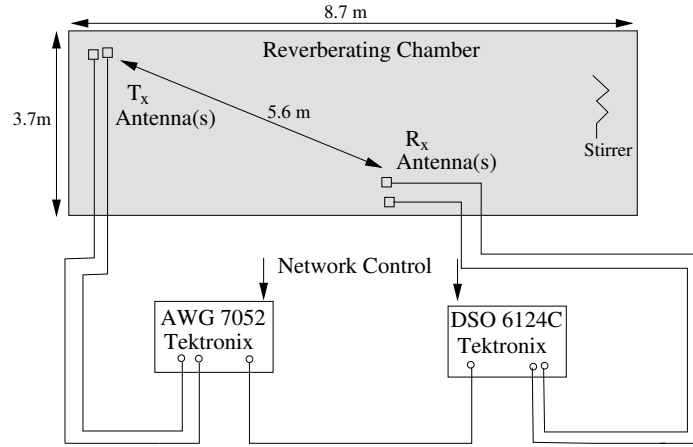


Figure 2.32: Experimental setup for different multi-antenna configurations in the RC

configurations. FIG. 2.33 shows two CMAs placed inside the RC. The height of the transmitter and the receiver is 1 m from the ground. The distance between the transmitter and receiver is 5.6 m. The channel sounding pulse with a rise time of 200 ps (see FIG. 2.19) and the time reversed MCR are generated through the AWG. The received signal is measured by a DSO. The DSO captures the MCR of the channel as well as the TRR. The DSO is operated in average mode so that 256 samples are taken and averaged together to reduce the impact of noise.

### 2.7.1.2 Experimental Results

FIG. 2.34 shows power delay profile (PDP) of the received TR signal in RC for SISO, SIMO, MISO and MIMO configurations for a fixed transmitted power with both co-polar and cross-polar antenna orientations. It is evident that MIMO, MISO and SIMO TR have a better TR peak performance compared to SISO-TR. The comparison for all TR characteristics for these configurations is summarized in Table 2.9. The received peak power of the received signal is normalized to the SISO-TR received peak power. The normalized peak power (NPP) improves with SIMO, MISO and MIMO configurations. MIMO-TR outperforms SISO, SIMO and MISO TR for the same transmitted power. For instance, NPP MIMO-TR is 4.02 dB and 5.16 dB and more than SISO-TR for co-polar and cross-polar antenna orientations respectively.

As for the other TR properties, the performance of all the configurations remains almost the same. The configurations which have multiple antennas at the transmitter (MISO and MIMO) have a better FG and IAP than the configurations having one antenna at the transmitter (SISO and SIMO). The SSR remains almost constant for all configurations. The RMS delay spread also remains constant for all configurations. As SSR and RMS delay spread affect the ISI, therefore, all the configurations have a similar signal to interference (SIR) performance. However, the bit rate of the system can be increased taking advantage from the multiplexing gain of multi-antennas configurations.



Figure 2.33: The interior of the reverberation chamber with two conical monopole antennas

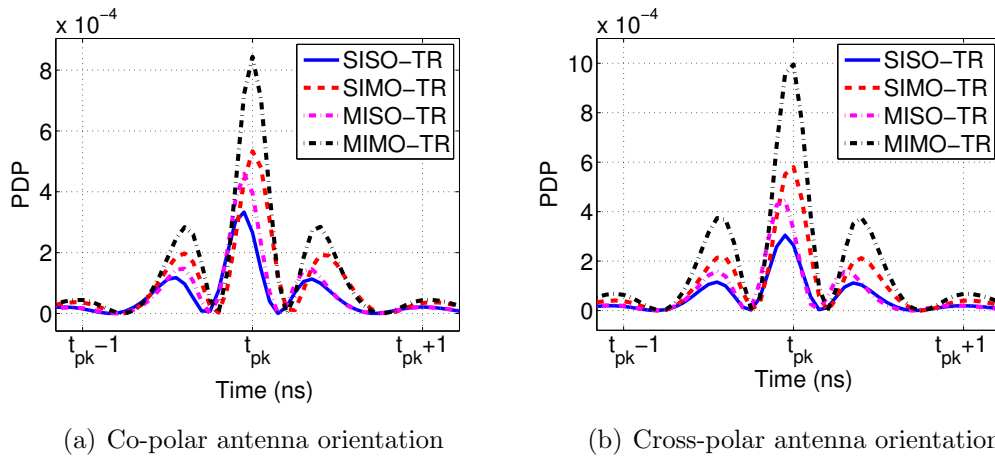


Figure 2.34: PDP of the received TR signal with SISO, SIMO and MIMO configurations

## 2.7.2 SISO and SIMO-TR in the Indoor Environment

Experiments are carried out in the indoor environment for SISO and SIMO configurations for a cross-polar antenna orientation for both LOS and NLOS environments. The experimental setup has already been discussed and can be seen from FIG. 2.18.

### 2.7.2.1 Experimental Results

FIG. 2.35 shows for both LOS and NLOS configurations, the power delay profile (PDP) of the received TR signal in an indoor environment with SISO and SIMO configurations for a fixed transmitted power. It is obvious that SIMO TR has a

TR Property	Co-polar antenna orientation				Cross-polar antenna orientation			
	SISO	SIMO	MISO	MIMO	SISO	SIMO	MISO	MIMO
$\sigma_{\tau}^{MCR}(\mu s)$	2.21	2.11	2.19	2.08	2.21	2.11	2.17	2.21
NPP (dB)	0	2.01	1.37	4.02	0	2.79	1.667	5.16
FG (dB)	26.05	24.62	27.32	27.41	28.02	27.47	30.46	30.67
SSR (dB)	4.51	4.29	4.93	4.68	4.22	4.32	4.43	4.24
IAP (dB)	3.59	4.09	5.02	5.94	3.40	4.50	5.20	5.89
$\sigma_{\tau}^{TR}(ns)$	0.54	0.57	0.50	0.50	0.52	0.54	0.48	0.55

Table 2.9: Time Reversal characteristics in the reverberation chamber with different polarizations and multi antenna configurations

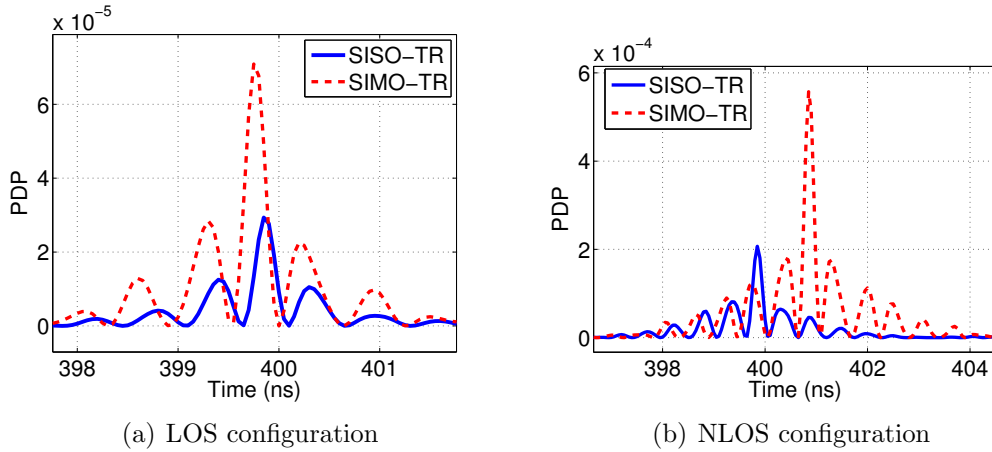


Figure 2.35: PDP of the received TR signal with SISO and SIMO configurations in an indoor environment

better TR peak performance compared to SISO-TR. TABLE 2.10 compares different TR properties with SISO-TR and SIMO-TR in the indoor environment. The NPP with SIMO-TR is 4.30 dB and 3.81 dB greater than SISO-TR for LOS and NLOS environments respectively. All other TR properties are very similar for SISO and SIMO-TR. NLOS environment has larger values for RMS delay spread of the MCR ( $\sigma_{\tau}^{MCR}$ ) but the RMS delay spread for the TR signal ( $\sigma_{\tau}^{TR}$ ) is in the same range for both LOS and NLOS environments.

## 2.8 Multiplexing Gain of SIMO-TR

For the TR scheme, multiple input single output (MISO) TR has been used in the literature to exploit the diversity gain offered by the MISO configuration [61, 62]. As described in SECTION 2.7 that the upper bound to the multiplexing gain in a classic MIMO system is  $\min(N_t, N_r)$ . From the TR perspective, a novel transmission approach for time reversal (TR) ultra wide-band (UWB) communication system is

TR Property	LOS		NLOS	
	SISO-TR	SIMO-TR	SISO-TR	SIMO-TR
NPP (dB)	0	4.30	0	3.81
FG (dB)	10.17	9.65	12.67	13.16
SSR (dB)	4.05	4.90	3.7	3.98
IAP (dB)	5.79	5.16	4.14	4.98
$\sigma_{\tau}^{TR}(ns)$	11.7	14.46	13.29	13.16
$\sigma_{\tau}^{MCR}(ns)$	18.35	16.07	23.21	22.17

Table 2.10: Time Reversal characteristics in the indoor environment with different SISO and SIMO configurations

proposed which increases the multiplexing gain with the increase in the number of antennas at the receiver i.e. even though  $\min(N_t, N_r)$  has a value of 1, yet the multiplexing gain keeps on increasing with the increase in the receiving antennas. Therefore, with this approach, an increased capacity of the system is achieved. This scheme has been registered as a patent by IETR [77] and we have submitted another article on this topic as well [78].

Block diagram of the proposed transmission scheme is shown in FIG. 2.36. A single antenna transmitter system is used for data transmission and M multiple simple receivers are used for data reception. It is assumed that the transmitter has perfect knowledge of the CSI, i.e. channel responses between the transmitter and M receiving antennas are known at the transmitter end. The first step is serial to parallel conversion of the input data. The input data is converted into M parallel data lines and passed through the pre-filter whose response is the time reversed version of the CIR between the transmitter and the intended receiver. All the filters must have the same length so that addition step after the pre-filter stage can be carried out. The M signals are added together and transmitted into the channel. The transmitted signal can be written as:

$$X(t) = \sum_{k=1}^M d_k A_k h_k(-t) \quad (2.10)$$

where  $d_k$  is the input serial data,  $A_k$  is the normalization coefficient for the  $k_{th}$  time reversed CIR ( $h_k(-t)$ ). The normalization coefficient for the proportional power allocation can be mathematically written as:

$$A_k = \frac{1}{\sqrt{M} \|h_k(t)\|} \quad (2.11)$$

where  $\|\cdot\|$  denoted the Frobenius norm operation. The transmitted signal convolves with M unique channels and each channel encodes the transmitted signal for its particular received antenna. The received signal at the  $j_{th}$  receiving antenna is expressed as:

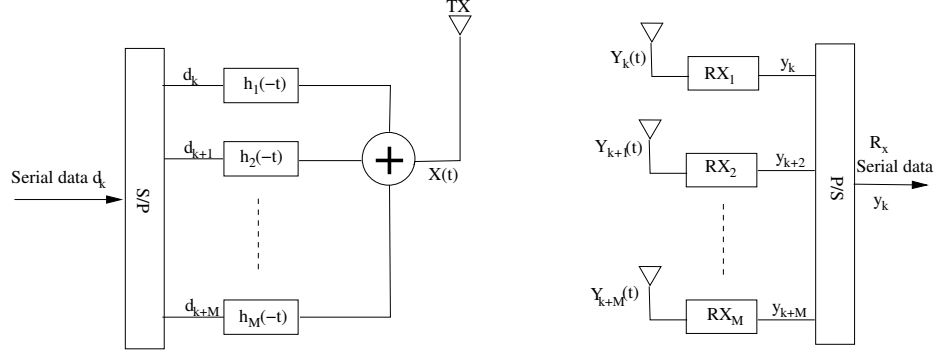


Figure 2.36: Block diagram of the novel transmission approach for SIMO-TR

$$Y_j(t) = X(t) \star h_j(t) + n(t) = \underbrace{\sum_{k=1, k \neq j}^M d_k A_k R_{jk}^{cross}(t)}_{Interference} + \underbrace{d_j A_j R_{jj}^{auto}(t)}_{Signal} + \underbrace{n(t)}_{Noise} \quad (2.12)$$

where  $R_{jj}^{auto}(t)$  is the auto-correlation function of the CIR,  $h_j(t)$  and  $R_{jk}^{cross}(t)$  is the cross-correlation function of the CIRs  $h_j(t)$  and  $h_k(t)$ . Thus the received signal consists of one useful signal and  $M - 1$  interference signals. The strength of the interfering signals depends on the correlation between the intended channel and the other channels. The correlation between channels depends on the delay spread, angular spread and the effective de-correlation distance between the receiving antennas. In the case of small separation between the antennas, the mutual coupling is high which causes the variation of the radiation pattern of the antennas [79], therefore, the observed channel responses via closely separated antennas are greatly modified. However, if the separation between the antennas is more than  $\frac{\lambda}{2}$  ( $\lambda$  is the wavelength of the lower frequency of the frequency band), the greater the separation between the antennas, the lesser is the correlation between the channels. At every receiving antenna, the signal is detected and passed to the parallel-to-serial converter to complete the communication chain.

### 2.8.1 Capacity Comparison of the TR Multi Antenna Configurations

For AWGN channel, the maximum bit rate which a system can achieve for a error free communication is given by famous Shannon's formula:

$$C = B \log_2 \left( 1 + \frac{S}{N} \right) \quad (2.13)$$

where  $C$  is the capacity of the channel in bits per second (bps),  $B$  is the bandwidth of the system ( $Hz$ ) and  $\frac{S}{N}$  is the signal to noise ratio (SNR). In the following the capacity

is considered in  $bps/Hz$ , as bandwidth of all the configurations to be compared is the same. The maximum data rate for a TR scheme can also be written in a similar way. Assuming no inter symbol interference, and considering zero mean independent and identically distributed (i.i.d.) BPAM transmit symbols, the maximum data rate can be written as:

$$C_{SISO} = \log_2\left(1 + \frac{S}{N}\right) \quad (2.14)$$

where  $\frac{S}{N}$  is the received SNR.

For the MISO-TR, as the received signal quality increases with the increase in the transmitting antennas ( $M$ ), therefore, the received power increases by a factor of  $M$ . Assuming zero ISI, the capacity of MISO-TR is given as:

$$C_{MISO} = \log_2 \left[ 1 + M \frac{S}{(N + I)} \right] \quad (2.15)$$

where  $I$  is the interference caused by the multiple antennas at the transmitter.

The proposed transmission approach converts the input serial data into  $M$  parallel data streams that are pre-filtered by the time reversed CIRs between the transmitter and  $M$  receiving antennas. The filtered signals are added together and transmitted into the channel. The received signal at every receiver has one dominant signal and  $M - 1$  negligible interference signals (if the channels are un-correlated). Thus, each receiving antenna enables the transmission of a data symbol. In this way, the system can have a multiplexing gain which increases with the number of receiving antennas. Thus maximum data rate or the capacity of the proposed transmission approach is ameliorated by factor  $M$  due to the  $M$ -parallel transmitted data in the SIMO-TR channel. However, with the constant total transmitted power  $P_0$ , the associated power for each transmitted data bit is reduced and the received peak signal amplitude per data bit is degraded by  $\frac{1}{\sqrt{M}}$  and the peak signal power is degraded by  $\frac{1}{M}$ .

Interference caused by the signals for non intended receiving antennas can affect the performance of the SIMO-TR scheme. However, if the CIRs are quasi orthogonal (uncorrelated channels), this interference will be minimal. Interference in the received symbol may also be caused due to the tail of the preceding symbol (ISI). The symbol rate is chosen in such a manner to limit ISI to a minimal level. Thus, neglecting the ISI, the capacity of a SIMO-TR system can be written as:

$$C_{SIMO} = M \log_2\left(1 + \frac{1}{M} \frac{S}{N + I}\right) \quad (2.16)$$

Looking at (2.16), we can find that the capacity of the SIMO-TR scheme is affected by  $M$  in two ways. On one hand, it increases linearly with the increase in  $M$ , but at the same time, it decreases with  $M$  logarithmically. The factor which makes the capacity increase with  $M$  overshadows the factor which decreases it especially for higher values of  $M$ . It suggests that the capacity on the SIMO-TR scheme increases significantly with the increase in the number of antennas at the receiver. FIG. 2.37 shows the capacity of the SISO-TR, MISO-TR for different number of transmitting

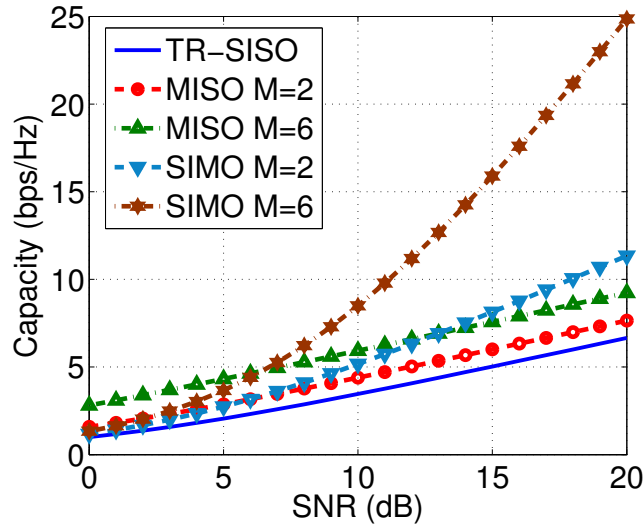


Figure 2.37: Capacity of the SISO-TR, MISO-TR with different number of antennas at the transmitting and SIMO-TR with different number of antennas at the receiving end.

antennas and the SIMO-TR for different number of receiving antennas. SIMO-TR results in significantly better capacity than MISO and SISO-TR for high values of SNR. For instance, for a SNR of 20 dB and  $M = 6$ , SIMO-TR gives 15.63 bps/Hz better performance than MISO-TR.

## 2.8.2 Experimental Validation of SIMO-TR

The proposed SIMO-TR is experimentally validated using two antennas at the receiver side in a reverberation chamber, which is an ideal test environment present inside the IETR laboratory, with the dimensions of  $8.7\text{ m} \times 3.7\text{ m} \times 2.9\text{ m}$ .

### 2.8.2.1 Experimental Setup

An experimental setup similar to the one shown in FIG. 2.32 is established in the RC. The only difference is that only one antenna is used at the transmitting end. A log-periodic antenna is used at the transmitting end and two identical CMAs are used at the receiving end. The radiation patterns of both antennas are uniform in the azimuth plane and are vertically polarized with a separation of 10 cm. The distance between the transmitter and the receiver is 6 m and the antennas are kept 1 m above the ground.

A very narrow pulse is generated with an AWG, which has a maximum sampling rate of 5 GS/s to measure the channel response. At the receiver end, the received signal is captured by a DSO with a maximum sampling rate of 40 GS/s. The DSO is operated in the average mode so that 256 samples of the received signals are recorded

and averaged together to reduce the noise. Once the channel responses of both channels are measured, the MCRs are truncated for 85% of the energy, reversed in time, added together, normalized to the equal power and then re-transmitted by using the AWG in the same channel. A very high quality signal is received at both of the receiving antennas.

FIG. 2.38 shows the PDP of the received signals at two antennas normalized to the maximum peak power of the SISO-TR scheme. As expected, the power of the peak is lesser than the peak power of the SISO-TR. It is the multiplexing gain and not the diversity gain which increases the capacity of the proposed transmission approach. The two signals have signal to side lobe ratio (SSR) of 7.5 dB which is better than the SSR of the SISO-TR (in the order of 5 dB) which suggests that the SIMO-TR will perform better in high data rate applications where SSR is of great importance.

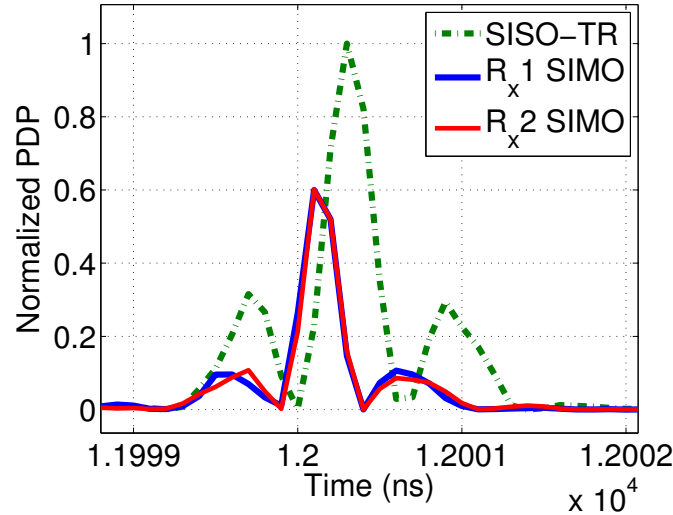


Figure 2.38: Power delay profile of the received signal with SISO-TR and two individual signals with SIMO-TR

## 2.9 Conclusion

In this chapter, we presented the validation procedure of the TR scheme. The validation of the TR scheme in the laboratory is performed to study different TR parameters using simulation, semi-measurement and measurement approaches.

In the simulation approach, existing channel models for UWB are used for the validation of the TR scheme. PDP of the pulsed UWB and the TR UWB are compared in different types of indoor environments i.e. residential, office and industrial environments. The received signal of the TR scheme is compressed in time. Furthermore, TR validation is carried out by using TD-TLM simulations in a metallic environment with

one side replaced by absorbers. The results suggest that the focusing zone expands in the direction where absorbing boundary is placed.

In the semi-measurement approach, the channel response of a typical indoor environment is measured by using the frequency domain instrument (VNA). Thereafter TR communication is simulated and spatial focusing of the TR scheme is analyzed. It is shown that in a typical indoor environment, the received peak power decreases by 10 dB for only 10 cm movement of the receiver. It is also studied that how different bandwidths affect the performance and the spatial focusing of the TR scheme by measuring the channel response over a rectangular surface in a reverberation chamber (RC). The results suggest that the dimension of the spatial focusing zone is controlled by the lower frequency of the bandwidth.

TR validation, followed by the parametric analysis of the TR scheme, is performed by using time domain instruments (AWG and DSO). Different TR properties such as normalized peak power (NPP), focusing gain (FG), signal to side-lobe ratio (SSR), increased average power (IAP) and RMS delay spread are compared for different configurations with combinations of different environments (LOS and NLOS) and different antenna orientations (co-polar and cross-polar). LOS co-polar configuration has the largest received peak power but the lowest SSR, whereas NLOS cross-polar configuration has the lowest received peak power and the highest SSR. For a given channel environment, LOS cross-polar configuration can be a good compromise with larger received power compared to NLOS configurations and equally good performance. Experiments are also performed in the RC and it is shown that the RC is a very favorable environment for TR.

TR validation is also performed with different bandwidths and it has been found that transmitted signals with higher bandwidths achieve better performance than the signal with lower bandwidths. Experiments are also performed for the TR scheme with different types of antennas. The results suggest that an omni-directional antenna performs better in the environments with a constant multi-path floor or where the direction of arrival for majority of the multi-paths is uniformly spread, whereas a directive antenna is expected to perform significantly better than the omni-directional antenna if the direction of arrival for most of the multi-paths matches with the main lobe of the radiation pattern of the antenna.

TR validation is also performed with different multi-antenna configurations. It has been found that with multi antenna configurations, a significantly better TR peak performance is achieved with all other properties remain comparable to the SISO-TR scheme. In the end, a multiplexing scheme is described using SIMO-TR scheme, where a multiplexing gain proportional to the number of receiving antennas is achieved and thus capacity of the TR scheme is ameliorated. A comparison of the capacity of the SIMO-TR and MISO-TR schemes is carried out and the results suggest that SIMO-TR scheme attains significantly higher capacity than MISO-TR scheme.



# Chapter 3

## Robustness of TR Scheme

### Contents

---

<b>3.1</b>	<b>Introduction</b>	<b>86</b>
<b>3.2</b>	<b>Experiments in RC</b>	<b>87</b>
3.2.1	Experimental Setup	88
3.2.2	Measurement Results and Analysis	88
<b>3.3</b>	<b>TR Robustness in Realistic Channels</b>	<b>98</b>
3.3.1	Measurement Procedure	98
3.3.2	Experiments With a Changing Environment	98
3.3.3	Experiments With a Moving Receiver	105
<b>3.4</b>	<b>Conclusion</b>	<b>107</b>

---

### 3.1 Introduction

As discussed in the previous chapters, the received signal in a time reversal (TR) system is considerably focused in spatial and temporal domains. As a result, the received power is concentrated within few taps and the effects of inter symbol interference (ISI) are greatly reduced. TR technique shifts the design complexity from the receiver to the transmitter. The receiver system becomes simpler than without TR and signal can be collected using a simple energy threshold detector. Spatial focusing enables very low co-channel interference in a multi cell system, resulting in an efficient use of bandwidth in the overall network.

The critics of the TR scheme claim that TR performance is highly dependent on the availability of the channel state information (CSI) at the transmitter. In case of non stationary channel, the performance of the TR scheme deteriorates rapidly. Therefore, one of the most important drawbacks of the TR scheme is considered as the necessity of regular channel estimation which makes the transmission system quite complicated. Similarly if imperfect channel is estimated, TR performance will be affected badly. However, if the TR system is robust and can resist the changes in the environment, frequency of estimation cycles will be less resulting in an increased throughput of the system. Similarly, the robustness of the TR scheme will help to withstand the imperfect channel estimation. To investigate the robustness of the TR system with respect to a time varying channel, a measurement campaigns are carried out in a mode stirred reverberation chamber (RC) and in the indoor environment. The RC is electrically large, high quality factor cavity that obtains statistically uniform fields by either mechanical stirring or frequency stirring [80]. RC is a highly controllable test environment and can be considered as a reference environment. It helps us to draw some important conclusions which otherwise are difficult to reach. A more detailed introduction of the RC is given in CHAPTER 2.

There are many factors which can change the channel of a communication system. If the transmitter and the receiver do not change their position, the time varying environment can cause the channel to change. The channel will also be changed if either the transmitter or the receiver changes its position. In this chapter, an experimental study for the robustness of TR technique is presented in varying channel environments. The experiments are performed inside the RC and in an indoor environment. In the RC, the channel is changed with the rotation of the stirrer present inside the RC or with the help of a precise robotic positionner to change the position of the receiver. The channel responses and the time reversal responses (TRR) are measured at varying positions of the stirrer and the receiver. Cross-correlation coefficients between the measured channel responses (MCR) and TRRs are studied for the signals of different bandwidths in a time varying channel environment. Furthermore, different TR properties like normalized peak power (NPP), signal to side-lobe ratio (SSR), focusing gain (FG) and increased average power (IAP) are studied with the varying channel for the bandwidths of 2.0 GHz, 1.5 GHz and 1.0 GHz. These results have been accepted for publication in [81].

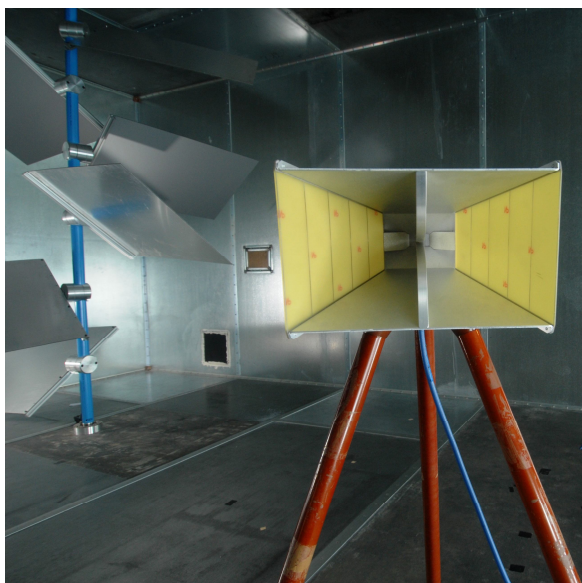


Figure 3.1: A snapshot of the interior of the reverberating chamber with horn antenna and the stirrer

Experiments for the robustness of the TR technique are also carried out in more realistic indoor environment. In the indoor environment, changes in the channel are induced with the presence of a person or metallic strips near a receiver terminal. Experiments are performed for three different bandwidths, i.e.  $2.0\text{ GHz}$ ,  $1.5\text{ GHz}$  and  $1.0\text{ GHz}$ . Cross-correlation coefficients between the MCRs and TRRs are studied for the signals of different bandwidths in the presence of induced variations. Thereafter, following a similar approach used for the RC, the impact of the induced variations on different TR properties is studied. Finally, TR robustness is studied in case of displaced receiver.

## 3.2 Experiments in RC

The reverberation chamber (RC) is a metallic chamber of dimensions  $8.7\text{ m} \times 3.7\text{ m} \times 2.9\text{ m}$  present inside IETR laboratory. All experiments are performed inside the RC which increases the wave reflections in the environment and allows accomplishing very high temporal and spatial focusing for a TR system. Two horn antennas are used as the transmitter receiver pair. The interior of the RC with a horn antenna and the stirrer is shown in FIG. 3.1.

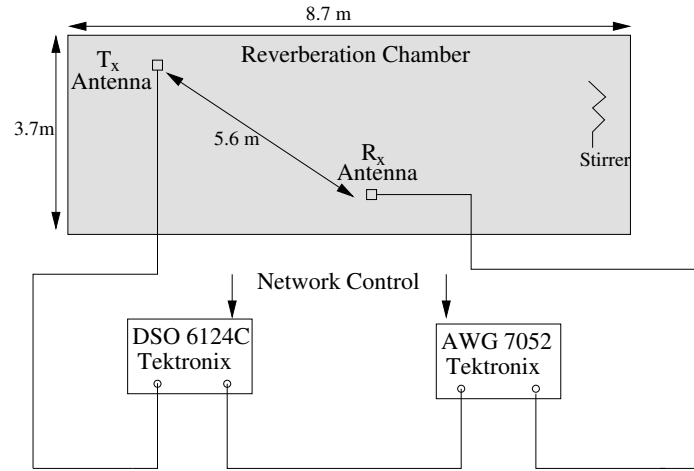


Figure 3.2: Measurement setup for the TR experiment in the reverberation chamber

### 3.2.1 Experimental Setup

The measurement setup is illustrated in FIG. 3.2. The channel sounding pulse and the time reversed MCR are generated through the arbitrary waveform generator (AWG 7052) having a maximum sampling rate of  $5\text{ GS/s}$ . The height of the transmitting antenna and that of the receiving antenna is  $1\text{ m}$  from the ground. Distance between the transmitter and receiver is  $4.5\text{ m}$ . The antennas are placed in such a manner so that the direct path is not received. The pulse is generated with the AWG which has a maximum sampling rate of  $5\text{ GS/s}$ . The receiver is a DSO with a maximum sampling rate of  $40\text{ GS/s}$ . The DSO captures the channel response. The time reversed version of the MCR is created through MATLAB and is retransmitted with the AWG in the same channel to measure the TRR which is captured by the DSO. The DSO is operated in average mode so that 32 samples are taken and averaged together to reduce the captured noise.

### 3.2.2 Measurement Results and Analysis

TR experiments are performed in a mode stirred reverberation chamber for different positions of the stirrer ( $\theta$ ) and the receiver and for the bandwidths of  $1\text{ GHz}$ ,  $1.5\text{ GHz}$  and  $2.0\text{ GHz}$ . Respective lower frequencies ( $f_L$ ) for these bands are  $1\text{ GHz}$ ,  $750\text{ MHz}$  and  $700\text{ MHz}$ . These bandwidths are selected because our system is lower bounded by the antenna as it filters the frequencies lower than  $0.7\text{ GHz}$  and upper bounded by the AWG because it can generate the frequencies up to  $2.7\text{ GHz}$ .

#### 3.2.2.1 Experiments with a Rotating Stirrer

The transmitter and the receiver do not change their position. The channel is changed with the precise rotation of the stirrer. The RC is very sensitive to the changes in the environment; a small movement of the stirrer can cause large changes in the channel.

FIG. 3.3 compares for different bandwidths, the cross-correlation coefficients ( $\rho_h(\theta^\circ)$ ) between the MCRs for rotation of the stirrer by  $\theta^\circ$  ( $h'_j(\theta^\circ)$ ) and the MCR at  $\theta = 0^\circ$  ( $h'_j(0^\circ)$ ). Mathematically, it can be written as:

$$\rho(\theta^\circ) = \frac{s_{0^\circ\theta^\circ}}{\sqrt{s_{0^\circ0^\circ} s_{\theta^\circ\theta^\circ}}} \quad (3.1)$$

where  $s_{0^\circ\theta^\circ}$  is the covariance of  $h'_j(0^\circ)$  and  $h'_j(\theta^\circ)$ ,  $s_{0^\circ0^\circ}$  and  $s_{\theta^\circ\theta^\circ}$  are the variances of  $h'_j(0^\circ)$  and  $h'_j(\theta^\circ)$  respectively. For the sake of clarity, the dependence of all these variables on time ( $t$ ) is omitted. The MCRs are rapidly de-correlated with the rotation of the stirrer. For  $\theta \geq 3^\circ$ , the MCRs of all bandwidths are almost totally de-correlated. Thus in a RC, rotation of the stirrer for the first few degrees plays a decisive role in analyzing the robustness of a system.

FIG. 3.4 compares for different bandwidths, the cross-correlation coefficients ( $\rho_y(\theta^\circ)$ ) between the TR received signals for different values of  $\theta$  ( $y_j(\theta^\circ)$ ) and the TR received signal  $y_j(0^\circ)$ . Comparing FIG. 3.3 and FIG. 3.4, it can be concluded that even if the MCR has changed from the original MCR, TRR has a sufficient correlation with the original TRR  $y_j(0^\circ)$ . For instance, for  $\theta = 1^\circ$ , the TR received signal ( $y_j(1^\circ)$ ) has a correlation coefficient in the order of 0.7 while the MCR has a correlation coefficient in the order of 0.2. The TR signals with higher bandwidths have somewhat higher correlation coefficients but there is not a stark difference between the correlation coefficients of the received signals of lower and higher bandwidths.

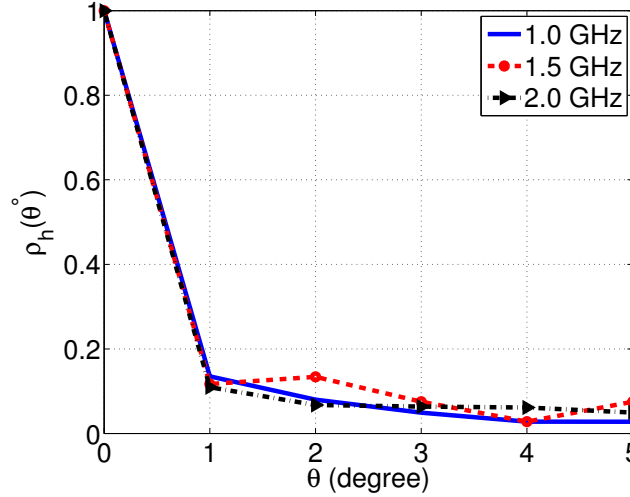


Figure 3.3: Cross-correlation coefficients ( $\rho_h(\theta^\circ)$ ) between the MCRs  $h'_j(\theta^\circ)$  and  $h'_j(0^\circ)$

FIG. 3.5a shows the Power Delay Profile (PDP) of the TR received signals in the RC for  $\theta \in \{0^\circ, 1^\circ, 2^\circ, 3^\circ\}$ , for the same transmitted signal ( $\theta = 0^\circ$ ) having a bandwidth of 2.0 GHz. The PDPs of the received signals for  $\theta \geq 1^\circ$  are separately shown in FIG. 3.5 b,c,d. It can be seen that for  $\theta \geq 1^\circ$  (FIG. 3.5b,c,d), even though

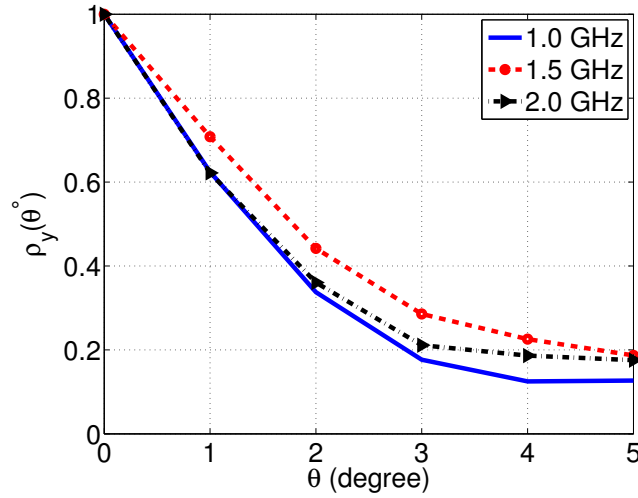


Figure 3.4: Cross-correlation coefficients ( $\rho_y(\theta^\circ)$ ) between the TR received signals  $y_j(\theta^\circ)$  and  $y_j(0^\circ)$

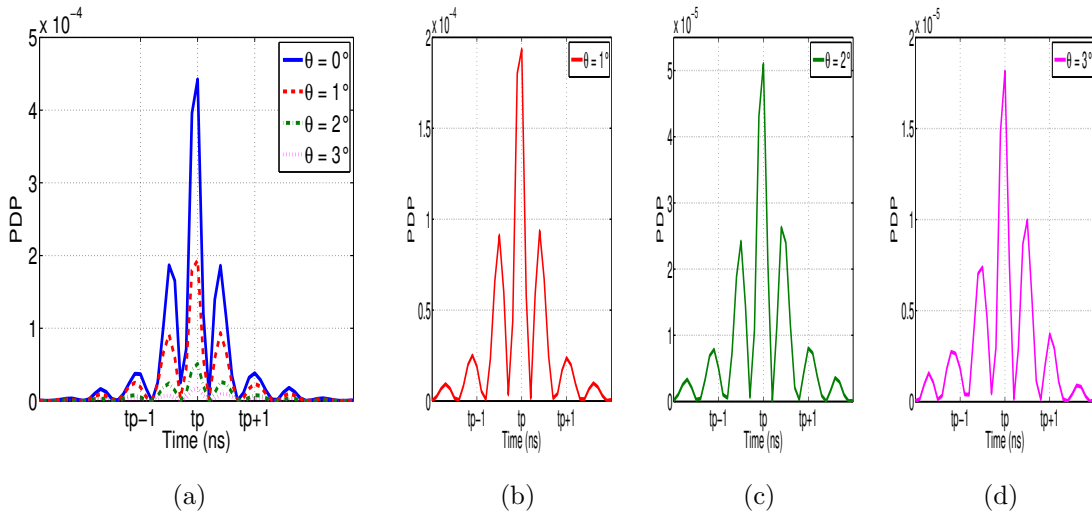


Figure 3.5: PDP of the TR received signals a)  $y_j(\theta^\circ)$  b)  $y_j(1^\circ)$  c)  $y_j(2^\circ)$  d)  $y_j(3^\circ)$  for a bandwidth of 2.0 GHz

the strength of received signal peak has reduced, the signals are focused in time and have a high signal to side-lobe ratio (SSR).

To investigate why the TR received signal does not degrade in the same way as MCR does, we evaluate the partial correlation of the measured MCRs  $h'_j(0^\circ)$  and  $h'_j(3^\circ)$  having a bandwidth of 2.0 GHz. The two MCRs are arbitrarily divided into

100 equal parts written as under:

$$\begin{aligned} h'_j(0^\circ) &= [a_1, a_2, \dots, a_{100}] \\ h'_j(3^\circ) &= [b_1, b_2, \dots, b_{100}] \end{aligned} \quad (3.2)$$

where  $a_i$  and  $b_i$  are vectors extracted from the two MCRs all having equal lengths.  $a_i$  can be written as:

$$a_i = \sum_{j=\frac{N(i-1)}{100}+1}^{\frac{N i}{100}} h'_j(0^\circ, j) \quad (3.3)$$

where  $N$  is total number of MCR taps. The vectors,  $b_i$ , can also be extracted in the same manner from the MCR,  $h'_j(3^\circ)$ . Length of both  $a_i$  and  $b_i$  is  $0.2 \mu s$ . Thereafter, the correlation coefficients of each  $a_i$  and its respective  $b_i$  are calculated as:

$$\rho(a_i, b_i) = \frac{s_{a_i b_i}}{\sqrt{s_{a_i a_i} s_{b_i b_i}}} \quad (3.4)$$

where  $s_{a_i b_i}$  is the covariance of  $a_i$  and its respective  $b_i$ ,  $s_{a_i a_i}$  and  $s_{b_i b_i}$  are the variances of  $a_i$  and  $b_i$  respectively. FIG. 3.6 shows the curve for these (100) partial correlations. Although the correlation coefficient for the MCR  $h'_j(0^\circ)$  and  $h'_j(3^\circ)$  is in the order of 0.1 (see FIG. 3.3), the partial correlation coefficients reveal some interesting facts. FIG. 3.6 shows that some parts of the MCR,  $h'_j(0^\circ)$ , have very strong correlation with their respective parts of the MCR  $h'_j(3^\circ)$ . Thus, a part of the MCR maintains its form and does not de-correlate. FIG. 3.7 shows the correlated parts of the two MCRs having a length of  $40 ns$ . This correlation affects the received signal peak and in spite of a totally de-correlated channel (in total), TR achieves high signal quality, i.e. high SSR and FG and relatively lower RMS delay spread.

Table 3.1 compares the RMS delay spread of the TR received signal and the MCR for different bandwidths. To reduce the noise components, signal taps having a power less than the threshold of 2% ( $-39 dB$ ) of the maximum peak power are forced to zero. Once a tap crosses the threshold, all the taps are included in the selected signal until the signal taps reaches a stage after which they never cross the threshold. FIG. 3.8a shows the TR received signal along with the selected signal for the delay spread for a rotation of the stirrer by  $\theta = 1^\circ$  ( $y_j(1^\circ)$ ) for a bandwidth of  $2 GHz$ . A small part of the signal is selected for the calculation of the delay spread. FIG. 3.8b shows the TR received signal for  $\theta = 5^\circ$  ( $y_j(5^\circ)$ ) for a bandwidth of  $2 GHz$ . As expected, a large part of the signal is selected for the calculation of the delay spread.

The comparison of the RMS delay spread (Table 3.1) shows that the RMS delay spread of the TR received signal is in the order of  $0.5-0.8 ns$  for the first three positions of the stirrer except for the signal of  $1 GHz$  bandwidth. For higher bandwidths, the RMS delay spread is lesser than the lower bandwidths. For instance, the RMS delay spread for the TR received signal  $y_j(2^\circ)$  for a bandwidth  $1 GHz$  is  $885.2 ns$ , where as the delay spread for  $y_j(2^\circ)$  with a bandwidth of  $2 GHz$  bandwidth is  $0.65 ns$ . Thus, the signals having larger bandwidth can resist the changes in the channel better than

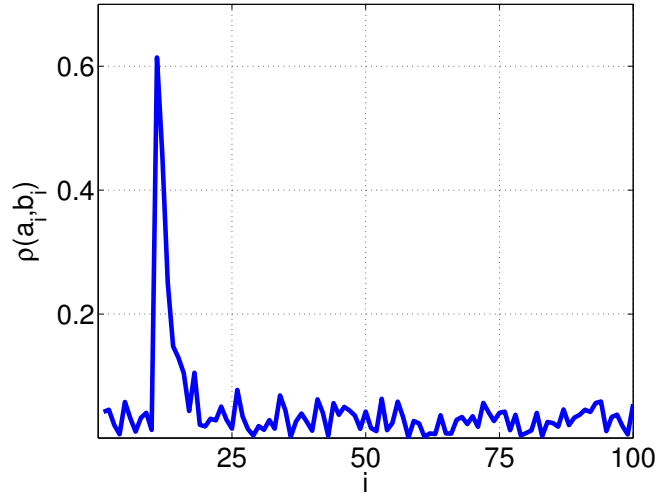


Figure 3.6: Partial correlation between the  $a_i$  and  $b_i$  extracted from MCRs  $h'_j(0^\circ)$  and  $h'_j(3^\circ)$  respectively for bandwidth of  $2.0\text{ GHz}$

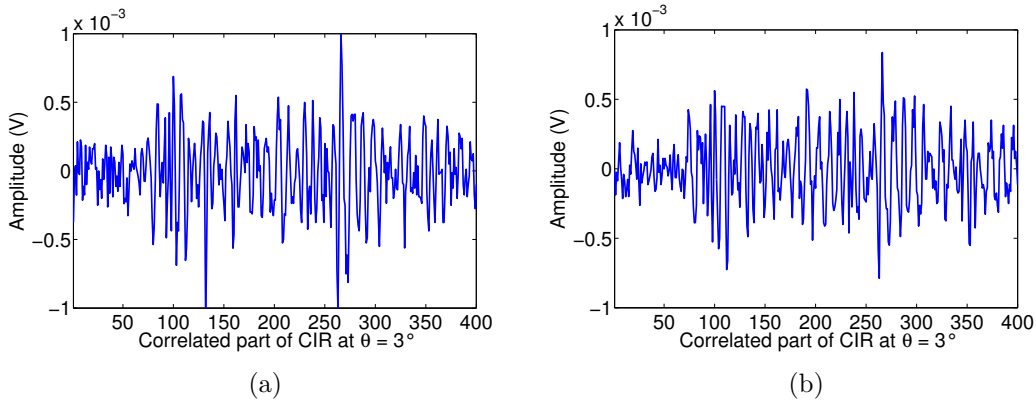


Figure 3.7: Correlated part of the MCRs  $h'_j(0^\circ)$  and  $h'_j(3^\circ)$  for a bandwidth of  $2.0\text{ GHz}$

the signals with lower bandwidths. As the stirrer moves by  $\theta = 3^\circ$ , a substantial increase in the RMS delay spread is observed. The robustness of the TR system is evident from these observations. Even if the channel is de-correlated from its original state ( $\theta = 1^\circ, 2^\circ$ ), the TR received signal has a very short delay spread especially for bandwidths  $\geq 1.5\text{ GHz}$ . For  $\theta \geq 3^\circ$ , it is quite large (in the order of  $1\text{-}3\ \mu\text{s}$ ) but still it is less than the RMS delay spread of the MCR which remains almost constant for all the positions of the stirrer (in the order of  $5.5\ \mu\text{s}$ ). Again one can note the difference in the RMS delay spread of signals of different bandwidths. The higher bandwidths always result in a lesser RMS delay spread.

$\theta$ (degrees)	Delay Spread of TR signal ( $\mu s$ )			Delay Spread of MCR ( $\mu s$ )		
	1.0 GHz	1.5 GHz	2.0 GHz	1.0 GHz	1.5 GHz	2.0 GHz
0	0.00078	0.00071	0.00055	5.38	5.29	5.50
1	0.00089	0.00077	0.00060	5.41	5.28	5.51
2	0.8852	0.00084	0.00065	5.41	5.28	5.50
3	2.6724	1.0906	1.2007	5.42	5.28	5.51
4	2.7110	1.7509	1.7118	5.42	5.27	5.50
5	2.6243	2.2131	1.9946	5.38	5.29	5.49

Table 3.1: Comparison of delay spread of the TR received signal ( $y_j(\theta^\circ)$ ) and the MCR ( $h'_j(\theta^\circ)$ ) for different  $\theta$  and bandwidths

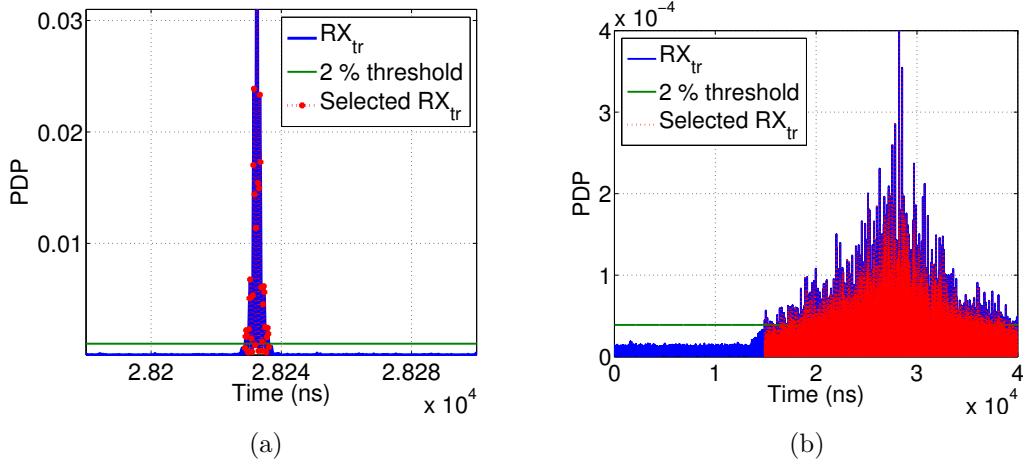


Figure 3.8: Received TR signal with a 2% threshold for a)  $\theta = 1^\circ$  b)  $\theta = 5^\circ$

FIG. 3.9 shows the effects of the rotation of the stirrer on different TR characteristics. Even though the MCR changes rapidly with  $\theta$ , received peak power does not decrease as severely with  $\theta$  (see FIG. 3.9a) as does the correlation coefficients of the MCR (see FIG. 3.3). More importantly, SSR does not degrade a great deal with  $\theta$  (see FIG. 3.9b). Thus, the signal quality remains almost constant. Focusing gain (FIG. 3.9c) and the increased average power (FIG. 3.9d) also decrease with  $\theta$  but the decrease can be considered small compared to the channel de-correlation. Thus, TR system can resist a change in the channel if a part of the channel is not totally de-correlated. TR system results in a good signal quality even if the channel is de-correlated (in total). It must be noted that the TR performance improves with the bandwidth for a same change in the channel environment. Thus for a given change in the channel environment, higher bandwidths result in a better robustness of the

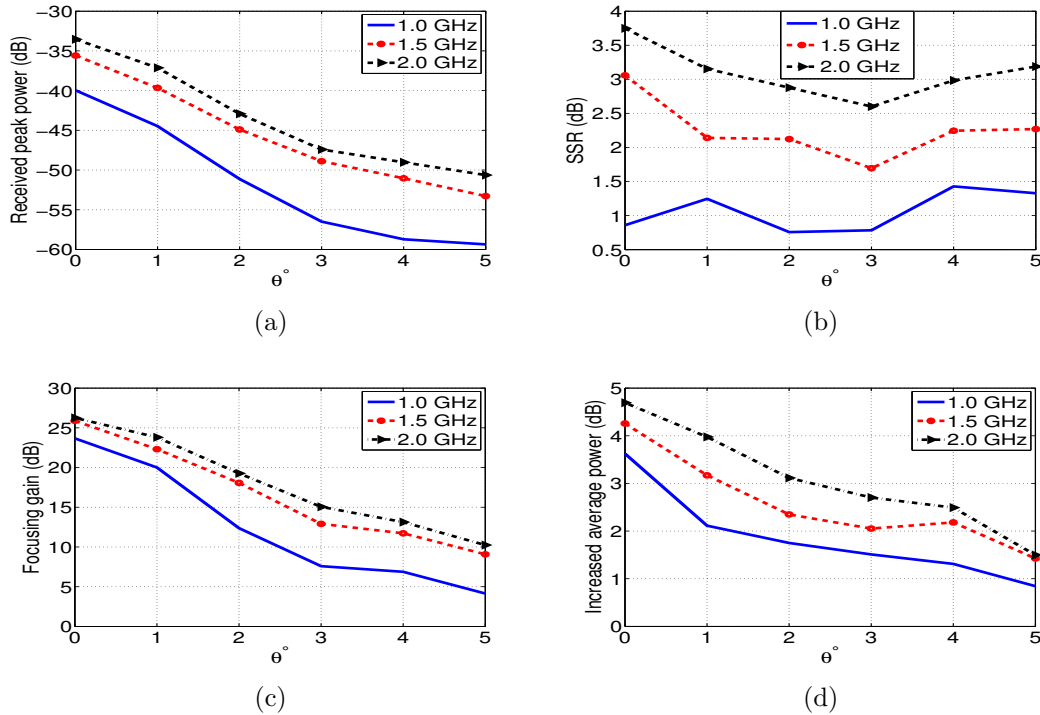


Figure 3.9: For varying  $\theta$  and different bandwidths, a) Received peak power b) Signal to side-lobe ratio c) Focusing gain d) Increased average power

TR system. However, the performance degradation with the change in the channel is similar for all the bandwidths as all the curves have similar slope.

The comparison of the TR properties shows that even with a very low correlated MCR, TR system gives a satisfactory performance. For instance, for  $\theta = 2^\circ$ , MCR has a correlation coefficient in the order of 0.1-0.2, TR system has a FG in the order of 18-19 dB, SSR in the order of 3 dB, increased average power in the order of 3-4 dB, for the bandwidths  $\geq 1.5$  GHz. For the signal of 1 GHz bandwidth however, the performance is not very good which highlights the importance of using higher bandwidth in a TR system.

### 3.2.2.2 Experiments with Moving Receiver

Experiments are also performed in the RC with a moving receiver. The receiver is moved in x and y direction in the pattern shown in FIG. 3.10, by using a precise robotic positionner with a spatial resolution of 2.5 cm. After 30 cm (equal to  $\lambda$  at 1 GHz) movement in the x direction, the receiver is moved 30 cm in the y direction. At  $y = 30$  cm, the receiver is again moved in the x direction till it reaches  $x = 0$  cm. TR experiments are performed for the different bandwidths i.e. 1 GHz, 1.5 GHz and 2 GHz which corresponds to the wavelengths ( $\lambda$ ) of 30 cm, 40 cm, 42.86 cm. The wavelengths  $\lambda$  for all these bandwidths are calculated for the lower frequency ( $f_L$ ) of

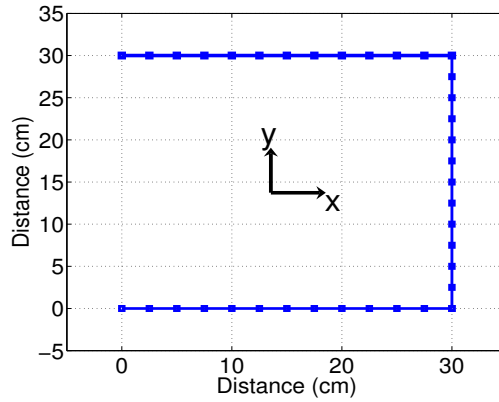


Figure 3.10: Pattern of the movement of the receiver for the TR experiments in the RC

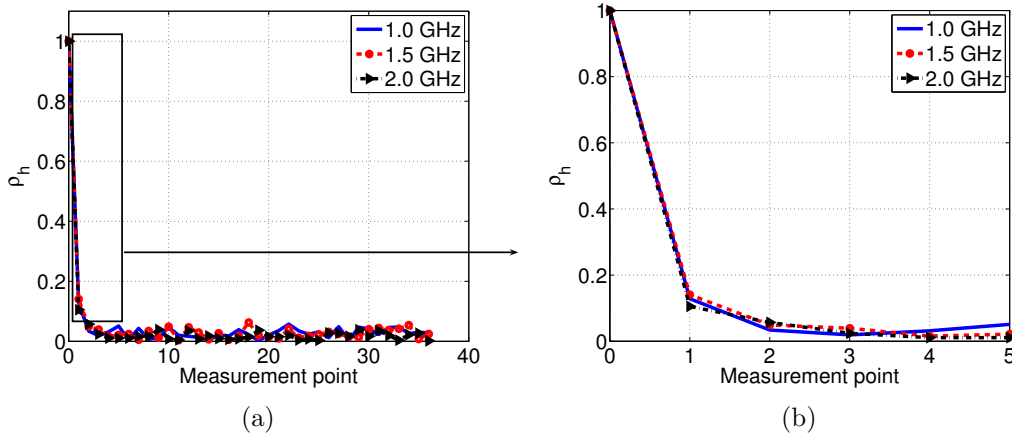


Figure 3.11: Cross-correlation coefficients ( $\rho_h$ ) of the MCR at a reference position and MCR at a) all measurement points b) first 6 measurement points

the bandwidth as the dimension of the focusing zone is governed by  $f_L$  [65]. FIG. 3.11 compares for different bandwidths, the cross-correlation coefficients ( $\rho_h$ ) of MCR at measurement point '0' ( $h'_j(0\text{ cm})$ ) and MCRs at other measurement points following the pattern of FIG. 3.10. Measurement point '0' corresponds to the reference position ( $x = 0\text{ cm}, y = 0\text{ cm}$ ). All other measurements are compared with this point. After a movement of  $\geq 10\text{ cm}$ , the MCR is almost totally de-correlated. The zoomed part of the figure for the first six measurement points is shown in FIG. 3.11b.

FIG. 3.12 shows for different bandwidths, the cross-correlation coefficients ( $\rho_y(d)$ ) between the TR received signals at different distances ( $d$ ) from the reference position ( $y_j(d\text{ cm})$ ) and the TR received signal at the reference position ( $y_j(0\text{ cm})$ ). It is observed that with  $10\text{ cm}$  movement of the receiver, which corresponds to  $\frac{\lambda}{3}$  at  $1\text{ GHz}$  and  $\frac{\lambda}{4}$  at  $750\text{ MHz}$ , the TR received signal is almost totally de-correlated.

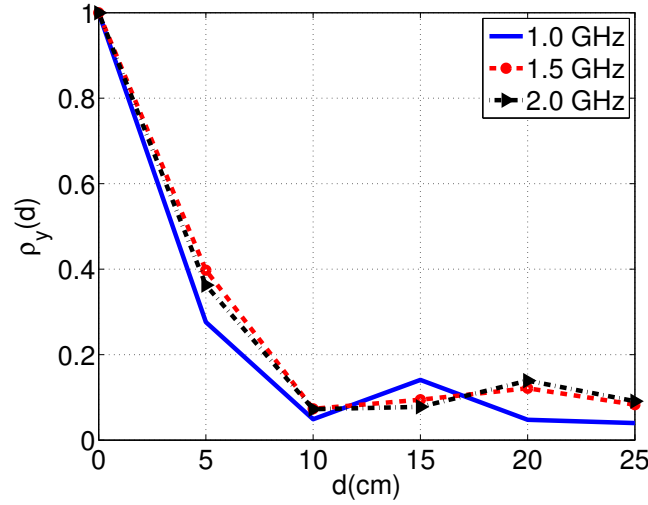


Figure 3.12: Cross-correlation coefficients ( $\rho_y(d)$ ) of the TR received signal at different distance ( $d$  cm) from the reference position ( $d = 0$  cm)

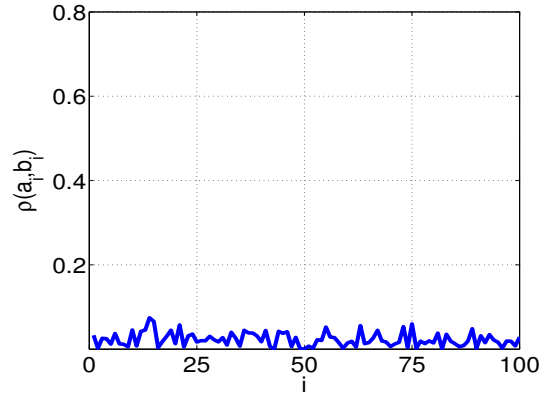


Figure 3.13: Partial correlation between  $a_i$  and  $b_i$  extracted from the MCRs  $h'_j(d = 0$  cm) and  $h'_j(d = 10$  cm) respectively for a bandwidth of 1.5 GHz

Thus, a little movement of the receiver results in a totally de-correlated TR received signal. In the case of moving receiver, as it was expected, the partial correlation also disappears quite rapidly.

FIG. 3.13 shows for a bandwidth of 1.5 GHz, the partial correlation between the MCR measured at the reference position ( $h'_j(0$  cm)), and the MCR measured at a distance of 10 cm ( $h'_j(10$  cm)). The distance of 10 cm corresponds to  $\frac{\lambda}{4}$  as  $f_L = 750$  MHz. Both MCRs are divided into 100 equal parts ( $a_i$  and  $b_i$ ) and then the correlation coefficients ( $\rho(a_i, b_i)$ ) between the respective parts are calculated from (3.4). It is observed that no part is highly correlated with its respective part. Thus, movement of the receiver in the order of  $\frac{\lambda}{4}$  entirely de-correlates the MCR.

Distance $d$ (cm)	Delay Spread of TR signal ( $\mu s$ )			Delay Spread of MCR ( $\mu s$ )		
	1.0 GHz	1.5 GHz	2.0 GHz	1.0 GHz	1.5 GHz	2.0 GHz
0	0.00063	0.00071	0.00057	5.58	5.55	5.68
5	0.0012	0.00085	0.00064	5.59	5.55	5.70
10	1.9761	1.1460	0.6491	5.60	5.54	5.70
15	2.5125	1.0799	1.4306	5.59	5.54	5.70
20	3.6471	2.4667	1.6635	5.58	5.51	5.69
25	3.7413	3.3665	2.1177	5.58	5.58	5.68

Table 3.2: For different bandwidths, comparison of delay spread of the TR received signal ( $y_j(d\text{ cm})$ ) and the MCRs ( $h'_j(d\text{ cm})$ ) at different distances ( $d\text{ cm}$ ) from the reference position ( $d = 0\text{ cm}$ )

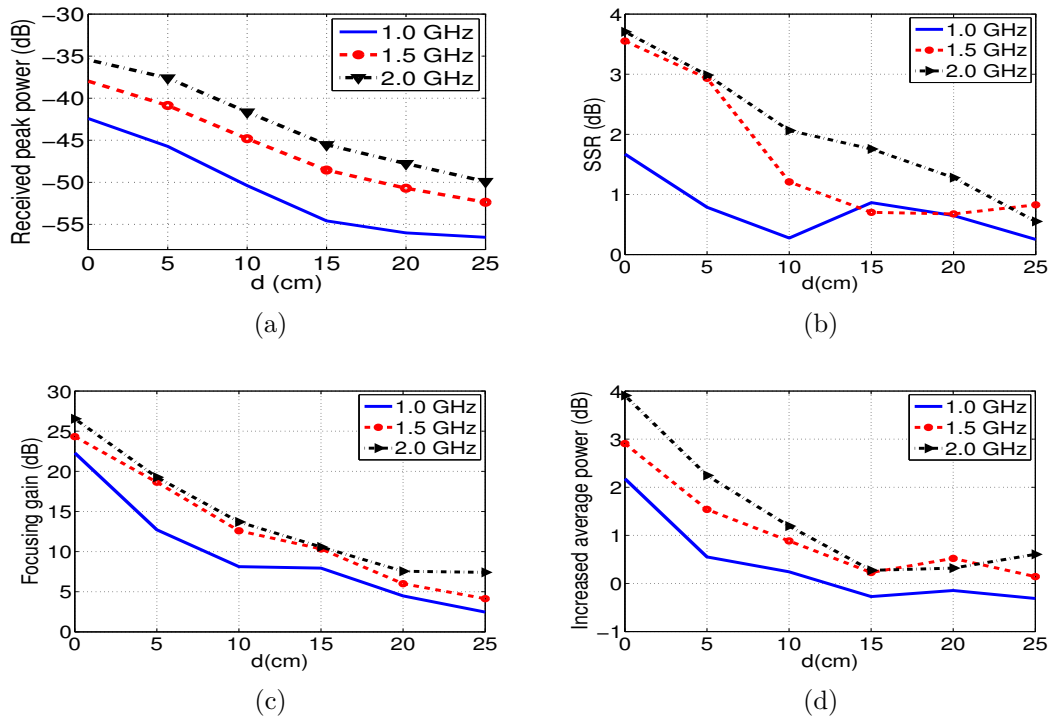


Figure 3.14: For varying positions of the receiver and different bandwidths, a) Received peak power b) Signal to side-lobe ratio c) Focusing gain d) Increased average power

Table 3.2 compares the RMS delay spread of the TR received signal and the MCR for movement of the receiver by 0-25 cm. For a 10 cm (or more) movement of the receiver, the RMS delay spread increases rapidly. However, the RMS delay spread is always less than the spread of the MCR. For higher bandwidths, delay spread is

always lesser than lower bandwidths but for a movement  $\geq 10\text{ cm}$ , the RMS delay spread of all bandwidths is in the order of  $1 - 4\ \mu\text{s}$ .

The effects of the channel change by the movement of the receiver are studied on different TR characteristics and are plotted in FIG. 3.14. The performance is degraded quite rapidly. Even for the higher bandwidths, the performance of the TR system becomes very poor after a small movement of the receiver. For instance for a  $20\text{ cm}$  movement of the receiver, the received peak power is decreased by  $15.28\text{ dB}$ , FG is decreased by  $19\text{ dB}$ , SSR is decreased by  $2.47\text{ dB}$  and the average increased power is decreased by  $3.66\text{ dB}$  for a bandwidth of  $2.0\text{ GHz}$ . Thus in a RC, a very small movement of the receiver degrades the performance substantially.

### 3.3 TR Robustness in Realistic Channels

In order to confirm the results in the RC, experiments are carried out in more realistic indoor environments. The robustness of the TR scheme is studied in two different indoor environments. The variations in the channel are introduced by the movement of the persons in the environment. Thereafter, to further modify the channel, metallic strips are placed in the environment. Experiments are performed for three different bandwidths, i.e.  $2.0\text{ GHz}$ ,  $1.5\text{ GHz}$  and  $1.0\text{ GHz}$ .

#### 3.3.1 Measurement Procedure

Experiments are performed to analyze the robustness TR scheme in the indoor environments. At first, the channel response is measured and the time reversal experiment is performed without any movement or change in the channel. Thereafter, TR experiments are performed in a non-stationary channel environment but with the same transmitted signal. There are two types of induced variations in the channel. In the first type, transmitter and the receiver do not change their position and channel is changed due to the changes in the environment. In the second type, transmitter or the receiver changes its position. TR experiments are performed for both types of variations. To include more generality in the results and ascertain the results two measurement campaigns are performed in two different indoor environments. For the second measurement campaign, the experiments are only performed for a bandwidth of  $2\text{ GHz}$ .

#### 3.3.2 Experiments With a Changing Environment

##### 3.3.2.1 Measurement Campaign 1

###### Experimental Setup

An experimental setup is established in a typical indoor environment (IETR laboratory) having the plan shown in FIG. 3.15. All rooms are furnished with office equipments: tables, PCs and seats. Moreover, there is a large reverberating chamber

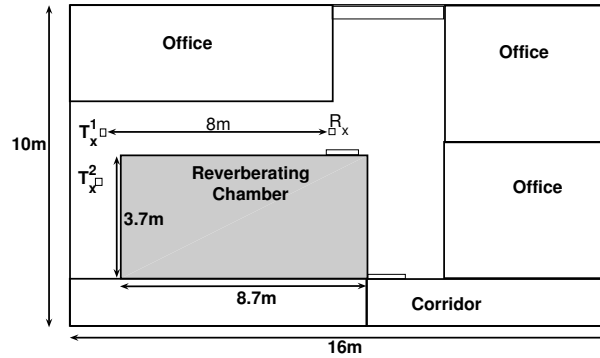


Figure 3.15: Measurement environment layout

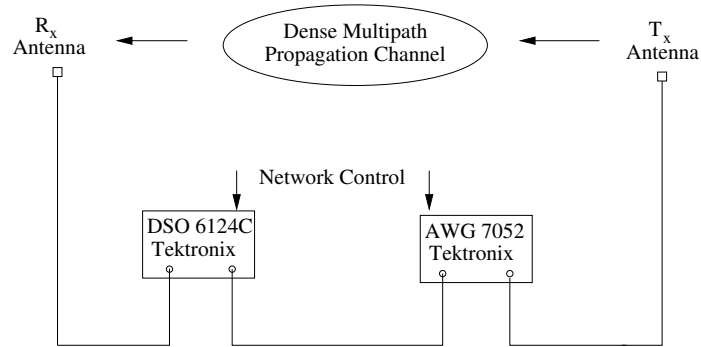


Figure 3.16: Experimental Setup

in the laboratory, which increases the wave reflections in the environment. The experimental setup is shown in FIG. 3.16. Two conical mono-pole antennas (CMA-118/A), are used as the transmitter and the receiver in a NLOS configuration. The distance between the transmitter and the receiver is 8.35 m. The height of the transmitting and receiving antennas is 1.8 m and 1 m from the ground respectively. The channel sounding pulse and the time reversed MCR are generated through the AWG having a maximum sampling rate of 5 GS/s. The receiver is a DSO with a maximum sampling rate of 40 GS/s. The DSO captures the channel response. Once the channel response is measured, the time reversed version of the MCR is created through MATLAB and is retransmitted with the AWG in the same channel to measure the TRR which is captured by the DSO. The DSO is operated in an average mode so that 1024 samples are taken and averaged together to reduce the captured noise.

### Induced Variations in the Channel

In the RC, a stirrer was used to induce the variations in the channel. In realistic channel environment, the changes in the channel are induced by the movement of the



Figure 3.17: Two metallic strips used to induce variations in the channel

people in the channel or by the displacement of the furniture. Therefore, experiments are performed for the following induced variations in the indoor channel environment:

1. Presence of one person near the receiving antenna
2. Presence of one metallic strip near the receiving antenna
3. Presence of one metallic strip near the receiving antenna and one near the transmitting antenna

The metallic strips used for the experiments are shown in FIG. 3.17. The positions near the terminals are chosen because they can most affect the channel. Thus in a way, these results represent a kind of worst case channel variations in the channel.

### Measurement Results

FIG. 3.18 shows for the different bandwidths, respective correlation coefficients of the original (without any change) MCR and the measured TRR with the MCRs and measured TRRs with different induced variations in the channel. The variations in the indoor channel caused by the movement of the people or by putting the metal strips in the channel (which is a sort of worst case in an indoor channel), do not de-correlate the channel completely. The correlation coefficients of the TRR is significantly higher than the correlation coefficients of the MCR for the same variation in the channel suggesting that the TR is more robust than the pulsed UWB systems.

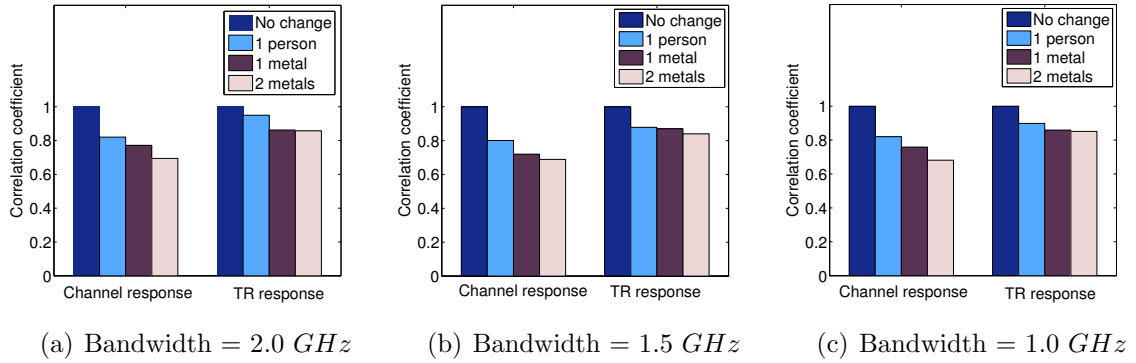


Figure 3.18: Correlation coefficient of the MCR and the TRR with different induced variations in the channel

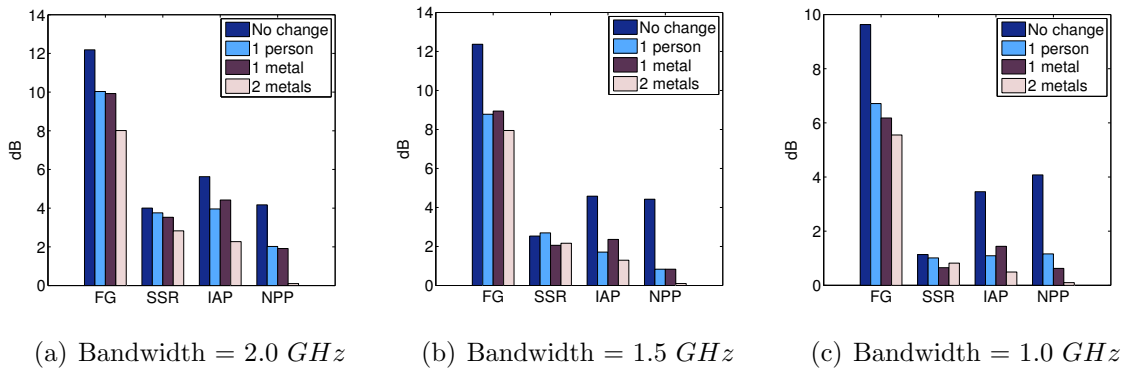


Figure 3.19: Relative strength of different TR properties with different induced variations in the channel

FIG. 3.19 shows the comparison of different TR properties with different induced variations in the channel for different bandwidths. FG, SSR, IAP and NPP are compared for different bandwidths and for different induced variations in the channel. For each bandwidth, the received peak power is normalized to the received peak power with the two metals placed in the channel because it is the lowest of all. Higher bandwidths have generally higher values of different performance metrics but generally the robustness of the TR scheme is not affected a great deal with the bandwidth of the transmitted signal. The deterioration in the performance with different induced variations is of the same order for all bandwidths. A very high FG is observed with all kind of variations in the channel. SSR does not change a great deal (ascertaining the results obtained in the RC). IAP decreases with the variations in the channel especially for lower bandwidth (1.5 GHz and 1.0 GHz).

FIG. 3.20 shows the PDP of the TR received signal with and without induced variations in the channel for a bandwidth of 2 GHz. Although the received signal strength decreases with the variations in the channel, the received signal has a very

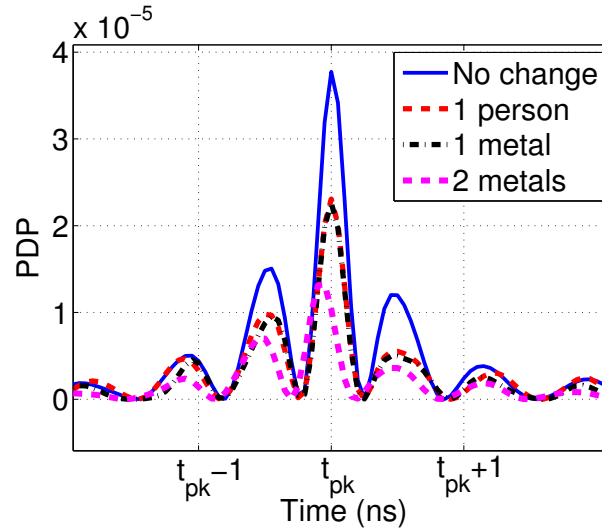


Figure 3.20: PDP of the received TR signal with different variations induced in the channel or a bandwidth of  $2.0\text{ GHz}$

good quality. Even with two metallic strips, for which the MCR has a correlation coefficient of 0.7, the received signal has a very good quality.

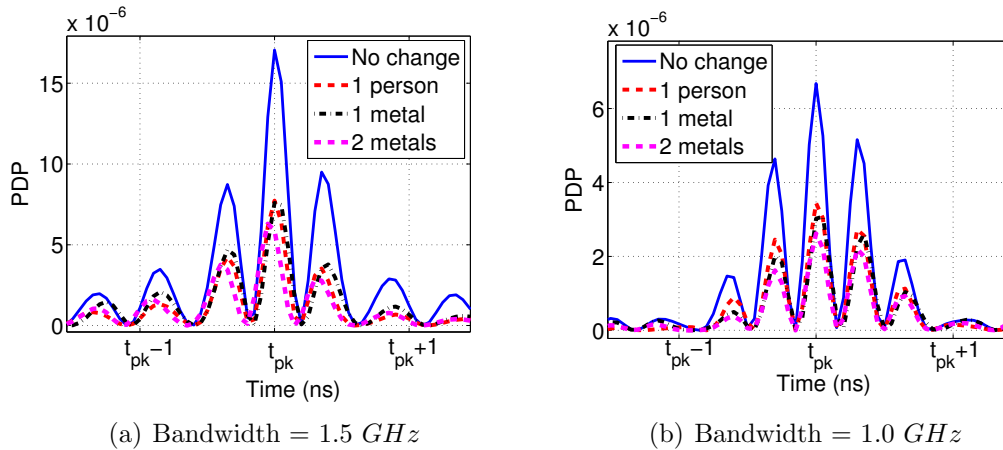


Figure 3.21: PDP of the received TR signal with different variations induced in the channel different bandwidths

FIG. 3.21 shows the PDP of the TR received signal with and without induced variations in the channel for a bandwidth of  $1.5\text{ GHz}$  and  $1.0\text{ GHz}$ . It is evident that the received signal is of very high quality and has a strong correlation with the received signal without modification in the channel. The received signal strength is however affected with the variations in the channel. This reduction in the power is strongly linked to the channel environment. In the above measurement layout, as both of the transmitter and the receiver are placed near the reverberation chamber,

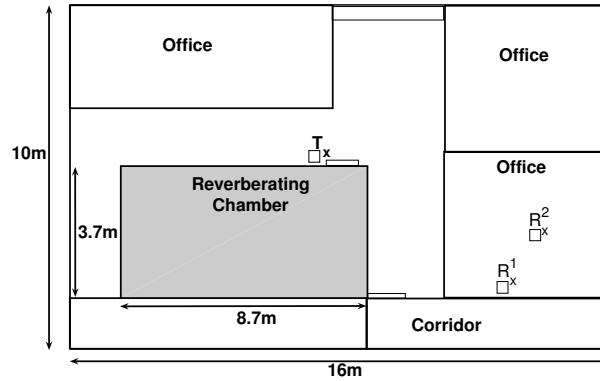


Figure 3.22: Measurement environment layout for the second measurement campaign

the received signal strength is affected with a variation in the channel especially near the terminals.

### 3.3.2.2 Measurement Campaign 2

To include more generality in the results and ascertain the results found by the previous experiment, experiments are conducted with different placement of the antennas in the environment with a bandwidth of  $2\text{ GHz}$ . This environment is relatively more typical indoor environment than the previous one (which has waveguide effects because of its layout). FIG. 3.22 shows the measurement layout of the second measurement campaign. Using the position 1, experiments are performed following the same procedure followed in the measurement campaign 1. Following variations are induced in the channel.

1. One person near the receiving antenna
2. One metallic strip and one absorber near the receiving antenna
3. Two metallic strips and one absorber near the receiving antenna

## Experimental Results

FIG. 3.23 shows respective correlation coefficients of the original (without any change) MCR and the measured TRR with the MCRs and measured TRRs with different induced variations in the channel for second measurement campaign. TRRs have significantly higher correlation coefficients as compared to the channel responses. For experiments with one person and one metallic strip, a very high correlation coefficient for the TRR is observed. The results of all these experiments suggest that although dependent on the environment, TR scheme is generally robust in every environment.

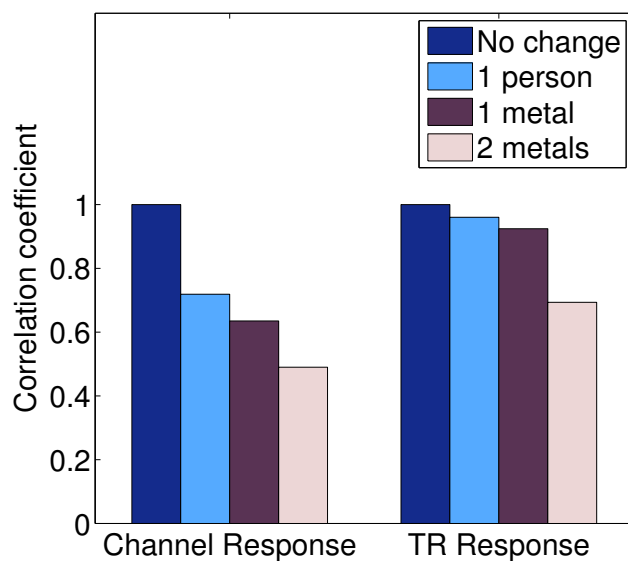


Figure 3.23: Correlation coefficient of the MCR and the TRR with different induced variations in the channel

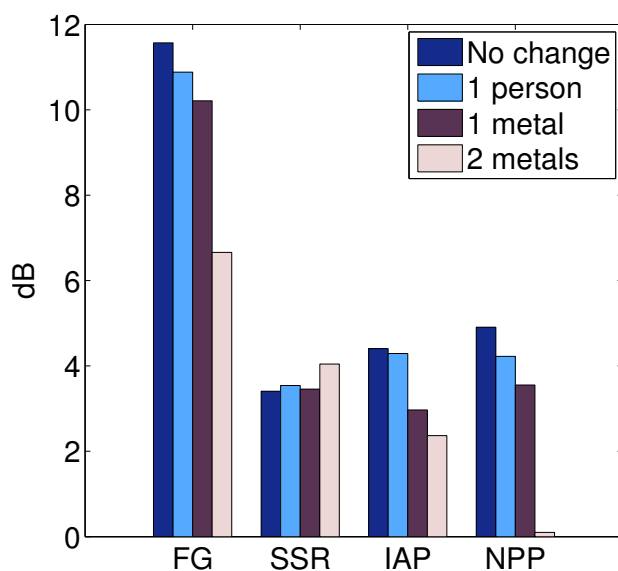


Figure 3.24: Relative strength of different TR properties with different induced variations in the channel for second measurement campaign

FIG. 3.24 shows the strength of different TR performance metrics for the second measurement campaign. One thing which is different from measurement campaign 1

is that for the induced variations in the channel with one person or one metallic strip, there is not much decrease in the focusing gain, increased average power and normalized peak power. SSR remains almost constant even with the induced variations in the channel. For instance, when the channel is modified by the presence of one person in the channel all TR properties experience only a minimal change although the modified and the original channel has a correlation coefficient of 0.7.

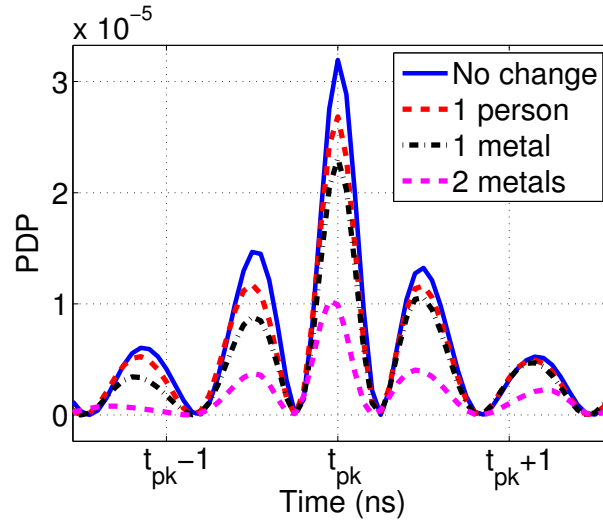


Figure 3.25: PDP of the received TR signal with different variations induced in the channel for a bandwidth of  $2.0 \text{ GHz}$

FIG. 3.25 shows the PDP of the TR received signal with and without induced variations in the channel for a bandwidth of  $2.0 \text{ GHz}$  for measurement campaign 2. The received signal with a presence of one person and one metallic strip in the channel has decreased only by  $0.7 \text{ dB}$  and  $1.35 \text{ dB}$  respectively. Thus, in an indoor channel TR scheme perform quite robustly even with the variations in the environment.

### 3.3.3 Experiments With a Moving Receiver

Experiments are also performed to study the effects of movement of the receiver on time reversal. The receiver is moved with a step of  $2.5 \text{ cm}$  for a bandwidth of  $2.0 \text{ GHz}$ . FIG. 3.26 shows the respective correlation coefficients of the MCRs ( $\rho_h(d)$ ) and the measured TRRs ( $\rho_y(d)$ ) at a distance  $d \text{ cm}$  with the MCR and measured TRR at  $d = 0 \text{ cm}$ . The measured TRR holds a better correlation with the original TRR even though the channel response is de-correlated almost completely. However, the de-correlation is sufficient to cause significant performance degradation of the TR scheme.

TABLE 3.3 summarizes different performance metrics for the displacement of the receiver up to  $30 \text{ cm}$  from the original position. The results give us some very interesting observations. The received peak power decreases with the movement of the

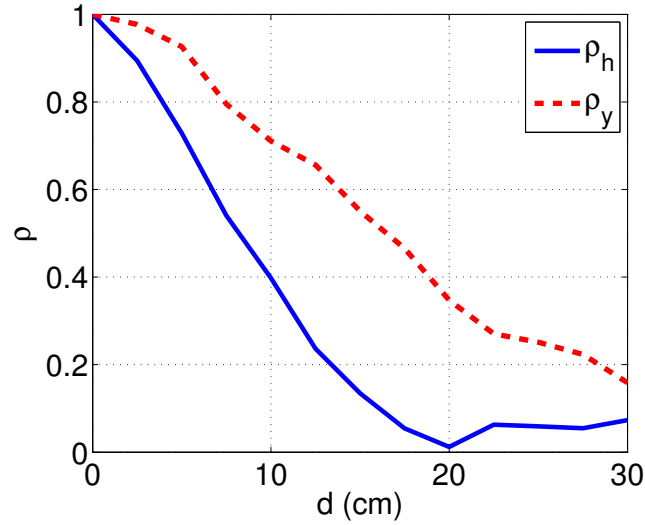


Figure 3.26: Respective correlation coefficients of the MCR ( $\rho_h(d)$ ) and the measured TRR ( $\rho_y(d)$ ) with the MCR and measured TRR at  $d = 0$  cm with different displacements of the receiver for a bandwidth of 2.0 GHz

receiver but it becomes somewhat static after almost 9 dB decrease in the received peak power. It is evident that the performance of the TR scheme deteriorates rapidly at first but then becomes somewhat saturated.

Distance	FG	IAP	SSR	NPP
0	11.87	4.64	3.85	0
5	10.28	3.97	3.40	-1.58
10	7.63	3.28	1.32	-4.24
15	5.60	2.39	0.06	-6.33
20	3.41	3.15	0.12	-8.59
25	2.01	2.82	1.35	-9.86
30	3.08	5.54	2.71	-8.78

Table 3.3: Comparison of different TR properties with different displacements of the receiver ( $d$  cm) with respect to the reference position ( $d = 0$  cm)

FIG. 3.27 shows the PDP of the TR received signal for different displacements of the receiver. The received peak power decreases considerably with the movement of the receiver but an interesting phenomenon is observed. Even though the received signals have been displaced by 20 cm and 30 cm, yet they have a peak (though significantly reduced) and the shapes of the two signals are very similar.

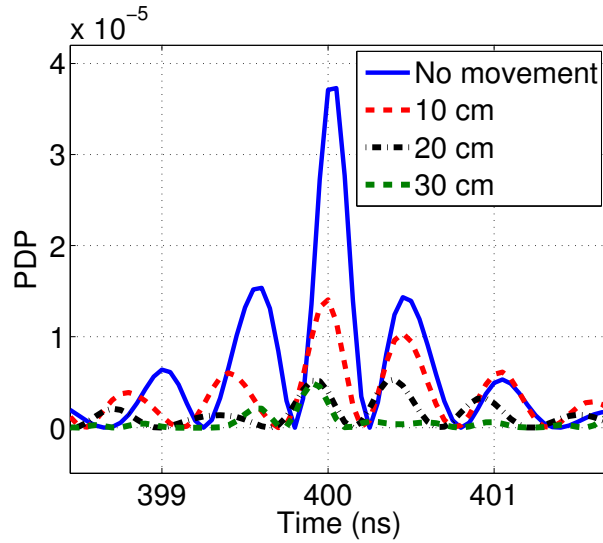


Figure 3.27: PDP of TR received signal with different displacements of the receiver

### 3.4 Conclusion

In this chapter, the robustness of a time reversal (TR) communication system is studied in a time varying channel environment. In the RC and the indoor environment, experiments are performed for the robustness of the TR scheme in a non stationary channel environment for three different bandwidths. In the RC, variations are induced with the rotation of the stirrer or the movement of the receiver. It has been found, that the bandwidth of the TR signal does not have a big impact on the robustness of the TR scheme. Higher bandwidths have generally better performance than the lower bandwidths but the degradation in the performance with the variations in the channel is of the same magnitude. The results suggest that TR system can give a robust performance even if the channel environment has changed partially. If the channel maintains some partial correlation with the previous channel, TR can give a good performance even if the total correlation of the channels is very low. For instance, channel impulse response with a  $2^\circ$  rotation of the stirrer has a correlation coefficient of 0.06 with the CIR of  $\theta = 0^\circ$ , but still the TR system achieves a RMS delay spread of only  $0.65 \text{ ns}$ , a focusing gain of  $19.26 \text{ dB}$ , signal to side lobe ratio of  $2.87 \text{ dB}$ , increased average power of  $3.15 \text{ dB}$ . On the other hand, if the receiver is displaced from its position, the channel gets totally de-correlated and does not maintain any partial correlation with the original CIR for a movement in the order of  $\frac{\lambda}{4}$ , where  $\lambda$  is the wavelength of lower frequency  $f_L$ . Thus, in a RC, TR system cannot support even a small movement of the receiver.

In the indoor environment, the variations in the channel are induced by the presence of a person, one metallic strip or two metallic strips in the channel near the receiver terminal. Higher bandwidths have generally higher values of different performance metrics but generally the robustness of the TR scheme is not affected a

great deal with the bandwidth of the transmitted signal. The deterioration in the performance with different induced variations is of the same order for all bandwidths. A very high FG is observed with all kind of variations in the channel. SSR does not change a great deal (ascertaining the results obtained in the RC). IAP decreases with the variations in the channel especially for lower bandwidths (1.5 GHz and 1.0 GHz).

These results are very important from the implementation point of view. In realistic environments, if the channel is changed due to the variation in the environment, e.g. movement of the people, the results suggest that channel will not de-correlate completely. In this case, TR robustness can play a vital role. There is no need to re-estimate the channel response if there are minor changes in the environment e.g. movement of the people. This property can be very attractive for WLAN and wireless streaming applications. However, when the receiver moves its position or there is significant change in the layout of the furniture, the performance of the TR scheme degrades rapidly, but nevertheless, the TRR maintains better correlation with the original TRR than the channel response maintains with the original channel response. Thus, TR is beneficial in a non stationary channel where variations are caused by the changes in the environment. The results suggest that realistic environments (such as typical indoor environment) create lesser number of multi-paths and are less sensitive to the changes in the environment than the RC.

# Chapter 4

## UWB Time Reversal Communication

### Contents

---

<b>4.1</b>	<b>Introduction</b>	<b>110</b>
<b>4.2</b>	<b>Novel Modulation Scheme for TR Communication</b>	<b>111</b>
4.2.1	Description of the Novel Modulation Scheme	111
4.2.2	Effects of Shift on the Received Signal	115
4.2.3	Theoretical Performance	116
4.2.4	Information Rate of the Modulation Scheme	117
4.2.5	Validation of the New Modulation Scheme by Experiments and Simulations	120
<b>4.3</b>	<b>High Data Rate TR Communication</b>	<b>127</b>
4.3.1	Experimental Setup	127
4.3.2	Experimental Results	128
4.3.3	Sub-Band TR Transmission Scheme	135
<b>4.4</b>	<b>Conclusion</b>	<b>138</b>

---

## 4.1 Introduction

The previous chapters of this thesis explained the validation and robustness of the TR scheme. Different properties of the TR scheme were studied including, TR peak performance, focusing gain, increased average power, signal to side lobe ratio and RMS delay spread etc. Although these parameters give an indication of how the TR scheme will perform in a communication system, they cannot be regarded as a direct performance metric for TR communication. True performance metrics for a communication system are bit error rate (BER), signal to interference ratio (SIR) and throughput.

Impulse radio ultra wide-band (UWB) is a communication technique in which high data rate can be achieved by making use of ultra large bandwidth. The ability of pulsed UWB to resolve individual multi-path components is exploited in the recent research for short range communication applications. However, large number of resolvable paths and low power limitations necessitate a complex receiver system. To collect the received signal energy, Rake, transmit-reference or the decision feedback auto-correlation receiver can be implied [47, 82, 83]. Each technique has different difficulties and drawbacks. In pulsed UWB communication systems, channel delay spread causes significant ISI. The performance of Rake receivers in the presence of such ISI is studied in a number of papers [45, 84].

In this chapter, high data rate TR communication is studied. In the first part of the chapter, we propose a novel modulation scheme which improves the data rate by spreading the transmitted data in a given large bandwidth, over the delay time [85]. This scheme has been registered as one of the patents by IETR [86] and an article has also been submitted on this subject [87]. Multiple data bits are packed in one time slot to add a new level of modulation along with the BPAM modulation. The packed data bits have quasi orthogonal waveforms and they cause minimum interference to the other bits. Thus, the received bits can be separated and demodulated quite easily. The BER performance of the new modulation scheme and the maximum achievable data rate are theoretically analyzed. Two separate measurement campaigns are carried out to analyze the performance of the modulation scheme. TR communication is simulated using the measurement results of the first measurement campaign. The simulated and the theoretical results are compared to each other. Furthermore, the performance of the new modulation scheme is compared with the performance of the quadrature amplitude modulation (QAM) and the pulse amplitude modulation (PAM) in an AWGN channel. With the second measurement campaign, the new modulation scheme is experimentally validated using time domain instruments. The performance of the proposed modulation scheme is compared for the two measurement campaigns.

In the latter part of the chapter, high data rate communication for a Time Reversal UWB communication system is experimentally studied for symbol times ( $T_s$ ) ranging from 64 ns to 1 ns (15.62 Mbps to 1 Gbps) using binary pulse amplitude modulation in dense multi-path propagation channels.

## 4.2 Novel Modulation Scheme for TR Communication

As mentioned in the previous chapters, in a TR communication scheme, time reversed CIR is used as a channel pre-filter. In the practical implementation of the TR system, the pre-coding filter is truncated in time to reduce the filter length and thus the system complexity. The truncated and time reversed channel response from the transmitting point  $i$  to the receiving point  $j$  is represented as  $h'_{ij}(-t)$ . The transmitted TR signal is normalized such that the average energy of the transmitted signal respects the limits of UWB spectral mask issued by FCC. For data communication purpose, the transmitted bits are modulated by binary pulse amplitude modulation (BPAM) scheme. The  $k^{th}$  symbol,  $d_k$ , of the symbol sequence is equal to 1 or -1 for the data bits 1 or 0 respectively. Therefore, the noiseless received signal at the intended receiver ( $j$ ) is written as:

$$y'(t) = A \underbrace{\sum_k d_k h'_{i,j}(-t + k T_s)}_{\text{Transmitted RF signal}} \star \underbrace{h_{ij}(t)}_{\text{CIR}} \quad (4.1)$$

where  $A$  is a normalization factor and  $T_s$  is the symbol duration. As the amplitude of the peak of the received signal is proportional to the energy of the transmitted signal (i.e.,  $\int h'_{i,j}{}^2 dt$ ), the truncation process decreases the peak of the received signal. Due to the BPAM, the polarity of the received peak signals is specified by the transmitted data bit and is used for the detection of the data bits.

### 4.2.1 Description of the Novel Modulation Scheme

An original technique for data modulation for time reversal systems has been proposed. We keep the BPAM modulation concept and add a second modulation level for the transmitted data. Let the CIR of the communication channel be represented by the classic tapped delay line model:

$$h(t) = \sum_{i=0}^{N-1} \alpha_i \delta(t - \tau_i) \quad (4.2)$$

where  $\delta(t)$  is the Dirac's delta function,  $N$  is the total number of taps in the CIR and  $\alpha_i$  and  $\tau_i$  are the respective amplitude and delay associated to the  $i^{th}$  tap. In the proposed scheme, the data bits ( $d_k$ ) which are the antipodal binary bits ( $\pm 1$ ) are divided into  $m$ -parallel lines using serial-to-parallel (S/P) conversion unit and then passed through multiple filter banks,  $\{K_1(t), K_2(t), \dots, K_m(t)\}$ , where subscript  $m$  is the number of bits transmitted in parallel giving us a modulation order  $M = 2^m$ .

FIG. 4.1 shows the conceptual block diagram of the new modulation scheme. The response of each filter is the shifted and truncated version of the original filter response  $h'(-t)$ . Let the measured, truncated and time reversed CIR with a length  $L < N$  tap

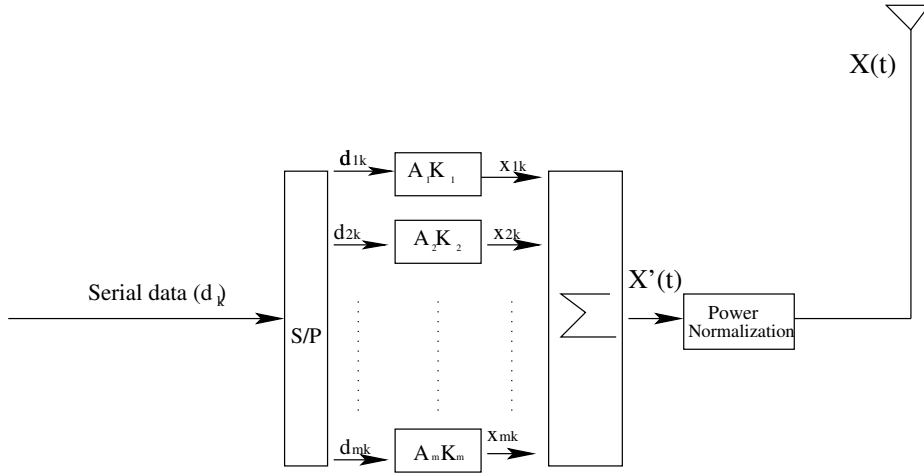


Figure 4.1: Conceptual block diagram of the new modulation scheme

be represented as:

$$h'(-t) = \sum_{i=0}^{L-1} a_i \delta(t - i \tau_s) \quad (4.3)$$

where  $L$  is the total number of the time reversal filter components having an equivalent length of  $T_{sig} = L \tau_s$  in seconds,  $a_i$  is the associated amplitude and  $i \tau_s$  is the associated delay of the multi-path components. The duration,  $\tau_s$ , is the time between two consecutive samples and depends on the maximum sampling rate of the time reversal filter. For instance, if the measured CIR is sampled with a sampling rate of  $5 \text{ GS/s}$ , the delay of  $\tau_s = 0.2 \text{ ns}$  is obtained between two consecutive samples, therefore the number of taps ( $L$ ) in filter having a length of  $50 \text{ ns}$  is  $L = 250$  samples or taps.

The responses of the filter banks are produced by shifting  $h'(-t)$  to either left or right and then forcing the shifted part to zero so that the shifted signal can be packed in the same signal duration. FIG. 4.2 shows the pattern of the left or right shift of  $l = 1, 2$  taps. As shown for the left shift of 1 tap, the last three taps are shifted to left by one tap and the slot for last tap is filled with zero. For the right shift of 1 tap, first three taps are shifted to right and then the slot for the first tap is filled with zero. If  $h'(-t)$  is shifted left or right by  $T_b = l_{opt} \tau_s$ , the expression is given by:

$$\begin{aligned} \text{right shift}(h'(-t, T_b)) &= \hat{h}(-t - T_b) = \left[ \text{zeros}(1, l_{opt}) \sum_{i=1}^{L-l_{opt}} a_i \delta(t - (l_{opt} + i) \tau_s) \right] \\ \text{left shift}(h'(-t), T_b) &= \hat{h}(-t + T_b) = \left[ \sum_{i=1}^{L-l_{opt}} a_{i+l_{opt}} \delta(t - i \tau_s) \text{zeros}(1, l_{opt}) \right] \end{aligned} \quad (4.4)$$

where  $\text{zeros}(1, l_{opt})$  is a vector containing  $l_{opt}$  number of zeros,  $l_{opt} \left( \frac{T_b}{\tau_s} \right)$  is the number of shifted taps required to exercise a shift of  $T_b$  and  $a_i$  is the coefficient of

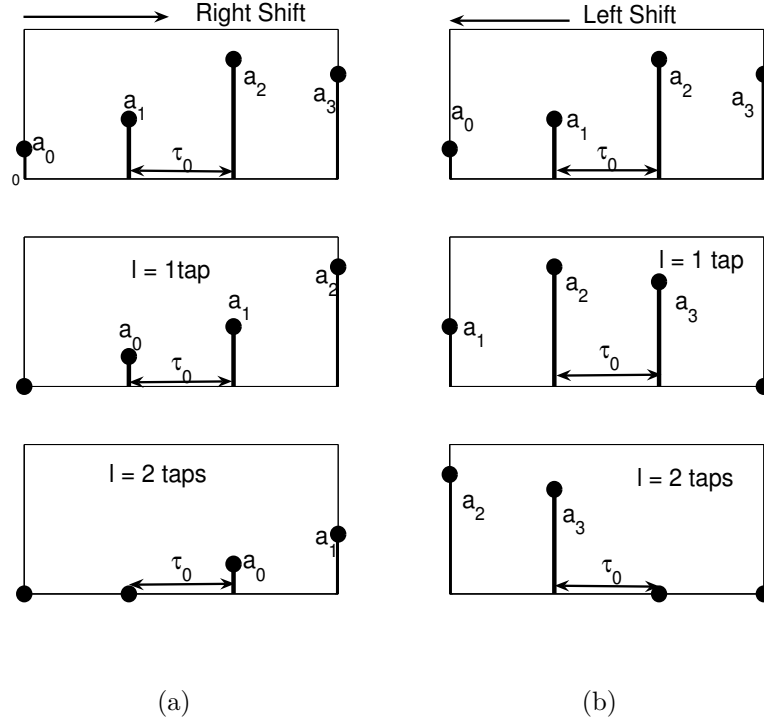


Figure 4.2: Pattern for the left and right shifts

$h'(-t)$  at the delay  $i\tau_s$ . Note that  $\hat{h}_j(-t - T_b)$  has  $L - l_{opt}$  non zero taps. As we have used only left shift for the new modulation scheme, the response of the  $i_{th}$  filter bank becomes  $K_i(t) = \hat{h}(-t + iT_b)$  with  $i \in \{0, \dots, m-1\}$ .

The signals after passing through the filter banks are then normalized to equal power and added together giving a waveform which can be written as:

$$X'(t) = \sum_{i=0}^{m-1} d_i A_i \hat{h}(-t + iT_b) \quad (4.5)$$

where the normalization factor  $A_i$  is given by the expression:

$$A_i = \frac{1}{\sqrt{\|\hat{h}(-t + iT_b)\|^2}} \quad (4.6)$$

where  $\|\cdot\|$  is the Frobenius norm operation. The normalization insures that each of the transmitted bits has equal power.

Due to addition of the signals, the power of the resulted waveform,  $X'(t)$ , is modified. To keep a constant transmitted power ( $P_0$ ) with the transmitter unit of the communication system, the signal  $X'(t)$  must be re-normalized. This power normalization allows the system to respect the transmit power regulations. In order to normalize the total transmit power to  $P_0$ , each bit is transmitted with a power of  $\frac{P_0}{m}$

resulting in a power of  $P_0$  in a time frame and periodic transmission of the frames is done with a period of  $T_s = T_{sig}$ . The resulting transmitted signal can be expressed as:

$$X(t) = \sum_k \frac{1}{\sqrt{m}} X'(t - kT_s) = \sum_k \frac{1}{\sqrt{m}} \sum_{i=0}^{m-1} d_{ik} A_i \hat{h}(-t + iT_b - kT_s) \quad (4.7)$$

The signal  $X(t)$  is transmitted in the propagation channel. The received signal can be written as:

$$\begin{aligned} R_x(t) &= h(t) \star X(t) + n(t) = h(t) \star \sum_k \frac{1}{\sqrt{m}} \sum_{i=0}^{m-1} d_{ik} A_i \hat{h}(-t + iT_b - kT_s) + n(t) \\ &= \sum_k \sum_{i=0}^{m-1} d_{ik} w_{rx_i}(t + iT_b - kT_s) + n(t) \end{aligned} \quad (4.8)$$

where  $w_{rx_i}(t + iT_b - kT_s) = h(t) \star \hat{h}(-t + iT_b - kT_s)$  is the received signal waveform for the  $i_{th}$  bit. Now if the channel delay spread is  $T_d$ , the received signal peak will be detected at  $t_{peak} = T_d + T_s$ . If  $m$  bits are transmitted simultaneously, peaks can be detected at:  $t_{peak_i} = t_{peak} + iT_b, \forall i \in \{0, \dots, m-1\}$ . Assuming a perfect synchronization, the received peaks for the  $i_{th}$  bit can be written as:

$$R_x(t_{peak_i}) = \sum_k \left[ \underbrace{d_{ik} w_{rx_i}(t_{peak} + iT_b - kT_s)}_{Signal} + \underbrace{\sum_{j=0, j \neq i}^{m-1} d_{jk} w_{rx_j}(t_{peak} + iT_b - kT_s)}_{Intra Symbol Interference} \right] + n(t) \quad (4.9)$$

The vectorial form for the  $k_{th}$  symbol can be written as:

$$\vec{z}_k = \vec{d}_k W_{rx} + \vec{\eta}_k \quad (4.10)$$

where  $\vec{z}_k$  is the decision variable,  $\vec{d}_k = (d_{0k}, \dots, d_{m-1k})$  is a vector of  $m$  transmitted bits in the  $k_{th}$  symbol,  $\vec{\eta}_k$  is the AWGN vector and the matrix  $W_{rx}$  is defined as:

$$W_{rx} = \begin{pmatrix} w_{0,0} & w_{0,1} & \cdot & \cdot & \cdot & w_{0,m-1} \\ w_{1,0} & w_{1,1} & \cdot & \cdot & \cdot & w_{1,m-1} \\ \cdot & \cdot & \cdot & \cdot & \cdot & \cdot \\ \cdot & \cdot & \cdot & \cdot & \cdot & \cdot \\ \cdot & \cdot & \cdot & \cdot & \cdot & \cdot \\ w_{m-1,0} & w_{m-1,1} & \cdot & \cdot & \cdot & w_{m-1,m-1} \end{pmatrix}$$

where  $w_{x,y} = w_{rx_x}(t_{peak} + yT_b - kT_s)$  with diagonal as the peaks of the *Signal* and the rest are the interference peaks.

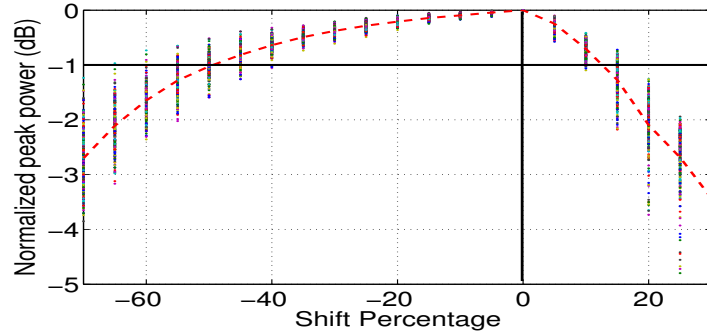


Figure 4.3: Received signal peak power with left and right shifts normalized to the peak with no shift

### 4.2.2 Effects of Shift on the Received Signal

In a TR communication system, as the received signal is the auto-correlation function of the CIR. The received signal peak is the sum of the square of the coefficients of CIR (from the properties of auto-correlation function). The transmitted signal for the new modulation scheme is given by (4.7). The received signal at the peak is given by (4.9). Neglecting the interference and the noise, the received signal peak for the  $j$ th bit of the  $k$ th symbol is written as:

$$R_x(t_{peak_{jk}}) = d_{jk} w_{rx_j}(t_{peak} + j T_b - k T_s) = d_{jk} A_j \left( \sum_{i=0}^{L-l_j-1} a_i^2 \right) \quad (4.11)$$

where  $a_i$  are the coefficients of taps of  $\hat{h}(-t + j T_b - k T_s)$  and  $l_j$  ( $j \frac{T_b}{T_s}$ ) are the number of taps required for a shift of  $j T_b$ . The received signal peak depends on the energy contents of  $(L - l_j)$  filter coefficients. Thus, the amplitude of the received peak decreases by the sum of the squared coefficients in the shifted part of the transmitted signal. Therefore with the new modulation scheme, the received signal peak reduces in proportion to the energy of the shifted part of the transmitted signal.

FIG. 4.3 shows the peak power of the received signal peak for the shifted signals normalized to the received peak with no shift. The signals are shifted by a percentage of the total number of taps in the transmitted signal. A set of 243 measured CIRs are used for the simulation. Experimental setup and the measurement procedure are explained in Section 4.2.5. The loss of the received peak power for transmitted signals corresponding to individual CIRs is represented by the dots and the dashed line is the mean of power loss. The power loss for left shift is lesser than the power loss for the right shift as the energy contained in the shifted parts of the right shift is greater than the energy contained in the shifted parts of the left shift. Although a combination of right and left shifts can be used for the communication, for the sake of simplicity we have only used left shift. In the rest of the chapter unless otherwise mentioned, a shift is meant to be a left shift.

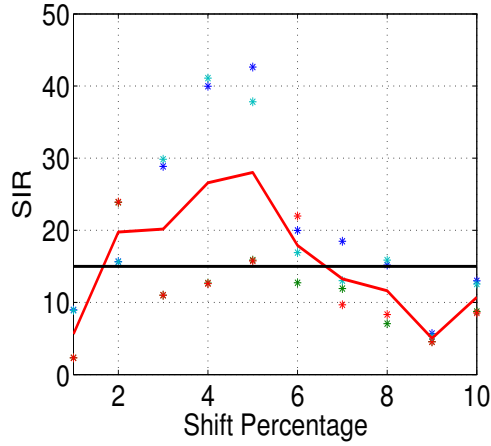


Figure 4.4: Average and bit by bit signal to interference ratio for the received signal with 4 simultaneous bits ( $m = 4$ ) with different shift steps (in percentage of the transmitted signal length ( $T_{sig}$ ))

In the proposed modulation scheme, the number of shifted samples is given by  $l_j = (j - 1) l_{opt}$  where  $j \in \{1, 2, \dots, m\}$  is one of the parallel data branches and  $l_{opt}$  is the optimal shift step. The choice of the shift step ( $l_{opt}$ ) is carried out under two conditions. The optimum shift step is the one which gives us an acceptable minimum signal to interference ratio (SIR) with the minimum possible shift. A small value of shift is required to restrict the power loss of the received peak due to the shift. Secondly, interference is introduced when multiple signals are packed in the same time slot. Thus, a shift percentage is required which gives an acceptable SIR for all the packed bits. The shift step which gives an acceptable SIR is not necessarily obtained for the large shift steps as the *Signal* part of the received signal decreases severely for high shift steps. FIG. 4.4 shows the SIR for  $m = 4$  with different shift steps. The figure was obtained for a measured CIR in an indoor environment. The stars ('\*') show the individual SIR for different bits while the solid line shows the mean SIR. If the minimum SIR is above a certain threshold (e.g. 15 dB), the shift percentage is acceptable. We found that even the small shift steps give a satisfactory SIR performance, thus we have chosen shift steps of 2% ( $0.02 T_{sig}$ ) and 5% ( $0.05 T_{sig}$ ) in our experiments.

### 4.2.3 Theoretical Performance

To evaluate the error probability of the new modulation scheme we suppose that the transmitted signals are quasi orthogonal and does not result in any significant intra symbol interference. With the new proposed technique,  $m$  simultaneous bits are transmitted and each bit has energy of  $\frac{E_s}{m}$ . The signal space representation of the new modulation scheme consists of  $m$  dimensions. FIG. 4.5 shows the signal space

representation of the new modulation scheme for  $M = 4$  ( $m = 2$ ) and  $M = 8$  ( $m = 3$ ).  $S(\vec{t})$  represents the received signal without noise and has an energy of  $E_s$ .

The transmitted signal is a sum of  $m$  orthogonal vectors, each having an energy of  $\frac{E_s}{m}$ . Let the received signal vector be  $X(\vec{t}) = S(\vec{t}) + N(\vec{t})$  where  $S(\vec{t})$  is the signal vector and  $N(\vec{t})$  is the noise vector. Then the symbol error probability for the transmission system can be written as:

$$P_s = 1 - P_c \quad (4.12)$$

where  $P_c$  is the probability of correct decision. Let the dimensions over which the signal space diagram is represented by  $x_1, x_2, \dots, x_m$ . Considering these vectors are statistically independent, the probability of the correct decision of a symbol can be written as:

$$P_c = Pr \left( \prod_{i=1}^m \overline{Proj X(\vec{t})/x_i} > 0 \right) = Pr \left( \prod_{i=1}^m \overline{Proj N(\vec{t})/x_i} > -\sqrt{\frac{E_s}{m}} \right) \quad (4.13)$$

where  $\overline{Proj(\cdot)/x_i}$  is the algebraic value of the projection of  $(\cdot)$  on the dimension  $x_i$ ,  $X(\vec{t})$  is the vectorial representation of the received signal and  $N(\vec{t})$  is the noise vector. Let the projection of  $N(\vec{t})$  on the dimension  $x_i$  be represented as  $p(n)$ , then  $P_c$  can be written as:

$$P_c = \left( \int_{-\sqrt{\frac{E_s}{m}}}^{+\infty} p(n) dn \right)^m = \left( 1 - \frac{1}{2} \operatorname{erfc} \left( \sqrt{\frac{E_s}{m N_0}} \right) \right)^m \quad (4.14)$$

The symbol error probability can be thus written as:

$$P_s = 1 - P_c \approx \frac{m}{2} \operatorname{erfc} \left( \sqrt{\frac{E_s}{m N_0}} \right) \quad (4.15)$$

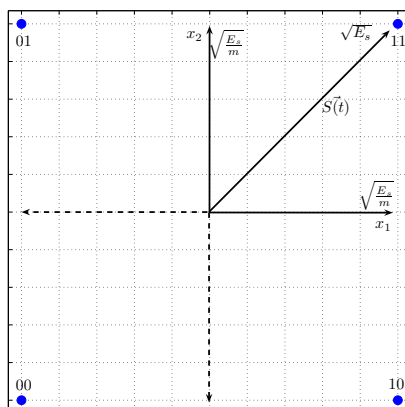
To find the bit error probability, from the geometrical symmetry we can say that probability of error in all of the individual bits are equal and thus the average of the bit error probability is equal to the error probability of one individual bit. The bit error probability can be therefore written as:

$$P_b = Pr \left( Proj \vec{N}/x_1 < -\sqrt{\frac{E_s}{m}} \right) = \int_{-\infty}^{-\sqrt{\frac{E_s}{m}}} p(n) dn = \frac{1}{2} \operatorname{erfc} \left( \sqrt{\frac{E_s}{m N_0}} \right) \quad (4.16)$$

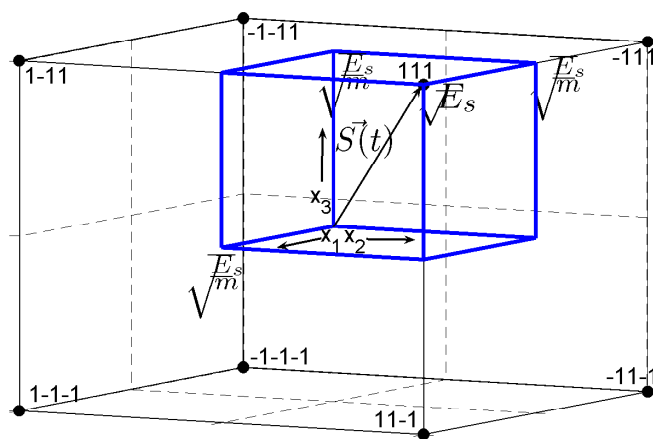
#### 4.2.4 Information Rate of the Modulation Scheme

For AWGN channel, the maximum bit rate which a system can achieve for a error free communication is given by the famous Shannon's formula:

$$C = B \log_2 \left( 1 + \frac{S}{N} \right) \quad (4.17)$$



(a)



(b)

Figure 4.5: Signal space representation of the new modulation scheme with  $M = 4$  and  $M = 8$

where  $C$  is the capacity of the channel in bits per second (bps),  $B$  is the channel bandwidth in  $Hz$  and  $\frac{S}{N}$  is the signal to noise ratio (SNR).

The maximum data rate for a TR scheme can also be written in a similar way. Assuming no inter symbol interference, and considering zero mean independent and identically distributed (i.i.d.) BPAM transmit symbols, the data rate can be written as:

$$C = \frac{1}{T_s} \log_2\left(1 + \frac{T_s S}{N_0}\right) \quad (4.18)$$

where  $T_s$  is the symbol time which is kept equal to the length of the truncated CIR ( $T_{sig}$ ),  $S$  is the received signal peak power and  $N_0$  is the zero mean noise power spectral density.

The proposed modulation scheme splits the input serial data into  $m$  parallel data streams that are transmitted simultaneously by shifting the transmitted signal and packing the multiple signals in the same time slot. In this way the system can have a sort of multiplexing gain without using any multi-antenna configuration. Thus the information rate of the proposed modulation scheme is ameliorated by a factor  $m$  due to the  $m$ -parallel transmitted data in the channel. However, with the constant transmitted power  $P_0$  for each  $T_s$ , the associated power for each transmitted data bit is reduced and the received peak signal amplitude per data bit is degraded by  $\frac{1}{\sqrt{m}}$  and the peak signal power is degraded by  $\frac{1}{m}$ . The second degradation term is imposed by the proposed shift operation of the TR-signal samples as described in the Section 4.2.2. Here we express the related peak signal power loss with factor  $k$ .

Another degradation factor is the interference. When multiple bits are transmitted simultaneously, there exists an interference caused by the adjacent bit within the symbol (intra symbol interference) and also there is interference in the received symbol due to the tail of the preceding symbol (inter symbol interference). As the symbols are transmitted with a symbol time equal to the length of the transmitted signal ( $T_s = T_{sig}$ ), the strength of the inter symbol interference signal is quite weak and is thus neglected. The temporal side lobes in the received signal for the adjacent bits cause the interference that reduces the system performance. This issue is reduced choosing the optimal shift step as described in the previous section. Thus for  $m$  simultaneously transmitted bits, and taking into account the  $k$  factor and the interference, (4.18) can be written:

$$C = \frac{m}{T_s} \log_2\left(1 + \frac{1}{m} \cdot \frac{k S}{(N + I)}\right) \quad (4.19)$$

where  $k$  is the variable which takes into account the peak power loss due to the shift operation,  $N = \frac{N_0}{T_s}$  is the noise power and  $I$  is the intra symbol interference which depends on the shift and the temporal sidelobes of the TR received signal. The overall data rate of the given modulation scheme is increased proportionally to the number of simultaneous bits ( $m$ ) and the degradation terms are varied by the logarithmic function with  $k$ ,  $I$  and  $\frac{1}{m}$ . If the interference is neglected ( $I = 0$ ) and  $k$  is kept close

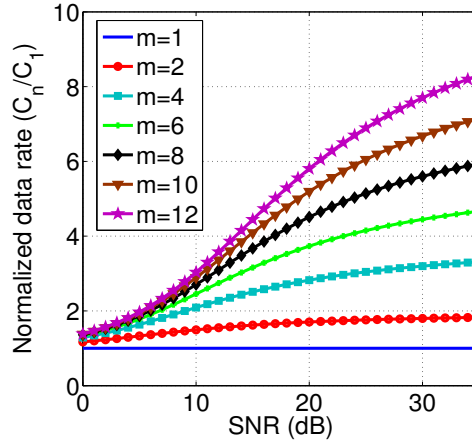


Figure 4.6: Data rate for  $m$  number of simultaneous bits normalized to the data rate of BPEM ( $m = 1$ )

to unity, i.e. the optimum performance of the modulation scheme is considered, the maximum data rate of the modulation scheme is simplified as:

$$C_{ideal} = \frac{m}{T_s} \log_2 \left( 1 + \frac{1}{m} \frac{S}{N} \right) \quad (4.20)$$

FIG. 4.6 shows the maximum data rate for different number of simultaneous transmitted bits ( $m$ ) normalized to the data rate for a BPAM transmitted signal ( $m = 1$ ). For each value of SNR, the data rate for a given  $m$ , is normalized to the corresponding data rate of a BPAM signal ( $m = 1$ ). It shows that with the new modulation scheme, the data rate increases significantly with  $m$  for a constant SNR especially for high SNR. For instance, for  $SNR = 20$  dB, the data rate increases by a factor of 2.82 for  $m = 4$ , 4.51 for  $m = 8$  and 5.19 for  $m = 10$ .

FIG. 4.7 shows for  $m = 3$  and  $m = 9$ , the maximum achievable data rate normalized to the data rate for a BPAM transmitted signal ( $m = 1$ ) against both SNR and SIR. Thus, the effects of ISI are included in this figure. The power loss due to the shift operation is neglected i.e.  $k = 1$ , thus the data rate is given by (4.19) with  $k = 1$ . It shows that an optimal performance is achieved at  $SIR \geq SNR$ .

#### 4.2.5 Validation of the New Modulation Scheme by Experiments and Simulations

To analyze the bit error rate performance of the new modulation scheme, two separate measurement campaigns are performed for two different typical indoor environments. Two different environments are chosen to include more generality in the results.

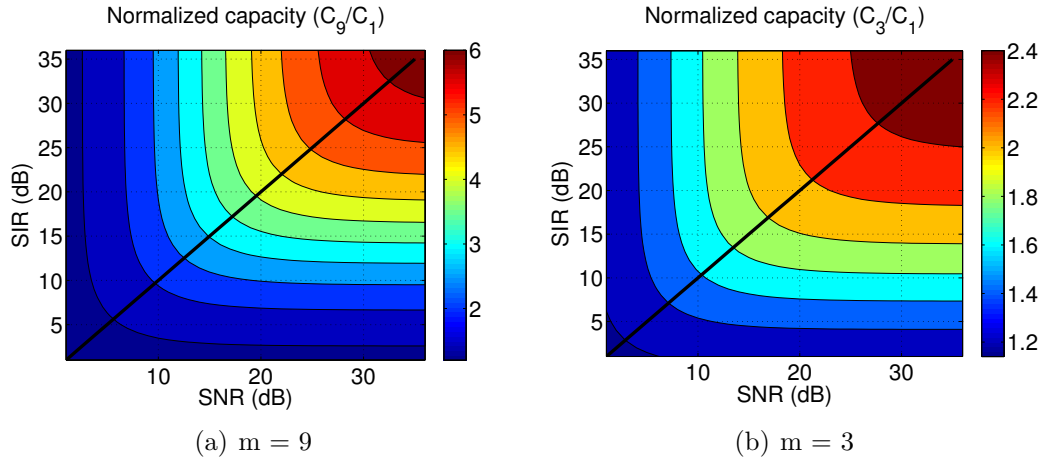


Figure 4.7: Data rate of the proposed modulation scheme against both SNR and SIR normalized to the data rate of  $m = 1$  for two different values of  $m$

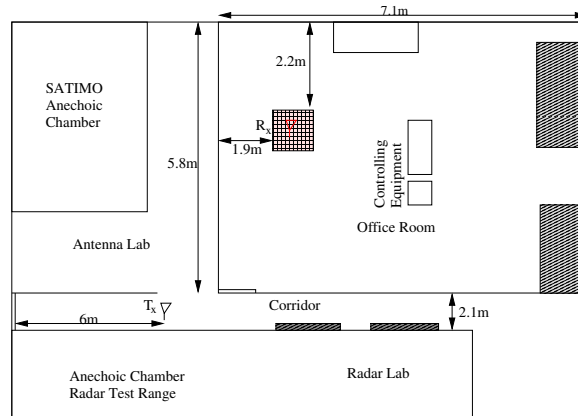


Figure 4.8: Environment layout of the first measurement campaign

#### 4.2.5.1 Measurement Campaign 1

In the first measurement campaign, the frequency responses are measured for varying positions of the receiver over a rectangular surface of  $65\text{ cm} \times 40\text{ cm}$ . A vector network analyzer (VNA) is used to measure the frequency responses. Thereafter, a TR communication is simulated and the BER performance of the new modulation scheme is analyzed.

#### Experimental Setup

Experiments are performed in a typical indoor environment. The environment is an office space of  $14\text{ m} \times 8\text{ m}$  in the IETR laboratory. FIG. 4.8 shows the environment layout of the first measurement campaign. The frequency responses of the channel in the frequency range of  $0.7 - 6\text{ GHz}$  are measured using a VNA with a frequency

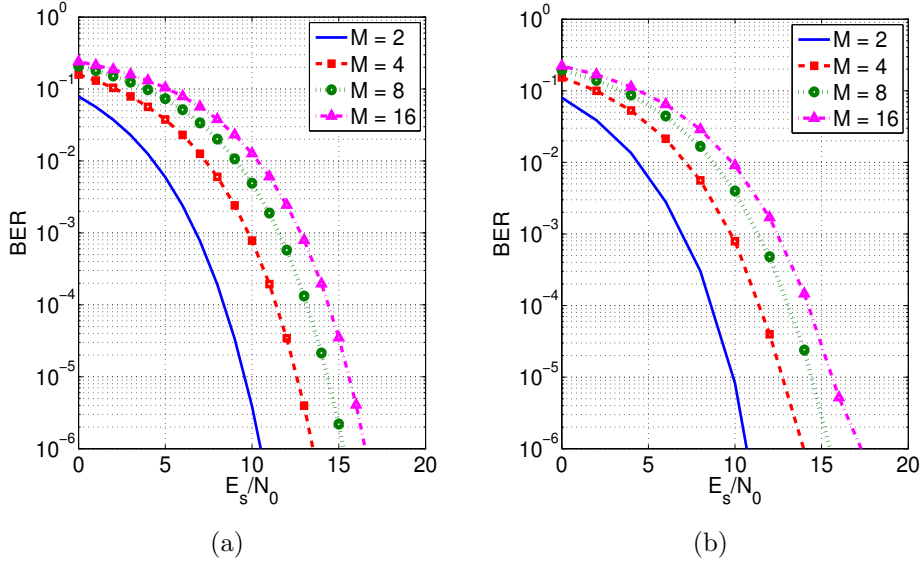


Figure 4.9: BER performance of the new modulation scheme for different modulation orders a) Theoretical curves b) simulated curves with a shift step of  $0.02 T_{sig}$

resolution of  $3.3 \text{ MHz}$ . Two wide-band conical mono-pole antennas (CMA) are used in a non line of sight (NLOS) configuration. The height of the transmitting and the receiving antennas is  $1.5 \text{ m}$  from the floor. The receiver is moved over a rectangular surface ( $65 \text{ cm} \times 40 \text{ cm}$ ) with a precise positioner system. Respective spatial resolution of  $2.5 \text{ cm}$  and  $5 \text{ cm}$  is used for the x-axis and y-axis of the horizontal plane. Thus 243 ( $27 \times 9$ ) measurements are taken over the rectangular surface. The frequency responses between the transmitting antenna and receiving virtual array (of 243 antennas) are measured. The time domain CIRs are computed using the inverse fast Fourier transformation (IFFT) of the measured frequency responses.

### BER Performance

The BER performance of the system is evaluated for different number of simultaneously transmitted bits. In the simulations, for each measured channel, 500000 symbols are transmitted to have enough data for statistical analysis.

Ideal theoretical curves for the new modulation scheme for multiple number of simultaneously transmitted bits (from (4.16)) are plotted in FIG. 4.9a. FIG. 4.9b shows the BER performance of the proposed modulation scheme based on simulations for different modulation orders. A shift step of 2% of the length of the transmitted signal ( $0.02 T_{sig}$ ) is kept and only left shift is used. The performance of the new modulation scheme is in strong agreement with the theoretical BER performance. A small shift percentage enabled a negligible loss in the received peak power and quasi orthogonal transmitted signals resulted in a very low intra symbol interference. It must be noted that the proposed modulation scheme gives a better performance

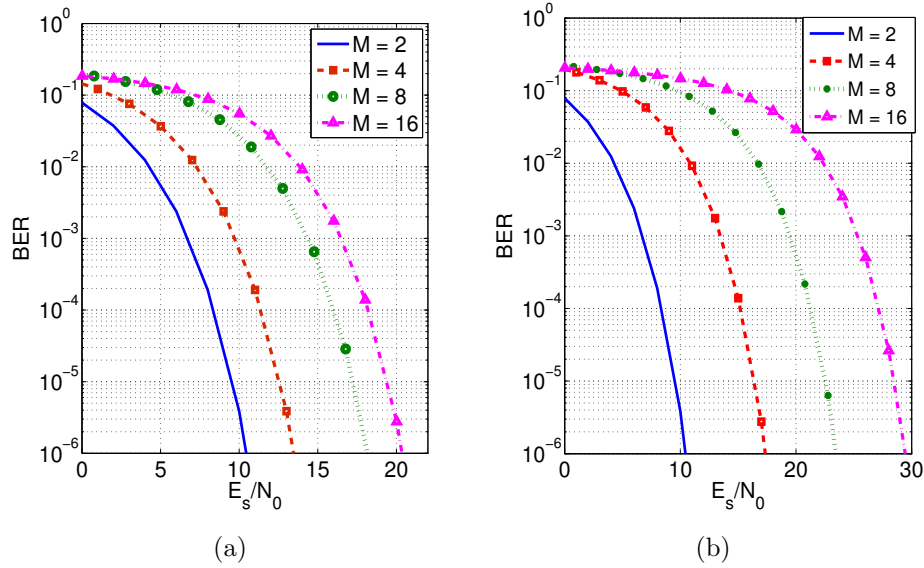


Figure 4.10: BER performance for different modulation orders in the AWGN channel for a) QAM b) PAM

than M-ary quadrature amplitude modulation (QAM) and PAM for  $M \geq 4$ . The theoretical performance of the error probability of these modulation schemes can be found in [17]. FIG. 4.10 shows the curves for the QAM and PAM modulation schemes in an AWGN channel for  $2 \leq M \leq 16$ . Comparing FIG. 4.9 and FIG. 4.10, it can be seen that the proposed modulation scheme outperforms QAM and PAM. For instance, for  $M = 4$ , the proposed modulation scheme gives similar performance to QAM, but  $3.88 \text{ dB}$  better performance than PAM for a fixed BER of  $10^{-6}$ . For higher modulation orders, the proposed modulation scheme even outperforms the QAM. For instance, for  $M = 16$ , the proposed modulation scheme gives a  $3.89 \text{ dB}$  and  $13 \text{ dB}$  better performance than QAM and PAM respectively for a fixed BER of  $10^{-6}$ .

It is interesting to note that for the new modulation scheme, bit energy to noise ratio,  $\frac{E_b}{N_0}$ , remains almost constant for all  $M$  for a given BER. Therefore, symbol energy to noise ratio,  $\frac{E_s}{N_0}$  follows the equation given below:

$$\frac{E_s}{N_0}(\text{dB}) = \frac{E_b}{N_0}(\text{dB}) + 10 \log_{10}(m) \quad (4.21)$$

where  $\frac{E_b}{N_0}$  is the bit energy to noise ratio. For instance, for a fixed BER of  $10^{-5}$ ,  $\frac{E_s}{N_0} = 10 \text{ dB}$  for  $M = 2$ . Same BER is achieved for a  $\frac{E_s}{N_0}$  of  $16 \text{ dB}$  for  $M = 16$ . These results are in agreement to (4.21). Therefore, with the new modulation scheme, the data rate is increased linearly while the  $\frac{E_s}{N_0}$  increases in proportion to the log term (4.21). This performance is only achieved for a small shift step. For higher shift steps, as we will see, the performance is not the same.

If a higher shift step is chosen, the power loss due to shift also affects the performance of the system. FIG. 4.11 shows the simulation curves for the BER performance

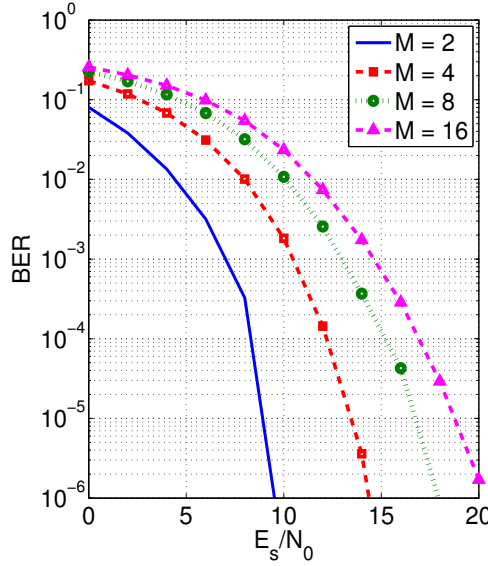


Figure 4.11: Simulation curves for BER performance of the new modulation scheme for different modulation orders with a shift step of  $0.05 T_{sig}$

of the system with a shift step of 5% ( $0.05 T_{sig}$ ). The effect of the power loss due to the shift is evident on the performance of the system. For example, for a fixed BER of  $10^{-5}$  and  $M = 16$ , a 2 dB degradation is observed with higher shift step of  $0.05 T_{sig}$  compared to the lower shift step of  $0.02 T_{sig}$  (see FIG. 4.11 and FIG. 4.9b).

#### 4.2.5.2 Measurement Campaign 2

A time domain validation of the new modulation scheme is performed by making use of time domain instruments: an arbitrary waveform generator (Tektronix AWG 7052) and a high speed digital storage oscilloscope (Tektronix DSO 6124C). For this purpose, a second measurement campaign is carried out in another typical indoor environment. The environment also has a reverberation chamber which increases the number of multi-paths at the receiver. In this case, the performance of the new modulation scheme is experimentally studied.

#### Experimental Setup

An experimental setup is established in a typical indoor environment (laboratory IETR) having the plan shown in FIG. 4.12. All rooms are furnished with office equipments: tables, PCs and seats. Moreover, there is a large reverberating chamber in the laboratory, which increases the wave reflections in the environment. Two Conical Mono-pole Antennas (CMA), are used as the transmitter and the receiver. The distance between the transmitter and the receiver is 8.5 m while the height is 1 m from the ground. The pulse is generated with an AWG, which has a maximum

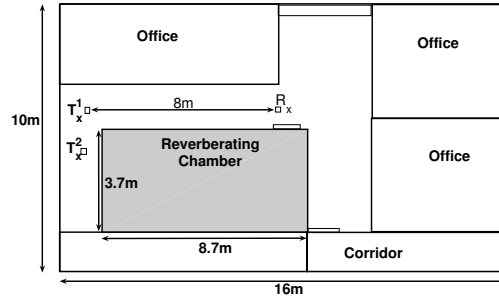


Figure 4.12: Measurement environment layout of the measurement campaign 2

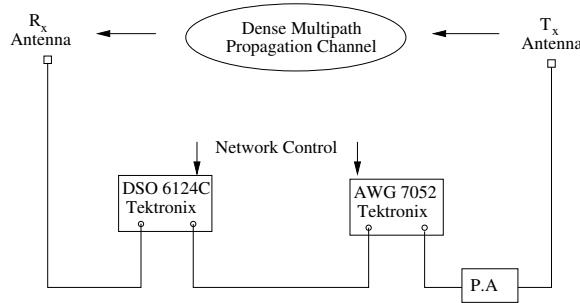


Figure 4.13: Experimental Setup of the measurement campaign 2

sampling rate of  $5\text{ GS/s}$ . At the receiver end, the signals are captured by a DSO with a maximum sampling rate of  $40\text{ GS/s}$ . The experimental setup is shown in FIG. 4.13.

Once the CIR is measured, 1000 transmitted symbols for different modulation orders are created through MATLAB and are re-transmitted in the same channel. A left shift percentage of 5% is kept for each  $M$ . The DSO is operated in average mode and the received signal is averaged 256 times so that the effects of the noise are compensated. FIG. 4.14 shows for  $M = 16$ , 3 consecutive frames of the measured received signal with the new modulation scheme detected through the DSO. All four peaks inside a time slot can easily be detected.

### BER Performance

To analyze the BER performance of the modulation scheme validated by the experiments, random noise is added in the received signal and the experiment is repeated in order to reach  $10^8$  transmitted bits for each  $M$ . FIG. 4.15 shows the BER performance of the new modulation scheme using the experimental results of measurement campaign 2 for different  $M$ . The performance of the modulation scheme with measurement campaign 2 is in good agreement with the results of measurement campaign 1 for a shift step of  $0.05T_{sig}$  (see FIG. 4.11 and FIG. 4.15). Even though the two measurement campaigns are carried in two different environments, their performance matches with good agreement. The performance can never match exactly as the curves

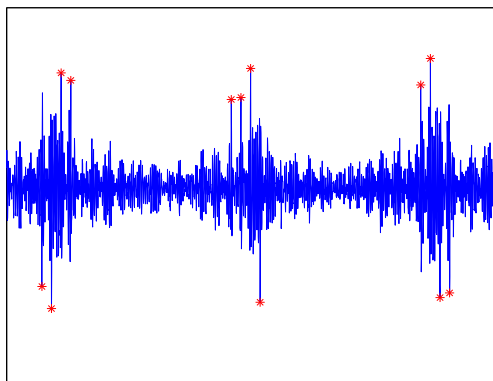


Figure 4.14: Received signal for  $M = 16$  with the new modulation scheme

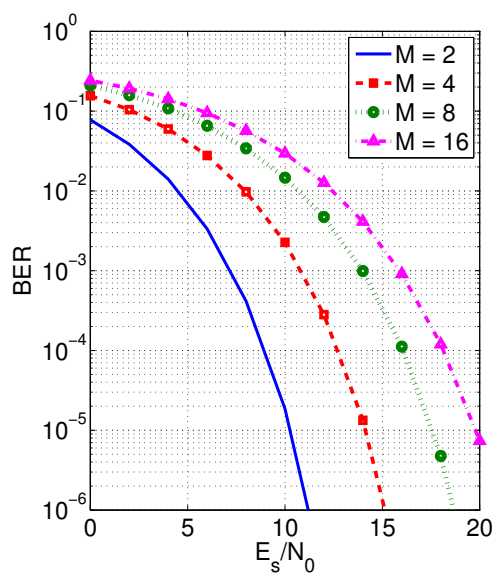


Figure 4.15: BER performance of the new modulation scheme for different modulation orders with using the experimental results of measurement campaign 2

for measurement campaign 1 are achieved by simulating the TR communication for a set of 243 measured CIR, while the performance of the campaign 2 is carried out for over one single channel. Furthermore, the time domain equipments are subjected to the inherent jitter which may reduce the received signal peak and may cause the degradation of the performance.

The novel modulation scheme performs very well when the amount of introduced shift is not very large. The data rate can be significantly increased compared to simple TR scheme. For a high data rate communication, large number of bits must be added in the same symbol duration. As the number of simultaneously transmitted bits increases, the amount of shift will increase no matter how small is the shift step. Larger shift step will eventually degrade the performance of the system. Therefore, a communication can be envisaged without the introduction of shift so that the limitations introduced by the shift can be avoided. In the next section, we present the results for very high data rate TR communication using BPAM. No shift is introduced and the same signal is transmitted with different symbol durations.

### 4.3 High Data Rate TR Communication

In this part of the chapter, we discuss the experimental validation of high data rate TR communication. High data rate TR communication is experimentally studied in a reverberation chamber (RC) and in a typical indoor environment. Without any processing or equalization at the receiver, experiments are done for different data rates ( $15.62 \text{ Mbps} \leq R_b \leq 1 \text{ Gbps}$ ) using binary pulse amplitude modulation (BPAM). *Signal*, *Interference* and *Noise* components are separated from the received signal and bit error rate (BER) performance of system is studied. In [88] a modified transmission scheme is proposed to reduce signal to side lobe ratio of the TR received signal. This modified TR scheme is used to improve the BER performance of a high data rate TR communication system. Experimental validation of the modified TR scheme is performed and its BER performance is compared with the classic TR scheme. Two research articles have been accepted for publication on this subject [89], [90].

#### 4.3.1 Experimental Setup

Experiments are done in a reverberation chamber (RC) and in an indoor environment. In the indoor channel, experiments are performed outside of office hours. The indoor environment consists of a laboratory rooms where a RC is also located (see Fig. 4.12). Consequently, the metallic walls of the RC help accomplishing a non line of sight (NLOS) propagation scenario. These rooms are also furnished with standard office equipments: tables, PCs and seats. Experimental setup in the indoor environment is shown in Fig. 4.13. Two conical mono-pole antennas (CMA-118/A), are used as the transmitter and the receiver. The distance between the transmitter and the receiver is 8.5 m in the indoor environment and 5.5 m in the RC. Antennas are always kept 1 m above the ground.

The pulse is generated with the AWG which has a maximum sampling rate of 5 GS/s. Because of such a high sampling rate, an extremely narrow channel sounding pulse with a power spectrum of DC-2.7 GHz and a rise time of 200 ps is generated with the AWG. In the indoor environment, the output signal of the AWG is amplified to a level to drive the power amplifier (P.A), Mini-Circuits ZHL-42. The given P.A provides a constant gain of 30 dB and covers the frequency range of 700 – 4200 MHz. The amplified signal is transmitted with an ultra wide-band CMA antenna having a frequency range of 0.7 – 18 GHz. Therefore, the effective bandwidth of the transmitted pulse is 0.7 – 2.7 GHz. In the RC, no PA is used. At the receiver end, the received signal is sampled and stored by using a DSO with a maximum sampling rate of 40 GS/s. To suppress the effects of the additive noise from the received signals, the DSO is operated in average acquisition mode and a common trigger signal is used to synchronize the AWG and the DSO. In the average acquisition mode, multiple samples of the received signals are measured at different time instants and then averaged together. Every sample measurement has a random noise, thus averaging multiple measured samples filters out the noise. Number of measurements for the averaging process improves the quality of the signal at the receiver. In our case, the received signals are averaged 256 times to reduce the noise considerably. The selected sampling rate of the DSO is 10 GS/s which results in a delay resolution of 0.1 ns. The acquisition time for operating in the average mode for the delay of 400 ns is in the order of few seconds. It is assumed that the channel remains quasi-static during this time interval.

### 4.3.2 Experimental Results

#### 4.3.2.1 Channel Estimation

The first step of the experiment is to estimate the channel response between the transmitting and receiving antennas. A short pulse with a rise time of 200 ps is transmitted in the channel with the AWG and the channel response is measured by the DSO with a sampling rate of 10 GS/s. To suppress the effects of noise from the received signals, the DSO is operated in average acquisition mode. The acquisitions are synchronized thanks to a wire trigger between the AWG and the DSO. Obviously this kind of synchronization is not realistic for a wireless application. However, the channel estimation is a separate research subject and not studied in the present paper. The averaged channel response is computed from 256 acquisitions. As the noise between each acquisition is different, we assume that it is filtered out from the measured channel response (MCR).

#### 4.3.2.2 Data Transmission

The MCR is then truncated such that the truncated version keeps 80% and 97% of the total energy in the RC and in the indoor environment respectively. The truncated MCR is then reversed in time and the RF signal to transmit is computed from

(4.1). Memory space of the AWG is restricted, therefore only a certain number of symbols can be transmitted simultaneously. For the lower values of  $T_s$ , larger number of symbols are accommodated in the given memory space than higher values of  $T_s$ . Therefore, for different  $T_s$ , different number of symbols are transmitted depending on memory space they acquire. For instance, in an indoor environment, number of transmitted symbols vary from 20000 to 1562 for  $T_s$  varying from 1 ns to 64 ns. Once the transmitted signal is created by using (4.1), the signal is then down sampled to 5 GS/s and transmitted by the AWG in the same channel. As the length of the channel response ( $T_{sig}$ ) is significantly larger than  $T_s$ , high ISI is present. Temporal compression property of the TR helps to reduce ISI. Nevertheless, at such high data rates ISI is the critical factor to limit the performance of the system. As the experiments are done in the RC and indoor, we suppose that the channels do not change during the measurement procedure.

#### 4.3.2.3 Signal, Interference and Noise Extraction

The received TR signal with multiple number of simultaneously transmitted symbols consists of *Signal*, *Interference* and *Noise* ( $S + I + N$ ) components. Depending upon  $T_s$ , *Interference* component varies significantly. For high data rates, *Interference* is the main contributor of the errors.

The received signal is recorded by the DSO. Contrary to the channel estimation phase, here the received signals are synchronized by a triggering sequence that is added to the data signals. The triggering signal consists of a time reversed MCR, which generates a strong pulse at the receiver and enables a stable triggering and data synchronization at the DSO. First, a single record is performed. This record is a combination of the *Signal*, *Interference* and *Noise* ( $S + I + N$ ) components with the DSO in the sample mode which acquires the signal at a given instant. Then, to suppress *Noise* contribution in the measured signal, the DSO is operated in the average mode. In this case, the received signals at 256 time instants are averaged together. At each time instant, a random noise is received along with the signal, therefore averaging the signal 256 times reduces the random noise considerably. We assume that the random noise is totally eliminated by the averaging procedure and the measured signal consists of only *Signal* and *Interference* contributions ( $S + I$ ). Finally, by transmitting only one symbol (thus no ISI) and operating the DSO in the average mode (thus no *Noise*), *Signal* is measured. Thus there are three measured signals;  $S$ ,  $S + I$  and  $S + I + N$ . From these measured signals we can separate the contributions of *Signal*, *Interference* and *Noise* in the received signal. The power of the measured signals is normalized through post processing such that every data symbol is transmitted with the same energy.

The amplitude distributions of  $S + I + N$  in an indoor environment for  $T_s = \{2, 8, 16, 64 \text{ ns}\}$  are shown in the FIG. 4.16 for  $SNR = 15 \text{ dB}$ . For  $T_s = 2 \text{ ns}$ , *Interference* is so high that the amplitude distribution cannot be separated between positive and negative parts. Same is the case for  $T_s = 8 \text{ ns}$ . However, for  $T_s = 16$  or  $64 \text{ ns}$ , negative and positive parts can easily be separated from the distribution. The dif-

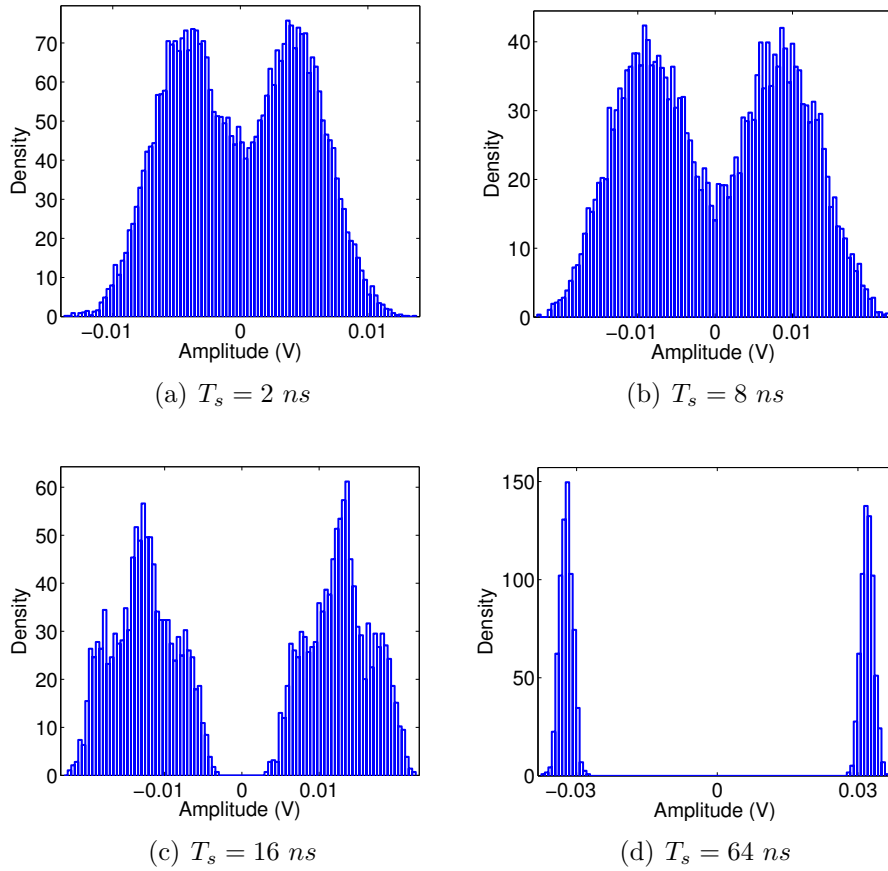


Figure 4.16: Amplitude distribution of the received signal without separating the *Interference* and *Noise* components for different values of  $T_s$

ference between the amplitude distributions of  $T_s = 16 \text{ ns}$  and  $T_s = 64 \text{ ns}$  is that the former is very close to the origin, suggesting that a little noise can cause an error whereas the latter is relatively far from the origin. Similar amplitude distributions are observed for  $S + I + N$  in the RC.

FIG. 4.17 shows the amplitude distribution of *Signal*, *Noise*, *Interference* and  $S + I + N$  in the RC for  $SNR = 15 \text{ dB}$  and  $T_s = \{1 \text{ or } 64 \text{ ns}\}$ . Separate sub-figures has been included for *Noise*, *Interference* and  $S + I + N$  distributions. At  $T_s = 1 \text{ ns}$ , the variance of *Interference* is greater than the variance of *Noise*. The combined power of *Noise* and *Interference* is so high that the distribution of the received signal ( $S + I + N$ ) cannot be separated into positive and negative parts. However, for  $T_s = 64 \text{ ns}$ , *Signal* power is greater than the combined power of *Noise* and *Interference*. Thus, the distribution of the received signal can easily be separated into positive and negative parts.

FIG. 4.18 shows *Signal*, *Noise* and *Interference* contributions for the first fifty symbols in the indoor environment for  $SNR = 15 \text{ dB}$  and  $T_s = \{1, 64 \text{ ns}\}$ . For  $T_s = 1 \text{ ns}$ , *Interference* limits the performance of the system and is much greater

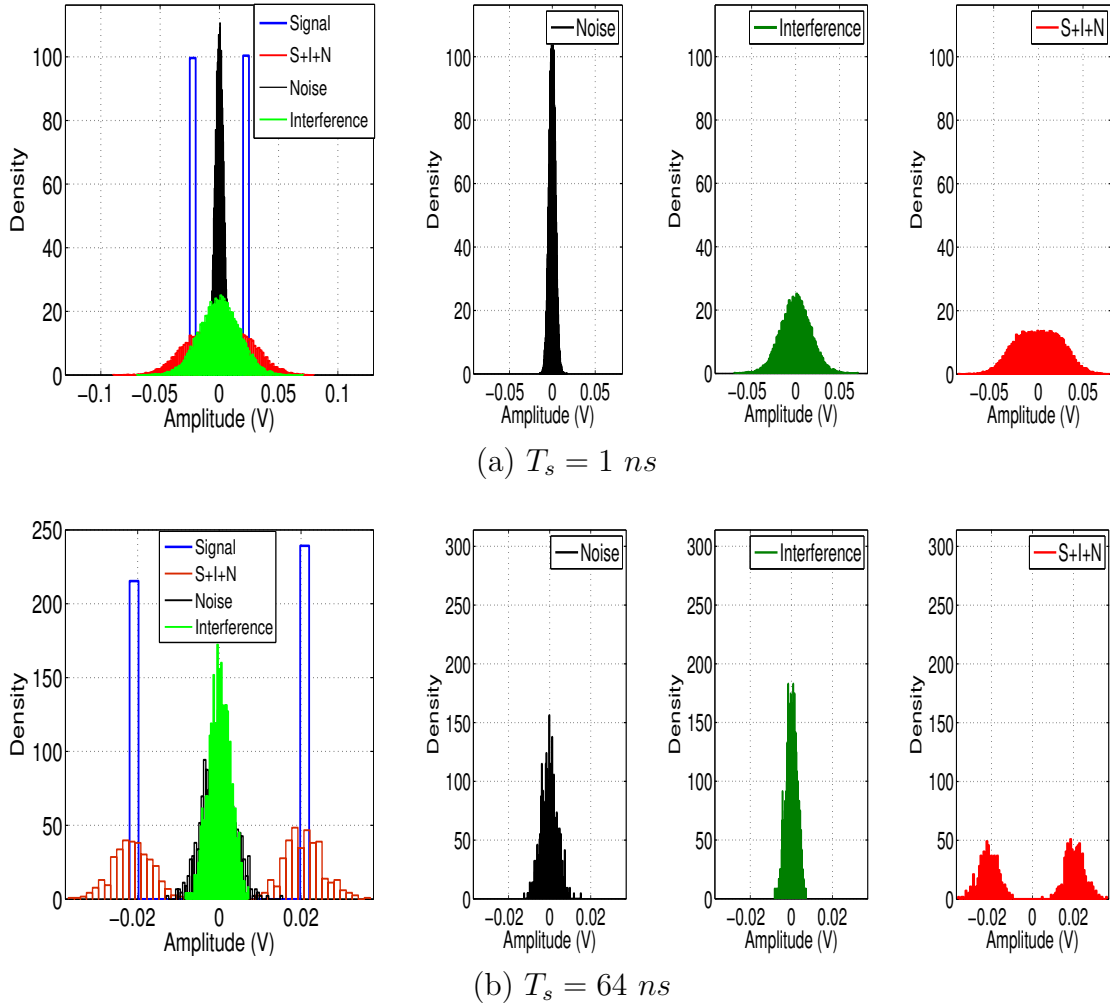


Figure 4.17: Amplitude distribution of *Signal*, *Interference* and *Noise* and the sum of three components for  $SNR = 15 \text{ dB}$  in a reverberation chamber for two different values of  $T_s$

than *Noise* (see FIG. 4.18 a). However for  $T_s = 64 \text{ ns}$ , *Signal* is quite stronger than *Noise* and *Interference* for  $SNR = 15 \text{ dB}$  (see FIG. 4.18 b).

#### 4.3.2.4 SIR and BER Performance of the Classical TR Scheme

Table 4.1 compares the signal to interference ratio (SIR) of the received signal peaks for two different propagation environments (RC and the indoor channel), for different  $T_s$  and  $SNR = 15 \text{ dB}$ . As expected, SIR increases with  $T_s$  for both channels. In the RC, SIR increases by 3 dB (or doubles) by doubling  $T_s$ , whereas in the indoor channel, SIR increases rapidly for  $T_s > 16 \text{ ns}$ . The ratio  $\frac{T_{sig}}{T_s}$  can help to interpret this rapid increase in SIR.  $T_{sig}$  is the length (in ns) of the transmitted (time reversed

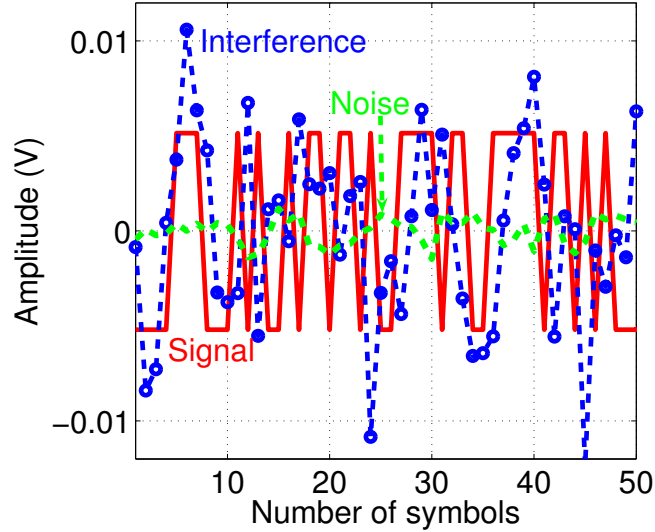
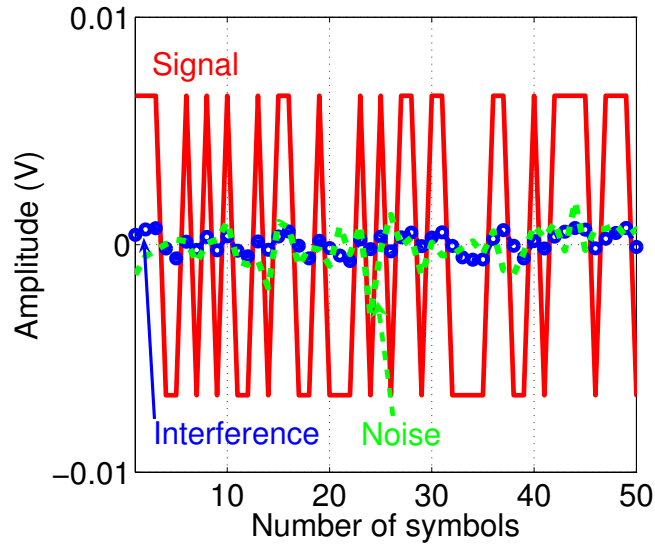
(a)  $T_s = 1 \text{ ns}$ (b)  $T_s = 64 \text{ ns}$ 

Figure 4.18: *Signal*, *Interference* and *Noise* component  $SNR = 15 \text{ dB}$  in an indoor environment for different values of  $T_s$

CIR) signal. In our case, it is directly proportional to the root mean square (RMS) delay spread of the CIR. In the RC for all values of  $T_s$ ,  $T_{sig}$  is much larger than  $T_s$ . However, in the indoor channel,  $T_{sig}$  becomes comparable to  $T_s$  when  $T_s \geq 32 \text{ ns}$ . A large increase (in the order of  $7 \text{ dB}$ ) in the SIR is observed when the ratio  $\frac{T_{sig}}{T_s}$  is close to 1. This explains the jump in the SIR for the indoor channel when  $T_s$  increases from  $16 \text{ ns}$  to  $32 \text{ ns}$  in the indoor channel.

$T_s$	RC		Indoor Channel	
	SIR (dB)	$\frac{T_{sig}}{T_s}$	SIR (dB)	$\frac{T_{sig}}{T_s}$
1	1.97	5020	1.11	70
2	4.91	2510	2.35	35
4	8.01	1255	6.54	17.5
8	10.87	627	10.50	8.7
16	13.26	314	13.23	4.3
32	16.56	157	20.09	2.2
64	19.09	78	23.43	1.1

Table 4.1: Comparison of SIR for different  $T_s$  in the reverberation chamber and in the indoor channel for  $SNR = 15$  dB with classic TR scheme

FIG. 4.19 shows the BER comparison for different  $T_s$  in the indoor channel. The SNR is varied by adding additive white Gaussian noise (AWGN) to *Signal + Interference* components measured from the signals averaged 256 times. For each SNR, BER is calculated for  $10^8$  transmitted bits. Similarly, BER is calculated for different data rates (data rate =  $\frac{1}{T_s}$ ) ranging from 15.62 Mbps to 1 Gbps. For  $R_b \leq 125$  Mbps, the BER performance is quite good. For instance for  $R_b = 125$  Mbps, a BER of  $10^{-3}$  is achieved for  $SNR = 16.2$  dB. For  $R_b < 125$  Mbps, the performance is even better. However, for higher data rates, the BER curves reach a plateau. Indeed, in such a case, the ISI dominates the BER. It must be noted that these data rates are raw data rates based on baseband communication without any equalization at the receiver.

The leveling out of the BER curves is a well known phenomenon for irreducible interference. Indeed, the temporal compression of TR is not perfect; the received TR signal has temporal side-lobes. These side lobes induce the irreducible interferences. Nevertheless, the experimental validation of high data rate TR gives us a range of the data rates for which the irreducible interference does not heavily affect the performance of the system. We can achieve data rates as high as 125 Mbps with the TR scheme in an indoor environment. Although these experimental results cannot be generalized, yet these results give us an idea of the performance of the TR scheme in realistic environments.

Fig. 4.20 shows the BER comparison for different  $T_s$  in the RC. Comparison of Fig. 4.19 and Fig. 4.20 suggests that for lower data rates ( $15.62$  Mbps  $\leq R_b \leq 125$  Mbps), the BER performance is better for the indoor channel. For higher data rates ( $250$  Mbps  $\leq R_b \leq 1$  Gbps), the BER performance is better in the RC. However, at these high data rates the curves have already reached a plateau. The term  $\frac{T_{sig}}{T_s}$  can help us to interpret this observation. As the ratio of the transmitted signal and the symbol time is quite high for the RC environment, therefore it results in a poor SIR performance compared to the indoor channel (see Table 4.1). SIR performance

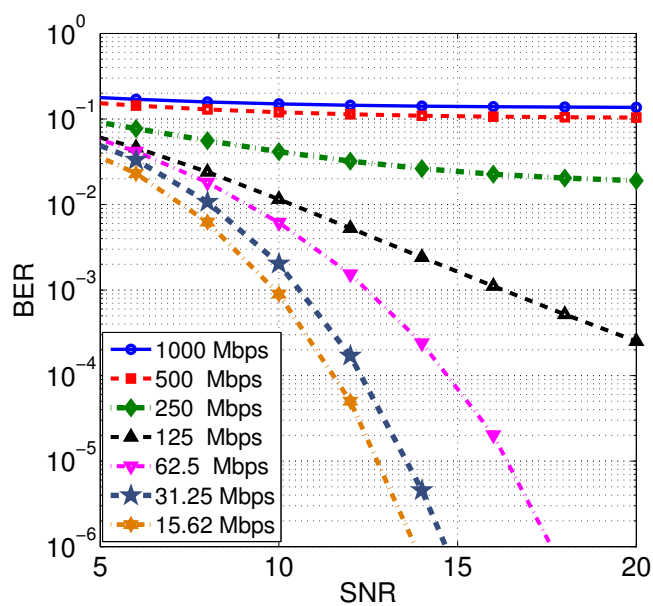


Figure 4.19: BER performance of TR system for  $1 \text{ ns} \leq T_s \leq 64 \text{ ns}$  in an indoor environment

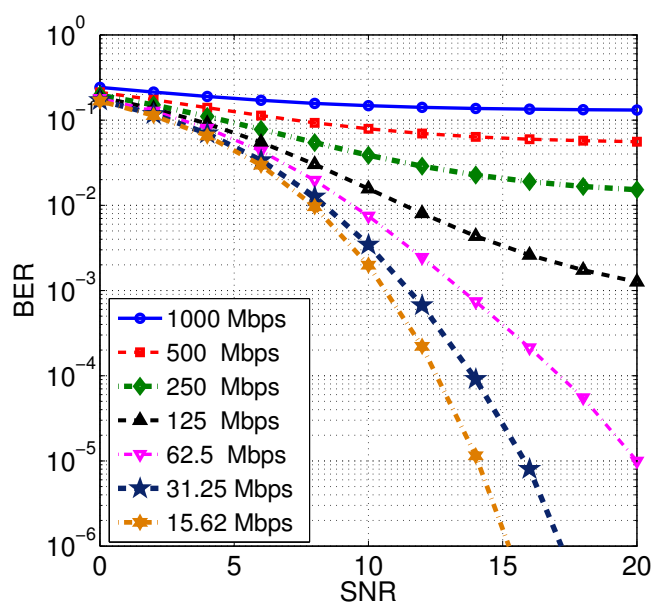


Figure 4.20: BER performance of TR system for  $1 \text{ ns} \leq T_s \leq 64 \text{ ns}$  in a reverberating chamber

in the RC is only better for very high data rates where curves for both environments saturate quite rapidly.

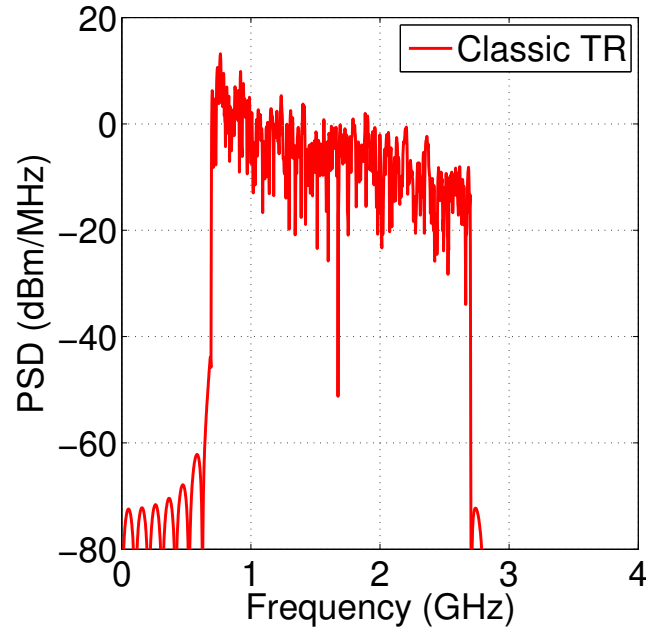


Figure 4.21: PSD of a classic TR transmitted signal

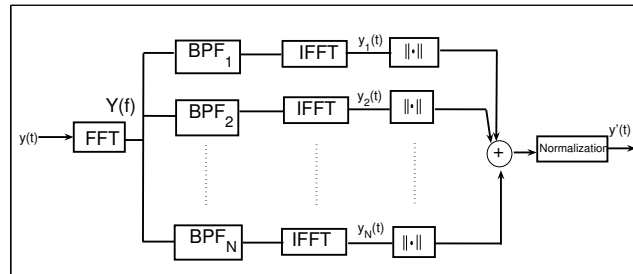


Figure 4.22: Block diagram of the modified TR scheme

### 4.3.3 Sub-Band TR Transmission Scheme

The TR signal has a very large bandwidth. In our case, it has a bandwidth of  $2\text{ GHz}$  with a center frequency of  $1.7\text{ GHz}$ . Fig. 4.21 shows the power spectral density (PSD) of a TR transmitted signal normalized to a constant power. The PSD is calculated using Welch's method [71]. The PSD of the TR transmitted signal depends on the effects of the propagation channel including path loss and the antenna effects. Therefore, PSD has a descending shape. The components of the signal at higher frequencies are attenuated as compared to the components at lower frequencies. This inherent property of the TR signal makes it difficult to employ efficiently to a UWB system. Thus, the transmitted signal must be attenuated so that it respects the UWB

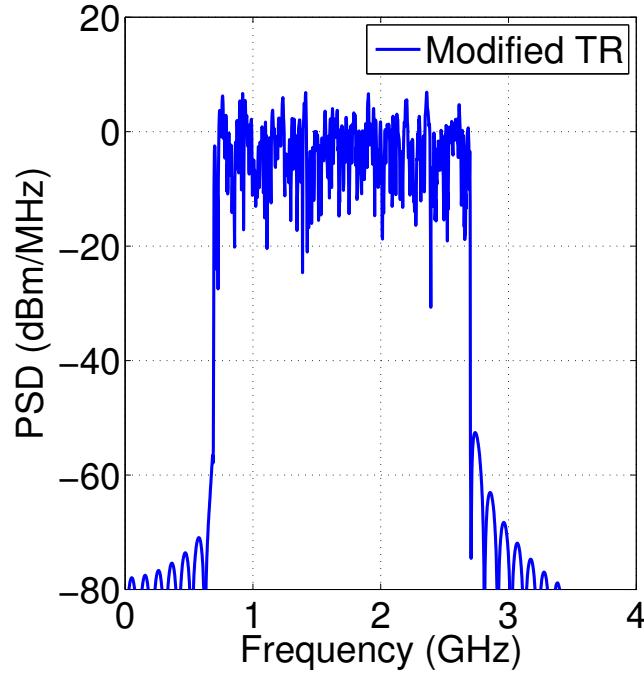


Figure 4.23: PSD of a modified TR transmitted signal

spectral mask (imposed by the Federal Communication Commission (FCC) [3]) over the whole band resulting in a poor spectral efficiency. However, if the PSD of the transmitted signal is flat, the TR system will then respect the UWB spectral mask with a better spectral efficiency. To achieve a flat PSD, total bandwidth of the time reversed signal is divided into  $N$  sub bands of equal power [88]. We call the scheme as Sub-Band TR Transmission Scheme (SB-TRTS). The power of each sub-band is normalized using equal power control (EPC) so that each sub-band contributes equally to the PSD. Let  $x_i$  be the signal for the  $i_{th}$  sub-band. Using EPC, it can be normalized as:

$$|x_i(t)|_{EPC} = \frac{x_i(t)}{\|x_i(t)\|} \quad (4.22)$$

where  $\|\cdot\|$  is the Frobenius norm operation.

In our case, the TR signal is divided into 10 sub bands of 200 MHz. The block diagram of the SB-TRTS is shown in FIG. 4.22. The filtering is achieved by transforming the signal in the frequency domain (FFT), then filtering the signal by band-pass filters, and transforming the signal back into the time domain (IFFT). In this way, the signals with precise bands are achieved. Once the signals are filtered with  $N$  sub bands, the signal of each sub-band is normalized to have an equal power using EPC. The normalized signals are then added together to form the transmitted signal for the SB-TRTS. The added signal must be again normalized so that it respects the UWB spectral mask. FIG. 4.23 shows the PSD of the TR signal of the SB-TRTS having a

$T_s$	SIR (dB)	$\frac{T_{sig}}{T_s}$
1	-0.14	75
2	2.24	37.4
4	5.97	18.7
8	11.83	9.35
16	17.10	4.67
32	20.05	2.33
64	26.60	1.16

Table 4.2: Comparison of SIR for different  $T_s$  in the indoor channel for  $SNR = 15$  dB with SB-TRTS

power normalized to a constant. As expected, PSD is flat and it is easier to respect the spectral mask.

The received signal with the SB-TRTS has a better SSR as compared to the classic TR, but it has a lower peak power as well for the same transmitted power [88]. We have used this scheme to achieve a better BER performance for a high data rate TR communication system. The experiments are performed with the SB-TRTS in the same way as were performed with the classic TR scheme.

#### 4.3.3.1 Experimental Results with SB-TRTS

Table 4.2 shows the SIR at the instants of decision for different  $T_s$  with the SB-TRTS. SIR is computed by following the same procedure adopted for the classic TR scheme. Comparing Table 4.1 and Table 4.2, it can be seen that the SB-TRTS has improved the SIR of the TR system for  $T_s \geq 8$  ns in an indoor environment.

FIG. 4.24 shows the BER performance of the SB-TRTS in an indoor environment. Comparing FIG. 4.19 and FIG. 4.24, it can be seen that the performance of the system has significantly improved with the SB-TRTS. For instance, SB-TRTS gives a 3 dB better performance than the classic TR scheme for a fixed BER of  $10^{-4}$  for a data rate of 125 Mbps. The SB-TRTS gives a 2.4 dB better performance than the classic TR scheme for the data rate of 62.5 Mbps for a fixed BER of  $10^{-6}$ . Thus, the flattening of the spectrum has worked as equalization and has improved the BER performance with the SB-TRTS. However, the performance has not improved for the data rates  $\geq 250$  Mbps where the curves reach a plateau for both the schemes.

With the validation of high data rate communication, TR can be thought of a potential transmission scheme for realistic applications, for example, WLAN and wireless streaming applications etc. The SB-TRTS has furthered improved the performance of the TR system. For the future work, study can be done by using an equalizer at the receiver but it will be a performance complexity trade off. The performance of

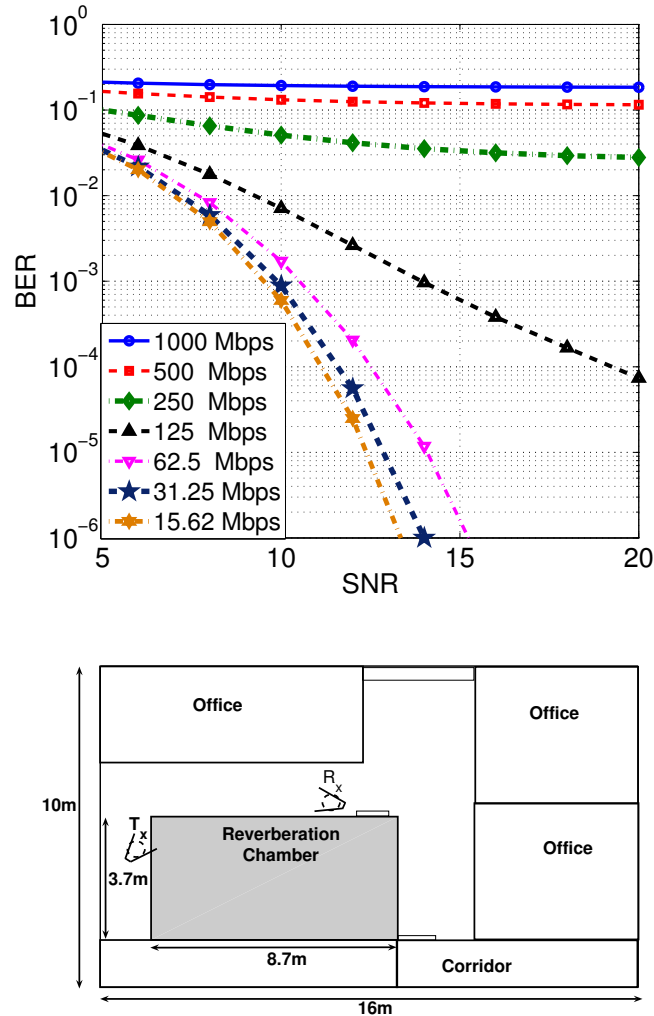


Figure 4.24: BER performance of TR system for  $1 \text{ ns} \leq T_s \leq 64 \text{ ns}$  in an indoor environment with sub-band filtering

the TR system can also be compared by using pulse position modulation scheme with classic TR and the SB-TRTS.

## 4.4 Conclusion

In this chapter, high data rate TR communication is discussed with two approaches. In the first approach, a novel modulation scheme is proposed for a time reversal (TR) ultra wide-band (UWB) communication system. The proposed modulation scheme adds a new level of modulation to the existing modulation scheme like bipolar pulse amplitude modulation (BPAM). Multiple bits are transmitted simultaneously by shifting the transmitted signal and packing them in the same time slot. The BER

performance of the new modulation scheme is theoretically studied. Thereafter, it is shown that for negligible interference and quasi orthogonal signals, the data rate of the modulation scheme increases linearly whereas the transmitted power must only be increased logarithmically. The validation of the modulation scheme is carried out with the help of two separate measurement campaigns. For the first measurement campaign, the frequency responses of a typical indoor channel are measured with a vector network analyzer and TR communication is simulated for the new modulation scheme. The bit error rate performance of the new modulation scheme is analyzed for different modulation orders. It is shown that for an optimal shift, theoretical and simulation performances of the modulation scheme are in strong agreement to each other. In the second measurement campaign, time domain instruments are used to measure the channel impulse response and the new modulation scheme is validated experimentally. It is shown that the experimental and the simulative results are in good agreement with each other. For high data rate communication, large number of bits must be added in the same symbol duration and the introduced shift will degrade the performance of the system. However, this scheme can be very useful for multi-user TR communication system where the shift is introduced on the signals of different users. Multi-user TR communication by using the proposed shift operation has been investigated in the next chapter.

In the second part of the chapter, results of high data rate communication experiments without any shift introduction are presented using BPAM. Experiments have been done in a typical indoor environment and in a reverberation chamber for different data rates ( $R_b$ ) ranging from 15.62 Mbps to 1 Gbps. *Signal*, *Interference* and *Noise* components are separated from the measured received signal and are compared for different  $T_s$  at a fixed SNR. It is observed that inter symbol interference increases with the decrease in  $T_s$  and saturates the BER performance. It is shown that the BER performance in the indoor channel is better than the reverberation chamber. Furthermore, experiments are performed using a sub-band TR transmission scheme (SB-TRTS) which divides the total bandwidth of the transmitted signal into multiple sub bands, each contributing equally to the power spectral density (PSD) and therefore improves the spectral efficiency of the system. This process helps to achieve a flat PSD. It is shown that the modified TR scheme performs a sort of equalization and significantly improves the BER performance. For instance the SB-TRTS gives a 2.4 dB better performance than the classic TR scheme for  $R_b = 62.5$  Mbps and a fixed BER of  $10^{-6}$ .



# Chapter 5

## Multi User TR Communication

### Contents

---

<b>5.1</b>	<b>Introduction</b>	<b>142</b>
<b>5.2</b>	<b>Circular Shift Time Reversal</b>	<b>142</b>
5.2.1	Effects of CSTR on Received Signal Peak	145
<b>5.3</b>	<b>Effects of CSTR on Signal to Interference Ratio (SIR)</b>	<b>146</b>
5.3.1	Experimental Setup	147
5.3.2	Simulation Results	147
<b>5.4</b>	<b>Modified Transmission Scheme</b>	<b>149</b>
5.4.1	Interference Analysis of the Proposed Scheme	150
5.4.2	Effects of Shift on Received Signal Peak	151
5.4.3	Experimental Setup and Simulation Results	153
<b>5.5</b>	<b>Conclusion</b>	<b>155</b>

---

## 5.1 Introduction

Multi-user communication can be envisaged as one the following two cases:

1. Down link: When a base station is communicating with the multiple users
2. Up link: When different users are communicating with the base station.

In case of multiuser communication, the base station normally transmits different signals for different users. Therefore, this broadcast is fundamentally different from the TV or radio broad case where the base station transmits same signal for all users. In this work, we have mainly focus on the first case described above; a transmitter communicating with multiple users with UWB time reversal (TR) technique.

In the CHAPTER 4, a novel modulation scheme is proposed for a time reversal (TR) ultra wide-band (UWB) communication system. Multiple bits are transmitted simultaneously by shifting the transmitted signal and packing them in the same time slot. In this chapter, multi-user TR communication is studied in detail by following the same approach. At first, we examine multi-user TR communication with a modified pre-filter using a circular shift operation (CSTR). Thereafter, the signals for different users are packed in a single time slot and are transmitted simultaneously. Consequently, better throughput is achieved. We have carried out the analytical study of CSTR scheme. Some inherent drawbacks in the scheme are highlighted. At first, amount of circular shift (CS) is varied for a given user and SIR performance of the CSTR scheme is independently analyzed for each user. The results on the SIR analysis of the CSTR scheme have been published in [64].

Thereafter, multi-user TR communication has been investigated by using the proposed shift operation (described in CHAPTER 4). This scheme addresses the limitations of the CSTR scheme and gives a significantly better performance than the TR and CSTR schemes. The improvement in the performance increases with the increase in the number of users. Mathematical expressions for the received signal and the interference of the proposed transmission scheme are derived. Experiments are performed in a typical indoor environment. The maximum number of simultaneous users is calculated with the proposed scheme. The results of our work on this subject have been published in [91]. In contrast to [63], our analysis considers a constant transmitted energy after the users are packed in a time slot, so that the comparison between the systems with different number of users becomes valid.

## 5.2 Circular Shift Time Reversal

If instead of time reversed channel impulse response (CIR), a circularly shifted time reversed CIR is used as a transmitter pre-filter, the resulting scheme can be called as Circular Shift Time Reversal (CSTR). CSTR can be further classified into left CSTR and right CSTR, depending upon the direction of the CS operation applied on signal

samples of the time reversed CIR. To elaborate the phenomenon of CSTR, one can consider a CIR,  $h(t)$ , with  $N$  multi-path taps, represented as:

$$h(t) = \sum_{i=1}^N \beta_i \delta(t - \tau_i) \quad (5.1)$$

where  $\beta_i$  and  $\tau_i$  are the amplitude and the delay of the CIR coefficient associated to the  $i_{th}$  tap. The time reversed version of the CIR is written as:

$$h(-t) = \sum_{i=1}^N a_i \delta(t - \tau_i) \quad (5.2)$$

where  $a_i = \beta_{N-i+1}$ . If  $h(-t)$  is circularly shifted to right by  $l$  taps, the resulting function is written as:

$$circshift(h(-t), l(right)) = \sum_{i=1}^l a_{N-l+i} \delta(t - \tau_i) + \sum_{i=l+1}^N a_{i-l} \delta(t - \tau_i) \quad (5.3)$$

The equation for the left circular shift can be written as:

$$circshift(h(-t), l(left)) = \sum_{i=1}^{N-l} a_{i+l} \delta(t - \tau_i) + \sum_{i=N-l+1}^N a_{i+l-N} \delta(t - \tau_i) \quad (5.4)$$

where  $l$  can have integer values:  $1 \leq l \leq N - 1$

FIG. 5.1 shows a time reversed CIR without any circular shift, with right and left circular shift (CS) of  $l$  taps ( $l = 3$ ). In a multiuser scenario, the interference at the peak increases with the number of simultaneous transmissions. Simultaneous transmission with the simple TR scheme means that the maximal peaks of the time reversed impulse responses intended for different users are aligned with each other in order to be transmitted. This results in the creation of the interference which is equal to the magnitude of the CIRs cross-correlations ( $R_{jk}^{cross}$ ). This interference will increase to the sum of  $M - 1$  cross-correlations for  $M$  simultaneous users. If CSTR is used instead of simple TR, the effects of the interference can be greatly reduced [63]. If symbols for more than one user are transmitted simultaneously with CSTR, the maximal peaks of the time reversed impulse responses will no longer be aligned with each other. The taps in the propagating channel containing more energy are multiplied by the taps of the transmitted signal with less energy and vice versa. This results in greatly reduced interference with CSTR [63].

The received signal for the right CSTR while neglecting the noise is written as:

$$R_{x,right}^{CSTR} = circshift(h(-t), l(right)) \star h(t) \quad (5.5)$$

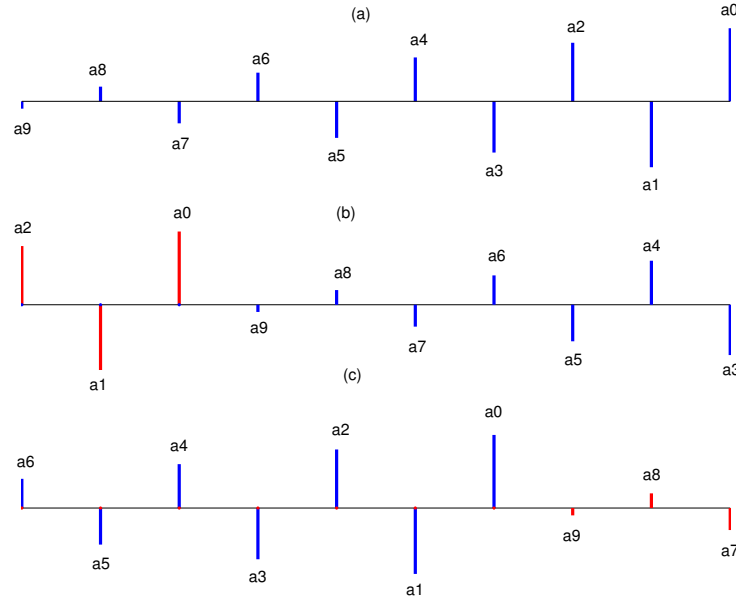


Figure 5.1: Time Reversed CIR a) without CS b) with right CS of 3 taps c) with left CS of 3 taps

Applying (5.3), the equation becomes:

$$R_{x,right}^{CSTR} = \underbrace{\left( \sum_{i=1}^l a_{N-l+i} \delta(t - \tau_i) \star \sum_{i=1}^N \beta_i \delta(t - \tau_i) \right)}_{Image} + \underbrace{\left( \sum_{i=l+1}^N a_{i-l} \delta(t - \tau_i) \star \sum_{i=1}^N \beta_i \delta(t - \tau_i) \right)}_{Signal} \quad (5.6)$$

The received signal for a right CSTR consists of two parts. The first part is the convolution of the first  $l$  taps of the right CSTR transmitted signal (i.e. the last  $l$  taps of the time reversed CIR moved to the start) with the CIR and the second part is the convolution of the rest of the taps with CIR. These two convolutions result in two signals with two significant peaks. We call the latter as *Signal* and the former as *Image*. The position of the *Signal* peak also moves from its position toward right by  $l$  taps. The distance between the position of the *Signal* and *Image* peaks is always equal to  $N$  taps. The received signal for left CSTR can be constructed in the same manner. As the number of shifted taps increases, the amplitude of the *Image* peak also increases depending upon the energy contained in the shifted taps.

Thus, the amplitude of the *Signal* and *Image* peaks depends directly on the energy of the taps responsible for their creation. To summarize, if  $l$  is the number of taps to be shifted then, the first  $l$  taps of the circularly shifted time reversed CIR are responsible for the creation of *Image* in case of right CSTR. In case of left CSTR, the

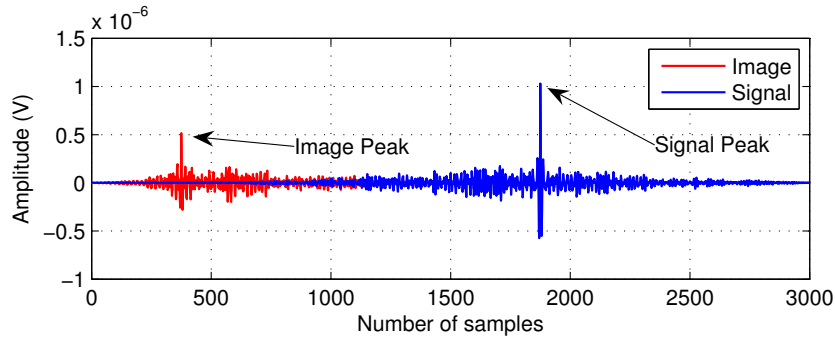


Figure 5.2: Received *Signal* and *Image* with right circular shift of  $0.25N$  taps

last  $l$  taps of the circularly shifted time reversed CIR are responsible for the creation of an *Image*.

Thus, the reduction in the interference with CSTR has its cost. On one hand, CSTR improves the performance of the system by reducing the interference caused by the simultaneous transmissions, but on the other hand, it results in the degradation of the system performance as the received signal peak amplitude is reduced with the increase of circular shift. This behavior of the CSTR was not elaborated by the authors in [63]. Thus, CSTR has its limits and we can get a better performance, only if these are taken into account. Otherwise, CSTR could lead to a very poor performance.

### 5.2.1 Effects of CSTR on Received Signal Peak

We have found that the received signal peak is reduced with CSTR depending upon the amount of the shift. The lost power appears as an *Image* and is thus lost. These *Image* and *Signal* are represented mathematically in (5.6). The amplitude of the *Image* peak becomes comparable to the amplitude of the *Signal* peak when the energy contained in the circularly shifted taps approaches to the energy contained in the rest of the taps.

FIG. 5.2 shows the received signal for a right CS of  $0.25N$  taps where  $N$  is the total number of taps in the transmitted signal. *Signal* and *Image* peaks can easily be distinguished.

FIG. 5.3 shows the variation of the received *Signal* peak power (normalized to the received peak power without CS) with CSTR using the 35 measured channels. The bold line shows the average variation over multiple measurements. The dashed line is our defined threshold that is considered as  $-3$  dB. This threshold should be selected according to the application and received power requirements. As shown, the received *Signal* peak power reduces as the percentage of the CS (either left or right) increases. The graph is plotted till left circular shift of  $0.70N$  taps and right circular shift of  $0.30N$  taps instead of more symmetric  $0.50N$  taps shift on both sides. These percentages are chosen because energy contained in the shifted taps for right

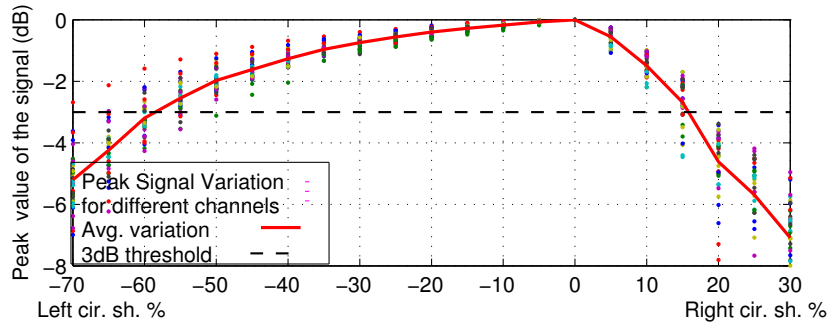


Figure 5.3: Variation of the received signal peak values normalized to the received signal peak without circular shift with different values of circular shift

CSTR is higher than energy contained in the shifted taps for left CSTR, resulting in a greater power loss with the right circular shift (see FIG. 5.1). Therefore, the allowable shift margin obtained from the threshold increases considerably with our choice of CS percentages.

When the sum of *Signal* and *Image* peak amplitudes is taken, it comes out to be equal to the amplitude of the received signal peak without any shift, ascertaining that the received signal peak is decomposed into a *Signal* peak and an *Image* peak after CS.

### 5.3 Effects of CSTR on Signal to Interference Ratio (SIR)

When symbols for more than one user are transmitted simultaneously, only one part amongst  $N$  simultaneously transmitted signal is intended toward a specific user. The rest  $N - 1$  parts are the Interferences for that user. In multiuser CSTR, the intended signals for different users are circularly shifted with different CS percentages. In [63], the CS percentage increases by 5% for every user. The authors have shown an improvement in the SIR curves with the CS. The maximum shift percentage studied in [63] is 20% for five simultaneous users. For more users, the percentage of CS must be increased. We have also considered a scenario of five simultaneous users but we have gradually increased the CS percentage for User5 till it reaches 30% (in both directions). The purpose is to study the effects of CS on SIR. The intended signals for five users are transmitted simultaneously with a CS difference of 3%. Thus every user receives four interferences along with its intended signal. We have varied (left and right) CS percentage for User5 from 12-30%. The CS percentages for other four users remain same (i.e. 0-9%). All these simulations are performed on the measured channel responses in a typical indoor environment.

### 5.3.1 Experimental Setup

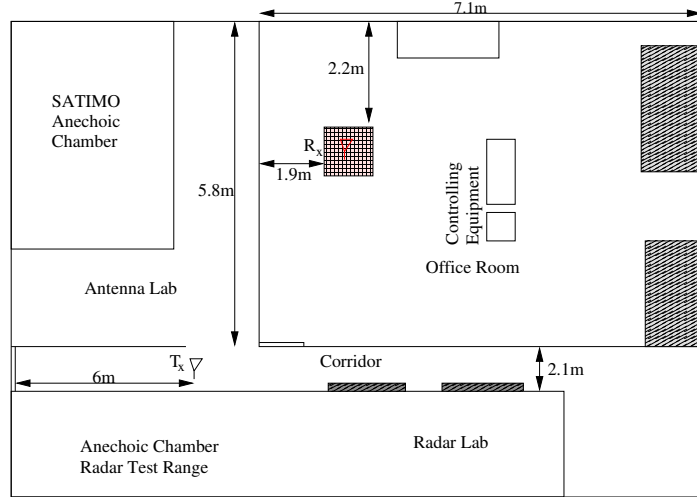


Figure 5.4: Measurement layout for the measurement in an indoor environment

Experiments are performed in a typical indoor environment. The environment is an office space of  $14\text{ m} \times 8\text{ m}$  in the IETR laboratory. FIG. 5.4 shows the measurement layout in a typical indoor environment of IETR lab. The frequency response of the channel in the frequency range of  $0.7 - 6\text{ GHz}$  is measured using vector network analyzer (VNA) with a frequency resolution of  $3.3\text{ MHz}$ . Two wide-band conical mono-pole antennas (CMA) are used in a non line of sight (NLOS) configuration. The height of the transmit antenna and the receive antenna is  $1.5\text{ m}$  from the floor. The receiver antenna is moved over a rectangular surface ( $65\text{ cm} \times 40\text{ cm}$ ) with a precise positioner system. Respective spatial resolution of  $2.5\text{ cm}$  and  $5\text{ cm}$  is used for the x-axis and y-axis of the horizontal plane. Thus, 243 ( $27 \times 9$ ) measurements are taken over the rectangular surface. The frequency responses between the transmitting antenna and receiving virtual array (of 243 antennas) are measured. The time domain CIRs are computed using the inverse fast Fourier transformation (IFFT) of the measured frequency responses.

### 5.3.2 Simulation Results

In the context of multiuser CSTR, it is important to study the system performance on user to user basis otherwise the results might not show the true picture of the scenario. For example, in our studied scenario with five simultaneous users, the performance of User1 will always be better than other users. The intended *Signal* for User1 does not undergo CS while all four of its *Interference* parts do undergo CS. The benefits are two folds; first its *Interference* is reduced considerably due to the CS and second no power is lost as an *Image*. Thus, if the total performance of the system is studied, it is not a fair representation. That is why, we have presented the curves for User5 which

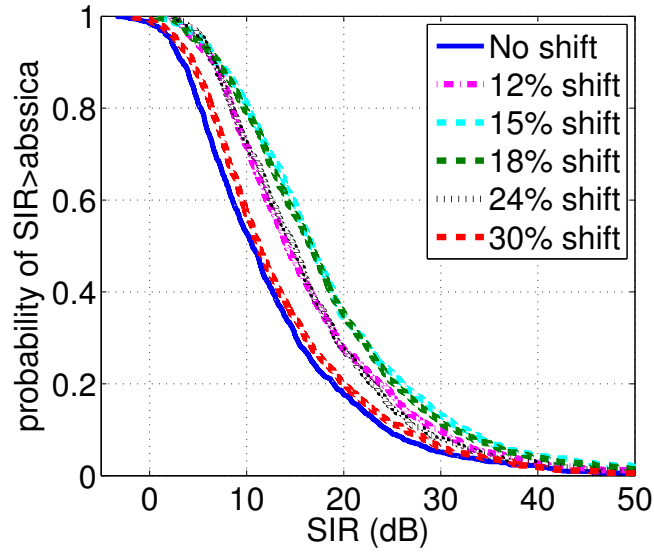


Figure 5.5: CDF of SIR with right circular shift for User5 with different shift %

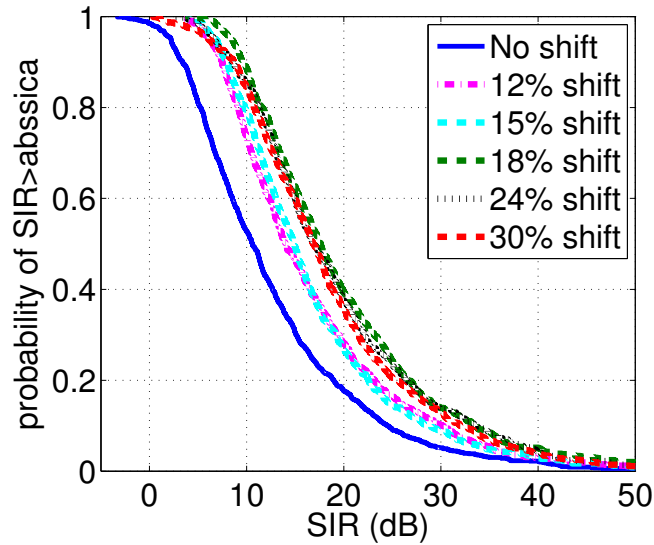


Figure 5.6: CDF of SIR with left circular shift for User5 with different shift %

is worst case i.e. its intended *Signal* undergoes largest CS while its *Interference* undergoes least CS.

The CSTR (left or right) scheme results in the reduction of the interference caused by the other users. This reduction in the interference results in an increase of SIR. To simulate the scenario of 5 simultaneous users, we have generated 1085 ( $35 \times 31$ ) combinations of 5 from the existing 243 measured CIRs. Figs. 5.5-5.6 show the curves of cumulative density function (CDF) of SIR for User5 for different (left and right) CS.

As shown, the performance is improved with CSTR. For right CSTR (FIG. 5.5), the improvement in SIR reaches its saturation state, and the performance degradation starts after certain value of CS (20%). This degradation in the performance after certain value of CS is due the reduction in received signal strength with CS. However, for left CSTR, the performance degradation is lesser as the reduction in the received signal strength is considerably lesser for left CSTR than right CSTR (see FIG. 5.6).

## 5.4 Modified Transmission Scheme

In this section, multi-user TR scheme is analyzed by modifying the CSTR and using our proposed shift operation (explained in CHAPTER 4). It is important to note, the proposed scheme is used in a multi-user scenario, therefore, simultaneous bits are intended for different users rather than the same user. We have omitted the detailed description of the transmission scheme, however, expressions for the transmitted and the received signals are presented as they have changed a little.

In a multi-user TR system, multiple signals for different users are transmitted simultaneously. Let the measured and truncated CIR from the transmitter to the user  $i$  be written as:

$$h'_i(-t) = \sum_{m=0}^{L-1} a_m^i \delta(t - m \tau_s) \quad (5.7)$$

where  $L$  is number of time reversal filter taps which corresponds to  $T_{sig} = L \tau_s$  in seconds,  $a_m^i$  is the associated amplitude and  $m \tau_s$  is the associated delay of the  $m_{th}$  multi-path component.  $\tau_s$  is the time between two consecutive samples and depends on the sampling rate of the time reversal filter. For instance, if the measured CIR is sampled with a sampling rate of 5 GS/s, the delay of  $\tau_s = 0.2 ns$  is obtained between two consecutive samples, therefore the number of taps ( $L$ ) in filter having a length of 50 ns is  $L = 250$  samples or taps. The transmitted signal for multi-user TR can be written as:

$$T_x(t) = \sum_k \sum_{i=0}^{N_u-1} \frac{1}{\sqrt{N_u}} d_{ik} A_i h'_i(-t - kT_s) \quad (5.8)$$

where  $d_{ik}$  is the  $k_{th}$  information bit of the  $i_{th}$  user,  $N_u$  is the total number of simultaneous users,  $T_s$  is the symbol duration and  $A_i$  is the normalization factor which can be written as:

$$A_i = \frac{1}{\sqrt{\|h'_i(-t - kT_s)\|^2}} \quad (5.9)$$

where  $\|\cdot\|$  is the Frobenius norm operation. The term  $\frac{1}{\sqrt{N_u}}$  insures that the signals for all the users are transmitted with a constant power. This is in contrast to [63], where this normalization has not been carried out resulting in an unfair comparison of the

performance with different number of users. The received signal for the  $j_{th}$  user and the  $k_{th}$  symbol while neglecting the noise can be written as:

$$R_{x_{kj}}(t) = \underbrace{\frac{1}{\sqrt{N_u}} d_{jk} h_j(t) \star h'_j(-t + jT_u - kT_s)}_{\text{Signal}} + \underbrace{\frac{1}{\sqrt{N_u}} \sum_{i=0, i \neq j}^{N_u-1} d_{ik} h_j(t) \star h'_i(-t + iT_u - kT_s)}_{\text{Interference}} \quad (5.10)$$

The responses of the modified filter are produced by shifting  $h'(-t)$  to either left or right and then forcing the shifted part to zero, so that the shifted signal can be packed in the same signal duration. With the process of filling the shifted taps with zeros, we get rid of the unwanted signal, which causes interference to the adjacent symbols (we named it as *Image* in [64]). As the taps, which result in an undesired signal are forced to zero, the received peak signal increases for an equal transmitted power. The details of the shift procedure have already been described in CHAPTER 4.

The transmitted signal with the modified transmission scheme can be thus written as:

$$T_x(t) = \sum_k \sum_{i=0}^{N_u-1} \frac{1}{\sqrt{N_u}} d_{ik} A_i \hat{h}_i(-t + iT_u - kT_s) \quad (5.11)$$

where  $A_i = \frac{1}{\sqrt{\|\hat{h}(-t+iT_u-kT_s)\|^2}}$  and the term  $\frac{1}{\sqrt{N_u}}$  insures that power transmitted for different number of users is constant. The received signal for the  $k_{th}$  symbol of the  $j_{th}$  user can be written as:

$$R_{x_{kj}}(t) = \underbrace{\frac{1}{\sqrt{N_u}} d_{jk} h_j(t) \star \hat{h}_j(-t + jT_u - kT_s)}_{\text{Signal}} + \underbrace{\frac{1}{\sqrt{N_u}} \sum_{i=0, i \neq j}^{N_u-1} d_{ik} h_j(t) \star \hat{h}_i(-t + iT_u - kT_s)}_{\text{Interference}} \quad (5.12)$$

### 5.4.1 Interference Analysis of the Proposed Scheme

To analyze the worst case performance, it is assumed that the transmitter communicates with all users at the same time. Therefore, TR received signal in a multi-user scenario consists of a sum of one auto-correlation function and  $N_u - 1$  cross-correlation functions. The  $N_u - 1$  cross-correlation functions cause multi-user interference. The

received signal peak is the sum of the square of the coefficients of CIR (from the properties of auto-correlation function). The interference term at the time of the peak ( $t_{peak}$ ) for the  $j$ th user in a simple TR scheme can be written as:

$$I_{j_{simple\ TR}}(t_{peak}) = \sum_{i=1, i \neq j}^{N_u} \sum_{m=0}^{L-1} b_{mi} \times a_{mj} \quad (5.13)$$

where  $b_{mi}$  are the coefficients of the time reversed CIR  $h'_i(-t + iT_u - kT_s)$  (from 5.10) specific to the user  $i$ ,  $a_{mj}$  are the coefficients of  $h_j(t)$ . As (5.13) uses simple TR transmission scheme, the high powered taps of  $h'_i(-t)$  and  $h'_j(-t)$  are approximately in the same time interval. Therefore, taps in the propagating channel containing more energy are multiplied by the taps of the transmitted signal with more energy resulting in a relatively higher interference.

To calculate the interference of the modified transmission scheme, we assume that the transmitted signal for the intended receiver is not shifted. Then by using (5.12) and (5.13), interference at the peak of the intended signal is then written as:

$$I_{j_{mod\ TR}}(t_{peak}) = \sum_{i=0, i \neq j}^{N_u-1} \sum_{m=0}^{L-l-1} b_{(m+l)i} \times a_{mj} \quad (5.14)$$

where  $b_{mi}$  and  $a_{mj}$  are the same coefficients used in (5.13). Here, the interference is the product of  $L - l$  coefficients (as  $l$  taps are forced to zero). Furthermore, (5.14) suggests that in case of modified TR scheme, the taps in the propagating channel containing more energy are multiplied by the taps of the transmitted signal with less energy and vice versa. Therefore, interference is reduced with the new proposed transmission scheme. This reduced interference helps to improve the bit error rate (BER) performance of the system.

### 5.4.2 Effects of Shift on Received Signal Peak

In a TR communication system, as the received signal is the auto-correlation function of the CIR, the received signal peak is the sum of the square of the coefficients of CIR. Neglecting the interference and the noise, the received signal peak with the modified TR scheme for the  $k$ th symbol of the  $j$ th user is written as:

$$R_{x_{mod\ TR}}(t_{peak_{jk}}) = d_{jk} A_j \left( \sum_{m=0}^{L-l_j-1} a_m^2 \right) \quad (5.15)$$

where  $a_i$  are the coefficients of taps of  $\hat{h}(-t + jT_b - kT_s)$  and  $l_j$  ( $j \frac{T_b}{T_s}$ ) are the number of taps required for a shift of  $jT_b$ . The received signal peak depends on the energy contents of  $(L - l_j)$  filter coefficients. Thus, the amplitude of the received peak decreases by the sum of the square coefficients in the shifted part of the transmitted signal. Therefore with the new modulation scheme, the received signal peak reduces in proportion to the energy of the shifted part of the transmitted signal.

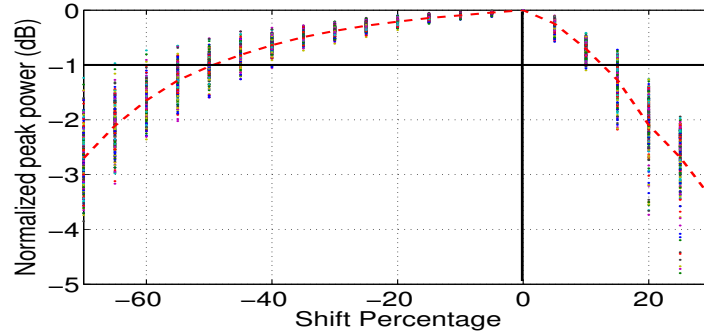


Figure 5.7: Received signal peak power with left and right shifts normalized to the peak with no shift

FIG. 5.7 shows the peak power of the received signal peak for the shifted signals normalized to the received peak with no shift. The shift percentage corresponds to the percentage of the total length of the transmitted signal. A set of 243 measured CIRs are used for the simulation. The experimental setup and the measurement procedure are explained in Section 5.4.3. The loss of the received peak power for transmitted signals corresponding to individual CIRs is represented by the dots and the dashed line is the mean of power loss. To calculate the maximum number of simultaneous users that a system can support, we must take the decision in accordance to the threshold (say  $-3$  dB) which can vary for different applications.

For a  $-3$  dB threshold, our system can support a shift percentage of  $0.70L$  taps for left shift and  $0.25L$  taps for right shift (see FIG. 5.7). Thus, the number of users with the proposed scheme can be written as:

$$N_u^{mod.TR} = \lfloor \frac{0.95 \times L}{\delta} \rfloor = \lfloor \frac{0.95 \times T_{sig}}{\Delta TR} \rfloor \quad (5.16)$$

where  $\lfloor \cdot \rfloor$  denotes the floor operator,  $L$  is the total number of taps in the transmitted signal,  $\delta$  is the shift percentage between two simultaneous users,  $T_{sig}$  is the channel length in seconds and  $\Delta TR$  is shift separation between two users in seconds. For the same threshold, the previously proposed scheme in [63] can only support a shift of  $0.75L$  which is contrary to their claim of 100% shift (as power loss with circular shift operation was not considered by the authors). The power loss for left shift is lesser than the power loss for the right shift, as the energy contained in the shifted parts of the right shift is greater than the energy contained in the shifted parts of the left shift. Although a combination of right and left shifts can be used for the communication, for the sake of simplicity, we have only used left shift. In the rest of the chapter unless otherwise mentioned, a shift is meant to be a left shift.

Power spectral density (PSD) of the transmitted signal of a TR communication system takes into account the effects of the antennas and the propagation channel including the path loss. In contrast to the pulse signal, the spectrum of a TR signal has a descending shape with increasing the frequency, because the higher frequency

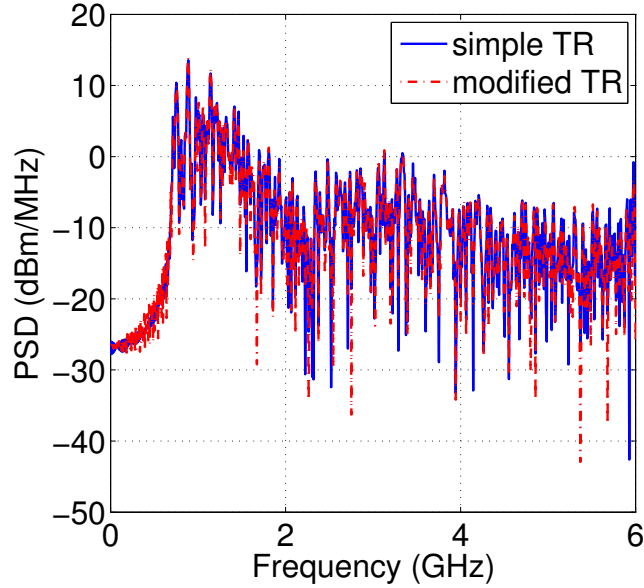


Figure 5.8: PSD of transmitted signal with simple TR and modified TR schemes

components experience a greater path loss as compared to the lower frequency components in the spectrum. FIG. 5.8 shows the PSD plots of the transmitted signal with simple TR and modified TR schemes where a left shift of  $0.20N$  taps is carried out for both TR schemes. The plots of both schemes have a descending shape. The maximum spectral power is experienced at the same frequency. Therefore, both the signals must be attenuated with the same factor in order to respect the UWB spectral mask proposed by FCC. Frequency selectivity of the transmitted signals is similar for the two schemes. In short, the both schemes have resembling spectral properties.

### 5.4.3 Experimental Setup and Simulation Results

Experiments are performed in a typical indoor environment. The environment is an office space of  $14\text{ m} \times 8\text{ m}$  in the IETR laboratory. The frequency response of the channel in the frequency range of  $0.7\text{--}6\text{ GHz}$  is measured using vector network analyzer (VNA) with a frequency resolution of  $3.3\text{ MHz}$  and two wide-band conical mono-pole antennas (CMA) in non line of sight (NLOS) configuration. The height of the transmitter antenna and the receiver antenna is  $1.5\text{ m}$  from the floor. The receiver antenna is moved over a rectangular surface ( $65\text{ cm} \times 40\text{ cm}$ ) with a precise positioner system.

The frequency responses between the transmitting antenna and receiving virtual array are measured. The time domain CIRs are computed using the inverse fast Fourier transformation (IFFT) of the measured frequency responses.

### 5.4.3.1 BER Performance

In the proposed transmission scheme, one user is separated with the other by a shift of a fixed number of taps. This separation is named as  $\delta$ , which is a percentage of total number of taps in the transmitted signal. Signal for User 1 is transmitted without any shift. As discussed in Section 5.4.1, interference between users is greatly reduced with the proposed modulation scheme. To study the impact of the reduced interference, we evaluate the BER performance with the proposed scheme using left shift for 5, 10 and 15 simultaneous users for  $\delta = 0.05 L$ .

From the measured CIRs, we generate almost  $35 \times (35 - N_u - 1)$  combinations for simulating different number of simultaneous users ( $N_u$ ). For every combination of simultaneous users, 10000 symbols are transmitted which makes it sufficient for statistical analysis. The measured CIR is truncated for 90% energy contained in the CIR. Thus, the transmitted symbol has a length of 55 ns and a per user bit rate of 18 Mbps. Perfect synchronization and no ISI effects are assumed. Signal to noise ratio (SNR) is varied by varying the noise variance, as:

$$SNR = P_j / \sigma_{noise}^2 \quad (5.17)$$

where  $P_j$  is the power of the received signal at its peak and  $\sigma_{noise}^2$  is the noise variance. Bipolar pulse amplitude modulation (BPAM) is used for these simulations. The received signal  $y_j(t)$  is sampled at its peak and is detected based on ideal threshold detection, given as:

$$\text{Detected bit} = \begin{cases} 1 & \text{if } y_j(t_{peak}) \geq 0 \\ 0 & \text{if } y_j(t_{peak}) < 0 \end{cases} \quad (5.18)$$

FIG. 5.9a-c shows the BER performance of the simple TR, TR with circular shift operation and the modified TR scheme for 5, 10 and 15 simultaneous users. The modified TR scheme outperforms the other two schemes especially for higher number of simultaneous users (10, 15). For instance, for 10 simultaneous users, the modified TR scheme results in a 1.4 dB better performance than the TR with circular shift for a BER of  $10^{-4}$ . The simple TR scheme has already reached a plateau. To perform an analysis in the presence of extreme multi-user interference, BER performance is studied for 15 simultaneous users. FIG. 5.9d compares the performance of the three schemes for 15 simultaneous users. The modified TR scheme gives significantly better performance than the other two schemes. The improvement is in the order of 4.5 dB or more.

If a system has a large number of users, the users experiencing higher shift percentages will give poorer performance than the users experiencing lower shift percentages. To have a consistent system, we propose to rotate the shift percentages for different users so that no user is subjected to permanent high shift percentage.

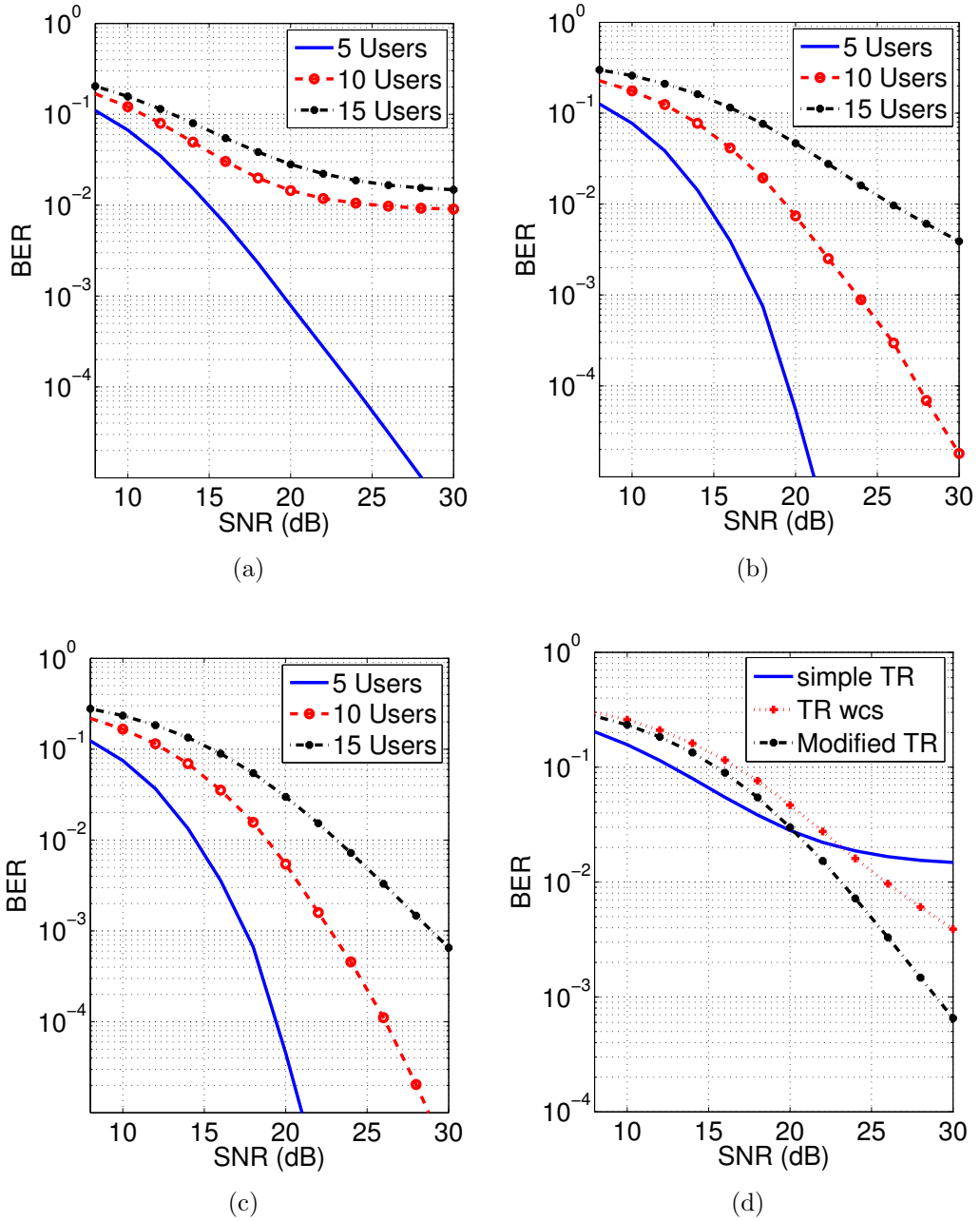


Figure 5.9: BER performance with 5, 10, and 20 simultaneous users with a) simple TR b) TR with circular shift c) modified TR scheme d) 15 simultaneous users with all three schemes for  $\delta = 0.05 L$  taps

## 5.5 Conclusion

In this chapter, multi-user TR communication has been studied. Multi-user TR is examined using a circular shift operation (CSTR) and is compared with the simple

TR scheme. It is shown that in a multi-user scenario, CSTR reduces the interference considerably and results in a better SIR performance than simple TR scheme. However the SIR improvement reaches its limit and the performance starts degrading due to the reduction in the received peak with the circular shift. Thus, CSTR can result in a very poor performance for some users with high values of circular shift, especially in the case of right CSTR. It is also shown that the reduction in the received peak power depends directly on the power of the shifted taps. Furthermore, a modified transmission scheme for a multi-user TR system is proposed. With the help of mathematical derivations, it is shown that the interference in the modified TR scheme is reduced compared to simple TR scheme. Limitations of the proposed scheme are studied and an expression for maximum number of simultaneous users is proposed. It is shown that the modified TR scheme outperforms simple TR and TR with circular shift scheme, especially at higher number of simultaneous users. For instance for 15 simultaneous users, the modified TR scheme improves the performance in the order of 4.5 *dB* or more for a constant BER.

# General Conclusion and Prospects

This PhD thesis is an effort to elaborate the application of time reversal (TR) technique to ultra wide-band (UWB) and MIMO communication systems. TR is a concept which can be applied to the signals of any type and of any bandwidth. Classically, TR has been applied to acoustics and under water applications. UWB received signals are spread in time and have a very high multi-path resolution. As a consequence, a complex receiver system is required to capture significant energy of the received signal. Therefore, UWB signals seem to be a perfect candidate for the application of TR scheme. TR scheme shifts the complexity from the receiver to the transmitter. TR received signal is very compressed in time and focused in spatial domain. These signals can be detected by means of relatively simple receivers. In this thesis, we have exploited TR scheme for the communication purpose. This thesis spans over the broad domains of propagation and data communication with the help of TR scheme. Some of our contributions on this research topic are:

- Validation of TR scheme using simulation, semi-measurement and measurement approach
- TR validation with multi-antenna configurations (MIMO)
- Robustness of TR scheme in a non stationary channel environment
- A novel modulation scheme for TR communication
- High data rate communication with TR scheme
- Multi-user communication utilizing the TR scheme

A great deal of experimental work has been carried out for the development of this thesis. The experimental validation of the TR scheme has a significance from the implementation point of view. Therefore, as a very first step, validation of the TR scheme has been performed in the laboratory using simulation, semi measurement and measurement approaches. The results of TR validation are presented in **Chapter 2**. With semi-measurement approach, spatial focusing of the TR scheme is analyzed. It is shown that in a typical indoor environment, the received peak power decreases in the order of 10 *dB* for only 10 *cm* movement of the receiver. The effects of different bandwidths on the spatial focusing of the TR scheme are also examined. **The results**

suggest that the dimension of the spatial focusing zone is controlled by the lower frequency of the bandwidth.

In the measurement approach, TR validation is carried out by using time domain instruments (AWG and DSO) in different dense multi-path channel environments. A parametric analysis of the TR scheme is carried out based on the experimental results for different configurations with combinations of different environments (LOS and NLOS) and antenna orientations (co-polar and cross-polar). In the indoor environment, **LOS co-polar configuration has the largest received peak power but the lowest SSR, whereas NLOS cross-polar configuration has the lowest received peak power and the highest SSR. For a given channel environment, LOS cross-polar configuration can be a good compromise with larger received power compared to NLOS configurations and equally good performance.** Experiments are also conducted in the RC and it is shown that the RC is a very favorable environment for TR.

Furthermore, **it has been found that transmitted signals with higher bandwidths achieve better performance than the signals with lower bandwidths.** Experiments are also performed for the TR scheme with different types of antennas. The results suggest that **an omni-directional antenna performs better in the environments with a constant multi-path floor or where the direction of arrival for majority of the multi-paths is uniformly spread, whereas a directive antenna is expected to perform significantly better than the omni-directional antenna if the direction of arrival for most of the multi-paths matches with the main lobe of the radiation pattern of the antenna.**

TR validation is also performed with different multi-antenna configurations. The results suggest that **MIMO-TR outperforms all other configurations.** In the end, a novel multiplexing scheme is described where **a multiplexing gain proportional to the number of receiving antennas with SIMO-TR scheme is achieved and thus capacity of the TR scheme is ameliorated. Furthermore, the results suggest that SIMO-TR scheme attains significantly higher capacity than MISO-TR scheme.**

The performance of a TR system was expected to be highly dependent on a perfect channel state information (CSI) at the transmitter end. It was suggested that although TR can potentially result in a very simple receiver, the dependence on the CSI would degrade the performance of the system in a time varying channels. Therefore, we carried out a series of experiments that eventually show that **the TR system is robust and can resist the changes in the channel.** These results are presented in **Chapter 3.** Measurement campaigns are conducted in a mode stirred reverberation chamber (RC) and in the indoor environments. It has been found, that **if the channel maintains some partial correlation with the previous channel, TR can give a robust performance even if the total correlation of the channels is very low. Although higher bandwidths generally give better performance than the lower bandwidths, but the degradation in the performance with the variations in the channel is of the same magnitude.** On the other hand, if

the receiver is displaced from its position, the channel gets totally de-correlated and does not maintain any partial correlation with the original CIR for a movement in the order of  $\frac{\lambda}{4}$ , where  $\lambda$  is the wavelength of lower frequency  $f_L$ .

**In the indoor environment, it has been found that a very robust performance is achieved for different induced variations in the channel.** A very high FG is observed with all kind of variations in the channel. SSR does not change a great deal (ascertaining the results obtained in the RC). IAP decreases with the variations in the channel especially for lower bandwidths (1.5 GHz and 1.0 GHz). Again, the deterioration in the performance with different induced variations is of the same order for all bandwidths.

From the implementation point of view, these results are very important. In realistic environments, there will be no need to re-estimate the channel response if there are minor changes in the environment e.g. movement of the people. This property can be very attractive for WLAN and wireless streaming applications. Thus, TR robustness is more beneficial in a non stationary channel where variations are caused by the changes in the environment.

The second part of this thesis focuses on the communication using TR scheme. In **Chapter 4**, a novel modulation scheme is proposed for a TR UWB communication system. **Multiple bits are transmitted simultaneously by shifting the transmitted signal and packing them in the same time slot.** It is shown that for negligible interference and quasi orthogonal signals, the data rate of the modulation scheme increases linearly whereas the transmitted power must only be increased logarithmically. The validation of the modulation scheme is carried out with the help of two separate measurement campaigns. The results suggest that **for an optimal shift, theoretical and simulation performances of the modulation scheme are in strong agreement to each other.** The scheme is experimentally validated with the second measurement campaign. For high data rate communication, larger values of shift step will be required which eventually degrade the performance of the system. Therefore, a communication can be envisaged without the introduction of shift so that the limitations introduced by the shift can be avoided. In the second part of the chapter, we present the results for very high data rate TR communication using BPAM without any introduction of shift. Experiments have been done in a typical indoor environment and in a reverberation chamber for different data rates ( $R_b$ ) ranging from 15.62 Mbps to 1 Gbps. **It is shown that the BER performance in the indoor channel is better than the reverberation chamber. Furthermore, with the sub-band TR transmission approach, a sort of equalization is achieved which significantly improves the BER performance.** For instance, the modified scheme gives a 2.4 dB better performance than the classic TR scheme for  $R_b = 62.5$  Mbps and a fixed BER of  $10^{-6}$ . With the validation of high data rate communication, TR can be thought of a potential transmission scheme for realistic applications for example WLAN and wireless streaming applications etc.

In **Chapter 5**, multi-user TR communication has been studied. The scheme introduced in **Chapter 4** is used for multi-user TR communication system. At first, we

examine multi-user TR communication with a modified pre-filter using a circular shift operation (CSTR). It is shown that in a multi-user scenario, CSTR reduces the interference considerably and results in a better SIR performance than simple TR scheme. However with the introduction of circular shift, a reduction in the received peak power has been found which depends directly on the power of the shifted taps. Thereafter, multi-user TR communication has been investigated by using the proposed shift operation (proposed in **Chapter 4**). Limitations of the proposed scheme are studied and an expression for maximum number of simultaneous users is proposed. It is shown that **the modified TR scheme outperforms simple TR and TR with circular shift scheme, specially at higher number of simultaneous users**. For instance, for 15 simultaneous users, the modified TR scheme improves the performance in the order of 4.5 dB or more for a constant BER.

The results presented in this thesis suggest that the TR UWB scheme is a promising and attractive transmission approach for future wireless local and personal area networks (WLAN & WPAN) and wireless streaming applications.

There are numerous prospects of the work carried out in this thesis:

- The results presented in different chapters can be extended. For example, experiments can be done in more generalized environments including outdoor environment
- TR experiments can be conducted with different types of waveforms
- High data rate communication can be examined by using the equalizer at the receiver and a performance-complexity trade-off analysis can be carried out
- Theoretical work can be performed on the capacity calculations of the TR scheme in different UWB channel models
- The performance of the TR system can also be compared by using pulse position modulation scheme with classic TR and the modified TR schemes
- Real time communication with TR can be experimentally studied
- A practical demonstrator can be built showing TR communication

# Research Publications

## Book Chapters

- I. H. Naqvi, G. El Zein, Time Reversal Technique for Ultra Wide-band and MIMO Communication Systems, Wireless Communication, InTech Publishers (Accepted for publication)

## International Journals

- I. H. Naqvi, G. El Zein, G. Lerosey, J. de Rosny, P. Besnier, A. Tourin, M. Fink, “Time Reversal UWB Communication: Experimental Study for High Data Rates in Dense Multipath Propagation Channels”, IET Journal of Antenna and Propagation, vol. 4, No. 5, pp 643–650, doi : 10.1049/iet-map.2009.0188
- I. H. Naqvi, A. Khaleghi, G. El Zein, “ Time Reversal UWB Communication System: A Novel Modulation Scheme with Experimental Validation ”, Eurasip Journal on Wireless Communications and Networking (JWCN), vol. 2010, doi:10.1155/2010/398401.
- I. H. Naqvi, P. Besnier, G. El Zein, “ On the Robustness of a Time Reversal UWB System in Non Stationary Channel Environments ”, IET Journal of Antenna and Propagation (Submitted)
- A. Khaleghi, I. H. Naqvi, G. El Zein, “ SIMO Time Reversal UWB Communication System: An Increased Capacity Transmission Approach ”, IET Electronics Letters (Under Preparation)

## National Journal

- I. H. Naqvi, G. El Zein, “ Retournement temporel: comparaison de système SISO, SIMO, MISO et MIMO avec les mesures dans le domaine temporel ”, Revue de l'Electricité et de l'Electronique (REE). Dossier: Propagation et Télé-détection. (Février 2010).

## International Conferences

- I. H. Naqvi, P. Besnier, G. El Zein, "Effects of Time Variant Channel on Time Reversal UWB System" Proceedings of The IEEE Global Communication Conference (IEEE GLOBECOM 2009), 30 November-4 December, 2009, Honolulu, Hawaii, USA.
- I. H. Naqvi, A. Khaleghi, G. El Zein, "Multiuser Time Reversal UWB Communication System: A Modified Transmission Approach", The 20th IEEE International Symposium On Personal, Indoor and Mobile Radio Communications (PIMRC '09).
- I. H. Naqvi, G. El Zein, G. Lerosey, J. de Rosny, P. Besnier, A. Tourin, M. Fink, "Time Reversal UWB Communication: Experimental Study for High Data Rates in Dense Multipath Propagation Channels", The Mosharaka International Conference on Communications, Propagation and Electronics (MIC-CPE 2009), February 6-8, 2009, Amman, Jordan.
- I. H. Naqvi, G. El Zein, "Time Domain Measurements for a Time Reversal SIMO System in Reverberation Chamber and in an Indoor Environment", The 2008 IEEE International Conference on Ultra-Wideband, (ICUWB 2008), Leibniz Universität Hannover, Germany, September 10-12, 2008.
- I. H. Naqvi, A. Khaleghi, G. El Zein, "Performance Enhancement of Multiuser Time Reversal UWB Communication System", Proceedings of The IEEE International Symposium on Wireless Communication Systems, (ISWCS '07), 16-19 October 2007, Trondheim, Norway.
- A. Khaleghi, G. El Zein, I. H. Naqvi, "Demonstration of Time-Reversal in Indoor Ultra-Wideband Communication: Time Domain Measurement", Proceedings of The IEEE International Symposium on Wireless Communication Systems, (ISWCS '07), 16-19 October 2007, Trondheim, Norway.
- I. H. Naqvi, G. El Zein, "Time Reversal UWB System: SISO, SIMO, MISO and MIMO Comparison with Time Domain Experiments", Journées Scientifiques CNFRS-URSI "Propagation et Télédétection", Paris, 24 - 25 Mars, 2009.

## Oral Presentations

- I. H. Naqvi, A. Khaleghi, G. El Zein, A. Tourin, "Miroirs à retournement temporel électromagnétiques pour les communications", Journées thématiques sur "la Propagation des Ondes, ses Applications, et ses Perspectives", Sous l'Egide du GDR IMCODE, Polygone Louis Néel, Grenoble, 20-21 Décembre, 2007 (oral presentaion).
- I. H. Naqvi, G. El Zein, "Time-Reversal in indoor ultra-wideband communication: experimental results", "RF&HYPER Europe 2008", September 30th, October 1st & 2nd 2008 at Paris Nord Villepinte, France (oral presentation).

# Bibliography

- [1] A. Khaleghi, G. El Zein, and I. Naqvi, “Demonstration of time-reversal in indoor ultra-wideband communication: Time domain measurement,” in *International Symposium on Wireless Communication Systems, ISWCS 2007*, pp. 465–468, Oct. 2007.
- [2] T. W. Barrett, “History of ultrawideband (UWB) radar & communications: pioneers and innovators,” in *Proc. Progress in Electromagnetics Symposium*, (Cambridge, MA, USA), July 2000.
- [3] FCC, “First report and order,” tech. rep., Federal Communications Commission, February 2002.
- [4] C. L. Bennett and G. F. Ross, “Time-domain electromagnetics and its applications,” *Proceedings of the IEEE*, vol. 66, pp. 299–318, March 1978.
- [5] J. D. Taylor, *Introduction to Ultra-Wideband Radar Systems*. Boca Raton: CRC Press, 1995.
- [6] C. Fowler, J. Entzminger, and J. O. Corum, “Assessment of ultra wideband (UWB) technology,” *IEEE Aerospace and Electronic Systems Magazine*, vol. 5, pp. 45–49, November 1990.
- [7] R. Scholtz, “Multiple access with time-hopping impulse modulation,” in *Proc. IEEE Military Communications Conference MILCOM '93.*, vol. 2, pp. 447–450, 11–14 Oct. 1993.
- [8] R. A. Scholtz, *Impulse radio in Wireless communications: TDMA vs. CDMA*. London: Kluwer Academic Publishers, 1997.
- [9] J. Foerster, E. Green, S. Somayazulu, and et al., “Ultra-wideband technology for short- or medium-range wireless communications,” *Intel Technology Journal*, 2001.
- [10] C. E. Shannon, “Communication in the presence of noise,” *Proceedings of the IRE*, vol. 37, pp. 10–21, Jan. 1949.
- [11] G. R. Aiello and G. D. Rogerson, “Ultra-wideband wireless systems,” *IEEE Microwave Magazine*, vol. 4, pp. 36–47, June 2003.

- [12] CEPT/ECC, "On allowing the use of the radio spectrum for equipment using ultra-wideband technology in a harmonised manner in the community," Commission Decision Document Number C(2007) 522,, European Communication Commission, February 2007.
- [13] D. Porcino and W. Hirt, "Ultra-wideband radio technology : potential and challenges ahead," *IEEE Communications Magazine*, vol. 41, pp. 66–74, July 2003.
- [14] IDA, "Singapore UWB programme frame work 2003," tech. rep., Infocomm development authority of Singapore, March 3 2003.
- [15] M. Z. Win and R. A. Scholtz, "Impulse radio: how it works," *IEEE Communications Letters*, vol. 2, pp. 36–38, Feb. 1998.
- [16] M. Weisenhorn and W. Hirt, "Robust noncoherent receiver exploiting UWB channel properties," in *International Workshop on Ultra Wideband Systems, Joint with Conference on Ultrawideband Systems and Technologies, Joint UWBST & IWUWBS, 2004*, pp. 156–160, 18–21 May 2004.
- [17] J. G. Proakis, *Digital Communications*. McGraw-Hill, 4th ed., 2001.
- [18] C. Rushforth, "Transmitted-reference techniques for random unknown channels," *IEEE transaction on Information Theory*, vol. 10, pp. 39–42, January 1964.
- [19] R. A. Scholtz, "The origins of spread spectrum communications," *IEEE Transaction on Communications*, vol. COM-30, pp. 822–854, May 1982.
- [20] A. Polydoros and K. Woo, "LPI detection of frequency-hopping signals using autocorrelation techniques," *IEEE Journal on Selected Areas on Communications*, vol. 3, pp. 714–726, Sep 1985.
- [21] J. Fisher, R. Kohno, M. M. Laughlin, M. Welborn, and et al, "DS-UWB physical layer submission to 802.15 task group 3a," tech. rep., IEEE, September 2005.
- [22] M. Welborn and W. Shvodian, "Ultra-wideband technology for wireless personal area networks - the IEEE 802.15.3/3a standards," in *Proc. IEEE Conference on Ultra Wideband Systems and Technologies, ICUWB 2003*, November 2003.
- [23] A. Batra and et al., "Multi-band OFDM physical layer proposal for IEEE 802.15 task group 3a," tech. rep., IEEE P802.15-03/268r1, February 2008.
- [24] A. Molisch, "Ultrawideband propagation channels-theory, measurement, and modeling," *IEEE Transactions on Vehicular Technology*, vol. 54, pp. 1528–1545, Sept. 2005.
- [25] R.-M. Cramer, M. Win, and R. Scholtz, "Impulse radio multipath characteristics and diversity reception," in *IEEE International Conference on Communications, ICC 1998*, vol. 3, pp. 1650–1654 vol.3, Jun 1998.

- [26] J. Foerster, "The effects of multipath interference on the performance of UWB systems in an indoor wireless channel," in *IEEE VTS Vehicular Technology Conference, VTC 2001-Spring*, vol. 2, pp. 1176–1180 vol.2, 2001.
- [27] S. Gaur and A. Annamalai, "Improving the range of ultrawideband transmission using RAKE receivers," in *IEEE Vehicular Technology Conference, VTC 2003-Fall*, vol. 1, pp. 597–601 Vol.1, Oct. 2003.
- [28] J. D. Parsons, *The Mobile Radio Propagation Channel*. Halstead Press, 1992.
- [29] J. Karedal, S. Wyne, P. Almers, F. Tufvesson, and A. Molisch, "Statistical analysis of the UWB channel in an industrial environment," in *IEEE Vehicular Technology Conference, VTC 2004-Fall*, vol. 1, pp. 81–85 Vol. 1, Sept. 2004.
- [30] C.-C. Chong, Y. Kim, and S.-S. Lee, "A modified S-V clustering channel model for the UWB indoor residential environment," in *IEEE Vehicular Technology Conference, VTC 2005-Spring*, vol. 1, pp. 58–62 Vol. 1, May-1 June 2005.
- [31] D. Cassioli, M. Win, and A. Molisch, "A statistical model for the UWB indoor channel," in *IEEE Vehicular Technology Conference, VTC 2001-Spring*, vol. 2, pp. 1159–1163 vol.2, 2001.
- [32] K. Siwiak and A. Petroff, "A path link model for ultra wide band pulse transmissions," in *IEEE Vehicular Technology Conference, VTC 2001-Spring*, vol. 2, pp. 1173–1175 vol.2, 2001.
- [33] J. Karedal, S. Wyne, P. Almers, F. Tufvesson, and A. Molisch, "UWB channel measurements in an industrial environment," in *IEEE Global Telecommunications Conference, 2004. GLOBECOM '04*, vol. 6, pp. 3511–3516 Vol.6, Nov.-3 Dec. 2004.
- [34] S. Ghassemzadeh, L. Greenstein, A. Kavcic, T. Sveinsson, and V. Tarokh, "UWB indoor delay profile model for residential and commercial environments," in *IEEE Vehicular Technology Conference, VTC 2003-Fall*, vol. 5, pp. 3120–3125 Vol.5, Oct. 2003.
- [35] J. Kunisch and J. Pamp, "Measurement results and modeling aspects for the UWB radio channel," in *Digest of Papers, IEEE Conference on Ultra Wideband Systems and Technologies, ICUWB 2002*, pp. 19–23, 2002.
- [36] D. Cox and R. Leck, "Distributions of multipath delay spread and average excess delay for 910-mhz urban mobile radio paths," *IEEE Transactions on Antennas and Propagation*, vol. 23, pp. 206–213, Mar 1975.
- [37] A. M. Hayar and G. M. Vitetta, "Channel models for ultra-wideband communications: an overview," in *15th Mobile and Communications Summit, 2005*, June 2005.

- [38] A. Saleh and R. Valenzuela, "A statistical model for indoor multipath propagation," *IEEE Journal on Selected Areas in Communications*, vol. 5, pp. 128–137, Feb 1987.
- [39] A. F. Molisch, K. Balakrishnan, D. Cassioli, C. Chong, and et. al., "IEEE 802.15.4a channel model-final report," tech. rep., IEEE 802.15.4a, 2005.
- [40] D. Cassioli, M. Z. Win, and A. F. Molisch, "The ultra-wide bandwidth indoor channel: from statistical model to simulations," *IEEE Journal on Selected Areas in Communications*, vol. 20, no. 6, pp. 1247–1257, 2002.
- [41] A. Molisch, J. Foerster, and M. Pendergrass, "Channel models for ultrawideband personal area networks," *IEEE Wireless Communications*, vol. 10, pp. 14–21, Dec. 2003.
- [42] H. Hashemi, "The indoor radio propagation channel," *Proceedings of the IEEE*, vol. 81, pp. 943–968, Jul 1993.
- [43] S. Venkatesh, J. Ibrahim, and R. Buehrer, "A new 2-cluster model for indoor UWB channel measurements," in *IEEE Antennas and Propagation Society International Symposium, 2004.*, vol. 1, pp. 946–949 Vol.1, June 2004.
- [44] W. Turin, R. Jana, S. Ghassemzadeh, C. Rice, and T. Tarokh, "Autoregressive modeling of an indoor UWB channel," in *Digest of Papers, IEEE Conference on Ultra Wideband Systems and Technologies, ICUWB 2002*, pp. 71–74, 2002.
- [45] A. Rajeswaran, V. Somayazulu, and J. Foerster, "RAKE performance for a pulse based UWB system in a realistic UWB indoor channel," in *IEEE International Conference on Communications, 2003. ICC '03.*, vol. 4, pp. 2879–2883 vol.4, May 2003.
- [46] S. Paquelet, L.-M. Aubert, and B. Uguen, "An impulse radio asynchronous transceiver for high data rates," in *International Workshop on Ultra Wideband Systems, Joint with Conference on Ultrawideband Systems and Technologies, Joint UWBST & IWUWBS 2004*, pp. 1–5, May 2004.
- [47] J. Choi and W. Stark, "Performance of ultra-wideband communications with suboptimal receivers in multipath channels," *IEEE Journal on Selected Areas in Communications*, vol. 20, pp. 1754–1766, Dec 2002.
- [48] M. Fink and et. al., "Time-reversed acoustics," *Rep. Progr. Phys*, vol. 63, pp. 1988–1955, 2000.
- [49] M. Fink, "Time-reversed acoustics," *Physics Today*, vol. 20, pp. 34–40, 1997.
- [50] M. Fink, "Time-reversed acoustics," *Scientific American*, vol. 1, pp. 91–97, 1999.

- [51] S. Catheline, M. Fink, N. Quiéffin, and R. Kiri Ing, "Acoustic source localization model using in-skull reverberation and time reversal," *Appl. Phys. Lett.*, vol. 90, pp. 063902–, 2007.
- [52] M. Fink, "Time reversal of ultrasonic fields-part i: Basic principles," *IEEE Transactions on Ultrasonics, Ferroelectrics and Frequency Control*, vol. 39, pp. 555–566, Sep 1992.
- [53] G. Edelmann, T. Akal, W. Hodgkiss, S. Kim, W. Kuperman, and H. C. Song, "An initial demonstration of underwater acoustic communication using time reversal," *IEEE Journal of Oceanic Engineering*, vol. 27, pp. 602–609, Jul 2002.
- [54] M. Fink, "Time-reversal acoustics in complex environments," *GEOPHYSICS*, vol. 71(4), pp. SI151–SI164, 2006.
- [55] A. Derode, M. Tanter, L. Sandrin, A. Tourin, and M. Fink, "Numerical and experimental time-reversal of acoustic waves in random media," *Journal of Computational acoustics*, vol. 9(3), pp. 991–998, 2001.
- [56] G. Lerosey, *Retournement temporel d'ondes électromagnétiques et application à la télécommunication en milieux complexes*. PhD thesis, Université Pierre et Marie Curie (Paris VI), 2006.
- [57] A. E. Akogun, R. C. Qiu, and N. Guo, "Demonstrating time reversal in ultrawideband communications using time domain measurements," in *International Instrumentation Symposium*, 2005.
- [58] C. Oestges, J. Hansen, S. M. Emami, A. D. Kim, G. Papanicolaou, and A. J. Paulraj, "Time reversal techniques for broadband wireless communication systems," in *European Microwave Conference (Workshop)*, 2004.
- [59] G. Lerosey, J. De Rosny, d. D. A. Tourin, A. a, and M. Fink, "Time reversal of wideband microwaves," *Appl. Phys. Lett.*, vol. 15, p. 154101, 2006.
- [60] I. Naqvi and G. El Zein, "Time domain measurements for a time reversal SIMO system in reverberation chamber and in an indoor environment," in *Digest of Papers, IEEE International Conference on Ultra-Wideband, ICUWB 2008*, vol. 2, pp. 211–214, Sept. 2008.
- [61] P. Kyritsi, G. Papanicolaou, P. Eggers, and A. Oprea, "MISO time reversal and delay-spread compression for FWA channels at 5 ghz," *IEEE Antennas and Wireless Propagation Letters*, vol. 3, pp. 96–99, 2004.
- [62] R. Qiu, C. Zhou, N. Guo, and J. Zhang, "Time reversal with MISO for ultrawideband communications: Experimental results," *IEEE Antennas and Wireless Propagation Letters*, vol. 5, pp. 269–273, Dec. 2006.

- [63] H. T. Nguyen, I. Kovacs, and P. Eggers, "A time reversal transmission approach for multiuser UWB communications," *IEEE Transactions on Antennas and Propagation*, vol. 54, pp. 3216–3224, Nov. 2006.
- [64] I. Naqvi, A. Khaleghi, and G. El Zein, "Performance enhancement of multiuser time reversal UWB communication system," in *International Symposium on Wireless Communication Systems, ISWCS 2007*, pp. 567–571, Oct. 2007.
- [65] A. Khaleghi and G. El Zein, "Signal frequency and bandwidth effects on the performance of UWB time-reversal technique," in *Antennas and Propagation Conference, 2007. LAPC 2007, Loughborough*, pp. 97–100, April 2007.
- [66] R. Qiu, C. Zhou, J. Zhang, and N. Guo, "Channel reciprocity and time-reversed propagation for ultra-wideband communications," in *IEEE Antennas and Propagation Society International Symposium*, pp. 29–32, June 2007.
- [67] H. Nguyen, J. Andersen, and G. Pedersen, "The potential use of time reversal techniques in multiple element antenna systems," *IEEE Communications Letters*, vol. 9, pp. 40–42, Jan. 2005.
- [68] T. Strohmer, M. Emami, J. Hansen, G. Papanicolaou, and A. Paulraj, "Application of time-reversal with MMSE equalizer to UWB communications," in *IEEE Global Telecommunications Conference, 2004. GLOBECOM '04.*, vol. 5, pp. 3123–3127 Vol.5, Nov.-3 Dec. 2004.
- [69] K. Usuda, H. Zhang, and M. Nakagawa, "Pre-Rake performance for pulse based UWB system in a standardized UWB short-range channel," in *IEEE Wireless Communications and Networking Conference, WCNC2004*, vol. 2, pp. 920–925 Vol.2, March 2004.
- [70] S. Imada and T. Ohtsuki, "Pre-RAKE diversity combining for UWB systems in IEEE 802.15 UWB multipath channel," in *International Workshop on Ultra Wideband Systems, Joint with Conference on Ultrawideband Systems and Technologies, Joint UWBST & IWUWBS, 2004*, pp. 236–240, May 2004.
- [71] P. Welch, "The use of fast fourier transform for the estimation of power spectra: A method based on time averaging over short, modified periodograms," *IEEE Transactions on Audio and Electroacoustics*, vol. 15, pp. 70–73, Jun 1967.
- [72] P. Kyritsi, P. Eggers, and A. Oprea, "MISO time reversal and time compression," in *Proc. URSI International Symposium on Electromagnetic Theory, 2004*.
- [73] S. S. Mo, N. Guo, J. Q. Zhang, and R. C. Qiu, "UWB MISO time reversal with energy detector receiver over ISI channels," in *IEEE Consumer Communications and Networking Conference, CCNC2007*, pp. 629–633, Jan. 2007.
- [74] P. Guguen and G. El Zein, *Les techniques multi-antennes pour les réseaux sans fil*. Hermes Science Publishers, 2004.

- [75] I. H. Naqvi and G. El Zein, "Time reversal uwb system: SISO, SIMO, MISO and MIMO comparison with time domain experiments," in *Journées Scientifiques CNFRS-URSI "Propagation et Télédétection"*, 2009.
- [76] I. H. Naqvi and G. El Zein, "Retournement temporel en ulb: étude comparative par mesures pour des configurations multi-antennes," *Revue de l'Electricité et de l'Electronique (REE)*, vol. Dossier: Propagation et Télédétection., 2009.
- [77] A. Khaleghi and G. El Zein, "Procédé d'émission par un émetteur comportant une unique antenne, d'un ensemble de données à destination d'un récepteur comprenant des antennes," Brevet Français d'Invention, Bretagne Valorisation Réf BV/ DV 468, 2007.
- [78] A. Khaleghi, I. Naqvi, and G. El Zein, "SIMO time reversal UWB communication system: An increased capacity transmission approach," *IET Electronics Letters*, (Submitted) 2009.
- [79] A. Khaleghi, "Diversity techniques with parallel dipole antennas: Radiation pattern analysis," in *Progress in Electromagnetic Research (PIER 64)*, 2006.
- [80] D. A. Hill, "Electromagnetic theory of reverberation chambers," tech. rep., National Institute of Standards and Technology (US) Technical Note 1506, December 1998.
- [81] I. H. Naqvi, P. Besnier, and G. El Zein, "Effects of time variant channel on time reversal uwb system," in *Proc. of IEEE Global Communication Conference (GLOBECOM)*, 2009.
- [82] R. Hoor and H. Tomlinson, "Delay-hopped transmitted-reference RF communications," in *Digest of Papers, IEEE Conference on Ultra Wideband Systems and Technologies (ICUWB) 2002*, pp. 265–269, 21–23 May 2002.
- [83] R. J. Fontana, E. Richley, and J. Barney, "Commercialization of an ultra wideband precision asset location system," in *Proc. IEEE Conference on Ultra Wideband Systems and Technologies, ICUWB 2003*, pp. 369–373, 16–19 Nov. 2003.
- [84] A. Klein, I. Brown, D.R., D. Goeckel, and J. Johnson, C.R., "RAKE reception for UWB communication systems with intersymbol interference," in *IEEE Workshop on Signal Processing Advances in Wireless Communications, SPAWC 2003*, pp. 244–248, June 2003.
- [85] I. H. Naqvi, A. Khaleghi, and G. El Zein, "Time reversal UWB communication system: A novel modulation scheme with experimental validation," *Eurasip Journal on Wireless Communications and Networking (JWCN)*, (Submitted) 2009.
- [86] A. Khaleghi and G. El Zein, "Procédé de modulation pour les communications sans fil à retournement temporel," September 2007.

- [87] I. Naqvi, A. Khaleghi, and G. El Zein, "Time reversal uwb communication system: A novel modulation scheme with experimental validation," *Eurasip Journal on Wireless Communications and Networking*, vol. 2010, p. 12, 2010.
- [88] A. Khaleghi and G. El Zein, "Measurement and analysis of ultra-wideband time reversal for indoor propagation channels," *Springer, Wireless personal communications*, vol. Accepted with minor revisions, 2009.
- [89] I. Naqvi and et al., "Time reversal uwb communication: Experimental study for high data rates in dense multipath propagation channels," *IET Journal of Antenna and Propagation*, vol. 4, pp. 643–650, Sept. 2010.
- [90] I. Naqvi, G. El Zein, G. Lerosey, J. De Rosny, P. Besnier, A. Tourin, and M. Fink, "Time reversal uwb communication: Experimental study for high data rates in dense multipath propagation channels," in *The Mosharaka International Conference on Communications, Propagation and Electronics (MIC-CPE)*, 2009.
- [91] I. Naqvi, A. Khaleghi, and G. El Zein, "Multiuser time reversal uwb communication system: A modified transmission approach," in *IEEE International Symposium On Personal, Indoor and Mobile Radio Communications (PIMRC '09)*, 2009.